

Archive ouverte UNIGE

https://archive-ouverte.unige.ch

Thèse de privat-docent

2024

Open Access

This version of the publication is provided by the author(s) and made available in accordance with the copyright holder(s).	
Understanding bacterial molecular weapons	
Renzoni, Adriana Maria	

How to cite

RENZONI, Adriana Maria. Understanding bacterial molecular weapons. Privat-docent Thesis, 2024. doi: 10.13097/archive-ouverte/unige:177300

This publication URL: https://archive-ouverte.unige.ch/unige:177300

Publication DOI: <u>10.13097/archive-ouverte/unige:177300</u>

© This document is protected by copyright. Please refer to copyright holder(s) for terms of use.



Section Fundamental Médicine
Département de Médecine Génétique et
de Laboratoire

"UNDERSTANDING BACTERIAL MOLECULAR WEAPONS"

Thesis submitted to the Faculty of Medicine of the University of Geneva

for the degree of Privat-Docent by

Adriana RENZONI

Geneva

2023

SUMMARY	2
1. INTRODUCTION	3
1.1. ANTIMICROBIAL RESISTANCE, A WORLDWIDE PROBLEM.	3
1.2. RESISTANCE DEVELOPMENT UPON ANTIBIOIC TREATMENT OF S. AUREUS.	3
1.3. ANTIBIOTIC RESISTANCE AND S. AUREUS BACTERIAL DORMANCY	
1.4. Our contribution	
1.4.1 MECHANISMS UNDERLYING THE EMERGENCE OF BACTERIAL RESISTANCE UPON ANTIBIOTIC TREATMENT	8
1.4.1.1. Identification of trfA and trfB, two new genes involved in glycopeptide antibiotic resistance in S.	
aureus.	8
1.4.1.2. Genetic characterization and impact of $trfA$ and $trfB$ on glycopeptide and β -lactam resistance	9
1.4.1.3. Deciphering the molecular function of <i>trfA</i> in <i>S. aureus</i> .	
1.4.1.4. Characterization of the lipoprotein PrsA in both glycopeptide and oxacillin resistance	
1.4.1.5. PrsA affect B-lactam resistance by affecting membrane PBP2A levels.	
1.4.2 MECHANISMS UNDERLYING ANTIBIOTIC INDUCED BACTERIAL DORMANCY.	12
2. THESIS RELATED MANUSCRIPTS	13
2.1 Staphylococcus aureus antibiotic sensing pathways leading to antibiotic resistance	13
2.1.1. Whole genome sequencing and complete genetic analysis reveals novel pathways to Glycopeptide resistance	
Staphylococcus aureus.	13
2.1.2. Molecular bases determining Daptomycin resistance-mediated resensitization to B-lactams (see-saw effect	
Methicillin-Resistant Staphylococcus aureus.	
2.2 Understanding antibiotic induced dormancy in Staphylococcus aureus	
2.2.1 Insights into the global effect on <i>Staphylococcus aureus</i> growth arrest by induction of the endoribonuclease	
toxin	
2.2.2 1 John solubility controls Spx in Staphylococcus aureus: Implication for Mazer Toxin-antitoxin system regu	
2.2.3 MazF toxin causes alterations in <i>Staphylococcus aureus</i> transcriptome, translatome and proteome that unde	
bacterial dormancy.	
3. CONCLUSION AND PERSPECTIVES	27
4. REFERENCES	32

SUMMARY

Bacterial antibiotic resistance in different bacterial strains has been recognized for several decades as a world-wide problem. This is an alarming situation with still few alternatives to fight against. To face this problem, different aspects of antibiotic resistance have been considered such as identifying the bacterial molecular pathways leading to the development of resistance, identifying factors contributing to the spread of resistant bacteria, or finding alternatives for clinical treatment and clinical diagnostics. This Privat–Docent thesis compiles the efforts of my research programme that contributes to this world-wide problem. The never-ending history of bacterial antibiotic resistance is the result of its incredible capacity to continuously react and adapt to antibiotic attack. Bacteria use different strategic defences based on selection of gene resistant mutations or other mechanisms such as the unbelievable induction of their own metabolic dormancy. By applying several basic or innovative molecular techniques, such as nEMOTE, whole genome sequencing, ribosome profiling, RNA-seq, transmission and fluorescence microscopy techniques, we discovered a novel arsenal of weapons probably used in Staphylococcus aureus defence. We propose protein aggregation, degradation, and secretion systems, oxidative stress, cell-wall modification systems or even modulation of endoribonucleolytic enzymes or ribosome hibernation, as incredible defence weapons used by S. aureus to avoid antibiotic attack. Our scientific contribution allows us to propose new diagnostic tools and open several pathways for the discovery of new therapeutic targets.

1. INTRODUCTION

1.1. Antimicrobial resistance, a worldwide problem.

Antibiotic resistance is still a major global health threat, found in different bacterial pathogens and contributing to diminishing our ability to treat bacterial infections. It is such an alarming situation that in some cases few or any treatment option remains effective. Whenever a new antibiotic is introduced, bacteria react and generate different defense resistant mechanisms leading to ineffective antibiotics and poor clinical treatments (Windels, Van den Bergh, and Michiels 2020). The bacterial resistance appears due to bacteria carrying resistant mutations, plasmids or even due to the repetitive antibiotic administration that selects for natural resistant bacteria. The molecular mechanisms explaining antibiotic resistance include production of enzymes destroying antibiotics, decreased antibiotic permeability, and antibiotic target modification among other mechanisms. We can fight against this phenomenon by decreasing antibiotic usage and controlling transmission of resistant bacteria but also understanding the molecular resistant mechanisms behind (Reygaert 2018; Darby et al. 2023).

In the following paragraphs, I will expose some of the aspects of antibiotic resistance that we studied in *Staphylococcus aureus* (*S. aureus*). We focused our research work to understand the molecular development of resistance to the most useful antibiotics in *S. aureus* treatment, such as glycopeptides, oxacillin and daptomycin (section 1.2) and to understand an incredible and clever mechanism used by bacteria to avoid killing by antibiotics, named bacterial dormancy (section 1.3).

1.2. Resistance development upon antibioic treatment of S. aureus.

S. aureus is a bacterial pathogen causing severe clinical infections including bacteremia, endocarditis and frequently associated with heart valves, catheters, or orthopedic implant infections (Howden et al. 2010; Tong et al. 2015). Specifically, S. aureus resistant to methicillin (MRSA), is considered an important pathogen of healthcare and community associated infections.

Different antibiotics were developed and used to treat S. aureus infections, but S. aureus has successively overcome the antibiotic killing by developing antibiotic resistance. The first introduction of β-lactam penicillin antibiotic, was fought back by S. aureus producing a βlactamase enzyme, capable of inactivating the drug and resulting in penicillin resistance. βlactamase resistant antibiotics were then created, such as methicillin. Right after its introduction, S. aureus methicillin-resistant (MRSA) isolates appeared. Methicillin resistance was achieved by horizontal transfer of mecA gene(Hiramatsu et al. 2014). The mecA gene encoding PBP2A is the main determinant of the MRSA phenotype. The mec and bla loci encode the regulatory genes mecRI-mecI-mecR2 and blaR1-blaI respectively; together, they are responsible for the fine-tuning of mecA induction by β-lactams(Arede, Ministro, and Oliveira 2013; Berger-Bachi et al. 1992). Acquisition and expression of the mecA gene alone is not sufficient for a uniform resistance to β-lactams and other factors are required (De Lencastre et al. 1999). After identification of methicillin-resistance, glycopeptide antibiotics (vancomycin and teicoplanin) were then developed and became the therapeutic drugs of choice. MRSA-infected patients are frequently treated with glycopeptides generating a continuous, strong selective pressure for the emergence of MRSA isolates resistant to glycopeptides(Lowy 2003). Two different forms of resistance to glycopeptides have been identified in S. aureus: the exogenously acquired, highlevel resistance (VRSA) and the endogenous, low-level/intermediate resistance (GISA/VISA). The limited treatment options available for MRSA infections after the emergence of glycopeptide resistance prompted the development of new antibiotics, such as daptomycin, linezolid, tigecycline, ceftaroline and ceftobiprole. Among these new therapies, daptomycin is considered an optimal option since it is a drug not inferior to vancomycin for the treatment of MRSA infections (Shaw et al. 2015; Fowler et al. 2006) and it has remained active against S. aureus world-wide with no trends toward increased daptomycin resistance (Sader et al. 2015). As for other antibiotics, clinical isolates with reduced susceptibility to daptomycin, although rare, have been already detected and associated with therapeutic failure (Skiest 2006; Sader and Jones 2006). The mechanism of daptomycin resistance is multifactorial and involves changes in the bacterial cell membrane and wall (Bayer, Schneider, and Sahl 2013). Gene mutations linked to daptomycin resistance, include those in cell membrane and wall- associated genes (e.g. mprF and the two-component system YycFG, respectively), and others such as mutations in RNA polymerase subunits RpoB/C (Bayer, Schneider, and Sahl 2013; Cui et al. 2010). The most

clinically significant and relevant changes are those associated with mutations in *mprF* (Yang et al. 2009). In addition to *mprF*, resistance to daptomycin involves the upregulation of genes required for cell wall synthesis and turnover, including the two-component regulator vraSR (Mehta et al. 2012; Mishra et al. 2012).

Today, higher complexity is added to S. aureus antibiotic treatment by the recognized existence of antibiotic cross-resistance. We frequently observed cross-resistance of glycopeptides with daptomycin (Mishra et al. 2011; Cui et al. 2006; Camargo et al. 2008) but the exact molecular modifications leading to cross-resistant are still unknown. Chen et al (2015) recently characterize the evolution of the dual resistance in a series of MRSA blood isolates (Chen, Huang, and Chiu 2015). They show a sequential emergence of hVISA/daptomycin nonsusceptible MRSA strains after exclusive teicoplanin treatment. Glycopeptide and daptomycin cross-resistance is further demonstrated by clinical cases showing that the vast majority of daptomycin resistant strains isolated were previously hVISA/VISA and isolated under glycopeptides treatment (Bayer, Schneider, and Sahl 2013; Stefani et al. 2015). The molecular pathways involved in daptomycin/glycopeptide cross-resistance include vraRS, mprF and rpoB genes, but the exact mechanism is unknown (Bayer, Schneider, and Sahl 2013). Between βlactams and glycopeptide antibiotics, several studies have clearly shown common-resistant molecular pathways used by both antibiotics to generate resistance. For example, in vitro studies have shown that exposure to β-lactams can select for vancomycin hetero-resistant strains (hVISA) (Katayama et al. 2009) through trfA (Roch et al. 2014) or vraRS-regulated molecular pathway(s) (Howden, Peleg, and Stinear 2014). As trfA and vraRS are involved in cell wall metabolism, probably cell wall changes induced by β-lactams through trfA and/or vraRS pathways are affecting vancomycin targets and decreasing vancomycin-susceptibility. A similar situation is found in MRSA patients coinfected with gram-negative bacteria and treated with combinations of vancomycin and β -lactams. This combination selects for β -lactam induced vancomycin-resistant MRSA strains (BIVR) (Hososaka et al. 2006; Yamaguchi et al. 2009). BIVR are a subtype of MRSA showing resistance to vancomycin only in the presence of βlactams. This phenomenon is explained by the β-lactam induced peptidoglycan metabolism that produces large amounts of peptidoglycan precursors carrying D-Ala-D-Ala termini. Vancomycin tightly binds to D-Ala-D-Ala termini and consequently, the concentration of free vancomycin is

reduced below its minimal inhibitory concentration (MIC) levels allowing strains to grow. The exact mechanism that induces BIVR is unknown.

It is not surprising to identify common molecular pathways leading to resistance of cell wall active antibiotics. The primary cell wall targets are all found outside the cell. All conditions changing cell wall metabolism and secretion of targets may affect susceptibility profiles to these antibiotics. From the analysis of biochemical and genetical studies, the VraSR two-component system that is clearly involved in cell wall metabolism and affecting glycopeptide, daptomycin and β-lactam resistance. To identify other targets that play a role in cross-resistance mechanism, we focused on candidate genes affecting the secretion of cell wall antibiotic targets. One key protein is PrsA, a lipid-anchored protein that assists post-translocational folding of proteins at the outer surface of the cytoplasmic membrane in other gram-positif bacteria (Hyyrylainen et al. 2010). We have shown that PrsA is under VraSR regulation and that it affects glycopeptide, β-lactams and daptomycin resistance (Jousselin et al. 2012; Jousselin et al. 2015).

1.3. Antibiotic resistance and S. aureus bacterial dormancy.

Dormant bacteria can be tolerant to antibiotics because during growth arrest, the activity of antibiotic targets is diminished and leads to survival. Antibiotic tolerant bacteria survive antibiotics without carrying a resistance factor, and they can regrow after removal of the antibiotic (Keren et al. 2004; Balaban et al. 2019). Antibiotic tolerant bacteria are important because they play a role in the population phenomenon of antibiotic persistence, in which under drug pressure, most of the bacterial population will be rapidly killed by the antibiotic and tolerant cells will survive by slowing down its metabolism, entering into a dormant state (Bigger 1944; Dorr, Vulic, and Lewis 2010; Balaban et al. 2019).

The dormant and antibiotic tolerant bacteria explain the clinical occurrence of bacterial recurrent infections (Conlon et al. 2013; Conlon 2014; Proctor et al. 2014; Vulin et al. 2018). Indeed, the positive outcome of an antibiotic treatment is generally measured by the absence of bacterial detection in clinical samples. However, antibiotic treatment may induce bacterial dormancy, resulting in low bacterial counts in clinical specimens and in a false interpretation of a negative bacterial culture. The subsequent removal of the antibiotic treatment can allow bacteria to regrowth (Mok, Orman, and Brynildsen 2015) with a final clinical interpretation of a recurrent bacterial infection. This phenomenon emphasizes the

urgent need to understand the molecular pathway(s) leading to dormancy allowing future development of diagnostic detection tools.

Toxin-antitoxin systems (TAS) has been linked to bacterial dormancy (Mutschler et al. 2011; Masuda et al. 2012; Castro-Roa et al. 2013; Harms, Maisonneuve, and Gerdes 2016; Mok et al. 2015). One of the best characterized TAS involved in dormancy is MazEF, a type II TAS operon found in clinical important bacteria, such as *Staphylococcus aureus* (Sierra, Viollier, and Renzoni 2018). The MazF toxin activity is normally inhibited by MazE antitoxin during normal growth conditions. Upon stressed conditions, MazE is degraded by cellular proteases, liberating MazF toxin endoribonucleolytic activity leading to dormancy, however, thorough an unknown mechanism (Harms et al. 2018). See figure 2.

One key factor in understanding the role of MazEF in dormancy is the regulation of its components (Sierra, Viollier, and Renzoni 2018). The chromosomally encoded mazEF locus is located upstream and co-transcribed with the sigB operon that encodes for the alternative stress sigma factor B and its activity modulators, rsbUVW. MazEF transcription is activated by subinhibitory concentrations of erythromycin or tetracycline and regulated by the transcriptional regulators σ^B and SarA. Its cognate antitoxin MazE is regulated by proteolysis through ClpCP proteolytic complex together with the adaptor protein TrfA (Donegan et al. 2010; Donegan, Marvin, and Cheung 2014). To further understand MazEF biological function, following studies were conducted towards the identification of MazF endoribonucleolytic targets. As MazF toxin was found to be a sequence specific endoribonuclease that recognizes the pentad sequence U^ACAU of mRNAs and cleaves independently of ribosomes (Fu et al. 2007; Zhu et al. 2009), MazF cleavage motif was further used as a marker for identification of MazF target genes. A link between MazEF and virulence was for example proposed based on the identification and in vitro cleavage of selected virulence genes such as hla (α -hemolysin), spa (Protein A virulence factor), sigB (global regulator Sigma B) and sraP (adhesion factor)(Fu et al. 2009; Zhu et al. 2009). However, the molecular pathways linking dormancy and MazEF TAS are still unknown, despite that dormancy was the first phenotype described upon overexpression of MazF toxin (Sierra, Viollier, and Renzoni 2018).

1.4. Our contribution

My research program aims to investigate the mechanisms underlying 1-the emergence of bacterial resistance upon antibiotic treatment and 2-antibiotic induced bacterial dormancy in *S. aureus*. Using genetic and molecular analyses of glycopeptide susceptible and resistant pairwise strains obtained upon antibiotic treatment either in vivo or in vitro, we identified and proposed that protein degradation, protein aggregation and secretion systems are bacterial antibiotic defense mechanisms. As part of this defense arsenal, we also proposed the modulation of endoribonucleolytic enzymes and ribosome hibernation as defence weapons inducing *S. aureus* dormancy to avoid antibiotic attack. A summary of our contributions is described in the next section 1.4.1 and depicted in Figure 1 and 2. The most important contributions are described in section 2.

1.4.1 Mechanisms underlying the emergence of bacterial resistance upon antibiotic treatment.

1.4.1.1. Identification of *trfA* and *trfB*, two new genes involved in glycopeptide antibiotic resistance in *S. aureus*.

Our implication to understand *S. aureus* antibiotic resistance started by an exciting in-vivo observation: a glycopeptide (teicoplanin or vancomycin) resistant bacterial clone emerged in a rat model of subcutaneous tissue cages chronically infected with a glycopeptide-susceptible MRSA strain (Vaudaux et al. 2001). This glycopeptide-resistant clone (Tei^r strain 14-4) showed a 8-16-fold increase in teicoplanin MIC (16 mg/L) and a 2-4-fold increase in vancomycin MIC, compared to its parent susceptible strain (MRGR3). Re-infection of rat tissue cages with the Tei^r strain 14-4, selected a stable Tei^s revertant subclone isolated in one tissue cage and named strain 14-4rev. Tei^s 14-4rev exhibited complete loss of teicoplanin and vancomycin resistance, and emerged concomitantly with the nearly complete disappearance of its Tei^r parent 14-4 used for the challenge. These three strains are clonally linked, as assessed by pulsed-field gel electrophoresis (PFGE) and comparative genome hybridization analysis (CGH). However, CGH data revealed a complete disappearance of a small (1.8-kb) genomic region in Tei^s revertant 14-4rev compared to Tei^r 14-4 (Renzoni et al. 2009). **Strains MRGR3, 14-4 and 14-4rev strains**

and this genetic deletion, opened to our laboratory the opportunity to build up our research projects to understand antibiotic resistance emergence in *S. aureus*.

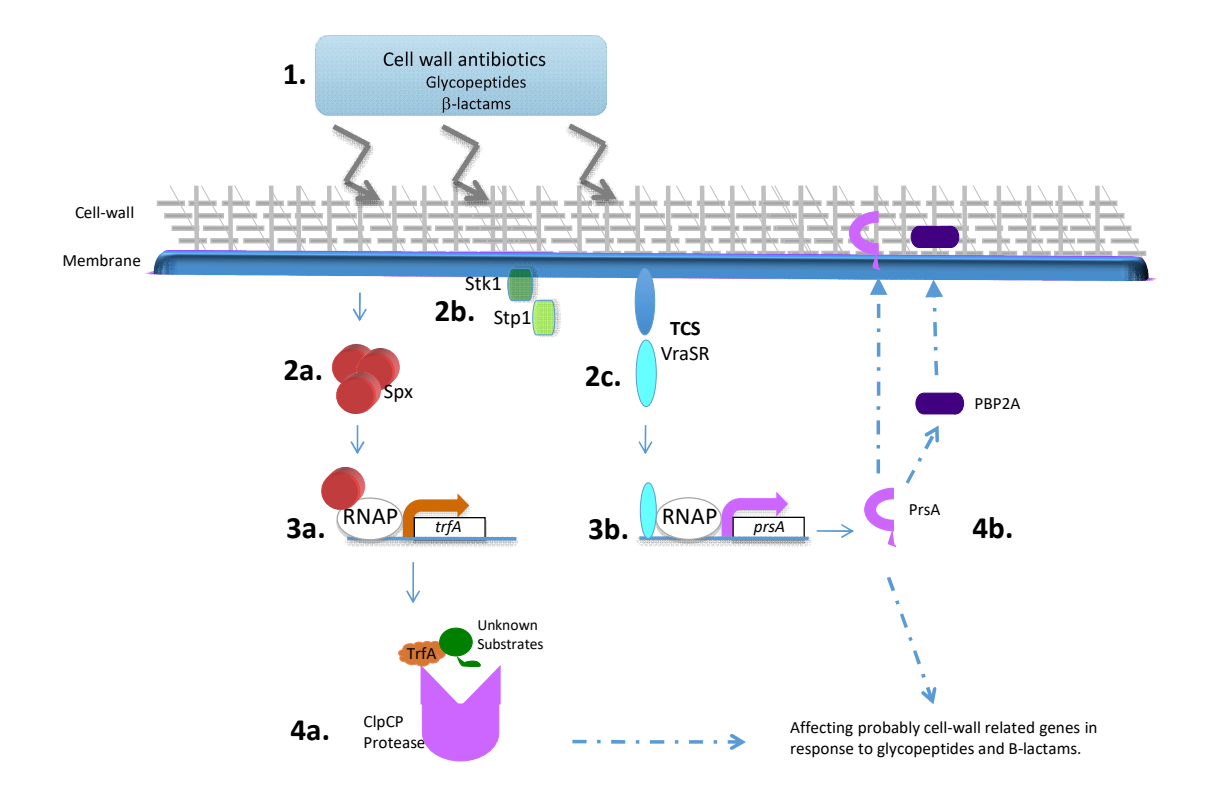


Figure 1. Schematic representation showing the key steps we identified to understand the emergence of antibiotic resistance in *S. aureus*. Our own phenotypic and molecular studies in the field highlighted the role of novel genes in *S. aureus* antibiotic resistance. 1. Cell wall antibiotic stress causes induction of multiple sensory pathways. 2. We uncovered three sensory pathways in our studies: Spx transcriptional regulator (2a), Stk1/Stp1 kinase-phosphatase system (2b) and VraRS two component system (2c). 3. We identified and studied trfA (3a) and prsA (3b), two candidate genes under control of Spx and VraRS sensory pathways, respectively. 4. TrfA is part of a bacterial proteolytic system probably controlling degradation of cell wall related proteins (4a). TrfA is necessary for β-lactam induced emergence of hVISA. PrsA is a membrane-anchored protein that regulates PBP2A cell-membrane amounts involved in β-lactam resistance (4b) and Daptomycin/B.lactam see-saw effect. It probably controls other cell wall related proteins.

1.4.1.2. Genetic characterization and impact of trfA and trfB on glycopeptide and β -lactam resistance.

As mentioned above, the small (1.8-kb) genomic segment deleted in the revertant Teis strain 14-4rev, compared to the Teir parent 14-4, contained only two genes, designated *trfA* and *trfB*, for teicoplanin resistance factors (Renzoni et al. 2009). As MRGR3 and its derivatives were found refractory to genetic manipulations, we evaluated the contribution of *trfA* and *trfB* to glycopeptide in the laboratory strain ISP794. A teicoplanin-resistant (TeiR) derivative strain ISP4-2-1 was selected from ISP794 by two *in vitro* passages on teicoplanin-containing agar.

Single or double trfA and/or trfB mutations restored teicoplanin and vancomycin susceptibilities to ISP794 parental levels. Conversely, complementation of trfA and/or trfB mutants restored glycopeptide resistance, suggesting that trfA and trfB genes are involved in glycopeptide resistance. Analyzing the impact of trfA and trfB on the clinical methicillin and glycopeptide-intermediate resistant (MRSA-GISA) NRS3 strain, we demonstrated a strong reduction in glycopeptide resistance but it also impacted the β -lactam antibiotic oxacillin resistance. Despite the genetic demonstration that trfA and trfB are contributing to glycopeptide resistance, their functional role is elusive. Indeed, no functional role has been reported in the field of antibiotic resistance for either trfA, trfB, or their homologs in other gram-positive bacteria.

1.4.1.3. Deciphering the molecular function of trfA in S. aureus.

- a) Putative link between oxidative stress and trfA. The trfA gene is related to mecA of B. subtilis encoding an adaptor protein implicated in multiple roles, notably proteolysis and genetic competence, but despite its strong sequence similarity with B. subtilis mecA, the function of S. aureus trfA remains largely unexplored. Northern blot analysis and 5' RACE mapping revealed that trfA was expressed monocistronically from three different promoters. Cell wall active antibiotic exposure led to both increased trfA transcription and enhanced steady-state TrfA protein levels. The trfA promoter regulation was not dependent upon the cell-wall stress sentinel VraSR and other sensory stress systems such as GraRS, WalkRK, Stk1/Stp1, and SigB. We discovered that the global oxidative stress regulator Spx controlled trfA transcription. This finding was also confirmed using a strain with enhanced Spx levels resulting from a defect in yjbH, encoding a Spx-interacting protein governing Spx proteolytic degradation. A collection of clinical GISA strains revealed significant steady state upregulation of trfA compared to corresponding susceptible parental strains further supporting a role for trfA in antibiotic resistance. These data provide strong evidence for a link between cell wall antibiotic stress and evoked responses mediated by an oxidative stress sensor (Jousselin et al. 2013).
- b) Link between trfA and the emergence of heterogeneous vancomycin-resistance (hVISA) in S. aureus. Glycopeptides select for heterogeneous vancomycin-resistance (hVISA) strains. However, in clinical situations hVISA strains have been isolated from patients without exposure to glycopeptides. In collaboration with Pr. François Vandenesch from Lyon University, we showed *in vitro* that subinhibitory concentration of different β -lactams can select hVISA

strains showing thickened cell-walls and without mutations in any known gene previously associated with glycopeptide resistance. Deletion of trfA gene was found to abolish the capacity of β -lactams to select for hVISA strains (Roch et al. 2014). These data suggest a link between b-lactam antibiotic stress, emergence of hVISA strains and trfA molecular function in S. aureus.

1.4.1.4. Characterization of the lipoprotein PrsA in both glycopeptide and oxacillin resistance. Our previous study (Renzoni et al. 2011), showed a limited number of genomic changes leading to glycopeptide resistance, including the VraSR operon, the master regulator of glycopeptide resistance. This observation prompted us to focus on VraR-regulated genes that are found to be highly expressed upon cell-wall antibiotic stress, such as *prsA*, a lipid-anchored protein of the parvulin PPIase family (peptidyl-prolyl *cis/trans* isomerase). We demostrated by both genetic and biochemical assays that *prsA* is directly regulated by the VraRS two-component system linked to cell-wall stress. Disruption of *prsA* does not affect macroscopic changes in cell wall_architecture or growth rate. Yet, disruption of *prsA*, leads to alterations in the sensitivity to glycopeptides and oxacillin resistance. Quantitative transcriptional analysis reveals that *prsA*, together with *vraR*, are coordinately upregulated in a panel of stable laboratory and clinical GISA strains compared to their susceptible parents (Jousselin et al. 2012).

1.4.1.5. PrsA affect B-lactam resistance by affecting membrane PBP2A levels.

It is known that β-lactam resistance in *Staphylococcus aureus* results from the expression of the extra penicillin binding protein PBP2A, which can catalyze DD-transpeptidation of peptidoglycan even in the presence of β-lactam antibiotics. Expression of the *mecA* gene, coding for PBP2A has been well studied. However, little is known about PBP2A protein expression and secretion to the outer surface of the membrane and its mechanism in acting as a peptidoglycan transpeptidase. PrsA is a lipid-anchored membrane protein, recognized to assist folding of extracellular proteins, such as penicillin binding proteins in *B. subtilis* and *L. monocytogenes*. We previously published that PrsA is involved in oxacillin and glycopeptide resistance in *S. aureus* and is transcriptionally regulated by the two-component system VraSR (Jousselin et al. 2012). We provide more interesting insights into the role of PrsA on β-lactam resistance. We report that deletion of PrsA causes a decrease in resistance to several β-lactam antibiotics in accordance with a decrease of PBP2A membrane amounts, without affecting *mecA* mRNA levels. By performing

PrsA structure-function analysis, we show that the N- and C-terminal chaperone domains of PrsA are critical features for PBP2A expression and oxacillin resistance. We propose that PrsA has a role in post-transcriptional maturation of PBP2A, possibly in export and/or folding of newly synthetized PBP2A (Jousselin et al. 2015). Unraveling the connection between PBP2A and secretion could reveal unexpected targets for innovative anti-infective strategies.

1.4.2 Mechanisms underlying antibiotic induced bacterial dormancy.

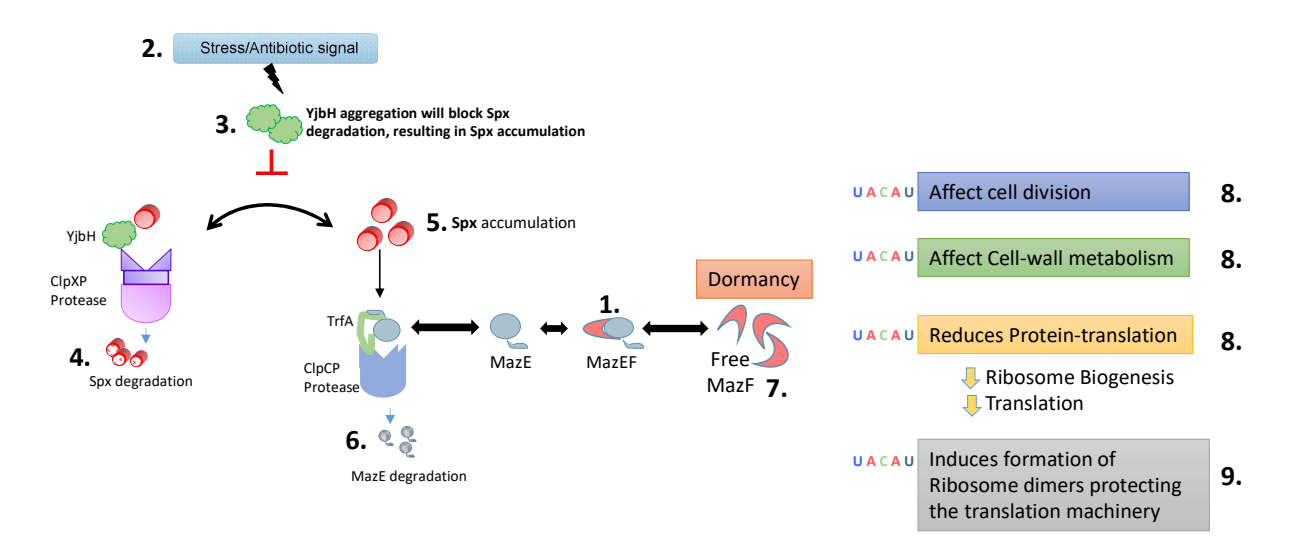


Figure 2. Proposed model linking antibiotic stress, toxin-antitoxin MazEF system and bacterial dormancy in *S. aureus*. (1) Under normal growth conditions, MazF endoribonuclease toxin (an enzyme cleaving RNA molecules) is sequestered by MazE antitoxin. (2) Upon an environmental stress, such as the presence of antibiotics, YjbH adaptor protein is aggregated (3), reducing Spx degradation through ClpXP protease system (4). As Spx is the transcriptional activator of *trfA* gene, the resulting accumulation of Spx (5) increases TrfA adaptor protein levels that will concomitantly result in MazE antitoxin degradation through ClpCP proteolytic system (6). MazE increased degradation will result in liberation of MazF toxin and inducing *S. aureus* dormancy (7). We identified the RNA motif recognized specifically by MazF to cleave RNA molecules (UACAU) and identify cell division, cell-wall metabolism, and protein translation related genes as targets for MazF cleavage (8). MazF overexpression induces cleavage of these RNA targets and formation of ribosome dimers (9) in agreement with growth bacterial arrest during dormancy.

All our projects related to study *S. aureus* bacterial dormancy are described in figure 2 and section 2. Briefly, we contributed with review publication in Biochemical and Biophysical Acta describing a compilation of all toxin antitoxin systems (TAS) described to date in *S. aureus* (Sierra, Viollier, and Renzoni 2018) and by studying different molecular steps leading to MazEF TAS regulation to understand the link of MazEF TAS and dormancy.

2. Thesis Related Manuscripts

2.1 Staphylococcus aureus antibiotic sensing pathways leading to antibiotic resistance.

2.1.1. Whole genome sequencing and complete genetic analysis reveals novel pathways to Glycopeptide resistance in *Staphylococcus aureus*.

PLoS ONE 6(6):e21577.

Glycopepetide resistance in *S. aureus* is known to occur via exogeneous and endogeneous mechanisms. Exogeneous acquisition of the *Enterococcus feacalis* VanA complex by horizontal gene transfer rendered *S. aureus* highly resistant to vancomycin (Minimum inhibitory concentration or MIC > 16 ug/ml). This modification in the peptidoglycan pentapeptide terminus from D-ala/D-ala to D-ala/D-lac (among others) (Cong, Yang, and Rao 2020). However, this exogeneous resistance is rare. In contrast, the endogeneous mechanism is more often observed. It arises from spontaneous mutations conferring a selective advantage to the presence of the antibiotic producing low level resistant strains (MIC >2 to < 16 ug/ml) (Hiramatsu 2001). It was clearly shown that during glycopeptide clinical treatment there is a progressive selection of bacteria showing increasing glycopeptide resistance and this has been linked to glycopeptide clinical failure. In light of these observations, we wanted to understand the molecular changes allowing survival of *S. aureus* during drug exposure.

Using whole genome sequencing, we identified genetic differences between isogenic teicoplanin-susceptible parental strain ISP794 (MIC 1 μ g/ml = Tei^S) and its stable *in-vitro* derived teicoplanin-resistant mutant ISP4-2-1 (MIC 8 μ g/ml = Tei^R). In Tei^R ISP4-2-1 strains, we uncovered mutations in *stp1* (encoding a serine/threonine phosphatase), *yjbH* (encoding an adaptor protein directing ClpXP-dependent degradation of the transcriptional regulator Spx) and in *vraS* (histidine kinase sensor of the TCS VraSR) genes. By standard genetic reconstructions, we demonstrated the role of each gene mutation in the emergence of glycopeptide resistance. All <u>single</u>, <u>pairwise</u> combinations, and a fully reconstructed <u>triple</u> mutant were evaluated for their contribution to low-level glycopeptide resistance (Figure 3).

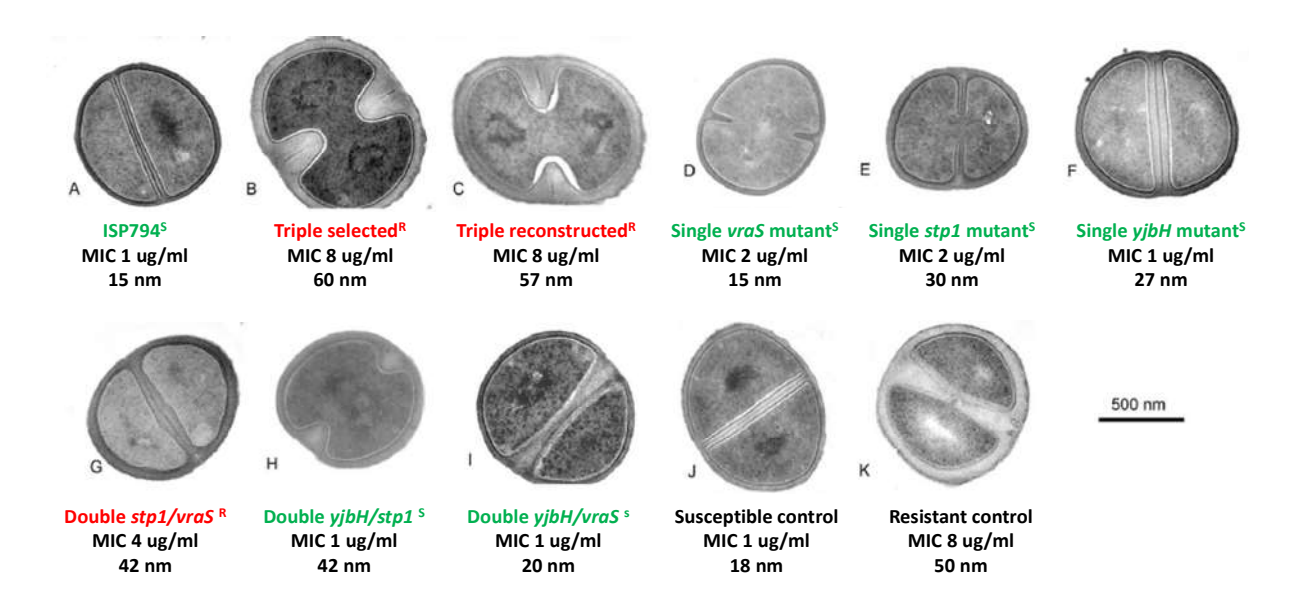


Figure 3. Transmission electron microscopy of the parental susceptible strain (A), the teicoplanin-resistant in vitro selected mutant ISP4-2-1 (B), the fully reconstructed triple mutant (C), all single mutants (D-F), each pairwise combinations (G-I) and susceptible and resistant control strains (J and K). Susceptible and resistant teicoplanin strains are denoted in green or red, respectively. Teicoplanin MIC and cell wall thickness (nm) are described below.

- 1. We found a synergistic cooperation on glycopeptide resistance between dual phosphosignalling systems (VraRS and Stk1/Stp1) combined with a more subtle contribution from YjbH, suggesting the activation of oxidative stress defences via Spx.
- 2. We found that all mutations contribute to significant alterations of the cell wall thickness, explaining their role on glycopeptide resistance.

This study was the first genetic demonstration for: 1- for the sequential emergence of mutations linked with the stepwise emergence of glycopeptide resistance and 2- for the presence of multiple sensor and stress pathways contributing simultaneously to glycopeptide resistance development. In particular, we identified two phospho-signalling systems and the oxidative stress molecular pathways (Renzoni et al. 2011).



Whole Genome Sequencing and Complete Genetic Analysis Reveals Novel Pathways to Glycopeptide Resistance in *Staphylococcus aureus*

Adriana Renzoni*, Diego O. Andrey, Ambre Jousselin, Christine Barras, Antoinette Monod, Pierre Vaudaux, Daniel Lew, William L. Kellev

Service of Infectious Diseases, Geneva University Hospitals, Geneva, Switzerland

Abstract

The precise mechanisms leading to the emergence of low-level glycopeptide resistance in *Staphylococcus aureus* are poorly understood. In this study, we used whole genome deep sequencing to detect differences between two isogenic strains: a parental strain and a stable derivative selected stepwise for survival on 4 µg/ml teicoplanin, but which grows at higher drug concentrations (MIC 8 µg/ml). We uncovered only three single nucleotide changes in the selected strain. Nonsense mutations occurred in *stp1*, encoding a serine/threonine phosphatase, and in *yjbH*, encoding a post-transcriptional negative regulator of the redox/thiol stress sensor and global transcriptional regulator, Spx. A missense mutation (G45R) occurred in the histidine kinase sensor of cell wall stress, VraS. Using genetic methods, all single, pairwise combinations, and a fully reconstructed triple mutant were evaluated for their contribution to low-level glycopeptide resistance. We found a synergistic cooperation between dual phospho-signalling systems and a subtle contribution from YjbH, suggesting the activation of oxidative stress defences via Spx. To our knowledge, this is the first genetic demonstration of multiple sensor and stress pathways contributing simultaneously to glycopeptide resistance development. The multifactorial nature of glycopeptide resistance in this strain suggests a complex reprogramming of cell physiology to survive in the face of drug challenge.

Citation: Renzoni A, Andrey DO, Jousselin A, Barras C, Monod A, et al. (2011) Whole Genome Sequencing and Complete Genetic Analysis Reveals Novel Pathways to Glycopeptide Resistance in Staphylococcus aureus. PLoS ONE 6(6): e21577. doi:10.1371/journal.pone.0021577

Editor: Malcolm James Horsburgh, University of Liverpool, United Kingdom

Received February 10, 2011; Accepted June 3, 2011; Published June 27, 2011

Copyright: © 2011 Renzoni et al. This is an open-access article distributed under the terms of the Creative Commons Attribution License, which permits unrestricted use, distribution, and reproduction in any medium, provided the original author and source are credited.

Funding: This work was supported by the Swiss National Science Foundation grant 3100A0-120428 (WLK) and 310030-125109 (DL) and an F. Hoffmann-La Roche MD-PhD training grant (DOA). The funders had no role in study design, data collection and analysis, decision to publish, or preparation of the manuscript.

1

Competing Interests: The authors have declared that no competing interests exist.

* E-mail: Adriana.Renzoni@hcuge.ch

Introduction

Methicillin-resistant *Staphylococcus aureus* (MRSA) infections is a major cause of morbidity and mortality worldwide, including in the health care setting. The mortality rate associated with invasive MRSA infections is significant and in the United States MRSA infections are now quoted as the leading cause of death by an infectious agent [1]. MRSA infections are particularly difficult to treat because of the development of antibiotic resistance and limited therapeutic options. Glycopeptide antibiotics (vancomycin and teicoplanin) are still the preferred drugs for treatment of serious hospital or community-acquired MRSA infections, despite reports of increasing numbers of glycopeptide-resistant MRSA isolates [2,3].

Glycopeptide resistance in *Staphylococcus* have emerged by two mechanisms. Highly glycopeptide-resistant *S. aureus* strains (VRSA; MIC≥16 µg/ml) acquired the exogeneous multigene VanA complex carried on transposon Tn1546 from *Enterococcus faecalis* by horizontal gene transfer. Fortunately, these events are infrequent and only few examples are known worldwide [4,5]. The second mechanism of resistance, termed endogenous or low-level (MICs with >2 µg/ml to <16 µg/ml), arises because spontaneous mutation(s) are thought to confer a selective survival advantage. Endogeneous resistance is thought to occur stepwise: emergence of resistance to low-antibiotic levels must be first acquired to allow

growth in progressively higher antibiotic concentrations [6,7]. The exact molecular mechanism(s) leading to endogeneous resistance to teicoplanin, or vancomycin, is/are unknown. A common resistance pathway has being suggested since in general reduced susceptibility to vancomycin strains also display reduced teicoplanin sensitivity. However, teicoplanin resistance can be acquired without alteration in vancomycin susceptibility [3,6].

Endogenous resistance is more often observed and clinical studies have linked glycopeptide clinical failure with progressive selection of bacterial isolates showing increasing glycopeptide resistance levels. In some reported cases, as little as a two-fold change in MIC altered clinical outcome [8,9]. Such concerns have resulted in the recent re-evaluation of clinical breakpoints for glycopeptides [10] (www.srga.org/). In light of these concerns, understanding the molecular changes permitting survival of *S. aureus* during drug challenge is of paramount importance.

Glycopeptides are non-penetrating cell wall acting antibiotics whose site of action lies outside the cell membrane, implying that changes in physical-chemical barriers, detection, signalling and response mechanisms could conceivably promote resistance. Several phenotypic responses leading to resistance are observed in some, but not all cases and include thicker cell wall, reduced autolysis and increased cell wall crosslinking [11,12,13,14,15,16,17]. These changes are thought to be correlated with a differential

expression of genes involved in cell wall metabolism. In several studies, point mutations occurring in only one gene (vraRS, graRS or tcaA) have been described and confirmed by genetic analysis to contribute to glycopeptide resistance [15,18,19]. No studies concerning the functional links between these pathways have been provided, however. Only one study has uncovered multiple mutations by sequence analysis when comparing Mu50 (VISA) and a revertant Mu50 Ω (VSSA) that were conclusively proven to contribute to low-level glycopeptide resistance [20].

In this study, we identified genomic changes using whole genome deep sequencing of a teicoplanin-susceptible and its teicoplanin-resistant derivative. Point mutations occurred in three genes and complete genetic analysis proved their causal link to glycopeptide resistance. We demonstrate multiple pathways contributing to glycopeptide resistance emergence including two types of phosphosignalling (histidine and serine/threonine) combined with a global redox/thiol stress sensor.

Results

Genomic sequencing of isogenic ISP794 and AR376 strains

To identify genomic changes selected during teicoplanin exposure, whole genome deep sequencing of both ISP794 and AR376 was performed. AR376 is an in vitro derived stable teicoplanin-resistant mutant from laboratory strain ISP794 [21].

Since ISP794 and AR376 are derivatives of the sequenced NCTC8325 strain (NCBI Accession No. NC_007795), we used this as a reference to evaluate genome coverage and facilitate contig assembly. Using Illumina-Solexa technology, we obtained 5,659,670 and 3,609,916 of 35-bp paired-end reads for ISP794 and AR376 strains, respectively, mapping the reference genome. The raw coverage depth was 35 and 23 times for ISP794 and AR376, respectively. Mapping covered 2,819,664 and 2,819,622 bases in ISP794 and AR376 strains, resulting in 99.8% and 99.6% of NCTC8325 genome coverage (2,821,361 bp), respectively. Most of the reference genome was covered sufficiently (minimum coverage of 3 read bases per reference base) to allow single nucleotide polymorphism (SNP) detection. The paired end information was used to detect with high confidence insertions and deletions (InDel).

SNP and InDel differences detected between ISP794 and AR376 strains

Computer analysis of interstrain differences between the assembled ISP794 and AR376 genomes first revealed 9 potential SNPs and 11 potential InDels. Each difference was subsequently re-examined by genomic DNA PCR amplification using appropriate primers and sequencing. Six potential SNPs and all InDel differences were rejected by this analysis. As shown in Figure 1, only 3 SNP differences apparently distinguished AR376 from its parental strain ISP794.

SNPs were detected in three different open reading frames corresponding to reference sequence tag SAOUHSC 00938,

Α

Genome position 8325	ISP794 Base	AR 376 Base	SNP in gene	Gene SAOUHSC	Gene N315	Change
912480	Т	А	yjbH	00938	SA 0860	K23stop
1137496	С	Т	stp1	01186	SA 1062	Q12stop
1974492	С	Т	vraS	02099	SA 1701	G45R

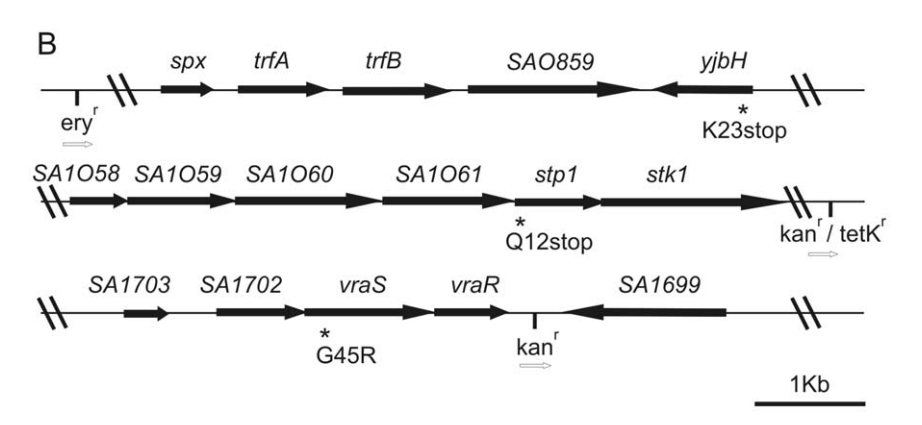


Figure 1. Genomic differences detected by whole genome sequencing. (A) Chromosomal location of detected SNPs and predicted protein changes. (B) Physical map of each locus containing *yjbH*(K23stop), *stp1*(Q12stop) and *vraS*(G45R). For genetic analysis, each mutation was tagged by site-specific insertion of a nearby selectable marker to facilitate strain constructions using bacteriophage-mediated transduction. doi:10.1371/journal.pone.0021577.g001

SAOUHSC 01186 and SAOUHSC 02099 genes (equivalent to N315 ordered sequence tags SA0860, SA1062 and SA1701, respectively). Similarity searches with SAOUHSC 00938 indicated the presence in Bacillus subtilis of a gene showing partial similarity and annotated as yjbH (SwissProt accession BG13137). In B. subtilis YjbH is an adaptor protein, which, together with ClpXP protease, regulates the degradation of the global transcriptional regulator Spx [22]. In S. aureus, YjbH is a hypothetical protein showing 34% identity and 73% amino acid sequence similarity with YibH of B. subtilis. The yjbH t/a SNP occurred at nucleotide position 67 generating a nonsense mutation at amino acid 23 (K23stop). The SAOUHSC 01186 gene encodes Stp1, a serine/threonine phosphatase [23]. The stp1 c/t SNP occurred at nucleotide position 34 generating a nonsense mutation at amino acid 12 (Q12stop). Finally, the SAOUHSC 02099 gene encodes the histidine kinase sensor VraS. The vraS c/t SNP occurred at nucleotide position 133 generating a missense mutation at amino acid 45 by substituting arginine for glycine (G45R) (Figure 1). The amino acid G45 in VraS is located in a region predicted to lie between two N-terminal transmembrane domains suggesting a possible role in extracellular signal sensing.

Genetic analysis of each SNP and its contribution to teicoplanin-resistance

To determine whether each individual SNP detected in AR376 contributed to reduced teicoplanin susceptibility, we first reengineered each SNP change by site-specific mutation or phage mediated transduction backcross in ISP794 (see Table 1). As judged by broth macrodilution MICs and confirmed by spot population analysis profiles (spot PAP assays), vraS(G45R), or stp1(Q12stop), led to reduced teicoplanin susceptibility (MIC = $2 \mu g/ml$) compared to the parent ISP794 (MIC = 1 μ g/ml) (Table 2). Spot PAP assays revealed detectably enhanced growth of both single mutants on MHA supplemented with increasing concentrations of teicoplanin, while no growth was observed with parent ISP794. Identical results were obtained when comparing a second independent isolate of each single mutant (Figure 2A). In contrast to vraS(G45R) and stp1(Q12stop) mutants, a small increase of growth was observed for yibH(K23stop) while no growth was observed for the parent ISP794. Growth was observed when 1×10^5 and 1×10^4 colony forming units were applied on MHA supplemented with 0.5 µg/ml of teicoplanin (Figure 2A). However, MIC analysis showed no difference between ISP794 and its isogenic yjbH(K23stop) mutant (MIC = 1 μ g/ml) (Table 2).

Complementation of either vraS(G45R) or stp1(Q12stop) mutants by a multicopy plasmid carrying the corresponding wild-type genes, led to restored sensitivity to teicoplanin (Figure S1). As yjbH(K23-stop) mutation has a subtle effect on teicoplanin resistance, complementation of the yjbH mutation was performed by introducing a multicopy plasmid carrying yjbH wild-type gene into the triple mutant (see below), a condition where its role could be readily assessed. We observed restored sensitivity of the triple mutant to levels comparable with the double mutant vraS(G45R)/stp1(Q12stop) mutant (Figure S1).

Collectively, we conclude that single *vraS* (G45R), *stp1* (Q12stop) and, to a lesser extent, *yjbH*(K23stop) mutations in parent ISP794 decreased teicoplanin susceptibility, however, none of the single mutations alone could account for the parental AR376 MIC levels. We conclude that some combination of these mutants must therefore contribute to the observed teicoplanin-resistant phenotype of AR376.

Effect of mutant combinations on teicoplanin resistance

We next analysed the drug resistance phenotypes of each of the three possible pairwise mutants: stp1/yjbH, stp1/vraS, and yjbH/

vraS. As shown in Figure 2B and Table 2, a further decrease of teicoplanin susceptibility was observed only with double mutant vraS(G45R)-stp1(Q12stop). Spot PAP assays revealed growth of the double vraS(G45R)-stp1(Q12stop) mutant on MHA supplemented with 2 μg/ml teicoplanin and showing a macrodilution MIC of 4 μg/ml. Notably, the double mutant displayed enhanced growth compared to either of the single mutants alone (Figure 2A and B, compare growth and log₁₀ -fold scale, teicoplanin 1 µg/ml panels, for the single stp1 or vraS mutants versus the stp1/vraS double mutant). In contrast, and as detected by spot PAP assay and macrodilution MIC, the other two pairwise mutants did not show any decrease in teicoplanin susceptibility (Figure 2B and Table 2). Interestingly, the decrease in teicoplanin susceptibility observed in vraS(G45R), or stp1(Q12stop) single mutants, was abolished by the yjbH(K23stop) mutation (Figure 2A, B and Table 2). These results suggest that the loss of yibH exerts a negative effect on the pathways leading to drug sensitivity changes engendered by vraS(G45R) or stp1(Q12stop) mutations.

Although the double mutant *vraS*(G45R)-*stp1*(Q12stop) decreased teicoplanin susceptibility, it still did not fully recapitulate the AR376 MIC levels. The effect on teicoplanin susceptibility of the fully reconstructed triple mutant was therefore tested. Genetic analysis of the re-engineered triple mutant revealed complete restoration of the teicoplanin resistance phenotype indistinguishable from AR376. Spot PAP assays revealed identical growth of both the triple mutant *vraS*(G45R) - *stp1*(Q12stop) - *yjbH*(K23stop) and AR376 on MHA supplemented with increasing concentrations of teicoplanin (Figure 2B) and identical macrodilution MIC levels were also observed (MIC = 8 μg/ml) (Table 2).

Effect of single mutations and their combinations on vancomycin susceptibility

The impact of all mutations was also examined for their contribution to changes in vancomycin susceptibility, despite the fact that the in-vitro derived teicoplanin-resistant AR376 strain showed only a 2-fold marginal increase in vancomycin MIC compared to its susceptible counterpart ISP794 (Table 2). Changes in vancomycin MICs were not as dramatic as the changes observed in teicoplanin MICs for the various mutant combinations (Table 2). Nevertheless, as shown in Figure 2C, similar results with teicoplanin susceptibilities were observed using the more sensitive log₁₀-scaled growth assay. Spot PAP assays revealed detectable enhanced growth of both single vraS(G45R) or stp1(Q12stop) mutants on MHA supplemented with 1 µg/ml of vancomycin compared to the susceptible strain ISP794. In contrast no difference was observed with yjbH(K23stop) mutant. At 2 µg/ml vancomycin concentration only AR376 showed growth and comparable colony formation as observed with control agar plates with no drug. Further analysis of all pairwise and triple mutants revealed a detectable decrease in vancomycin susceptibility only for the double vraS(G45R)-stp1(Q12stop) and reconstructed triple mutants. As previously noted above and in results presented in Figure 2B, we also observed that the yjbH(K23stop) mutation, when paired with either vraS(G45R) or stp1(K12stop) exerted a negative effect by reversing drug sensitivity changes arising from these single mutations.

Taken together, we conclude that all three SNPs were collectively responsible for the decreased glycopeptide susceptibility of AR376 strain. Furthermore, was(G45R) and stp1(Q12stop) mutations acted synergistically to reduce glycopeptide susceptibility while yjbH(K23Stop) contributed significantly to low level glycopeptide resistance in this strain only when paired with the dual phospho-signalling mutants. These results also reveal that although AR376 was originally selected for reduced susceptibility

Table 1. Strains and plasmids used in this study.

Strain/plasmid	Revelant genotype	Characteristics	Source/ reference
S. aureus			
RN4220	8325-4; r- m+, restriction defective laboratory strain		[55]
ISP794	8325 pig 131		[56]
AR376	ISP4-2-1		21
AR774	vraS (G45R)	ISP794, vraS (G45R) kan ^r nearby	This study
AR758	kan ^r nearby <i>vraS</i>	ISP794, <i>vraS</i> kan ^r nearby	32
AR756	vraS::ermB	ISP794, vraS::ermB	32
AR802	kan ^r nearby <i>stp1</i> (Q12stop)	AR376, stp1(Q12stop) kan ^r nearby	This study
AR860	kan ^r nearby stp1	ISP794, stp1kan ^r nearby	This study
AR826	stp1 (Q12stop)	ISP794, stp1(Q12stop) kan ^r nearby	This study
AR853	tetK ^r nearby stp1(Q12stop)	AR376, stp1(Q12stop) tetK ^r nearby	This study
AR858	vraS (G45R), stp1 (Q12stop)	ISP794, vraS (G45R) kan ^r nearby, stp1(Q12stop) tetK ^r nearby	This study
AR864	vraS (G45R), yjbH (K23stop)	AR376, stp1 kan ^r nearby	This study
AR854	stp1 (Q12stop), yjbH (K23stop)	AR376, <i>vra</i> S kan ^r nearby	This study
AR1077	ery ^r nearby <i>yjbH</i> (K23stop)	AR376, <i>yjbH</i> (K23stop) ery ^r nearby	This study
AR1079	yjbH (K23stop)	ISP794, yjbH(K23stop) ery ^r nearby	This study
AR1082	vraS (G45R), yjbH (K23stop), stp1 (Q12stop)	ISP794, vraS (G45R) kan ^r nearby, yjbH (K23stop) ery ^r nearby, stp1(Q12stop) tetK ^r nearby	This study
AR964	AR774/pAM1483		This study
AR1001	AR826/pAR992		This study
AR1085	AR1082/pAR973		This study
Sa <i>∆clpP</i>	8325-4 derived strain	clpP deleted strain	[57]
Δspx	8325-4 derived strain	spx deleted strain	27
spx ⁺	8325-4 Δspx, P _{spx} -spx::geh	spx deleted strain and chromosomally complemented with the intact copy of spx inserted into geh locus.	27
Plasmids			
pTYB12	N-terminal fusion IMPACT intein and chitin binding domain plasmid		New England (Biolabs)
pMK4	E.coli-S.aureus shuttle vector, amp ^r and cam ^r		[58]
pBT2	E.coli-S.aureus thermosensitive-shuttle vector, amp ^r and cam ^r		[59]
pBluescript II KS+	routine multicopy <i>E.coli</i> cloning vector amp ^r		Stratagene
pAR749	pBT2, vraS-G45R kan ^r nearby ts shuttle vector		This study
pAR712	pBT2, vraS-kan ^r -SA1699 intergenic ts shuttle vector		32
pAR784	pBT2, stp1-kan ^r nearby ts shuttle vector		This study
pAR787	pBT2, stp1-tet ^r nearby ts shuttle vector		This study
pAR1063	pBT2, <i>yjbH</i> -ery ^r nearby ts shuttle vector		This study
pAM1483	pMK4- 3.3 kb entire vraR operon and upstream promoter region Kpn-Pst		32
pAR992	pMK4- containing Not1-Kpn pHU promoter region, Kpn-Pst1 Stp1 gene		This study
pAR973	pMK4- containing Not1-Kpn pGlyS promoter region, Kpn-Pst1 <i>yjbH</i> gene		This study
pAM1101	pTYB12-SpxA (Nde-Pst)		This study

doi:10.1371/journal.pone.0021577.t001

to teicoplanin, the genetic changes also impact vancomycin susceptibility, *albeit* to a lesser degree in this strain background. The sensitivity of the spot PAP assay to reveal these subtle changes underscores its powerful application to unravelling the genetics of endogenous glycopeptide resistance.

Analysis of cell wall thickness by electron microscopy

Since the VraRS two-component sensor system regulates a response to cell wall stress and controls, in part, the expression of genes involved cell wall metabolism [24], and further, since stk1/

stp1 modulate cell wall metabolism [25], we analysed the cell wall thickness of all strains used in this study by transmission electron microscopy (Figure 3). As reference control strains, we first analysed the cell wall thickness of the glycopeptide resistant strain Mu50, which displays a significantly thicker cell wall (50.4 \pm 8 nm) than the glycopeptide susceptible control strain ATCC29213 (17.35 \pm 2.9 nm) (Figure 3A and 3B; [11]). Analysis of AR376 showed a significantly (p<0.001) thicker cell wall compared to its susceptible counterpart ISP794 and furthermore, this enhanced thickness was comparable to, and in fact greater than, Mu50. Both

Table 2. Glycopeptide susceptibility profiles of ISP794 and its

	MIC [*] μg/ml			
Strain	Teicoplanin	Vancomycin		
ISP794	1	2		
AR376	8	4		
vraS*	2	2		
stp1 [*]	2	2–4		
yjbH [*]	1	2		
vraS [*] /stp1 [*]	4	4		
stp1" yjbH" vraS"/stp1" vraS"/yjbH"	1	2		
stp1*/yjbH* vraS*/stp1*/yjbH*	1	2		
vraS*/stp1*/yjbH*	8	4		

MIC, Modal minimum inhibitory concentration measured by broth macrodilution. VraS, stp1* and yjbH* correspond to vraS (G45R), stp1 (Q12stop) and yjbH (K23stop) mutations, respectively. doi:10.1371/journal.pone.0021577.t002

of the stp1(Q12stop) and yjbH(K23stop) single mutations significantly increased (\$\phi < 0.001\$) cell wall thickness compared to the susceptible parental strains ISP794, while in contrast, no significant difference was observed between vraS(G45R) mutant and ISP794. Analysis of all pairwise mutants showed a significantly greater (p < 0.001) increase in cell wall thickness compared to ISP794; however, no double mutation attained AR376 cell wall thickness levels. Indeed, the observed mean thickness for both the stp1/vraS and stp1/vjbH mutations were significantly less (p<0.001) than AR376. Only the fully reconstituted triple mutant AR1082 showed comparable cell wall thickness as AR376 strain. It is worthwhile noting that the yjbH(K23stop) mutation enhanced cell wall thickness when paired with either stp1(Q12stop) or vraSG45R in these assays in contrast to the negative effect of yjbH(K23stop) on teicoplanin MIC and spot PAP assay growth (on either teicoplain or vancomycin) when paired with these mutants as described above. Apart from these changes in cell wall thickness, we did not observe overt changes in cell division such as aberrant septum formation or other peculiar morphology for any mutation examined.

Collectively, these results show that all mutations contribute to significant alterations in cell wall thickness in our strain background; however, the observed changes in cell wall thickness do not precisely correlate with the observed changes in glycopeptide susceptibility. We conclude that changes in glycopeptide sensitivities in this strain background must arise primarily from physiological changes other than pronounced changes in cell wall thickness.

YjbH negatively regulates Spx levels in S. aureus

A role for YjbH has not been previously described in S. aureus; however, in B. subtilis, YjbH acts as a post-transcriptional negative regulator of the global oxidative/thiol stress regulator Spx [26]. YjbH binds Spx and functions as an adaptor protein directing ClpXP-dependent degradation of Spx. Disruption of yjbH or clpP in B. subtilis is known to result in enhanced levels of Spx since its proteolytic turnover is greatly attenuated. A rise in Spx levels leads to substantial changes in gene expression profiles.

To address the hypothesis that S. aureus YjbH acts as a negative regulator of Spx analogous to its B. subtilis counterpart, we first examined Spx protein levels by western blot. As shown in Figure 4,

rabbit polyclonal anti-Spx antibody recognized purified S. aureus Spx migrating with the expected molecular weight of 15 kDa. No Spx was detected in a negative control S. aureus 8325-4 derived strain extract containing an internal disruption of spx, whereas Spx was strongly detected in cell extract lacking clpP as previously described [27]. Spx was also detected in an extract from AR376, harbouring the triple vraS(G45R)-stp1(Q12stop)-yjbH(K23stop) mutant combination. Importantly, comparison of extracts from ISP794 and its isogenic derivative AR1079 containing the yjbH(K23Stop) mutation, showed that Spx was undetectable in the presence of wild type yjbH, but clearly detectable in the presence of the yjbH(K23Stop). We conclude from these results that the loss of yjbH results in significant stabilization of Spx protein in S. aureus and that YjbH probably functions similarly to its B. subtilis counterpart by aiding Spx proteolytic turnover. Consequently, the triple mutant AR376 harbors changes in two distinct phosphosignalling pathways and possesses enhanced Spx protein levels arising from the loss of its negative regulator yibH.

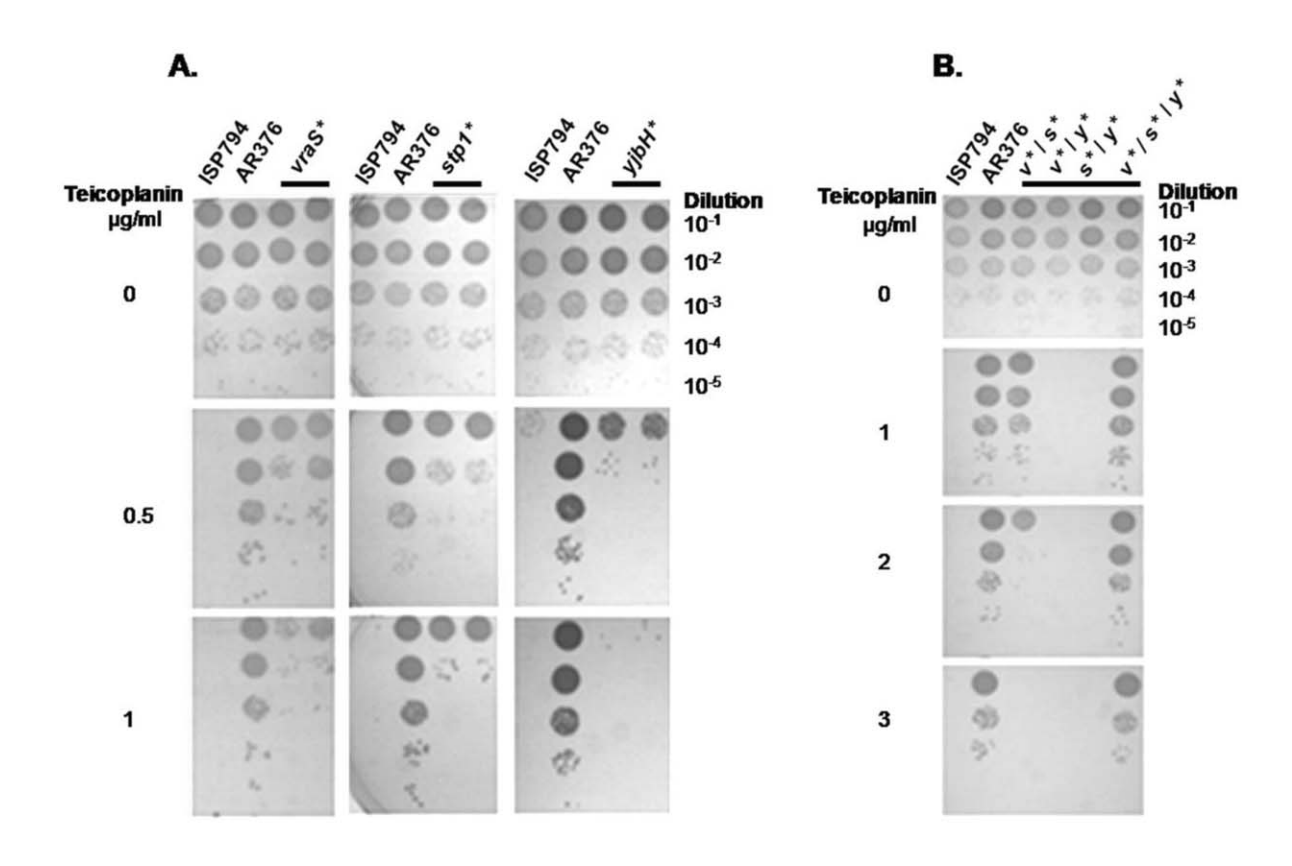
Influence of Spx and teicoplanin on transcription of msrA1 encoding methionine sulfoxide reductase in S. aureus

Several lines of evidence link oxidative stress and S. aureus responses to glycopeptide antibiotics. First, recent work suggests that the mode of killing by several classes of antibiotic, including glycopeptides, involves the endogenous production of reactive oxygen radicals [28]. Secondly, transcriptional profiling revealed that an oxidative stress defence gene, msrA1, encoding methionine sulfoxide reductase was among those genes most strongly upregulated in response to various cell wall active antibiotics, including glycopeptides, in S. aureus [29,30]. As msrA1 transcription is known to be positively regulated by Spx in B. subtilis [31], we hypothesized that a possible functional consequence of the loss of yjbH in AR376, would be enhanced transcription of Spx-dependent genes such as msrA1 (N315 ordered sequence tag SA1257). To explore this possibility, we tested whether msrA1 was indeed subject to Spxdependent transcription regulation in S. aureus.

The results (Figure 5A) show that in a Δspx strain, teicoplanin exposure resulted in no significant induction of msrA1 compared to uninduced control, whereas in the Δspx strain complemented with a chromosomally integrated copy of wild type spx, msrA1 induction was significantly induced more than 3-fold (p < 0.05) following exposure to teicoplanin. Indeed, in the absence of spx, even basal msrA1 transcript levels were significantly lower (p < 0.05) compared with msrA1 transcript levels in the spx complemented strain.

Since the yjbH(K23stop) mutation results in significant stabilization of Spx protein, we also analysed whether the steady state msrA1 transcription in the absence of drug induction was affected in either AR376 or the yjbH(K23stop) single mutant. Figure 5B shows that basal msrA1 transcript levels were indeed significantly higher (p < 0.05) in both AR376 and yjbH(K23stop) mutant compared to the parental strain ISP794. We conclude from these results that msrA1 is subject to transcriptional regulation dependent upon spx in S. aureus.

We also recently described the discovery of trfA (teicoplanin resistance factor A) as a gene whose loss restores glycopeptide sensitivity in AR376 [21]. We have found that *trfA* transcript levels are also significantly increased by the loss of yjbH and that the trfA promoter is also positively regulated by Spx (A. Renzoni, manuscript in preparation). Taken together, these findings strongly suggest that stabilization of Spx through disruption of yjbH results in important functional consequences within the cell since Spx positively regulates the expression of at least two genes, msrA1 and trfA, known to contribute to glycopeptide resistance.



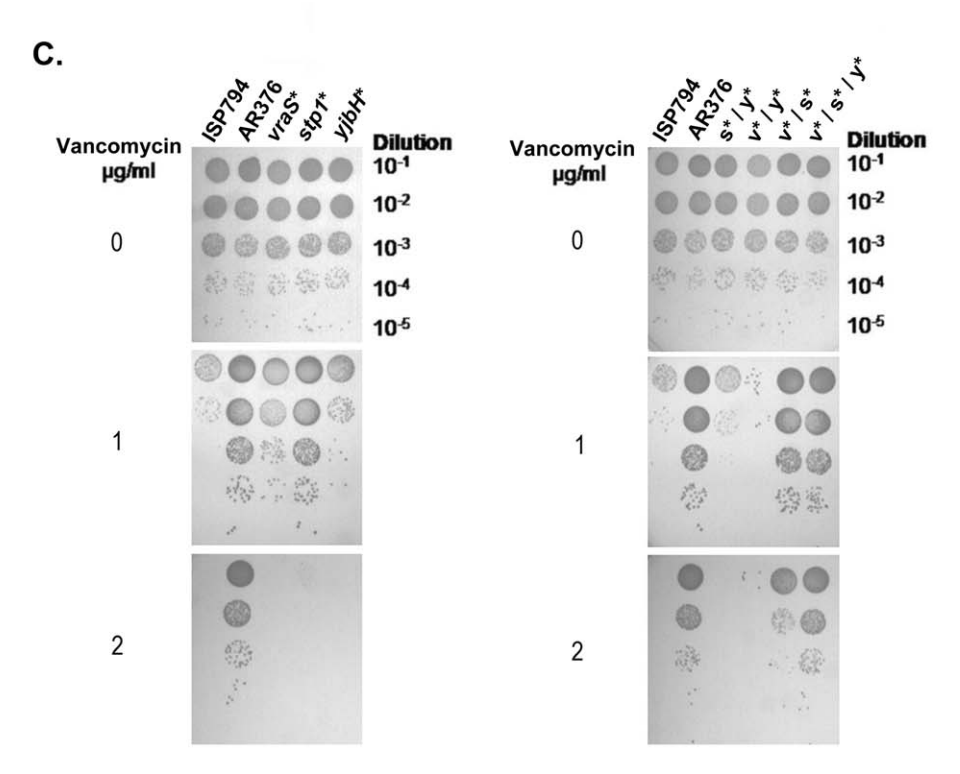
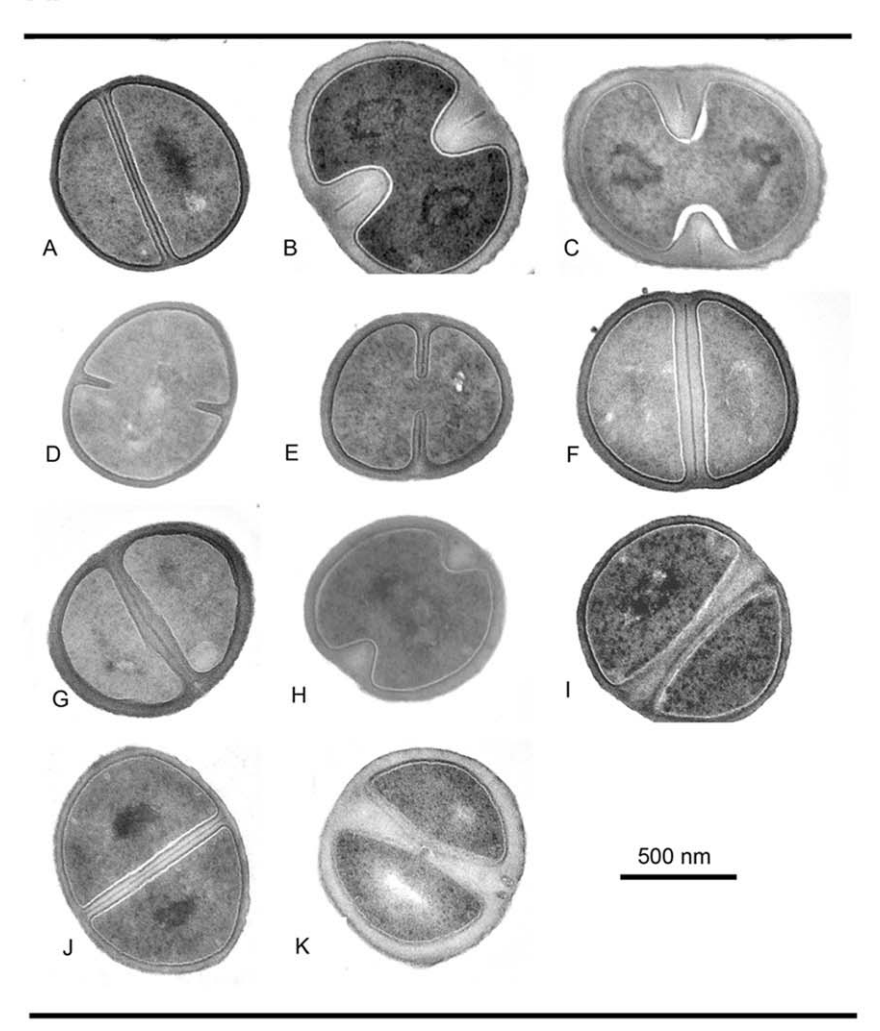


Figure 2. Stepwise genetic reconstitution of all SNP permutations and analysis of their contribution to glycopeptide resistance. (A and B) Teicoplanin spot plating population analysis (Spot PAP) on teicoplanin of ISP794 and each of its strain derivatives. Spot serial dilutions are indicated at the right margin. The first spot $10 \mu l$ corresponds to 1×10^5 colony forming units (CFU). Results for two independent isolates are shown for each single mutant (solid bar). For convenience, genes are marked with an asterisk such that $vraS^*$, $stp1^*$ and $yjbH^*$ correspond to vraS(G45R), stp1(Q12stop) and yjbH(K23stop) mutations, respectively. (C) Vancomycin spot plating population analysis (Spot PAP) of ISP794 and each of its strain derivatives. Conditions used were as in panels A, B. doi:10.1371/journal.pone.0021577.g002

A.



В.

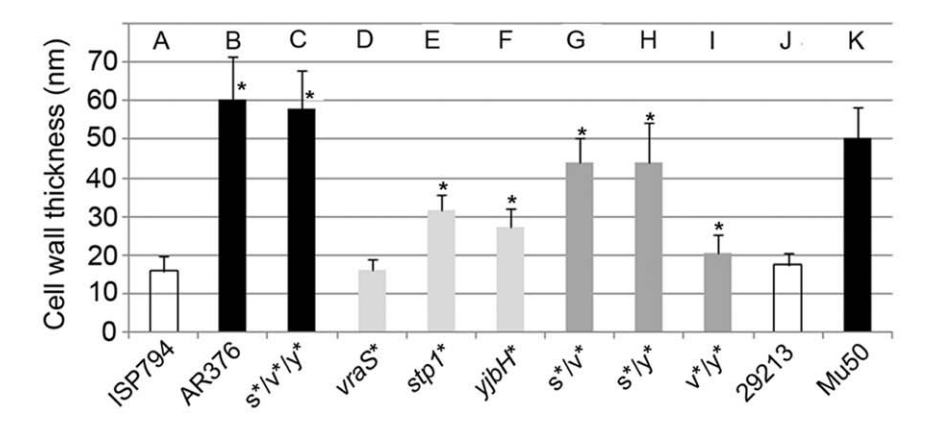


Figure 3. Cell wall thickness analysis. (A) Transmission electron microscopy showing one representative image of each bacterial strain used in this study, after growth in the absence of antibiotic to post-exponential phase on TSB media. Magnification ×37,000. Scale bar automatically inserted by the microscope imaging system is shown. (B) Quantification of cell wall thickness (nm) of each bacterial strain. Reported values correspond to the mean \pm SD (n = at least 40) of each bacterial strain. Asterisk (*) represents results significantly different by student's two-tailed t-test (p < 0.05) from ISP794.

doi:10.1371/journal.pone.0021577.g003

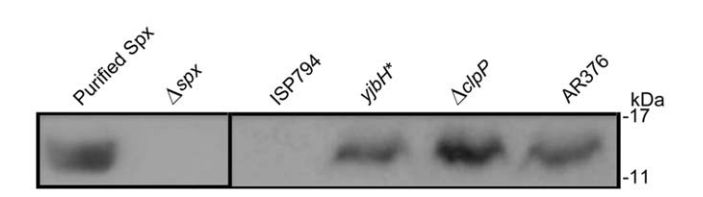


Figure 4. Western blot showing the effect of *yjbH*(K23stop) mutation on Spx protein levels. Total soluble protein extracts (50 μ g) from *S. aureus* strains were loaded per well in an SDS 15% acrylamide gel. Spx protein (15 kDa) was detected using rabbit-polyclonal anti-Spx antibodies. Purified-Spx protein (600 ng) (lane 1), Δ spx strain (lane 2), ISP794 containing wild-type *yjbH* gene (lane 3), *yjbH** correspond to *yjbH*(K23stop) mutant (lane 4), Sa Δ clpP strain (lane 5) and AR376 (lane 6). The position of protein markers are shown in the right margin.

doi:10.1371/journal.pone.0021577.g004

Effect of pre-existing *stp1*(Q12stop), *yjbH*(K23stop), *vraS*(G45R) or *spx* mutations on the emergence teicoplanin resistance in *S. aureus*

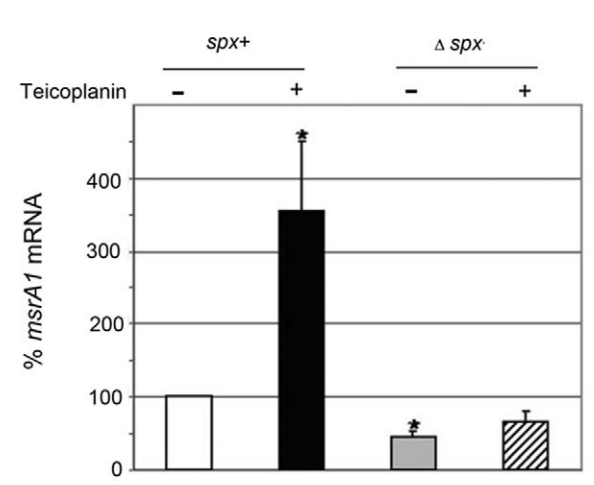
Since AR376 was originally obtained by stepwise cultivation on agar plates containing low levels of teicoplanin we wished to determine the extent to which each individual mutation identified in our study contributed to a change in a detectable frequency of emergence of teicoplanin resistant colonies using our standard assay conditions [21,32]. In light of our findings that disruption of yjbH altered Spx levels, we also tested the effect of spx deletion in the same assay. The results are shown in Table 3.

Compared to ISP794, strains harboring any of the three mutations, stp1(Q12Stop), yjbH(K23Stop) or vraS(G45R) - each backcrossed by bacteriophage mediated transduction into ISP794 and never having been previously exposed to glycopeptides, resulted in strongly enhanced frequency (from 4- to 10-fold) of emergence of low-level teicoplanin resistant colonies on MH agar plates. In contrast, loss of spx was associated with at least a 10-fold reduction in the frequency of emergence of teicoplanin resistant colonies compared to the identical strain background harboring a second wild-type copy of spx. We conclude that loss of spx reduced the emergence of teicoplanin resistant colonies while mutation in any of the three mutations discovered by genomic sequence analysis of AR376 enhanced the emergence of teicoplanin resistance.

Discussion

In the present study, we show by deep sequencing and genetic analysis that a laboratory selected low level teicoplanin intermediate resistant *S. aureus* strain has only three point mutations which distinguished it from its parental susceptible strain. These changes occur in two distinct (histidine kinase and serine/threonine kinase) phospho-signalling systems and in a gene contributing to a global oxidative/thiol stress defence response pathway. Moreover, we present evidence revealing a synergistic interaction between the dual phospho signalling pathways. The contribution of the third mutation in *yjbH* is subtle, and its properties suggest that it most probably exerts its effect following the first step acquisition of low level glycopeptide resistance mediated by the combined effects of *stp/vraS* mutations.

S. aureus glycopeptide resistance has been often correlated with morphological changes such as increased cell wall thickness, peptidoglycan crosslinking or decreased autolysis. Both vraS and stp1 are known to affect cell wall metabolism, although precisely how is unknown [23,24,33,34,35].



A.

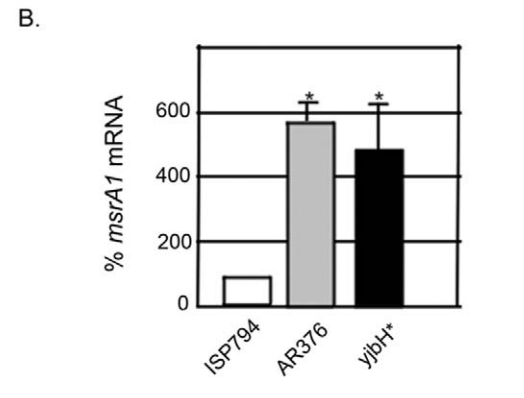


Figure 5. Effect of *spx* **on** *msrA1* **transcription.** (A) Steady-state levels of *msrA1* transcript of wild type strain (spx^{+}) compared to mutant Δspx strain, determined by qRT-PCR. Values represent the mean \pm SEM of four independent experiments performed in triplicate. Data are depicted setting spx^{+} values in the absence of teicoplanin as 100%. Asterisk (*) represents results significantly different by student's two-tailed t-test (p < 0.05) from spx^{+} without teicoplanin. (B) Steady-state levels of msrA1 transcript of ISP794 containing wild-type yjbH gene, AR376 and $yjbH^{*}$ containing both yjbH(K23stop) mutation, determined by qRT-PCR. Values represent the mean \pm SEM of three independent experiments performed in triplicate. Data are depicted setting ISP794 values as 100%. Asterisk (*) represents results significantly different by student's two-tailed t-test (p < 0.05) from ISP794. doi:10.1371/journal.pone.0021577.q005

The VraRS two-component system (TCS) responds to cell-wall active antibiotics [24,33]. Under cell wall stress, expression of *vraRS* and several cell wall biosynthetic genes are strongly upregulated. Disruption of the histidine kinase *vraS* gene blocks this transcriptional response and reduces β-lactam or glycopeptide resistance levels [32,33,36] Missense mutations in *vraS* altering the susceptibility to glycopeptides are commonly observed [17,20,37,38].

How *traS*(G45R) contributes to enhanced glycopeptide resistance is unknown. Amino acid 45 is located in the short region predicted to span two putative transmembrane segments and suggests a role in signal detection. The G45R mutation could also conceivably affect interaction with other regulatory proteins. For example, *B. subtilis* LiaF, a membrane protein, is thought to negatively regulate LiaS, a putative *S. aureus* VraS ortholog. *B. subtilis* LiaF is syngenic to *S. aureus* SA1702, and mutations in SA1702 have also been reported to affect glycopeptide resistance [17,38]. Indeed, a recent report suggests that *S. aureus* SA1702/

Table 3. Effect of the single point mutations and spx on the emergence of teicoplanin resistance.

Strain	Relevant genotype	No. bacteria under non-selective conditions T _o		No. bacteria under selective conditions T ₂		Frequency of emergence ¹	
		Mean (n = 7)	SEM	Mean (n = 7)	SEM	T ₂ /T ₀	%
ISP794	ISP794, rsbU ⁻	7.82×10 ⁺⁷	2.01×10 ⁺⁷	255	79	3.26×10 ⁻⁶	100 ³
AR1079	ISP794, <i>yjbH(K23stop)</i> ery ^r nearby	6.98×10 ⁺⁷	1.95×10 ⁺⁷	895	201	1.28×10 ⁻⁵	394
AR774	ISP794, vraS(G45R) kan ^r nearby	1.25×10 ⁺⁷	2.24×10 ⁺⁶	>1000 ²		8.00×10 ⁻⁵	>1000
AR826	ISP794, stp1(Q12stop) kan ^r nearby	2.80×10 ⁺⁷	5.73×10 ⁺⁶	>1000 ²		3.50×10 ⁻⁵	>1000
		Mean (n = 5)	SEM	Mean (n = 5)	SEM		
spx+	8325-4 Δ spx, P_{spx} -spx::geh	1.59×10 ⁺⁸	1.61×10 ⁺⁷	>1000 ²		>6.00×10 ⁻⁶	100 ⁴
Δspx	8325-4∆ <i>spx</i>	1.05×10 ⁺⁸	1.39×10 ⁺⁷	49	12	4.70×10 ⁻⁷	<10

¹Frequency of emergence expressed as the ratio of colony forming units (CFU) under selective (Teicoplanin 2 µg/ml) and non-selective conditions (No teicoplanin). Colony forming units were counted at 48 h. 37°C

YvqF and VraS directly interact lending support to the notion that SA1702/YvqF may modulate VraS signalling and detection of cell wall stress [39]

The vraS(G45R) mutation does not detectably increase VraR operon mRNA levels compared to its isogenic parent strain, or any gene (sgtB, prsA, htrA1, murZ) thought to be regulated by VraR that we tested by qRT-PCR and our experimental conditions. Nevertheless, this mutation by itself does result in pronounced changes in emergence of glycopeptide resistance frequencies. This result is curious, since in most reported cases, glycopeptide resistant bacteria show increased expression of vraR operon transcription compared to susceptible parental strains [24,37,40]. Nevertheless, one report, consistent with our findings, showed that increased transcription of vraS or vraRS operon is not essential for acquisition of low-level glycopeptide resistance [41]. A closer study of vraR operon regulation and VraR phosphorylation mechanisms is warranted to resolve precisely how VraS missense mutations disrupt signalling.

In S. aureus, Stp1 plays a role in phospho-signalling, together with Stk1 [23,34,35,42,43]. Stp1 (N315-SA1062), encodes a manganese-dependent serine/threonine phosphatase, capable of dephosphorylating Stk1 [23,34]. Stk1 is thought to be a membrane protein which possesses three extracellular PASTA domains (penicillin-binding protein and serine/threonine kinase associated domain) [44]. Stk1 or Stp1 have been shown to have a role in S. aureus virulence, cell wall metabolism and antibiotic resistance (for review see [25]). The effects of a single stp1 mutant, however, have not been tested for glycopeptide resistance [23,34,35,42,43]. To our knowledge, our work is the first study to report mutation in stp1 alone directly affecting glycopeptide resistance levels.

It is not known how stk1/stp1-mediated signalling contributes to the detection of antibiotic encounter and orchestration of cellular responses. One plausible hypothesis is that Stk1 senses some feature(s) of the cell wall assembly process via its PASTA domains and phosphorylates multiple downstream factors that coordinate proper assembly and quality control [44]. In the event of encounter with cell wall active drugs such as glycopeptides, Stk1 could conceivably signal damage and initiate a cascade of signalling events that permit survival in the face of drug stress. The loss of function of stp1 would have the predictable consequence of enhancing the duration of substrates phosphorylated by Stk1. Stk1 and Stp1 are only beginning to be understood in S. aureus, however. To date, several Stp1 client substrates have been described including the global accessory regulator SarA, MgrA, and the nucleoid organizing protein HU [43,45]. MgrA is known to be a major cell-wall autolytic regulator which modulates antibiotic resistance, including glycopeptides [45], providing a possible mechanistic link between signal systems and altered cell wall assembly.

Changes in cell wall thickening resulting from stp1 disruption appear to be strain dependent and divergent results have been reported for strains Newman and N315, for example [23,34,43]. The reason for these discrepancies is unknown and additional studies will be needed to resolve this important issue. The stp1(Q12stop) mutation present in our strain background nearly doubled cell wall thickness compared to ISP794. A recent metabolome study using 8325, a strain closely related to ISP794, detected striking coordinate increases in peptidoglycan intermediates depending upon the sequential action of MurA to MurF enzymes in a strain lacking stp1 compared to its isogenic parent [46]. These results strongly suggest that stk1/stp are indeed intimately involved in the regulation of cell wall biosynthesis.

A striking feature of our study is the enhanced glycopeptide resistance of the double stp1(Q12stop)/vraS(G45R) mutation compared to the resistance levels of the single mutants alone. This observation suggests the intriguing possibility that these signalling systems collaborate to modulate genes necessary to elicit drug resistance. Understanding the molecular mechanism of endogenous glycopeptide resistance arising from this dual signalling synergy is being vigorous pursued.

The yjbH(K23stop) mutation displays both positive and negative effects upon glycopeptide resistance. By itself, the yjbH(K23stop) mutation displays little contribution to glycopeptide resistance, whereas when combined as a double mutant with either the vraS(G45R) or stp1 null mutation, yjbH(K23stop) mutation reduces resistance. These findings suggest that mutation of yjbH exerts a negative influence on endogenous glycopeptide resistance achieved with either phosphosignalling pathway mutant alone. In contrast, when yjbH mutation is combined with the double mutant stp1(Q12stop)/vraS(G45R), a two-fold increase in modal teicoplanin

²Viable counts on agar containing 2 μg/ml of teicoplanin were too high to accurately measure using these conditions. More than 1000 CFU were estimated in each experiment.

 $^{^3}$ The effect of $rsbU^+$ on glycopeptide emergence is discussed in Galbusera et al (30). ISP794 emergence frequency was set equal to 100% for normalization and comparison.

 $^{^4}$ The emergence frequency was set equal to 100% for normalization and comparison with its derivative Δspx . doi:10.1371/journal.pone.0021577.t003

MIC was observed (4 to 8 μ g/ml) and was accompanied by increased colony counts indistinguishable from the parental triple mutant sequenced strain AR376. In this instance, yjbH clearly acts positively. The negative effects due to yjbH(K23stop) were also observed with vancomycin although its positive contribution to reduced susceptibility to this drug was less apparent in both spot PAP assays and modal MIC values. Future research will resolve in detail how YjbH and Spx contribute to glycopeptide resistance.

The drug resistance profiles of the three mutations detected in our study suggest that their temporal appearance was hierarchical. If either signalling mutation had occurred first, followed by yjbH, then the results we provide upon genetic reconstruction suggest little or no possibility for growth of the yjbH(K23stop)/stp1 or yjbH(K23stop)/vraS(G45R) mutation on teicoplain 2 µg/ml and thus little chance for continued selection. In contrast, it is reasonable to assume that the dual signalling mutants emerged first, followed by the acquisition of the yjbH mutation. This genetic order has the effect of pushing the teicoplanin MIC from 4 µg/ml to 8 µg/ml. It is thus tempting to speculate that the effect of yjbH, either by itself, or more likely through Spx, is manifest only when a threshold pre-existing level of glycopeptide resistance is attained.

We have shown that loss of yjbH leads to stabilization of Spx protein levels and provide evidence that Spx modulates the expression of at least two genes (msrA1 and trfA) involved in glycopeptide resistance. Spx is necessary for the upregulation of msrA1, encoding methionine sulfoxide reductase, an enzyme required to combat oxidative stress. msrA1 (SA1257) is transcribed as a four-gene operon (SA1254-SA1257) and induced by several cell wall active antibiotics [24,29,30,33]. In addition, activating oxidative stress defences is a plausible strategy to combat antibiotic stress since recent studies reveal that several antibiotics, including glycopeptides, kill cells by promoting the production of endogenous reactive oxygen species [28,47,48].

Teicoplanin resistance factor A, encoded by *trfA*, is also regulated by YjbH and Spx (A. Renzoni, manuscript in preparation). TrfA is important for glycopeptide resistance in several strain backgrounds including AR376 used in this and other studies, although its precise function has yet to be established [21]. Studies are underway to dissect which precise pathways are affected by the *trfA* mutation.

The three mutations uncovered in our study each contribute to enhanced cell wall thickness, although vraS(G45R) evokes only minimal change by itself and acts in conjunction with either of the other mutations. These findings could partly explain the reduced glycopeptide sensitivites observed in some, but not all of our strains, since in many instances no change in glycopeptide MICs were detected despite strong changes in cell wall thickness. To date, the majority of clinical glycopeptide resistant strains exhibit cell wall thickening [3,11]; however, reduced susceptibility to glycopeptides can be achieved without alterations in cell wall thickness [49,50]. Other metabolic changes must be affected by the mutations uncovered in our study which modulate low level glycopeptide resistance. While herein we present a detailed analysis suggesting an intricate interplay among signalling pathways in one particular strain, it is certainly possible that additional genes and pathways contributing to the acquisition of endogeneous glycopeptides resistance will be uncovered.

Materials and Methods

Bacterial strains and culture conditions

Bacterial strains used in this study are listed in Table 1. The NCTC8325 strain ISP794 (MIC = 1 μ g/ml) and its teicoplanin-derivative AR376 (MIC = 8 μ g/ml) are MLST type ST8 (3-3-1-14-4-3) and were described previously [21]. All *S. aureus* and *E. coli*

strains were grown in Mueller-Hinton broth (MHB) and Luria-Bertani medium, respectively. When required, media were supplemented with the following antibiotics: 15 $\mu g/ml$ chloramphenicol, 5 $\mu g/ml$ erythromycin, 40 $\mu g/ml$ kanamycin, and 3 $\mu g/ml$ tetracycline.

Genome sequencing

Genomic DNA (gDNA) was prepared from an overnight culture grown in MHB at 37°C as previously described [21]. Solexa technology was used to sequence the genomic DNA of both ISP794 and AR376 strains on an Illumina Genome Analyzer GAII (Illumina; Fasteris, SA, Geneva, Switzerland). The quality-controlled filtered reads, followed by alignment to the reference sequence NCTC8325 strain, were used to generate a consensus sequence for both ISP794 and AR376 strains, using the IUPAC ambiguity code. The generated consensus ISP794 and AR376 sequences were then compared to detect SNPs and InDel differences. All detected SNPs and InDels were subsequently verified or rejected by PCR of relevant genomic DNA and capillary sequencing. Additional details are available upon request.

Construction and analysis of genetic point mutants

To test the contribution of each individual mutation to glycopeptide resistance, or reconstruct all possible combinations, we used genetic linkage analysis by conveniently tagging each mutation with a nearby resistance marker (Figure 1B), using pBT2 thermosensitive plasmid [21]. All plasmids were first electroporated into non-restricting strain RN4220 prior to electroporation into ISP794 and its derivative strains. After growth with applied marker selection at a non-permissive temperature for pBT2 replication, double cross-over events were screened using antibiotic markers and all linked mutants were confirmed by PCR and sequencing. We also verified in every case that the insertion of the antibiotic-resistant marker alone did not alter the susceptibility phenotype to either teicoplanin or vancomycin. The intergenic regions chosen were devoid of known small regulatory RNAs. While we cannot exclude that the markers used confer some changes to the cell which we do not detect, they are importantly neutral with respect to all assays used in this study to measure glycopeptide susceptibility. All antibiotic-linked SNP mutations were subsequently backcrossed to ISP794 using bacteriophage Φ80α-mediated generalized transduction. In some cases, allelic exchange using nearby markers linked to the wild type locus were used to remove one or several point mutations and restoration of wild type sequence. Non-cell wall active antibiotic selectable markers kanamycin, tetracycline, and erythromycin were obtained as previously described [21,32]. Details of the construction of each single, pairwise, or reconstituted triple mutation are indicated below. In no case did we observe that single, double mutants, or the reconstructed triple mutant displayed altered growth rates or detectable fitness changes compared to ISP794.

Generation of point mutant vraS(G45R) in ISP794

VraS(G45R) point mutation linked to a kanamycin-resistant marker was constructed in ISP794 as follows: a chromosomal fragment containing a nucleotide change in position 133 (C to T) of vraS open-reading frame (ORF) to generate an amino acid change from glycine to arginine, was amplified from ISP794 using primers described in Table S1. A restriction site (Bgl2) was used to ligate a kanamycin resistance marker at position 1972957 (NCTC 8325 genome sequence coordinates).

The resulting plasmid, pAR749, was electroporated into vraS::ermB mutant (described in [32] selecting for kanamycin resistance. Double cross-over events were screened on agar

containing 40 µg/ml kanamycin and then replica streaked on 15 μg/ml chloramphenicol and 5 μg/ml erythromycin plates to screen for chloramphenicol and erythromycin-sensitive but kanamycin-resistant colonies. Clone AR774a was selected and used to backcross vraS(G45R) linked to kanamycin resistant marker to ISP794 using Φ80α lysates. A single mutant vraS(G45R) clone, AR774, was retained for further study.

Generation of stp1(Q12stop) and yjbH(K23stop) single mutants in ISP794

A similar strategy was used to generate stp1(Q12stop) mutant in ISP794 strain. We first pre-marked strain AR376 by targeted insertion of a kanamycin resistance marker nearby the stp1 gene (chromosomal locations 1142731 and 1142744 from NCTC 8325 genome sequence coordinates), using primer pairs described in Table S1. A restriction site (Bgl2) was used to insert a kanamycin resistant marker as described above. The resulting plasmid, pAR784, was electroporated into AR376, selecting with 40 µg/ ml kanamycin and then replica streaked on 15 µg/ml chloramphenicol plates to screen for chloramphenicol-sensitive but kanamycin-resistant colonies. Clone AR802 was chosen and used to backcross the stp1(O12stop) linked to kanamycin resistant marker to ISP794 using bacteriophage generalized transduction with $\Phi 80\alpha$ lysates. A single mutant stp1(Q12stop) AR826 was retained for further study.

To generate the yibH(K23stop) mutant, strain AR376 was premarked by targeted insertion of an erythromycin resistance gene nearby yjbH gene in position 905525 (NCTC 8325 genome sequence coordinates) using plasmid pAR1063 generated with primers described in Table S1. One colony was selected and designated AR1077. Transfer of yjbH(K23stop) mutation into ISP794 strain was next performed by bacteriophage transduction using Φ80α lysates of AR1077 selecting for erythromycinresistance marker. A single mutant yjbH(K23stop), AR1079, was fully verified by PCR and sequence analysis and retained for further study.

Generation of pairwise and triple mutants

The double mutant vraS(G45R)-stp1(Q12stop) was constructed as follows: we first pre-marked strain AR376 nearby stp1 gene (AR853) using plasmid pAR787 as described above, but instead inserting a tetracycline resistance marker at the same chromosomal location as we had inserted the kanamycin marker. Transfer of the stp1(Q12stop) mutation to vraS(G45R) mutant (AR774) was next performed by bacteriophage transduction using $\Phi 80\alpha$ lysates of AR853 selecting for the tetracycline-resistance marker. The selected kanamycin and tetracycline-resistant transductant (AR858) was analysed for acquisition of both vraS(G45R) and stp1(Q12stop) mutations by sequencing. The double mutant vraS(G45R)-yjbH(K23stop) was constructed as follows: we premarked strain ISP794 nearby stp1 gene (AR860) using plasmid pAR784 as described above, but instead inserting a kanamycin resistance marker. Transfer of the *stp1* wild-type gene to AR376 was next performed by bacteriophage transduction using $\Phi 80\alpha$ lysates of AR860 selecting for the kanamycin-resistance marker. The selected kanamycin-resistant transductant (AR864) was analysed for acquisition of wild-type *stp1* gene by allelic exchange and the presence of both vraS(G45R) and yjbH(K23stop) mutations by sequencing. To construct the double mutant stp1(Q12stop)yjbH(K23stop), we pre-marked strain ISP794 with a kanamycin resistance marker nearby wild-type vraS gene (AR758) using plasmid pAR712 as previously described [32]. Transfer of wildtype vraS gene to AR376 was next performed by bacteriophage transduction using Φ80α lysates of AR758 selecting for the kanamycin-resistance marker. The selected kanamycin-resistant transductant (AR854) was analysed for acquisition of wild-type vraS gene and the presence of both stp1(Q12stop) and yjbH(K23stop) mutations by sequencing.

Finally, to reconstruct the vraS(G45R)-stp1(Q12stop)-yjbH(K23stop) triple mutant, we transferred the yjbH(K23stop) mutation from AR376 by bacteriophage transduction using $\Phi 80\alpha$ lysates of AR1077 to the double mutant vraS(G45R)-stp1(K23stop) (AR858) selecting for the erythromycin-resistance marker. The selected erythromycin, kanamycin and tetracycline-resistant transductant (AR1082) was analysed for acquisition of vraS(G45R), stp1(Q12stop) and yjbH(K23stop) mutations by sequencing.

Plasmids for complementation

Plasmid pMK4 was used to express the entire wild-type vraR operon under control of its own promoter and stp1 or γjbH under the control of the heterologous p_{HU} or p_{GlvS} promoters (Table 1). Briefly, pMK4 plasmid containing Notl-Kpn p_{GlyS} or p_{HU} promoters were obtained as described [51,52]. PCR fragments containing vraR operon, or promoterless stp1 or yjbH were cloned into Kpn-Pst1 restriction sites using primers described in Table S1. All constructions were sequenced verified. Plasmids constructed in E. coli were first introduced into strain RN4220 prior to transformation of the corresponding mutant strains. Plasmids for negative controls in these experiments were either empty pMK4, or pMK4 harboring a heterologous gene, namely GFPuv4, driven by the same p_{HU} or p_{GlvS} promoters.

Minimal inhibitory concentration (MIC) and population analysis

Broth macrodilution MIC assays were performed in triplicate as previously described according to CLSI (Clinical and Laboratory Standards Institute) standard procedures [21]. Results were reported as the modal MIC values. The spot PAP method was used to assess population analysis, as previously described [21,32]. Bacterial cultures were adjusted to 0.5 MacFarland standard $(1.5 \times 10^8 \text{ bacteria/ml})$, corresponding to an $OD_{600} = 0.1$. Serial \log_{10} dilutions (resulting in a range 10^{-1} to 10^{-5}) were prepared, then aliquots of each dilution (10 µl) were spotted on freshly prepared MH agar (MHA) containing different concentrations of teicoplanin or vancomycin. Viable colonies were examined after 48 h at 37°C. The results reported were consistant across at least five independent assays. It is important to emphasize that the MIC values reported throughout our studies were determined using broth macrodilution; this method may give higher values than other susceptibility testing methods. Indeed, a recent study conducted in our laboratory indicates that microdilution methods tend to underestimate glycopeptide resistance [53].

Purification of recombinant Spx protein and antibody production

The open reading frame of the spx gene (SA0856 N315) was PCR amplified with primers indicated in Table S1 and cloned in pBluescriptII KS+. A sequenced verified spx fragment was next subcloned into E. coli expression vector pTYB12 (New England Biolabs) using Nde1-Pst1 sites, generating plasmid pAM1101. Nterminal intein-recombinant Spx protein was then purified using chitin affinity column (IMPACT system, New England Biolabs) as follows: E. coli strain ER2566 (New England Biolabs) containing pTYB12-Spx protein was grown in Luria-Bertani media containing carbenicillin at 100 μ g/ml until an OD_{600} of 0.7, induced with 0.4 mM isopropyl-β-D-1-thiogalactopyranoside (IPTG) for an additional 2 h30 min at 22°C with vigorous shaking. Bacteria

were harvested by low speed centrifugation, resuspended in buffer containing 0.1% Tween 20, followed by affinity chromatography and intein-mediated proteolytic cleavage of the affinity tag with 50 mM DTT. Recombiant Spx protein was eluted with 20 mM Tris-HCl pH 7.5, 500 mM NaCl and 1 mM EDTA, according to the manufacturer's recommendations. Thiol-induced intein cleavage resulted in the N-terminal attachment of three additional amino acids AlaGlyHis. Protein concentrations were determined using Bradford reagent (BioRad) and a bovine serum albumin standard. Recombinant Spx protein was stored at 4°C and used to generate polyclonal antibodies using the Rabbit ExpressTM extended protocol (Pickcell Laboratories, Netherlands).

Western blot analysis

Total protein extracts were obtained as follows: 10 ml of an overnight culture of S. aureus strains in MHB were harvested. After centrifugation, cell pellets were washed and resuspended in 500 uL TES (10 mM Tris pH 7.5, 1 mM EDTA and 0.1% SDS). Bacterial cells were disrupted by adding 500 µl of acid washed glass beads (100-200 micron, Sigma) and using FastPrep cell disrupter (MP Biomedicals). The cell debris were separated from soluble protein extracts by centrifugation for 10 min at 4°C at 17000 rpm (JA-20 rotor Beckman) followed by a second centrifugation step to remove additional insoluble and aggregated proteins (30 min, 4°C, 17000 rpm). Supernatant was removed and proteins were concentrated on Amicon spin columns (4 kDa cutoff, Milian, Geneva, Switzerland). Protein concentrations were determined by Bradford assay (Bio-Rad). Aliquots of total proteins $(50 \mu g)$ were loaded on 15% SDS-PAGE gels and blot transferred onto a polyvinylidene difluoride membranes (PVDF, Bio-Rad). After blocking using 5% (w/v) low fat milk in phosphate buffered saline, membranes were probed with a 1:1500 dilution of Spx antibody followed by incubation with a secondary HRPconjugated goat anti-rabbit antibody (1:10,000 BioRad). Chemiluminescence was detected using the Western Pico Super Signal reagent (Pierce).

Assays for emergence of teicoplanin resistance

Emergence of glycopeptide resistance was performed as previously described [21,32]. Overnight bacterial cultures were adjusted to McFarland 2.0 in 0.9% NaCl and ca. 3×10^8 CFU/ ml were plated on Muller Hinton agar (BD BBL 211438) containing the indicated freshly prepared teicoplanin concentration and incubated for 48 h at 37°C. To determine the frequency of emergence, serial dilutions of each culture were also plated on MHB plates without drug. Results are expressed as the mean ± SEM of seven independent experiments for ISP794, AR774, AR826, AR1079 and five independent experiments for spx+ and Δspx . A subset of colonies was retested by replica plating on selective agar plates to estimate the percentage of false positives (persisters cells which score as susceptible upon replating on selective medium) arising in each experiment. False positive rate of CFUs detected in the emergence assay were found to be 5-20% depending upon the experiment. The raw data are reported without correction and thus calculated emergence frequencies represent an upper limit. ISP794 used in this study is defective in rsbU. The effects of this mutation, its restoration, and the role of sigB in the emergence of teicoplanin resistance in this strain background have been thoroughly addressed in our previous study [32].

Total RNA extraction

Overnight cultures of 8325-4spx-c and $8325-4\Delta spx$ were diluted and grown at 37°C for 4 h in MHB without shaking. When

indicated, sub-inhibitory concentrations of teicoplanin (0.5 $\mu g/ml)$ were added and incubated for an additional hour. Bacteria were harvested and RNA extraction was performed as previously described [21]. The absence of contaminating DNA was verified by PCR using qRT-PCR probes in the absence of reverse transcription.

Quantitative real-time qRT-PCR

mRNA levels were determined by quantitative RT-PCR (qRT-PCR) using the one-step reverse transcriptase qPCR Master Mix Kit (Eurogentec, Seraing, Belgium) as described [54]. Primers and probes were designed using PrimerExpress software (version 1.5; Applied Biosystems), and obtained from Eurogentec. *MsrA1* primers (from SA1257) and probe are: *msrA1*-334F 5′GGAAG-TAACCTCTGGATCAAACGT, *MsrA*1-415R 5′CCCTACT-TATGAACAGGTATGTACGAAT and *msrA1*-359T 5′ATTTG-TACTGCTTCGACATGGCCGGTT. 16S primers and probe are described [54]. Reverse transcription and PCR were performed using primers and probes at a concentration of 0.2 and 0.1 μM, respectively. The *msrA1* mRNA levels were normalized on the basis of their 16S rRNA levels, which were assayed in each round of qRT-PCR as internal controls as described [54].

Transmission electron microscopy

S. aureus strains were grown on TSB at 37°C under shaking conditions until post-exponential phase. One milliter of postexponential phase bacteria was pelleted by low speed centrifugation, washed with PBS and fixed for 30 min in PBS containing 4% (v/v) glutaraldehyde. Fixed cells were further treated with 2% osmium tetroxide in buffer and immersed in a solution of 0,25% uranyl acetate to enhance membrane contrast. The pellets were dehydrated in increasing concentrations of ethanol followed by pure propylene oxide, then embedded in Epon resin. Thin sections for electron microscopy were stained with uranyl acetate and lead citrate and observed in a Technai 20 electron microscope (FEI Company, Eindhoven, The Netherlands). Digital images were captured at 37,000×. Cell wall thickness was determined using equatorial sections and four independent measurements for each image from random placement of a cardinal point grid. The reported values represent the mean of at least 40 independent images for each strain.

Supporting Information

Figure S1 Complementation of either yjbH(K23stop), stp1(Q12stop) or vraS(G45R) mutants by multicopy plasmid carrying wild-type genes. (A) Spot plating population analysis of each single mutant and its corresponding complemented strain on teicoplanin. V* and s* complementation was tested on teicoplanin containing 0.5 μg/ml. Spot serial dilutions are indicated at the right margin. As yibH(23stop) mutation has a subtle effect on teicoplanin resistance, complementation of the yjbH mutation was performed by introducing a multicopy plasmid carrying wild-type yjbH gene into the triple strain mutant, a condition where its role could be unambiguously assessed. Y* complementation was tested on teicoplanin containing 2 µg/ml. For convenience genes marked with an asterisk such as v*, s* and y* correspond to vraS(G45R), stp1(Q12stop) or yjbH(K23stop) mutations, respectively. (TIF)

Table S1 Primers used in this study. (DOC)



Acknowledgments

We thank Dorte Frees and Hanne Ingmer (Royal Veterinary and Agricultural University, Denmark) for kindly supplying *S. aureus spx* and *clp* mutant strains, Laurent Farinelli, Loic Baerlocher and the bioinformatic staff of Fasteris S.A. (Geneva) for their attention to our custom sequencing needs, and Michelangelo Foti and the staff of the University of Geneva Medical School ultrastructure core facility.

References

- DeLeo FR, Chambers HF (2009) Reemergence of antibiotic-resistant Staphylococcus aureus in the genomics era. J Clin Invest 119: 2464–2474.
- Maclayton DO, Hall RG, 2nd (2007) Pharmacologic treatment options for nosocomial pneumonia involving methicillin-resistant Staphylococcus aureus. Ann Pharmacother 41: 235–244.
- Howden BP, Davies JK, Johnson PD, Stinear TP, Grayson ML (2010) Reduced vancomycin susceptibility in Staphylococcus aureus, including vancomycinintermediate and heterogeneous vancomycin-intermediate strains: resistance mechanisms, laboratory detection, and clinical implications. Clin Microbiol Rev 23: 99–139.
- Perichon B, Courvalin P (2009) VanA-type vancomycin-resistant Staphylococcus aureus. Antimicrob Agents Chemother 53: 4580–4587.
- Zhu W, Murray PR, Huskins WC, Jernigan JA, McDonald LC, et al. (2010)
 Dissemination of an Enterococcus Inc18-Like van Plasmid, Associated with Vancomycin-Resistant Staphylococcus aureus. Antimicrob Agents Chemother.
- Hiramatsu K (2001) Vancomycin-resistant Staphylococcus aureus: a new model of antibiotic resistance. Lancet Infect Dis 1: 147–155.
- Berger-Bachi B, McCallum N (2006) State of the knowledge of bacterial resistance. Injury 37 Suppl 2: S20–25.
- Tenover FG, Sinner SW, Segal RE, Huang V, Alexandre SS, et al. (2009) Characterisation of a Staphylococcus aureus strain with progressive loss of susceptibility to vancomycin and daptomycin during therapy. Int J Antimicrob Agents 33: 564–568.
- Lodise TP, Graves J, Evans A, Graffunder E, Helmecke M, et al. (2008) Relationship between vancomycin MIC and failure among patients with methicillin-resistant Staphylococcus aureus bacteremia treated with vancomycin. Antimicrob Agents Chemother 52: 3315–3320.
- Tenover FC, Moellering RC, Jr (2007) The rationale for revising the Clinical and Laboratory Standards Institute vancomycin minimal inhibitory concentration interpretive criteria for Staphylococcus aureus. Clin Infect Dis 44: 1208–1215.
- Cui L, Ma X, Sato K, Okuma K, Tenover FC, et al. (2003) Cell wall thickening is a common feature of vancomycin resistance in Staphylococcus aureus. J Clin Microbiol 41: 5–14.
- Cui L, Lian JQ, Neoh HM, Reyes E, Hiramatsu K (2005) DNA microarraybased identification of genes associated with glycopeptide resistance in Staphylococcus aureus. Antimicrob Agents Chemother 49: 3404–3413.
- Howden BP, Johnson PD, Ward PB, Stinear TP, Davies JK (2006) Isolates with low-level vancomycin resistance associated with persistent methicillin-resistant Staphylococcus aureus bacteremia. Antimicrob Agents Chemother 50: 3039–3047.
- Sieradzki K, Tomasz A (2003) Alterations of cell wall structure and metabolism accompany reduced susceptibility to vancomycin in an isogenic series of clinical isolates of Staphylococcus aureus. J Bacteriol 185: 7103–7110.
- Maki H, McCallum N, Bischoff M, Wada A, Berger-Bachi B (2004) tcaA inactivation increases glycopeptide resistance in Staphylococcus aureus. Antimicrob Agents Chemother 48: 1953–1959.
- Neoh HM, Cui L, Yuzawa H, Takeuchi F, Matsuo M, et al. (2008) Mutated response regulator graR is responsible for phenotypic conversion of Staphylococcus aureus from heterogeneous vancomycin-intermediate resistance to vancomycin-intermediate resistance. Antimicrob Agents Chemother 52: 45–53.
- Mwangi MM, Wu SW, Zhou Y, Sieradzki K, de Lencastre H, et al. (2007) Tracking the in vivo evolution of multidrug resistance in Staphylococcus aureus by whole-genome sequencing. Proc Natl Acad Sci U S A 104: 9451–9456.
- Kuroda M, Kuwahara-Arai K, Hiramatsu K (2000) Identification of the up- and down-regulated genes in vancomycin-resistant Staphylococcus aureus strains Mu3 and Mu50 by cDNA differential hybridization method. Biochem Biophys Res Commun 269: 485–490.
- Meehl M, Herbert S, Gotz F, Cheung A (2007) Interaction of the GraRS twocomponent system with the VraFG ABC transporter to support vancomycinintermediate resistance in Staphylococcus aureus. Antimicrob Agents Chemother 51: 2679–2689.
- Cui L, Neoh HM, Shoji M, Hiramatsu K (2009) Contribution of vraSR and graSR point mutations to vancomycin resistance in vancomycin-intermediate Staphylococcus aureus. Antimicrob Agents Chemother 53: 1231–1234.
- Renzoni A, Kelley WL, Barras C, Monod A, Huggler E, et al. (2009) Identification by genomic and genetic analysis of two new genes playing a key role in intermediate glycopeptide resistance in Staphylococcus aureus. Antimicrob Agents Chemother 53: 903–911.

Author Contributions

Conceived and designed the experiments: AR WLK. Performed the experiments: AR DOA AJ CB AM. Analyzed the data: AR WLK PV DL. Wrote the paper: AR WLK.

- Garg SK, Kommineni S, Henslee L, Zhang Y, Zuber P (2009) The YjbH protein of Bacillus subtilis enhances ClpXP-catalyzed proteolysis of Spx. I Bacteriol 191: 1268–1277.
- Beltramini AM, Mukhopadhyay CD, Pancholi V (2009) Modulation of cell wall structure and antimicrobial susceptibility by a Staphylococcus aureus eukaryotelike serine/threonine kinase and phosphatase. Infect Immun 77: 1406–1416.
- Kuroda M, Kuroda H, Oshima T, Takeuchi F, Mori H, et al. (2003) Twocomponent system VraSR positively modulates the regulation of cell-wall biosynthesis pathway in Staphylococcus aureus. Mol Microbiol 49: 807–821.
- 25. Ohlsen K, Donat S (2010) The impact of serine/threonine phosphorylation in Staphylococcus aureus. Int J Med Microbiol 300: 137–141.
- Nakano S, Nakano MM, Zhang Y, Leelakriangsak M, Zuber P (2003) A regulatory protein that interferes with activator-stimulated transcription in bacteria. Proc Natl Acad Sci U S A 100: 4233

 –4238.
- Pamp SJ, Frees D, Engelmann S, Hecker M, Ingmer H (2006) Spx is a global effector impacting stress tolerance and biofilm formation in Staphylococcus aureus. J Bacteriol 188: 4861–4870.
- Kohanski MA, Dwyer DJ, Hayete B, Lawrence CA, Collins JJ (2007) A common mechanism of cellular death induced by bactericidal antibiotics. Cell 130: 797–810.
- Utaida S, Dunman PM, Macapagal D, Murphy E, Projan SJ, et al. (2003) Genome-wide transcriptional profiling of the response of Staphylococcus aureus to cell-wall-active antibiotics reveals a cell-wall-stress stimulon. Microbiology 149: 2719–2732.
- McCallum N, Spehar G, Bischoff M, Berger-Bachi B (2006) Strain dependence of the cell wall-damage induced stimulon in Staphylococcus aureus. Biochim Biophys Acta 1760: 1475–1481.
- You C, Sekowska A, Francetic O, Martin-Verstraete I, Wang Y, et al. (2008)
 Spx mediates oxidative stress regulation of the methionine sulfoxide reductases operon in Bacillus subtilis. BMC Microbiol 8: 128.
- 32. Galbusera E, Renzoni A, Andrey DO, Monod A, Barras C, et al. (2010) Site-specific mutation of Staphylococcus aureus VraS reveals a crucial role for the VraR-VraS sensor in the emergence of glycopeptide resistance. Antimicrob Agents Chemother.
- Gardete S, Wu SW, Gill S, Tomasz A (2006) Role of VraSR in antibiotic resistance and antibiotic-induced stress response in Staphylococcus aureus. Antimicrob Agents Chemother 50: 3424–3434.
- Debarbouille M, Dramsi S, Dussurget O, Nahori MA, Vaganay E, et al. (2009) Characterization of a serine/threonine kinase involved in virulence of Staphylococcus aureus. J Bacteriol 191: 4070–4081.
- Donat S, Streker K, Schirmeister T, Rakette S, Stehle T, et al. (2009)
 Transcriptome and functional analysis of the eukaryotic-type serine/threonine kinase PknB in Staphylococcus aureus. J Bacteriol 191: 4056–4069.
- Yin S, Daum RS, Boyle-Vavra S (2006) VraSR two-component regulatory system and its role in induction of pbp2 and vraSR expression by cell wall antimicrobials in Staphylococcus aureus. Antimicrob Agents Chemother 50: 336–343.
- Katayama Y, Murakami-Kuroda H, Cui L, Hiramatsu K (2009) Selection of heterogeneous vancomycin-intermediate Staphylococcus aureus by imipenem. Antimicrob Agents Chemother 53: 3190–3196.
- Kato Y, Suzuki T, Ida T, Maebashi K (2010) Genetic changes associated with glycopeptide resistance in Staphylococcus aureus: predominance of amino acid substitutions in YvqF/VraSR. J Antimicrob Chemother 65: 37–45.
- McCallum N, Meier PS, Heusser R, Berger-Bachi B (2011) Mutational analyses
 of open reading frames within the vraSR operon and their roles in the cell wall
 stress response of Staphylococcus aureus. Antimicrob Agents Chemother 55:
 1391–1402.
- Renzoni A, Barras C, Francois P, Charbonnier Y, Huggler E, et al. (2006) Transcriptomic and functional analysis of an autolysis-deficient, teicoplaninresistant derivative of methicillin-resistant Staphylococcus aureus. Antimicrob Agents Chemother 50: 3048–3061.
- 41. Howden BP, Smith DJ, Mansell A, Johnson PD, Ward PB, et al. (2008) Different bacterial gene expression patterns and attenuated host immune responses are associated with the evolution of low-level vancomycin resistance during persistent methicillin-resistant Staphylococcus aureus bacteraemia. BMC Microbiol 8: 39.
- Tamber S, Schwartzman J, Cheung AL (2010) Role of PknB kinase in antibiotic resistance and virulence in community-acquired methicillin-resistant Staphylococcus aureus strain USA300. Infect Immun 78: 3637–3646.



- Burnside K, Lembo A, de Los Reyes M, Iliuk A, Binhtran NT, et al. (2010) Regulation of hemolysin expression and virulence of Staphylococcus aureus by a serine/threonine kinase and phosphatase. PLoS One 5: e11071.
- 44. Paracuellos P, Ballandras A, Robert X, Kahn R, Herve M, et al. (2010) The extended conformation of the 2.9-A crystal structure of the three-PASTA domain of a Ser/Thr kinase from the human pathogen Staphylococcus aureus. J Mol Biol 404: 847–858.
- Chen PR, Nishida S, Poor CB, Cheng A, Bae T, et al. (2009) A new oxidative sensing and regulation pathway mediated by the MgrA homologue SarZ in Staphylococcus aureus. Mol Microbiol 71: 198–211.
- Liebeke M, Meyer H, Donat S, Ohlsen K, Lalk M (2010) A metabolomic view of Staphylococcus aureus and its ser/thr kinase and phosphatase deletion mutants: involvement in cell wall biosynthesis. Chem Biol 17: 820–830.
- Kohanski MA, DePristo MA, Collins JJ (2010) Sublethal antibiotic treatment leads to multidrug resistance via radical-induced mutagenesis. Mol Cell 37: 311–320
- 48. Dwyer DJ, Kohanski MA, Collins JJ (2009) Role of reactive oxygen species in antibiotic action and resistance. Curr Opin Microbiol 12: 482–489.
- Boyle-Vavra S, Carey RB, Daum RS (2001) Development of vancomycin and lysostaphin resistance in a methicillin-resistant Staphylococcus aureus isolate. I Antimicrob Chemother 48: 617–625.
- Pfeltz RF, Singh VK, Schmidt JL, Batten MA, Baranyk CS, et al. (2000) Characterization of passage-selected vancomycin-resistant Staphylococcus aureus strains of diverse parental backgrounds. Antimicrob Agents Chemother 44: 294–303.
- Andrey DO, Renzoni A, Monod A, Lew DP, Cheung AL, et al. (2010) Control
 of the Staphylococcus aureus toxic shock tst promoter by the global regulator
 SarA. J Bacteriol 192: 6077–6085.

- Tu Quoc PH, Genevaux P, Pajunen M, Savilahti H, Georgopoulos C, et al. (2007) Isolation and characterization of biofilm formation-defective mutants of Staphylococcus aureus. Infect Immun 75: 1079–1088.
- 53. Vaudaux P, Huggler E, Bernard L, Ferry T, Renzoni A, et al. (2010) Underestimation of vancomycin and teicoplanin MICs by broth microdilution leads to underdetection of glycopeptide-intermediate isolates of Staphylococcus aureus. Antimicrob Agents Chemother 54: 3861–3870.
- Vaudaux P, Francois P, Bisognano C, Kelley WL, Lew DP, et al. (2002) Increased expression of clumping factor and fibronectin-binding proteins by hemB mutants of Staphylococcus aureus expressing small colony variant phenotypes. Infect Immun 70: 5428–5437.
- Kreiswirth BN, Lofdahl S, Betley MJ, O'Reilly M, Schlievert PM, et al. (1983)
 The toxic shock syndrome exotoxin structural gene is not detectably transmitted by a prophage. Nature 305: 709–712.
- Stahl ML, Pattee PA (1983) Confirmation of protoplast fusion-derived linkages in Staphylococcus aureus by transformation with protoplast DNA. J Bacteriol 154: 406–412.
- Frees D, Qazi SN, Hill PJ, Ingmer H (2003) Alternative roles of ClpX and ClpP in Staphylococcuss aureus stress tolerance and virulence. Mol Microbiol 48: 1565–1578.
- Sullivan MA, Yasbin RE, Young FE (1984) New shuttle vectors for Bacillus subtilis and Escherichia coli which allow rapid detection of inserted fragments. Gene 29: 21–26.
- Bruckner R (1997) Gene replacement in Staphylococcus carnosus and Staphylococcus xylosus. FEMS Microbiol Lett 151: 1–8.

2.1.2. Molecular bases determining Daptomycin resistance-mediated resensitization to B-lactams (see-saw effect) in Methicillin-Resistant *Staphylococcus aureus*.

(Antimicrobial Agents and Chemotherapy 61:e01634-16)

Methicillin resistance in *Staphylococcus aureus* (MRSA) results from the acquisition of a modified penicillin-binding protein, named PBP2A, which is unable to bind B-lactam antibiotics. The lipopeptide antibiotic Daptomycin (DAP) is one clinical choice for treatment of these MRSA strains. However, development of resistance to DAP in MRSA strains (DAPR/MRSA) is observed, due to mutations in genes associated with cell-wall changes, such as *mprF* mutation. Interestingly, the emergence of DAP resistance actually makes MRSA strains more sensitive to B-lactams. In fact the combination therapy of DAP with B-lactams such as Oxacillin, Nafcillin, Cefotaxime or Imipenem, result in killing of DAPR/MRSA strains. This seemingly paradoxical effect, where resistance to B-lactam antibiotics decreases while DAP resistance increases in an MRSA strains, is known as the see-saw effect. However, the exact mechanism by which DAP and B-lactams work together to kill these bacteria is unknown. **Through a stepwise analysis of penicillin-binding proteins and proteins involved in membrane metabolism, we have identified here a potential mechanism that explains the effective killing of DAPR/MRSA by DAP and B-lactam combination treatment.**

When DAP treatment is administered alone, it affects DAPS/MRSA strains by inducing changes in cell morphology and causing the delocalization of peptidoglycan insertion. As expected, no such effects are observed when treating DAPR/MRSA strains with DAP alone. Only the combination treatment of DAP and OXA can affect DAPR/MRSA strains. To further understand the effect of DAP/OXA combination treatment on DAPR/MRSA strains, we analyzed cell wall using fluorescence microscopy. Our observations revealed a displacement of penicillin-binding proteins (PBP1 and 2) leading to the delocalization of peptidoglycan insertion. This suggests that changes in PBPs play a role in sensitizing DAPR/MRSA strains to B-lactams.

We observed that upon DAP/OXA treatment, both the transcription and protein production of PBP2A, the key PBP responsible of B-lactam resistance, increase. However, PBP2A protein is unexpectedly highly secreted from cells. This observation suggest a model in which the sensitization of DAP^R strains to B-lactams could be associated with a decrease of cell-membrane PBP2A. This unusual secretion of PBP2A can possibly be explained by changes in lipoprotein modifications

present in DAP^R strains, which are the result of the *mprF* mutation. These changes in lipprotein modifications may have a cascading effect on the location and function of PrsA, a chaperon protein required for the correct PBP2A membrane folding and activity (Figure 4). **Improper membrane folding and activity of PBP2A can explain B-lactam sensitization of DAP^R/MRSA strains** (Renzoni et al. 2017).

In conclusion, the combined DAP/OXA treatment appears to trigger several events on DAP^R/MRSA strains. The upregulation of PBP2A, its unexpected secretion, and the alteration of lipoprotein modifications collectively contribute to the sensitization of these strains to B-lactam antibiotics.

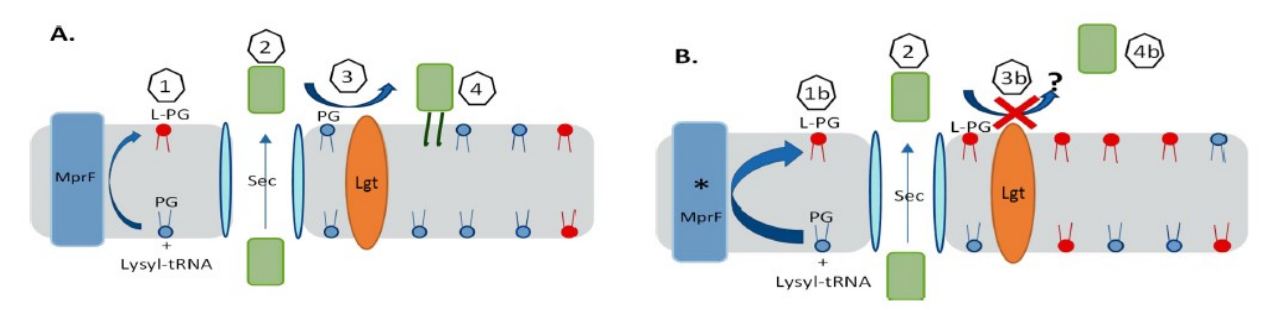


Figure 4. Proposed model of MprF (A) or MprF* (B) to explain PrsA anchorage.

- 1. MprF uses cytosolic lysyl-tRNA to convert phosphatidylglycerol (PG) to lysyl phosphatidylglycerol (L-PG).
- **1b.** The enhanced transferase and/or flippase activity of mutated MprF (*MprF) increases the proportion of L-PG compared to that of phosphatidylglycerol in the outer membrane leaflet.
- 2. Prelipoprotein PrsA (green rectangle) is secreted, which probably occurs through the Sec pathway.
- 3. Phosphatidylglycerol is used by the Lgt enzyme to lipid modify the PrsA lipobox cysteine.
- 3b. No PrsA lipid modification occurs. Indeed, the increased L-PG or decreased PG amounts inhibits Lgt-mediated acyl transfer
- 4. Lipidated membrane-anchored PrsA helps with the posttranslational maturation of PBP2A.
- 4b. No maturation of PBP2A occurs, due to failure of lipidated membrane-anchored PrsA.





Molecular Bases Determining Daptomycin Resistance-Mediated Resensitization to β -Lactams (Seesaw Effect) in Methicillin-Resistant Staphylococcus aureus

Adriana Renzoni, a William L. Kelley, b Roberto R. Rosato, c Maria P. Martinez, c Melanie Roch,^c Maryam Fatouraei,^c Daniel P. Haeusser,^d William Margolin,^d Samuel Fenn, e Robert D. Turner, e Simon J. Foster, e Adriana E. Rosatoc

Hopitaux Universitaires de Genève, Service of Infectious Diseases, Geneva, Switzerlanda; University of Geneva Medical School, Department of Microbiology and Molecular Medicine, Geneva, Switzerland^b; Department of Pathology and Genomic Medicine, Center for Molecular and Translational Human Infectious Diseases Research, Houston Methodist Research Institute, Houston, Texas, USAc; Department of Microbiology and Molecular Genetics, McGovern Medical School, University of Texas, Houston, Texas, USAd; Krebs Institute, University of Sheffield, Sheffield, United Kingdome

ABSTRACT Antimicrobial resistance is recognized as one of the principal threats to public health worldwide, yet the problem is increasing. Infections caused by methicillin-resistant Staphylococcus aureus (MRSA) strains are among the most difficult to treat in clinical settings due to the resistance of MRSA to nearly all available antibiotics. The cyclic anionic lipopeptide antibiotic daptomycin (DAP) is the clinical mainstay of anti-MRSA therapy. The decreased susceptibility to DAP (DAP resistance [DAP^r]) reported in MRSA is frequently accompanied by a paradoxical decrease in β -lactam resistance, a process known as the "seesaw effect." Despite the observed discordance in resistance phenotypes, the combination of DAP and β -lactams has been proven to be clinically effective for the prevention and treatment of infections due to DAPr MRSA strains. However, the mechanisms underlying the interactions between DAP and β -lactams are largely unknown. In the study described here, we studied the role of mprF with DAP-induced mutations in β -lactam sensitization and its involvement in the effective killing by the DAP-oxacillin (OXA) combination. DAP-OXA-mediated effects resulted in cell wall perturbations, including changes in peptidoglycan insertion, penicillin-binding protein 2 (PBP 2) delocalization, and reduced membrane amounts of PBP 2a, despite the increased transcription of mecA through mec regulatory elements. We have found that the VraSR sensor-regulator is a key component of DAP resistance, triggering mutated mprF-mediated cell membrane (CM) modifications that result in impairment of PrsA location and chaperone functions, both of which are essential for PBP 2a maturation, the key determinant of β -lactam resistance. These observations provide for the first time evidence that synergistic effects between DAP and β -lactams involve PrsA posttranscriptional regulation of CM-associated PBP 2a.

KEYWORDS MRSA, daptomycin, seesaw effect, β -lactams, PrsA, β -lactams

taphylococcus aureus has a proclivity for developing multidrug resistance (e.g., methicillin-resistant S. aureus [MRSA]), and infections with this pathogen result in enhanced attributable mortality (1). Since its FDA approval in 2003, the cyclic anionic lipopeptide antibiotic daptomycin (DAP), produced by Streptomyces roseosporus (2), has become the clinical mainstay of anti-MRSA therapy due to its potent staphylocidal

Received 27 July 2016 Returned for modification 1 September 2016 Accepted 12 October 2016

Accepted manuscript posted online 24

Citation Renzoni A, Kelley WL, Rosato RR, Martinez MP, Roch M, Fatouraei M, Haeusser DP, Margolin W, Fenn S, Turner RD, Foster SJ, Rosato AE. 2017. Molecular bases determining daptomycin resistance-mediated resensitization to β-lactams (seesaw effect) in methicillin-resistant Staphylococcus aureus. Antimicrob Agents Chemother 61:e01634-16. https://doi.org/10.1128/AAC.01634-16.

Copyright © 2016 American Society for Microbiology. All Rights Reserved.

Address correspondence to Adriana E. Rosato, aerosato@HoustonMethodist.org.

activity (3). The mechanism of action of DAP involves the disruption of the cytoplasmic membrane (CM) function, leading to its depolarization and causing cell death (4). However, there have been a number of reports in which initially DAP-susceptible (DAPs) MRSA strains developed DAP-resistant (DAPr) phenotypes during clinical treatment failures (5, 6). DAPr strains obtained from patients with therapeutic failure have a number of gene mutations linked with DAP resistance, including mutations in genes associated with the CM (e.g., mprF) and the cell wall (CW) (e.g., the two-component system YycFG), as well as other mutations, such as mutations in RNA polymerase subunits RpoB and RpoC (7). However, the most clinically significant and relevant changes are those associated with mutations in mprF (5, 6). In previous studies, we demonstrated by using sets of isogenic DAPs and DAPr strains that, in addition to mprF, resistance to DAP involves the upregulation of genes involved in CW synthesis and turnover, including the two-component regulator and CW stress stimulon vraSR (6). Together, these observations led us to postulate that both CM and CW components contribute to decreased susceptibility to DAP.

Interestingly, we and others have observed both in vitro (8–10) and in vivo (8, 11, 12) that DAP resistance sensitizes MRSA to β -lactams, notably, oxacillin (OXA), a process known as a "seesaw effect" (8). Indeed, we have demonstrated that combinations of DAP with OXA (in vitro) or nafcillin (NAF) (in vivo), as well as other β -lactams, such as cefotaxime (CTX), which targets penicillin-binding protein 2 (PBP 2), and carbapenems, such as imipenem (IPM), that target PBP 1, displayed strong synergistic interactions resulting in activity against DAP-resistant MRSA isolates (8). Although the DAP- β lactam combination is extensively used in clinical settings for the treatment of MRSA infections associated with decreased susceptibility to DAP (8), the mechanistic bases of the seesaw effect remain to be elucidated.

The PrsA protein is required for resistance to oxacillin as well as glycopeptide antibiotics in S. aureus (13, 14). In Gram-positive bacteria, such as Bacillus subtilis and Listeria monocytogenes, PrsA is a membrane-anchored protein that catalyzes the posttranslocational folding of exported proteins and is essential for their stability as they cross the bacterial cell membrane-cell wall interface (15, 16). In B. subtilis, PrsA is required for the folding of penicillin-binding proteins (PBPs) and lateral cell wall biosynthesis; in the absence of PrsA, four PBPs (PBP 2a, PBP 2b, PBP 3, and PBP 4) become unstable (17). Additionally, in L. monocytogenes, PrsA2 contributes to bacterial pathogenesis and virulence (18). Expression of prsA is induced when it encounters cell wall-active antibiotics, and induction is dependent upon the activity of VraSR, the cell wall stress two-component system (14). Importantly, the same authors reported that cells were more susceptible to oxacillin in the absence of PrsA, suggesting that PrsA may be involved in oxacillin resistance in concert with VraSR, PBP 2, and PBP 2a (14). Recent PrsA structure and function analyses revealed that PrsA modulates PBP 2a protein levels independently of the staphylococcal cassette chromosome mec element (SCCmec) background of the strains (13). Regulation of PBP 2a expression at the transcriptional level involves mecl, mecR, and blaRZ, which may vary in different SCCmec types, but less is known about the posttranscriptional maturation and proper localization of PBP 2a.

In the present study, we demonstrate that DAPr-mediated mprF mutations result in significant changes in cell wall synthesis by influencing the function of PrsA, which correlates with reduced amounts of β -lactam-induced PBP 2a. This work provides evidence that MprF and PrsA are important for the sensitization to β -lactams during DAP resistance in MRSA (the seesaw effect) and contributes new insights into the mechanisms associated with this effect.

RESULTS

Daptomycin-induced cytoplasmic membrane and cell wall changes. Despite considerable evidence pointing to the action of DAP on the CM, the CW has also been suspected to be an important target, as recently shown in B. subtilis (19, 20). We used fluorescence microscopy to visualize the effects of DAP on both CM and CW functions.

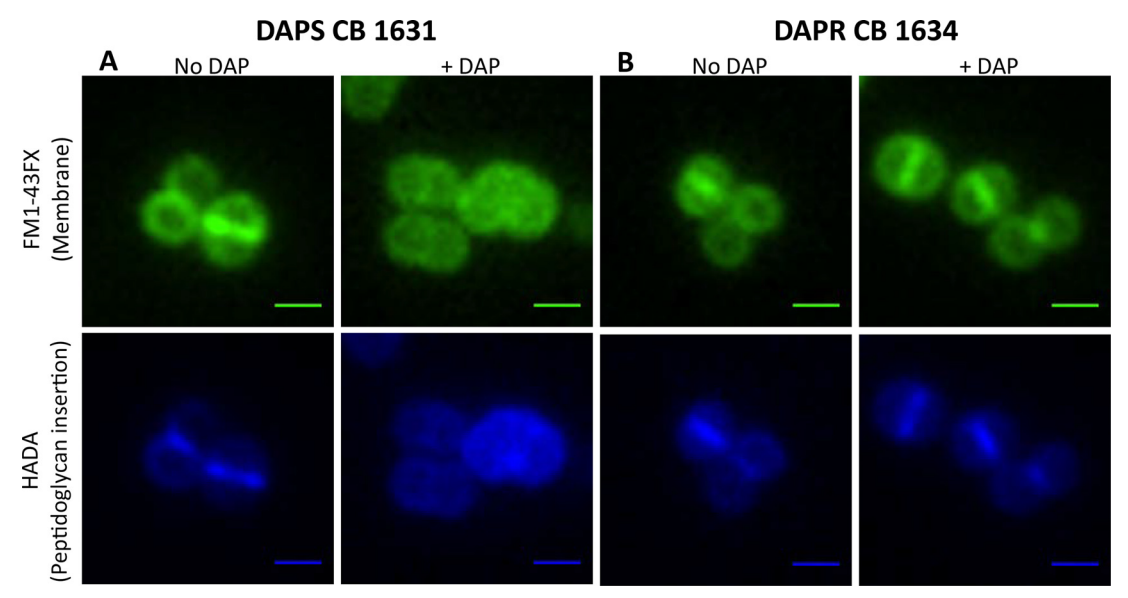


FIG 1 Effects of DAP on the cytoplasmic membrane and cell wall of the DAPs CB1631 (A) or DAPr CB1634 (B) bacterial strain. Bacteria were grown in TSB (with or without DAP) at 37°C to late exponential phase (2.5 h) and labeled for 5 min with FM1-43FX (membrane; top) or HADA (peptidoglycan insertion; bottom). A Nikon inverted epifluorescence microscope was used. Exposure and contrast settings were optimized for each image; i.e., the brightness was not comparable between fields. Scale bars are 1 µm.

When DAPs CB1631 cells were treated with DAP, they displayed significant morphological changes at the CM level (Fig. 1A, FM1-43FX staining, top), including shape abnormalities and size heterogeneity compared with the shapes and sizes of untreated control cells (Fig. 1A, No DAP). All the cells contained DNA, as judged by DAPI (4',6-diamidino-2-phenylindole) staining (not shown), indicating that DAP did not cause significant alterations to the nucleoid.

This observation was corroborated by analysis of the pattern of nascent peptidoglycan insertion using the fluorescent p-amino acid derivative 7-hydroxycoumarin 3-carboxylic acid (HCC)-3-amino-p-alanine (HADA). Exposure of DAPs CB1631 to DAP induced the delocalization of peptidoglycan insertion (Fig. 1A, bottom), suggesting that PBPs were displaced from the division septum, where CW synthesis normally takes place. Importantly, none of the changes described in DAPs CB1631 were observed in the DAPr CB1634 counterpart (Fig. 1B, right). These observations are in agreement with the hypothesis that DAP induces dramatic effects on both the CM and CW in S. aureus.

Effects on cell wall rearrangements during exposure to a combination of DAP and β -lactams. We previously observed that DAP-mediated sensitization to β -lactams occurred with those β -lactams that preferentially target PBP 1 or PBP 2, including NAF (PBP 1, PBP 2), IPM (PBP 1), and CTX (PBP 2), whereas no changes were observed with β-lactams targeting PBP 4, such as cefoxitin (FOX), or PBP 3, such as cefaclor (CEC) (8, 21, 22). Similar effects were observed in other in vitro-selected DAPr mutants obtained from DAPs CB1631 (DAPr CB1631 mutants) and CB5011 (DAPr CB5011 mutants) (8). Collectively, these observations suggest that the seesaw effect involves CW modifications.

To address this in more detail, we stained cells with Bodipy FL-vancomycin (VAN), which has been used extensively to detect the localization of newly synthesized peptidoglycan in Gram-positive bacteria (23, 24). DAPr CB1634 cells were grown without or with the DAP-OXA combination and then stained with Bodipy FL-VAN (10 min) for detection of peptidoglycan by fluorescence microscopy (Fig. 2). In the untreated control, Bodipy FL-VAN intensely stained the complete equatorial cell septa and faintly stained the side walls; in contrast, cells grown in the presence of DAP-OXA showed mostly delocalized Bodipy FL-VAN staining (Fig. 2A). These results are consistent with the delocalized peptidoglycan insertion patterns observed by HADA staining (Fig. 1) and suggest that the coadministration of DAP with β -lactams causes dramatic

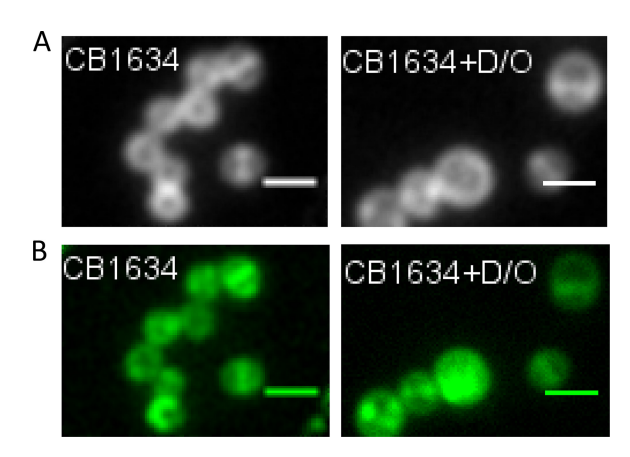


FIG 2 Localization of PBP 2-GFP fusions in DAPr cells treated with OXA, DAP, or DAP-OXA. (A) The DAPr CB1634 strain producing PBP 2-GFP was grown with or without sublethal concentrations of DAP-OXA (D/O; $0.5 \times$ MIC), followed by labeling with Bodipy FL-VAN, fixation, and imaging by fluorescence microscopy. (B) DAPr CB1634 cells producing PBP 2-GFP were induced with IPTG in the presence or absence of DAP, OXA, or the DAP-OXA combination, fixed, and imaged by fluorescence microscopy. Scale bars are 1 μ m.

local effects on the CW in DAP^r cells similar to those observed in DAP^s cells (CB1631), such as displacement of PBPs from the septum. In fact, studies of the labeling of newly synthesized CW with fluorescein-conjugated VAN in *S. aureus* have suggested that most CW synthesis is confined to the division septum, where both PBP 1 and PBP 2 are localized (25).

To investigate further the hypothesis that the combined effects of DAP and β -lactams on the CW contribute to the delocalization of PBPs, particularly PBP 1 and PBP 2, we generated a CB1634 derivative strain expressing an IPTG (isopropyl- β -Dthiogalactopyranoside)-regulated PBP 2-green fluorescent protein (GFP) fusion protein. Analysis of untreated cells of the CB1634 strain expressing PBP 2-GFP showed that the PBP 2-GFP protein clearly localized to the equatorial cell septa (Fig. 2B). In contrast, exposure to the DAP-OXA combination resulted in a diffused and delocalized distribution of PBP 2-GFP, in agreement with the results in Fig. 2A. Similar observations were made by using the same approach with a PBP 1-GFP fusion protein (data not shown). We next wanted to determine the activity of PBPs by measuring their affinity of binding to a fluorescent β -lactam, Bocillin FL. The DAP CB1634 strain was exposed to DAP (1 μ g/ml), OXA (0.5 μ g/ml), and DAP-OXA (1 μ g/ml and 0.5 μ g/ml, respectively), and PBPs, separated by sodium dodecyl sulfate (SDS)-PAGE, were analyzed for their ability to bind Bocillin FL. As shown in Fig. 3, DAPr CB1634 cells treated with DAP-OXA and subsequently labeled with Bocillin FL displayed decreased levels of PBP 1, PBP 2, and PBP 3, whereas no changes were observed with either DAP or OXA alone or both DAP and OXA. However, since we have previously shown that inhibition of PBP 3 by CEC did not result in a seesaw effect when CEC was combined with DAP (8), the present results may indicate that PBP 1 and PBP 2 have a relevant role in the DAP-associated seesaw effect and restoration of susceptibility to β -lactams in DAP^r MRSA strains.

Sensitization to β -lactams during DAP resistance is associated with decreased production of PBP 2a. β -Lactam resistance in MRSA involves the horizontal acquisition of the mecA gene, which encodes PBP 2a, a PBP with a low affinity for β -lactams that can mediate cell wall assembly when the normal staphylococcal PBPs (PBPs 1 to 4) are inactivated by these agents (25). To determine a potential role for PBP 2a in the DAP-mediated seesaw effect observed in the DAPr strains, PBP 2a protein expression levels were analyzed by Western blotting using cell membrane protein extracts prepared from CB1634 cells treated with OXA, DAP, and the DAP-OXA combination. PBP 2a induction was observed in untreated control cells, but no PBP 2a induction was observed after DAP treatment, while, as expected, the levels of PBP 2a increased significantly after exposure to OXA (Fig. 4A). Importantly, in DAP-OXA-treated CB1634

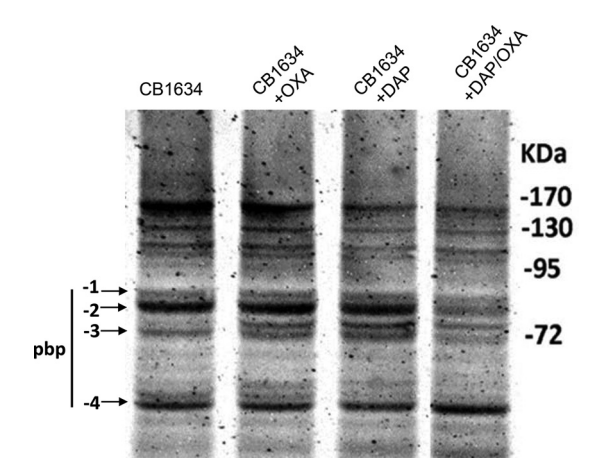
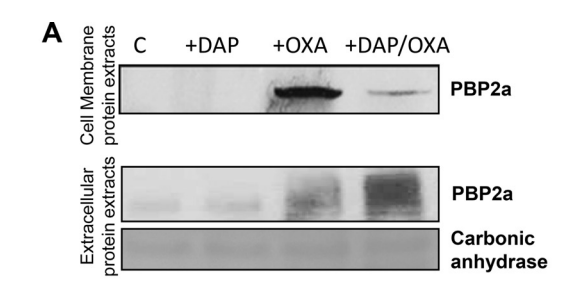


FIG 3 Analysis of PBPs from CB1634 cells treated with OXA, DAP, or DAP-OXA. Membrane preparations obtained from CB1634 cells untreated or treated with OXA (0.5 µg/ml), DAP (1 µg/ml), or DAP-OXA (0.5 μ g/ml and 1 μ g/ml, respectively) were analyzed for the detection of penicillin-binding proteins 1 to 4. Equal amounts (20 µg) of Bocillin FL-labeled membrane proteins were separated by 10% SDS-PAGE. Arrows, fluorescently labeled PBPs.

cells, there was a marked reduction in PBP 2a levels compared to those after OXA induction. Analysis of extracellular extracts normalized to their optical density at 600 nm (OD_{600}) showed increased amounts of extracellular PBP 2a in extracts from the CB1634 strain treated with DAP-OXA, while no extracellular PBP 2a was detected in extracts from the untreated control sample (Fig. 4A). A slight increase in the extracellular amounts of PBP 2a was also observed in extracts from OXA-treated cells, consistent with increasing amounts of cell membrane-associated protein. These results strongly suggest that PBP 2a localization to the CM is altered, which in turn would be associated with the DAPr phenotype-mediated seesaw effect.

To determine whether the reduction of PBP 2a levels observed with the DAP-OXA combination was linked to alterations in mecA transcriptional regulation, we evaluated mecA mRNA levels in the absence and presence of DAP, OXA, and DAP-OXA by real-time reverse transcription-PCR (RT-PCR) analysis. We found that mecA transcription in the CB1634 strain displayed significant induction by OXA alone, an effect that was further enhanced in the case of induction by the combination OXA-DAP (Fig. 4B); a modest induction was also observed upon exposure to DAP. These results do not correlate with the changes in the levels of the CM-associated PBP 2a protein after treatment with the various drug combinations and thus cannot be attributed solely to changes in the level of transcription of the mecA gene. Furthermore, the results strongly suggest that these alterations during the seesaw effect may critically interfere with the normal synthesis/function of the CW.

We next wanted to establish whether DAP-induced mutations in mprF, which are potentially associated with changes in the CM, may play a role in PBP 2a and the changes to the CW observed during the seesaw effect. To address this, we analyzed PBP 2a protein levels using membrane protein extracts from DAP^r CB1634, CB1634 ΔmprF, and CB1634 ΔmprF complemented with either wild-type (WT) mprF or a previously isolated mprF mutant with an L-to-F amino acid change at position 826 (mprFL826F) that is associated with decreased susceptibility to DAP (6). As depicted in Fig. 4C, the cellular levels of membrane-associated PBP 2a were sharply increased by exposure to OXA in all strains compared to the levels in either the corresponding untreated controls or DAP-treated cells. Importantly, the strong reduction of PBP 2a levels in the parental CB1634 strain exposed to DAP-OXA (Fig. 4A) was not observed in the CB1634 $\Delta mprF$ strain, strain MAR17 (Fig. 4C). Interestingly, complementation of MAR17 with WT mprF (strain MAR18) resulted in the same PBP 2a profile detected in MAR17, indicating that there were no differences in the amount of CM-associated protein between OXA- and DAP-OXA-treated cells. However, PBP 2a levels were significantly reduced in CB1634



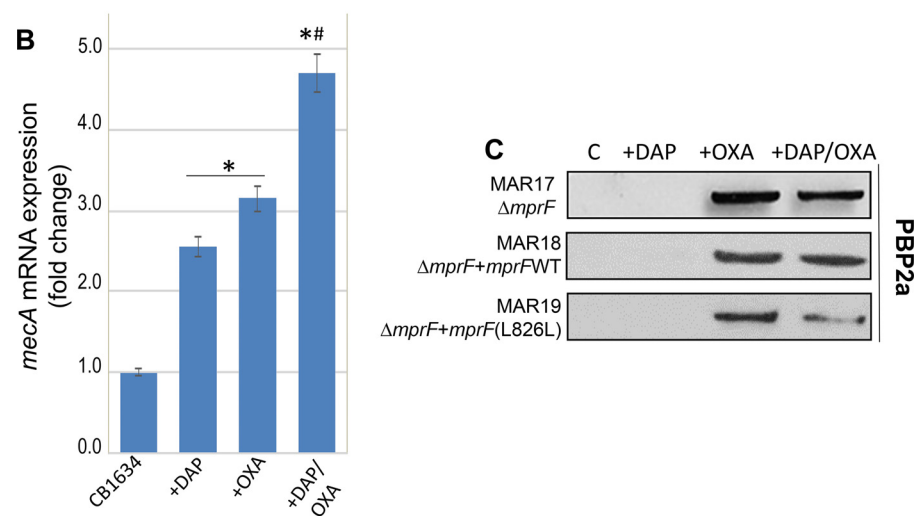


FIG 4 Sensitization to β-lactams during DAP resistance is associated with decreased production of PBP 2a. (A) Western blot analysis of the PBP 2a protein in membrane and extracellular protein extracts from DAPr CB1634 cells grown without (control [C]) or with DAP, OXA, or the DAP-OXA combination. Carbonic anhydrase was used as a loading control. (B) RT-PCR analysis showing *mecA* gene expression in DAPr CB1634 cells grown without or with DAP, OXA, or the DAP-OXA combination. *, the fold change was significantly higher than that for the CB1634 control (no antibiotic) (P < 0.05); #, the fold change was of the PBP 2a protein in membrane protein extracts from CB1643 Δ*mprF* (MAR17), CB1634 Δ*mprF mprF* (WT) (MAR18), and CB1634 Δ*mprF mprFL826F* (MAR19) cells grown without (control) or with DAP, OXA, or the DAP-OXA combination.

 $\Delta mprF$ complemented with mprFL826F (strain MAR19), following the same pattern observed in the parental CB1634 strain displaying the seesaw effect. These results indicate that the DAP-mediated changes in mprF and/or the CM associated with the DAPr phenotype alter the membrane levels of PBP 2a and thereby may interfere with the normal synthesis/function of the CW.

Functional role of *mprF* mutations on peptidoglycan cross-linking and DAP availability during DAP^r and the seesaw effect. Given the effects of altered MprF on PBP 2a levels, we next wanted to determine the influence of *mprF* mutations on the DAP-mediated seesaw effect. Phenotypic analysis comparing DAP^r CB1634 and its CB1634 Δ *mprF* counterpart showed that inactivation of *mprF* led to increased susceptibility to DAP (DAP MICs, 4 μ I/ml and 0.25 μ I/ml, respectively) and increased resistance to OXA (OXA MICs, 0.5 μ I/ml and 32 μ I/ml, respectively) (Table 1). Importantly,

TABLE 1 MICs of DAP and OXA for DAP $^{\rm r}$ CB1634 and $\it mprF$ derivatives determined by Etest

2.03.			
	MIC (μg/ml)		
Strain	DAP	OXA	
CB1634	4	0.5	
CB1634 ΔmprF	0.25	32	
CB1634 ΔmprF mprF (WT)	0.75	32	
CB1634 ΔmprF mprFL826F	3	1	

Downloaded from https://journals.asm.org/journal/aac on 27 March 2023 by 195.65.152.110.

complementation of CB1634 \(\Delta mprF \) with WT mprF did not revert the phenotype (DAP and OXA MICs, 0.75 μ g/ml and 32 μ g/ml, respectively). In contrast, complementation with mprFL826F restored the resistance to DAP (MIC, 3 μ g/ml) and decreased the level of resistance to OXA (MIC, 1 µg/ml), reestablishing the DAP-mediated seesaw effect (Table 1). Similar results were observed with the DAPs-DAPr pair CB5011 and CB5012 mprFL826F (data not shown).

We next determined the impact of mprF mutations and the implications of altered levels of PBP 2a on the CW during the DAP-mediated seesaw effect. The muropeptide composition of peptidoglycan was measured in DAPr CB1634 cells untreated and treated with DAP-OXA after separation by reverse-phase high-performance liquid chromatography (HPLC). Analysis of the HPLC profiles revealed marked differences in CW cross-linking in CB1634 cells with or without DAP-OXA treatment (Fig. 5A), showing that exposure to DAP-OXA resulted in a significant decrease in the amount of highly cross-linked oligomer muropeptides (peaks 17 to 22), which should reduce the rigidity of the CW. These results are in accordance with our data showing that exposure of DAPr strains to DAP-OXA reduces the levels of PBP 2a associated with the CM, which in turn could lead to the observed CW rearrangements and increased oxacillin susceptibility.

To investigate the role of mprF in the CW composition, notably taking into account the observations described above, we compared the muropeptide profiles of CB1634 with those of the CB1634 ΔmprF mutant. While no differences in the profiles between the two strains were observed in the absence of antibiotics (Fig. 5B, top), the addition of OXA showed significant enrichment of monomeric and dimeric components in the CB1634 ΔmprF strain (Fig. 5B, middle). These mprF-dependent effects were further enhanced by coexposure to DAP and OXA (Fig. 5B, bottom), providing a plausible explanation for the ability of the mprF deletion in DAPr strains to reverse the increased susceptibility to OXA during the seesaw effect, as shown in Table 1.

Cross talk between MprF and PrsA proteins. To understand further the molecular mechanism linking the mprFL826F mutation with decreased PBP 2a levels in the CM and peptidoglycan cross-linking during the seesaw effect, three basic observations were important to consider. First, we recently demonstrated that PrsA, a lipoprotein acting as a posttranslocational chaperone, is involved in β -lactam resistance by affecting the amounts of PBP 2a in the CM (26); in addition, prsA expression is regulated by the two-component system VraSR (14). Second, we have shown that acquisition of DAPr involves the upregulation of genes controlling CW synthesis and turnover, including vraSR (6). Unpublished transcriptome RNA sequencing (RNA-Seq) results suggest that the vraSR and prsA genes in the DAPr CB1634 strain are upregulated compared to their level of regulation in the DAPs CB1631 strain, suggesting a link between the mprFL826F mutation present in CB1634 and changes in the expression of both the vraSR and prsA genes. Third, MprF has been shown to be involved in the modification of the membrane phospholipid phosphatidylglycerol, which in turn acts as a substrate for the Lgt enzyme that modifies lipoproteins, such as PrsA (27).

In light of these observations, we hypothesized that DAPr-associated mprF mutations could affect the ability of PrsA to associate with the CM and, consequently, affect its functional activity. To test whether PrsA and MprF are mutually interconnected during the DAPr-mediated seesaw effect, we first evaluated the cellular levels of PrsA and the localization of PrsA in both the CM and extracellular protein extracts (Fig. 6). Consistent with the results of RNA-Seq analysis, we observed that steady-state levels of PrsA in the CM were higher in CB1634 than CB1631 (Fig. 6A). Interestingly, the levels of PrsA, which was almost undetectable in the absence of mprF (CB1634 ΔmprF), were restored by complementation with mprFL826F (CB1634 ΔmprF mprFL826F) but not with WT mprF (CB1634 ΔmprF mprF) (Fig. 6A). Concomitant analysis of extracellular extracts for which the ${\rm OD}_{600}$ was normalized showed increased amounts of extracellular PrsA in the corresponding CB1634 \(\Delta mprF \) and CB1634 \(\Delta mprF \) mprF (WT) strains, while no extracellular PrsA was detected in extracts from the CB1634 ΔmprF mprFL826F strain

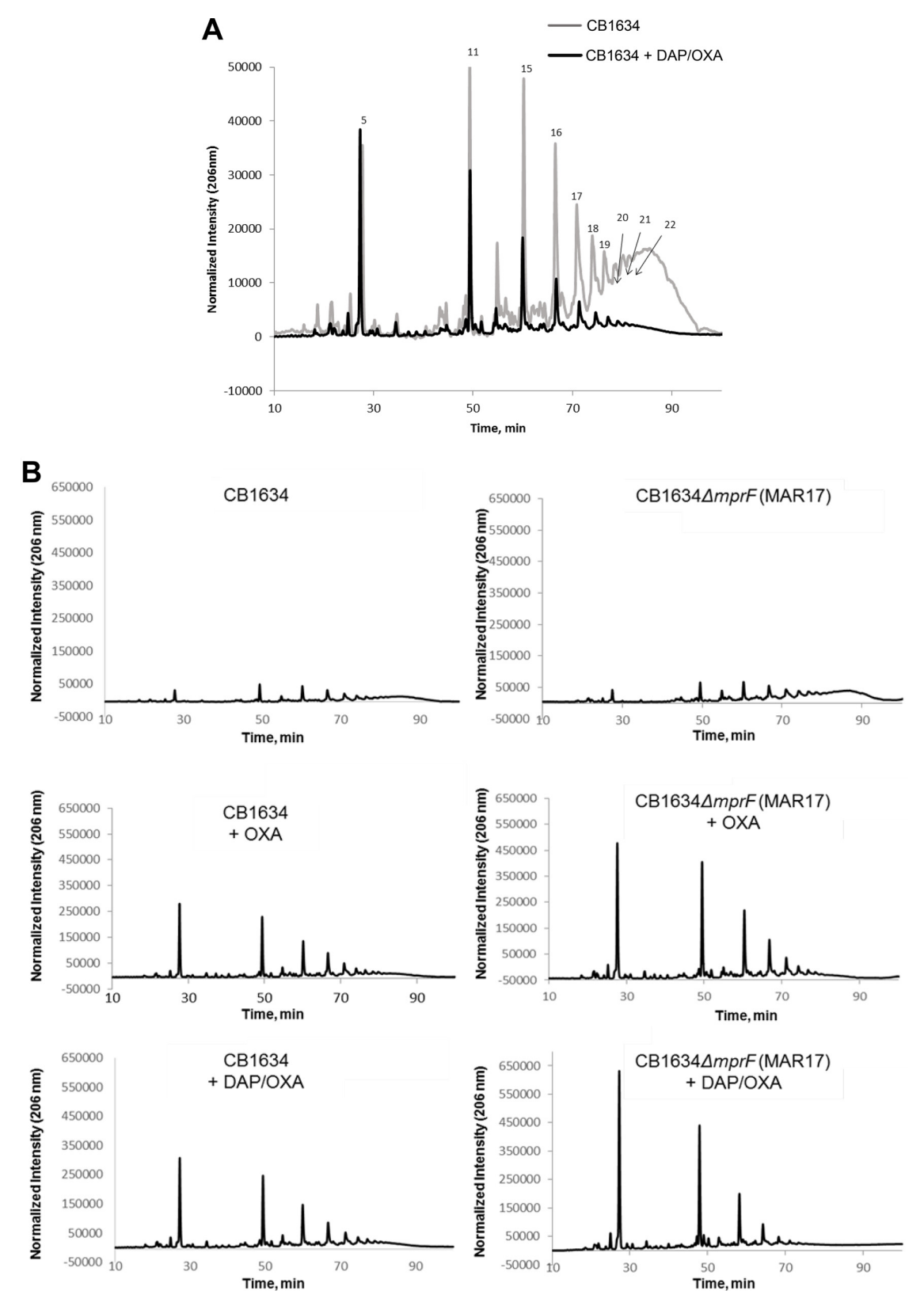


FIG 5 (A) Effect of the DAP-OXA combination on peptidoglycan cross-linking. The peptidoglycan muropeptide composition of DAPr CB1634 strains grown without or with the DAP-OXA combination was analyzed by reverse-phase HPLC. Peaks numbered 17 to 22 denote highly cross-linked oligomer muropeptides. (B) Effect of *mprF* deletion on peptidoglycan cross-linking in the presence of OXA or the DAP-OXA combination. The peptidoglycan muropeptide composition of DAPr CB1634 (left) and DAPs CB1634 $\Delta mprF$ (right) strains grown without or with OXA or the DAP-OXA combination was analyzed by reverse-phase HPLC.

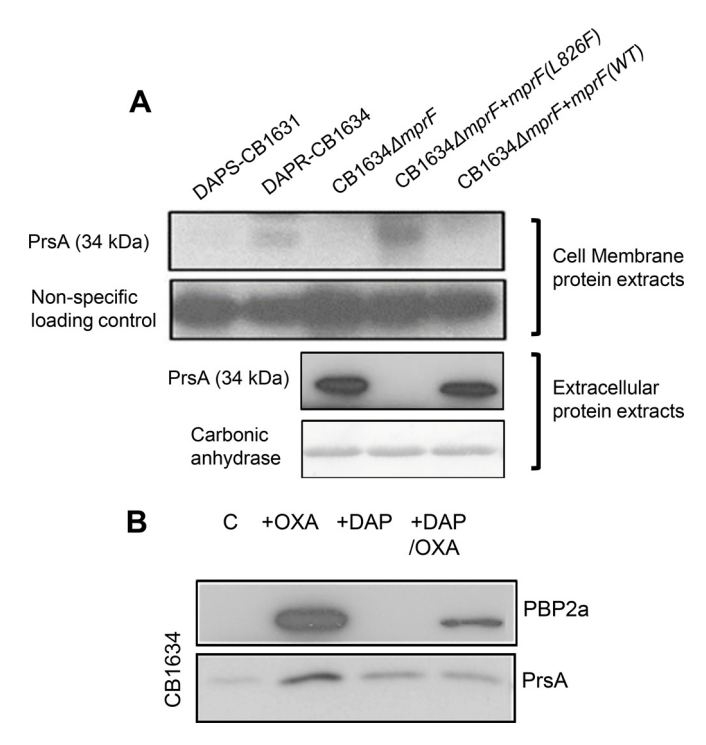


FIG 6 Effect of mprF mutations on PrsA membrane localization. (A) Western blot analysis of the PrsA protein in membrane protein extracts (top) and extracellular protein extracts (bottom) from DAPs CB1631, DAPr CB1634, CB1643 AmprF, CB1634 AmprF mprF (WT), and CB1634 AmprF mprFL826F cells grown without antibiotics. Carbonic anhydrase was used a loading control. (B) Western blot analysis for PBP 2a and PrsA in membrane extracts from DAPr CB1634 cells grown without (control [C]) or with OXA, DAP, or the DAP-OXA combination.

(Fig. 6A). These results strongly suggest that PrsA localization to the CM is altered by the mprF mutation and that this in turn is associated with the DAPr phenotype.

PrsA-mediated effects on CM-associated PBP 2a are triggered by the mprFL826F mutation. Since DAP-mediated effects during the seesaw effect involve alterations in PBP 2a levels in the membrane (Fig. 4A) and taking into account the PrsA-mediated regulatory role in β -lactam resistance via modulation of PBP 2a (13), we hypothesized that during the acquisition of DAPr, cell membrane modifications triggered by mutations in mprF alter PrsA membrane localization and, consequently, PBP 2a membrane levels. To test this idea, we measured PBP 2a and PrsA protein levels in CM extracts prepared from CB1634 (carrying mprFL826F) grown in the absence or presence of DAP, OXA, and the DAP-OXA combination. As shown in the Western blot in Fig. 6B, PBP 2a and PrsA protein membrane levels were increased upon OXA stress, but consistent with our hypothesis, the DAP-OXA combination resulted in decreased cell membrane levels of PBP 2a that correlated with a concomitant reduction in the levels of PrsA. Taken together, our results strongly suggest that despite the DAP-OXAinduced transcriptional upregulation of mecA, the mprF-dependent loss of CManchored PrsA results in the depletion of PBP 2a. Thus, the acquisition of DAPr via an mprF-dependent mechanism results in levels of PBP 2a insufficient to sustain resistance to β -lactams, an effect mediated by the altered cell membrane localization of PrsA.

Homogeneous DAPr MRSA strains do not display the seesaw effect without DAP induction. In previous studies, we reported that two DAPr strains, CB5036 and CB5014, with mutations in the central domain of MprF, P314L and S377L, respectively, did not display the DAP-mediated seesaw effect; i.e., their OXA MICs remained the same (512 µg/ml) in both strains of pairs of DAPs-DAPr strains (strains CB5035 [DAPs] and CB5036[DAPr] and strains CB5013 [DAPs] and CB5014[DAPr]) (8). However, as we described previously, the DAP-OXA combination was still effective against them (8). These strains are called homogeneous MRSA because they express a uniformly high

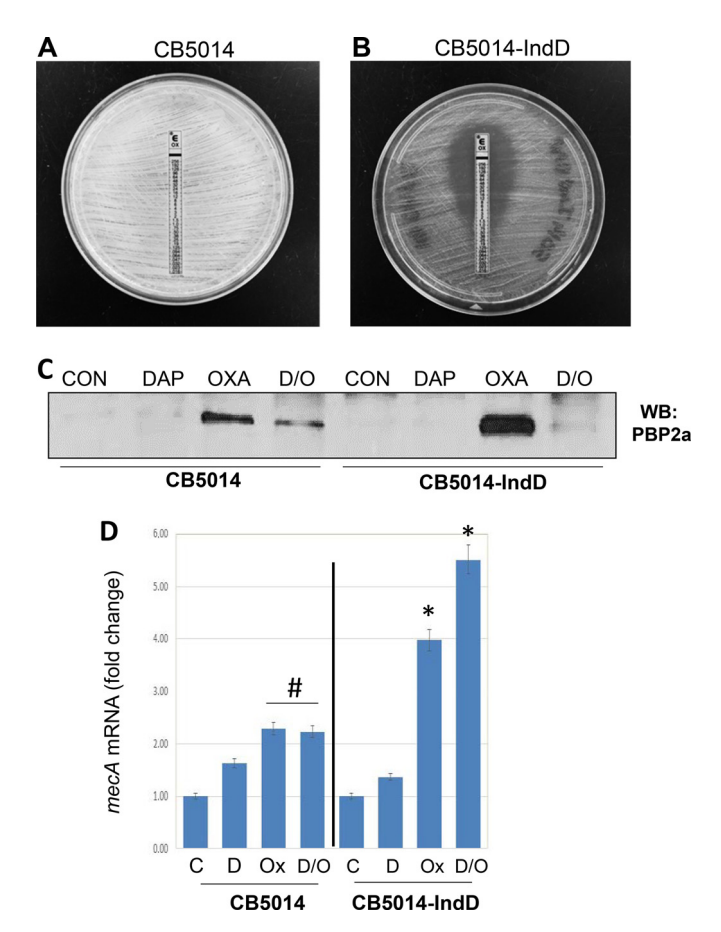


FIG 7 Homogeneous DAPr MRSA strains do not display the seesaw effect without DAP induction. DAPr strain CB5014 grown overnight in the absence (A) and in the presence (B) (strain CB5014IndD) of sublethal concentrations of DAP (0.5 \times MIC with 2 μ g/ml 50 mg/liter Ca²), after which the adjusted inoculum was plated onto MH agar containing 0.5imes MIC of DAP (2 μ g/ml). OXA Etest strips were placed on the plates, and the plates were incubated for 24 h. (C) Western blot (WB) analysis of the PBP 2a present in cell membrane extracts collected from cells as described in the legend to panel A. (D) Quantitation of mecA mRNA by real-time RT-PCR using RNA prepared from CB5014 and CB5014IndD. Relative fold changes are shown; 16S rRNA was used as an internal control. # and *, the fold change was significantly greater than that for the control (P < 0.05 and P < 0.01, respectively). C, control; D, daptomycin; Ox, oxacillin; D/O, daptomycin-oxacillin.

level of β -lactam resistance different from that seen in the heterogeneous MRSA strains (e.g., CB1634) whose cell populations are able to express differential levels of resistance and that are mostly associated with lower MICs (1 to 32 μ g/ml).

We hypothesized that the absence of DAP selection prevented detection of the seesaw effect in these strains. We tested this idea by growing cultures of DAPr strain CB5014 in the presence of a sublethal concentration (0.5 \times MIC) of DAP (2 μ g/ml DAP, 50 mg/liter Ca²⁺), after which the adjusted inoculum was plated onto Mueller-Hinton (MH) agar containing 0.5× MIC of DAP (2 μ g/ml). OXA Etest strips were placed on the plates, and the plates were incubated for 24 h, after which a pronounced decrease in the OXA MIC from 512 µg/ml to 1 µg/ml was observed (Fig. 7A and B); this strain with low-level resistance induced by DAP is referred as CB5014IndD. Similar results were obtained with DAP^r strain CB5036 (data not shown). In support of these observations, PBP 2a was detectable in membrane extracts from CB5014 grown overnight without DAP induction and then exposed to DAP-OXA, whereas under the same conditions, the levels of the protein in CB5014IndD became almost undetectable (Fig. 7C). These results are consistent with the appearance of the DAP-mediated seesaw effect, as it was displayed only in the CB5014IndD strain. Furthermore, as shown above for CB1634 (Fig. 4A), the absence of PBP 2a in cell membrane extracts collected from CB5014IndD was

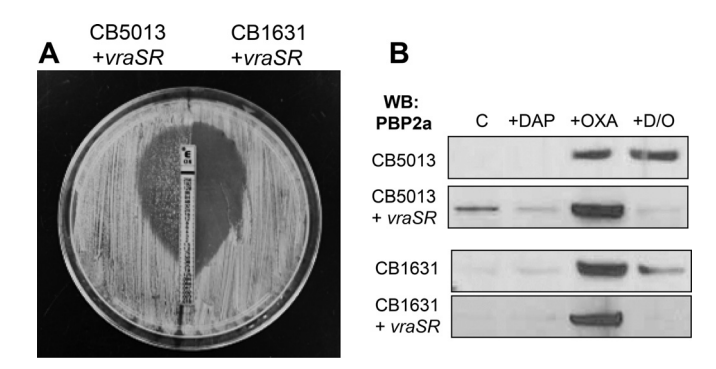


FIG 8 VraSR- and DAP-mediated seesaw effect. (A) CB5013+vraSR and CB1631+vraSR were grown overnight, after which the adjusted inoculum was plated onto MH agar, OXA Etest strips were placed on the plates, and the plates were incubated at 37°C for 24 h. (B) Western blot analysis of the PBP 2a present in cell membrane extracts collected under the indicated conditions from DAPs CB5013 and CB1631 and their corresponding vraSR-overexpressing counterparts (CB5013+vraSR and CB1631+vraSR, respectively).

not related to a decrease in the levels of mecA mRNA transcription: in the presence of OXA, either alone or in combination with DAP, mecA expression was highly induced (~4- and 5.6-fold, respectively; Fig. 7D). CB5014 exposed to OXA or OXA-DAP also showed increased levels of mecA expression, although the level of expression was lower than that observed in CB5014IndD (Fig. 7D). Together, these data suggest that homogeneous DAP^r MRSA strains rely upon DAP induction-mediated factors to express the seesaw phenotype.

Role of VraSR in the DAP-mediated seesaw effect. As mentioned above, we previously demonstrated the critical role played by the VraSR two-component regulatory system in the acquisition of DAPr (20) Moreover, DAPr strains, including the CB5014 and CB5035 homogeneous MRSA strains, expressed higher levels of vraSR than their corresponding DAPs counterparts (20). To further elucidate and understand the mechanistic role of DAP-induced vraSR expression and the seesaw effect, we overexpressed vraSR in the corresponding DAPs CB5013 (OXA MIC, 512 μ g/ml) and CB1631 (OXA MIC, 32 µg/ml) strains. This resulted in vraSR expression levels similar to those observed in the corresponding DAPr counterparts, CB5014 and CB1634, as determined by RT-PCR (data not shown). Phenotypic analyses performed by the OXA Etest showed that CB5013 overexpressing vraSR (strain CB5013+vraSR) and CB1631 overexpressing vraSR (strain CB1631+vraSR) displayed both DAP-mediated seesaw effects, i.e., decreased DAP susceptibility (DAP MICs, 4 µg/ml) and oxacillin resistance (OXA MICs, 0.25 and 0.5 μg/ml for DAPs CB5013+vraSR and CB1631+vraSR, respectively; Fig. 8A). Moreover, analysis of the mprF DNA sequences in these strains revealed amino acid changes that were identical to those present in their DAPr counterparts (\$337L in CB5014 and L826F in CB1634), demonstrating that the increased expression of vraSR mediated by DAP leads to polymorphisms in mprF. To investigate further the potential role of increased vraSR expression mediated by DAP in changes in antibiotic susceptibilities related to the seesaw effect, we analyzed the PBP 2a levels in cell membrane lysates from strains CB5013 and CB1631+vraSR. As depicted in Fig. 8B, increased PBP 2a levels were observed at the baseline in CB5013+vraSR compared to those observed in the other strains. When all strains were exposed to OXA alone, they showed increased amounts of cell membrane-associated PBP 2a. Importantly however, membrane-associated PBP 2a was undetectable following exposure to DAP-OXA in both strains expressing higher levels of vraSR, consistent with the seesaw effect described above.

To gain further insights into potential differences between the strains displaying the seesaw effect, i.e., CB1634 and CB5014IndD, we compared the overall gene expression profiles of the strains by comparing RNA-Seq data after exposure to OXA or DAP-OXA. Expression of approximately 322 genes was significantly altered (determined by a P value of <0.05 and a more than 2-fold difference in the level of expression before and

after exposure to OXA or DAP-OXA; see Table S1 in the supplemental material). Among these genes, relevant observations obtained when the gene expression of CB5014IndD and CB1634 was compared after exposure to DAP-OXA included the upregulation of vraSR mRNA (~6-fold), accompanied by increased levels of expression of transcripts for the vraSR target genes pbp2 (~4-fold) and sqtB (~3.5-fold). In addition, mecA mRNA was also highly upregulated (\sim 21- and 5-fold in strains exposed to DAP-OXA and OXA, respectively), as were mRNAs for mecl and mecRI (~5- and 3-fold). Other genes that were upregulated included those coding for proteins involved in the synthesis of peptidoglycan precursors (murA to murG, femAB, and mraW, the levels of expression of which were increased between 6- and 3.9-fold), while downregulated genes were associated with other gene class families, i.e., genes involved in biosynthesis and metabolic pathways, such as those for iron (fer, fmhA), histidine (hisG, hisH), and gluconate (gntP, gntK). Together, these results provide strong evidence supporting the key mechanistic role played by the increased expression of vraSR following DAP exposure and its implication in the process leading to the acquisition of DAP resistance and the concomitant seesaw effect.

DISCUSSION

DAP targets the bacterial CM, causing rapid membrane depolarization and cell death (2). Decreased susceptibility to DAP in S. aureus has been reported to lead to clinical failures in patients with MRSA deep-site infections, such as endocarditis and abscesses (28-30). Previously, we identified two major factors that mutually cooperate in the acquisition of DAP resistance; one is related to the cell membrane (mrpF mutations), and the second affects cell wall factors (VraSR) (6). Moreover, we observed that the DAPr phenotype was accompanied by increased susceptibility to OXA, the so-called seesaw effect. Previously, a concomitant rise in the level of vancomycin resistance with decreased β -lactam resistance has been reported in some clinical vancomycin-intermediate S. aureus (VISA) and vancomycin-resistant S. aureus (VRSA) strains. In VISA strains, the mechanism remains undefined, with some strains showing excision of SCCmec carrying mecA, while in others mecA is retained (31, 32). In contrast, in VRSA strains, the loss of β -lactam resistance seems to be associated with the inability of PBP 2a to utilize the UDP-N-acetylmuramic acid-depsipeptide (p-Ala-p-Lac) cell wall precursor produced in VRSA for transpeptidation, leaving PBP 2 to be essential for the synthesis of the abnormally structured cell wall (33). To date, the precise mechanism responsible for the seesaw effect mediated by DAP resistance in MRSA still remains to be elucidated.

Based on the findings of the present study, we postulate that DAP-induced mprF mutations at the CM level cause alterations that affect the localization and functions of important proteins involved in cell wall construction. In this context, it has previously been noted that subinhibitory concentrations of DAP induce aberrant and asymmetric division septa in B. subtilis (20), reinforcing the notion that DAP may target both the CM and CW. Working on the hypothesis that, by targeting the CM, DAP perturbs the lipid environment of membrane-bound enzymes involved in peptidoglycan synthesis, moderately disrupting CW assembly, we found that exposure of DAPr cells to a combination of DAP and β -lactams led to the delocalization of peptidoglycan synthesis from the division septum, redistributing this activity around the cell wall. We and others have observed that the seesaw effect is mainly achieved by β -lactams targeting the PBP 1 and/or PBP 2 protein that localizes at the septum of S. aureus and, furthermore, that this effect does not depend on other peptidoglycan synthesis enzymes (34). Recently, it has been demonstrated that peptidoglycan synthesis in S. aureus can rely solely on PBP 1 and PBP 2 after seven of the nine peptidoglycan synthesis proteins are removed (34). The observation that only β -lactams targeting PBP 1 or PBP 2 are capable of killing cells during exposure to DAP-OXA supports the idea that perturbations to these proteins are largely sufficient for the MRSA sensitization observed during the seesaw effect.

Importantly, we found that sensitization to β -lactams in DAP^r strains containing mutant mprF alleles was associated with decreased levels of cell membrane-associated

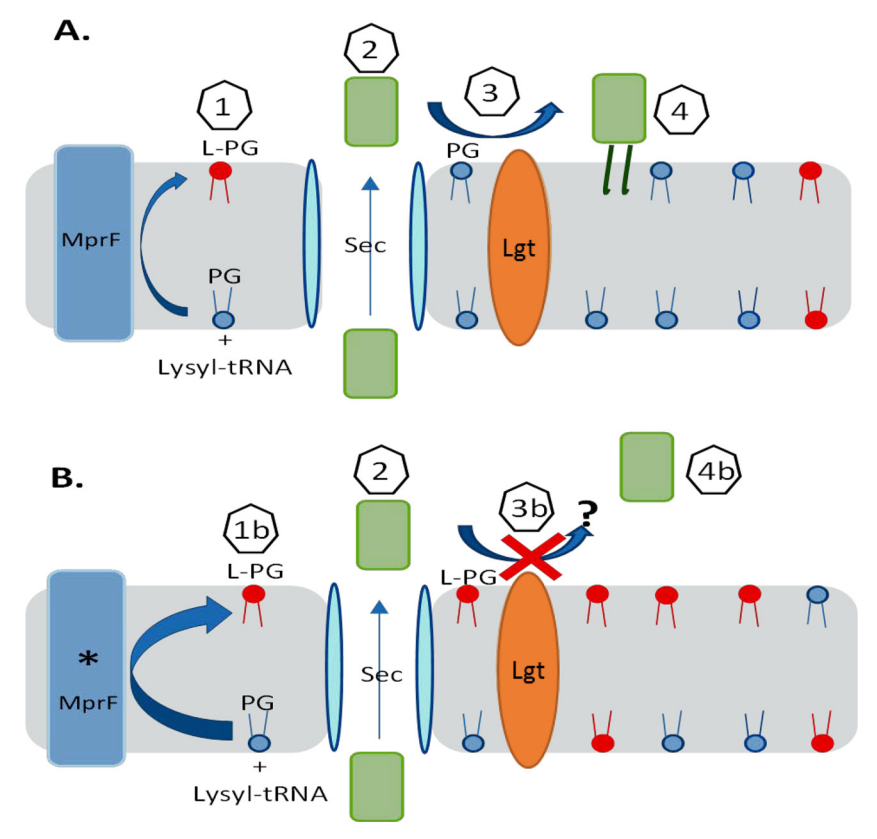


FIG 9 Proposed model of MprF (A) or mutated MprF (* MprF) (B) affecting lipoprotein PrsA anchorage. Step 1, MprF uses cytosolic lysyl-tRNA to convert phosphatidylglycerol (PG) to lysyl phosphatidylglycerol (L-PG); step 1b, the enhanced transferase and/or flippase activity of mutated MprF increases the proportion of L-PG compared to that of phosphatidylglycerol in the outer membrane leaflet; step 2, prelipoprotein PrsA is secreted, which probably occurs through the Sec pathway; step 3, phosphatidylglycerol is used by the Lgt enzyme to lipid modify the PrsA lipobox cysteine; step 3b, inhibition of Lgt-mediated acyl transfer to PrsA occurs due to increased L-PG amounts/reduced phosphatidylglycerol amounts in the outer membrane leaflet; step 4, lipidated membrane-anchored PrsA helps with the posttranslational maturation of PBP 2a; step 4b, failure to produce lipidated membrane-anchored PrsA occurs.

PBP 2a. MprF is involved in the modification of phosphatidylglycerol, which acts as a substrate for Lgt to modify lipoproteins, such as PrsA, with lipid moieties (27). The present evidence highlights potential mutual interactions between MprF and PrsA during DAPr. In fact, it is plausible to postulate that cell membrane modifications triggered by DAPr-mediated mutated MprF may affect both PrsA location and chaperone functions, which are required for PBP 2a folding. In support of the importance of posttranscriptional regulation, we observed reduced amounts of cell membraneassociated PBP 2a in DAP-OXA-treated cells, despite the increased transcription of mecA through mec regulatory elements. These findings are in agreement with recent observations by Jousselin et al. suggesting that PBP 2a is a related substrate of PrsA (13), although we cannot rule out the possibility that PrsA may also influence the septal localization of PBPs, specifically, PBP 1 and PBP 2, which are associated with the seesaw effect and are PrsA substrates in three Gram-positive bacterial pathogens (18).

We have previously established a role for the lipoprotein PrsA as an important mediator of both glycopeptide and oxacillin resistance, with the latter occurring through its effect on the potential proper maturation of PBP 2a (13, 14). A consideration of MprF and the biosynthesis of lipoproteins, such as PrsA, suggests a plausible model to explain the seesaw effect linking DAP nonsusceptibility and decreased resistance to certain antistaphylococcal β -lactams in MRSA strains (Fig. 9).

The integral membrane protein MprF uses cytosolic charged lysyl-tRNA to lysinylate

phosphatidylglycerol and subsequently flips lysyl phosphatidylglycerol (L-PG) to the outer leaflet of the cytoplasmic membrane. Mutated MprF showing enhanced enzymatic transferase and/or flippase activity results in a significantly increased proportion of L-PG in the membrane compared to that of peptidoglycan, as well as the generation of membrane L-PG asymmetry by the selective accumulation of L-PG in the outer leaflet (35, 36).

Prelipoproteins mature sequentially by secretion, lipidation of the lipobox cysteine embedded within the signal sequence by phosphatidylglycerol and Lgt acyltransferase, and finally, signal sequence cleavage by Lsp (37, 38). The study of LgtA in Escherichia coli demonstrated that the S. aureus enzyme could fully compensate for the E. coli enzyme (39). Further high-resolution X-ray structure and function analysis of the E. coli enzyme revealed mechanistic features consistent with an active site facing the periplasm and acquisition of the phosphatidylglycerol substrate from the outer membrane leaflet (40). Phosphatidylglycerol is used as a substrate lipid by at least four enzymes, MprF, LtsA, Cls1/2, and Lgt, to control the biosynthesis of L-PG, the polymerization of lipoteichoic acid glycerol phosphate, cardiolipin, and the lipidation of lipoproteins, respectively. Only LtsA is essential, indicating that the activities provided by the other enzymes when phosphatidylglycerol is used as a substrate are facultative (27, 36). Since LtsA governs an essential process mediating the production of lipoteichoic acid, it is reasonable to ask, what permits lipobox lipidation to continue, if at all, in DAPr strains arising from mutated MprF (or enhanced GraRS activity driving MprF production) as L-PG accumulates and the amount of phosphatidylglycerol diminishes in the outer membrane leaflet?

We hypothesize that disruption of lipoprotein anchorage by inhibition of Lgtmediated acyl transfer contributes to the seesaw mechanism. Our model predicts that the proper function of PrsA in particular is disrupted, and this is in accordance with our experimental findings. Failure to produce sufficient lipidated PrsA would impair PrsAdependent posttranslational maturation of PBP 2a, allowing transpeptidase activity to be susceptible to β -lactams. Of course, we cannot exclude the possibility of the existence of alternative scenarios in which other lipoproteins, such as DsbA, could affect protein function (41) or in which the membrane electrostatic charge has effects on membrane-associated sensory processes that regulate cell wall biosynthesis (26). In support of the specific role of PrsA, we have produced a PrsA lipobox cysteine mutant that we could not detect in membrane extracts by Western blot analysis, suggesting that it is unstable and degraded or fails to anchor and is lost (A. Jousselin and A. Renzoni, unpublished data).

The intriguing observation that some DAPr strains do not display a seesaw effect unless they are preinduced with sublethal levels of DAP prompted us to investigate in more detail the role of VraSR. Indeed, we found that overproduction of VraSR in DAPs strains decreased susceptibility to DAP and increased susceptibility to β -lactams, similar to the findings obtained with LiaFSR, a pivotal regulator of DAPr in enterococci (42). In the absence of DAP, the three-component regulatory system LiaFSR is turned off by the negative interaction of LiaF with LiaS. LiaS responds to membrane stress by phosphorylating LiaR, which leads to changes in the levels of transcription of several downstream operons that affect CM homeostasis (42). Interestingly, in enterococci the ability of several β -lactams, especially ampicillin (AMP), ceftaroline (CPT), and ertapenem (ERT), to provide synergistic activity with DAP and prevent the emergence of DAP nonsusceptibility has also been demonstrated (43, 44).

In S. aureus, VraS belongs to a subfamily of kinases that sense cell envelope stress and do not contain extracellular sensor domains (45). Although the transmembrane helices of this subgroup have been proposed to be involved in stress sensing, the precise mechanism of VraS-like kinase activation remains unknown. We propose that exposure of DAP^r strains to DAP-OXA determines the reorganization of the membrane structure through the induction of changes in phospholipid composition which may activate VraSR signaling by promoting VraS dimerization and downstream events, including autophosphorylation of VraS, phosphorylation of VraR, and gene regulation.

TABLE 2 Strains and primers used in this study

Strain or primer	Description or sequence	Reference or source
S. aureus strains		
CB5011	Daptomycin susceptible	6
CB5012	Daptomycin-resistant strain isogenic to CB5011, mprFL826F	6
CB5013	Daptomycin susceptible	6
CB5014	Daptomycin-resistant strain isogenic to CB5013, mprFS377L	6
CB1631	Daptomycin susceptible	6
CB1634	Daptomycin-resistant strain isogenic to CB1631, mprFL826F	6
MAR17	CB1634 ΔmprF::cat	6
MAR18	MAR-17/pMPRF-1 (wild type)	6
MAR19	MAR-17/pMPRF-2 (L826F mutant)	6
CB5013+VraSR	Entire vraS and vraR sequences cloned into pAW8	This study; 49
CB1631+VraSR	vraS and vraR sequences cloned into pAW8	
Primers and probes		
PrsA-F	AGTTAATGATAAGAAGATTGACGA	
PrsA-R	GAAGGGCCTTTTCAAATTTATCTTT	
VraSR-F	GGTGCAACGTTCCCATATTGTATTGT	
VraSR-R	GGCTTCAACTCATGGGCTTTGGCAA	
mprF-F	GGTGGCTTTATTGGTGCAGGCG	
mprF-R	GATGCATCGAAAACATGGAA	
mecA-F	TGCCTAATCTCATTGTGTTCCTGTAT	
mecA-R	CGGTGCTGAAACTTTCACAATATAAT	
pbp2-GFPF (DPH407)	GATAGCGGCCGCATGACGGAAAACAAAGGATCTTCTC	
pbp2-GFPR (DPH408)	GAAGGGATCCTTAGTTGAATATACCTGTTAATCCACCG	
16S-F	TCCGGAATTATTGGGCGTAA	
16S-R	CCACTTTCCTCTTCTGCACTCA	

Based on our observations, we postulate that the induction of changes by DAP, such as those seen in the CB5014IndD strain, may favor the oligomerization of VraR, which in turn may form a constitutively activated tetramer with a high affinity for DNA, even in the absence of phosphorylation, favoring the development of DAP resistance and the seesaw effect phenotype, as in heterogeneous DAPr MRSA strain CB1634. We are currently studying the differences in VraR oligomerization among DAPr clinical strains that may explain the differences between heterogeneous and homogeneous DAPr MRSA strains.

In summary, the present study addresses the mechanistic bases and significance of sensitization to β -lactams linked to DAP^r in clinical MRSA strains. The combination of DAP and β -lactams has gained increased acceptance for the treatment of MRSA infections produced by DAP^r strains, resulting in clinical successes. We demonstrate that VraSR is a key determinant of DAP resistance, leading to mutations in mprF that may impair PrsA chaperone functions, which are required for the posttranscriptional maturation of PBP 2a; these effects may account for the resensitization of DAPr strains to cell wall-specific β -lactams. Continued progress in understanding DAP's mode of action and its impact on the CM/CW machinery will provide fundamental insights into MRSA biology that may potentially be translated into the discovery of new therapeutic targets.

MATERIALS AND METHODS

Bacterial strains and antibiotics. All clinical strains used in this study are listed in Table 2. Trypticase soy agar with 5% sheep blood (BBL, Sparks, MD) was used for the subculture and maintenance of S. aureus. Staphylococcus aureus and E. coli were grown in Mueller-Hinton broth (MHB). Standard reference antibiotics, tetracycline (TET; 3 µg/ml), chloramphenicol (CM; 10 µg/ml), and oxacillin (OXA; concentration range, 0.5 to 10 μ g/ml) were obtained from Sigma, St. Louis, MO, or United States Biochemicals, Cleveland, OH. Daptomycin (DAP) was provided by Cubist Pharmaceuticals/Merck (Lexington, MA). DAP and OXA were used at concentrations adjusted on the basis of the MICs for the parental strains and genetic mutants. Calcium was added at a concentration of 50 mg/liter for DAP. Antimicrobial susceptibility to OXA was determined according to the guidelines of the Clinical and Laboratory Standards Institute (46). DAP MICs were determined by Etest (AB Biodisk, Solna, Sweden).

Membrane protein extraction. For the isolation of membrane proteins, strains were grown in MHB until mid-exponential phase, and pellets were resuspended in 600 μ l of phosphate-buffered saline (PBS). Bacterial cells were disrupted by adding glass beads and using a FastPrep cell disrupter (MP Biomedicals,

Santa Ana, CA), and the lysate was centrifuged at 8,000 imes g for 10 min at 4°C. The supernatant fraction was centrifuged for an additional 5 min at 8,000 imes g at 4°C to remove the beads, and then the supernatant was transferred to ultracentrifuge tubes and centrifuged at 45,000 rpm in a Thermo Sorvall WX Ultra series WX80 centrifuge (Thermo Scientific, Waltham, MA) for 1 h at 4°C. The membrane pellet was resuspended in PBS, and total membrane proteins were quantified by the Bradford protein assay (Thermo Fisher) and stored at -80° C.

Secreted protein preparation. Bacteria were grown in MHB until the OD₆₀₀ was approximately 0.3. Then, the samples were centrifuged for 10 min at 4,000 rpm and the supernatant was passed through $0.22-\mu m$ -pore-size membrane filters (Millex). Samples were normalized by adjustment of the volume to equal the sample OD, and 20 μg of carbonic anhydrase (Sigma) was added as an internal spike control as described previously (14). Samples were concentrated in Amicon 10,000-molecular-weight-cutoff centrifugal filters (Millipore) to a final volume of 40 μ l.

Western blotting. Proteins (15 μ g) were separated on 4 to 12% bis-Tris gels and blot transferred onto pure nitrocellulose blotting membranes (Pall Life Science). The membranes were blocked using 5%low-fat milk in PBS. PBP 2a was probed with monoclonal anti-PBP 2a antibody (Slidex MRSA detection kit; bioMérieux, France) at a 1/2,000 dilution, followed by incubation with a secondary alkaline phosphatase-labeled goat anti-rabbit IgG(H+L) antibody at a 1/5,000 dilution. The labeled protein signal was detected using an SRX/101A film processor (Konica Minolta).

DNA manipulation and sequencing. Chromosomal DNA was prepared by using a Qiagen genomic DNA preparation kit (Qiagen, Inc., Valencia, CA) according to the manufacturer's directions. Sequencing of all PCR amplification products was performed at the Nucleic Acid Research Facility at Genewiz (South Plainfield, NJ). Analysis of the mprF sequence in wild-type strains and mutants was performed by using mprF-specific primers as previously described (6). Consensus sequences were assembled from both orientations with Lasergene (v12) software (DNAStar, Madison, WI). The S. aureus N315 sequence (GenBank accession number BA000018) was used as a reference control.

RNA extraction and RNA-Seq. Total RNA was extracted using an RNeasy isolation kit (Qiagen). The concentration and integrity of the RNA samples were assessed by A_{260}/A_{280} spectrophotometry and gel electrophoresis. RNA samples were cleaned and treated with DNase following the manufacturer's recommendations to avoid potential DNA contamination. RNA was prepared from CB1634 cells collected at exponential phase of growth under the different conditions in the absence and presence of DAP, OXA, and DAP-OXA. The genome-wide transcript sequencing libraries were prepared according to the manufacturer's instructions (ScriptSeg; EpiCenter) and sequenced on a MiSeg instrument (Illumina). Differential gene expression was determined by CLC Genomic Workbench and Lasergene software; differences consisting of >1.5-fold differences in the levels of expression with a P value of <0.05 after application of the Bonferroni correction for multiple comparisons were considered significant.

Analysis of gene expression by RT-PCR. Real-time reverse transcription-PCR (RT-PCR) analysis for RNA samples was done using a SensiMix SYBR one-step kit (Qantace/Bioline, Taunton, MA) according to the manufacturer's protocol. The level of gene expression compared with that for a sample considered the reference (value = 1) was determined using $\log_2 - (\Delta \Delta C_7)$, where C_7 represents the threshold cycle value. The change (n-fold) in the transcript level (ΔC_{τ}) was calculated using the following equations: $\Delta C_T = C_T$ for test DNA – C_T for reference cDNA, $\Delta \Delta C_T = \Delta C_T$ for the target gene – ΔC_T for 16S rRNA, and amount of target = $2^{-\Delta\Delta CT}$. The quantity of cDNA for each experimental gene was normalized to the quantity of 16S cDNA in each sample. The oligonucleotide primers used in this study are shown in Table 2.

Microscopy, labeling, and imaging of DAPs and DAPr cells. Parental DAPs strain CB1631 and resistant DAPr strain CB1634 were grown to exponential phase in tryptic soy broth (TSB) in the absence and presence of DAP (0.25 and 1 μ g/ml, respectively) at 37°C and labeled for 5 min with either HADA (which stains nascent peptidoglycan insertion), FM1-43FX (which stains the cell membrane), DAPI (which stains DNA), or vancomycin (which stains nascent D-alanyl-D-alanine incorporation into the CW) (Sigma) mixed with a Bodipy FL conjugate of vancomycin (VAN-Bodipy FL; Molecular Probes) to a final concentration of 0.8 μ g/ml. Images were obtained with a Nikon inverted epifluorescence microscope. For studies on the localization of PBP 2, the corresponding gene, pbpB, was expressed as an N-terminal GFP fusion protein in CB1634. Genomic DNA was PCR amplified using Phusion DNA polymerase and primers pbp2-GFPF (DPH407) and pbp2-GFPR (DPH408) (Table 2). PCR fragments were digested with Notl and BamHl and ligated into a cleaved pEA18 vector in frame with gfp (originally cloned from pDSW207) to generate pDH177 in E. coli AG111 competent cells. The gfp-pbpB fragment, including the B. subtilis spoVG ribosome binding site sequence of pEA18, was subcloned from pDH177 by digestion with HindIII and BamHI and ligated into the cleaved pCL15 vector to generate pDH178. pDH178 was initially cloned into E. coli AG1111 (Promega Wizard) and transformed into S. aureus RN4220 by electroporation. The plasmid was then transduced from RN4220 into S. aureus CB1634 using phage 80α . CB1634 cells containing the gfp-pbpB gene in pDH178 were induced with IPTG in the presence of OXA, DAP, or DAP-OXA to localize PBP 2a during DAP-OXA synergistic effects. Cells were fixed in 2.8% formaldehyde (FA) and 0.04% glutaraldehyde (GA) in growth medium for 15 min at room temperature. The cells were collected by centrifugation at $8,000 \times g$ for 5 min, washed once in PBS, treated with Vectashield antifade reagent, and visualized by fluorescence microscopy with an Olympus BX60 epifluorescence microscope containing a ×100 oil immersion objective (numerical aperture, 1.4). Images were captured with a Hamamatsu Orca charge-coupled device camera using HCImage software.

Labeling of PBPs with Bocillin FL. Bocillin FL labeling of 100 µg of membrane proteins was performed with 100 μ M Bocillin FL (Molecular Probes), with which the proteins were incubated for 30 min at 35°C. The reaction was stopped by adding $4 \times$ SDS-PAGE sample buffer. The labeled membrane

Downloaded from https://journals.asm.org/journal/aac on 27 March 2023 by 195.65.152.110.

protein concentrations were determined by the Bradford protein assay, 15 μg was loaded on a 10% bis-Tris gel, and the proteins were detected using a ProteinSimple imager-FluorChem E system (GE Healthcare).

Peptidoglycan purification and analysis. Exponentially growing cells (OD₆₀₀, 0.5) grown on MHB untreated and treated with OXA, DAP, and DAP-OXA were boiled in 4% SDS, deproteinized by treatment with pronase and trypsin, treated with 48% hydrofluoric acid (HF) at 4°C for 16 h, and washed several times with 0.25 M Tris-HCl and water before lyophilization. Purified peptidoglycan was digested with 25 μg/ml of mutanolysin (Sigma). The soluble muropeptides were reduced with sodium borohydride. The reaction was stopped by the addition of phosphoric acid, and the supernatant containing peptidoglycan was analyzed in an LC-20AB HPLC equipped with an SPD-20A UV detector (Shimadzu). The separation of muropeptides was performed in a Jupiter Proteo column (C₁₈, 250 by 4.6 mm, 4 μm, 90 Å; Phenomenex). Twenty microliters of sample was eluted at 0.5 ml/min for 5 min with 95% mobile phase A (100 mM sodium phosphate buffer, pH 3.0, containing 0.00025% sodium azide) and 5% mobile phase B (methanol), and then the proportion of mobile phase B was increased up to 30% at 120 min, as previously described (47). Detection was performed at 206 nm, and peaks were identified by comparison with the elution profile for peptidoglycan from the COL strain, as previously reported (48).

Statistical analyses. Statistical tests were performed using SPSS (v17.0) software for Windows (SPSS Inc., Chicago, IL, USA). The survival data were plotted using the Kaplan-Meier method.

SUPPLEMENTAL MATERIAL

Supplemental material for this article may be found at https://doi.org/10.1128/AAC.01634-16.

TEXT S1, XLS file, 0.1 MB.

ACKNOWLEDGMENTS

We acknowledge Liliana Paz and Regina Fernandez for their contribution to this work.

We have no relevant financial interests to report.

This study was funded in part by Merck (formerly Cubist Pharmaceuticals), Lexington, MA, by NIH grant NIH-R56AI102503-01A1 (principal investigator, A. E. Rosato), and by Swiss National Science Foundation grants 310030-149762 (to A.R.) and 310030-146540 and 310030-166611 (to W.L.K.).

REFERENCES

- National Nosocomial Infections Surveillance System. 2004. National Nosocomial Infections Surveillance (NNIS) System Report, data summary from January 1992 through June 2004, issued October 2004. Am J Infect Control 32:470–485. https://doi.org/10.1016/j.ajic.2004.10.001.
- Baltz RH, Miao V, Wrigley SK. 2005. Natural products to drugs: daptomycin and related lipopeptide antibiotics. Nat Prod Rep 22:717–741. https://doi.org/10.1039/b416648p.
- Arbeit RD, Maki D, Tally FP, Campanaro E, Eisenstein Bl. 2004. The safety and efficacy of daptomycin for the treatment of complicated skin and skin-structure infections. Clin Infect Dis 38:1673–1681. https://doi.org/ 10.1086/420818.
- Baltz RH. 2009. Daptomycin: mechanisms of action and resistance, and biosynthetic engineering. Curr Opin Chem Biol 13:144–151. https:// doi.org/10.1016/j.cbpa.2009.02.031.
- Bayer AS, Mishra NN, Chen L, Kreiswirth BN, Rubio A, Yang SJ. 2015. Frequency and distribution of single-nucleotide polymorphisms within mprF in methicillin-resistant Staphylococcus aureus clinical isolates and their role in cross-resistance between daptomycin and host defense antimicrobial peptides. Antimicrob Agents Chemother 59:4930 – 4937. https://doi.org/10.1128/AAC.00970-15.
- Mehta S, Cuirolo AX, Plata KB, Riosa S, Silverman JA, Rubio A, Rosato RR, Rosato AE. 2012. VraSR two-component regulatory system contributes to mprF-mediated decreased susceptibility to daptomycin in in vivoselected clinical strains of methicillin-resistant Staphylococcus aureus. Antimicrob Agents Chemother 56:92–102. https://doi.org/10.1128/ AAC.00432-10.
- Friedman L, Alder JD, Silverman JA. 2006. Genetic changes that correlate with reduced susceptibility to daptomycin in Staphylococcus aureus. Antimicrob Agents Chemother 50:2137–2145. https://doi.org/10.1128/ AAC.00039-06.
- 8. Mehta S, Singh C, Plata KB, Chanda PK, Paul A, Riosa S, Rosato RR, Rosato AE. 2012. β -Lactams increase the antibacterial activity of daptomycin against clinical methicillin-resistant Staphylococcus au-

- reus strains and prevent selection of daptomycin-resistant derivatives. Antimicrob Agents Chemother 56:6192–6200. https://doi.org/10.1128/AAC.01525-12.
- Rand KH, Houck HJ. 2004. Synergy of daptomycin with oxacillin and other beta-lactams against methicillin-resistant Staphylococcus aureus. Antimicrob Agents Chemother 48:2871–2875. https://doi.org/10.1128/ AAC.48.8.2871-2875.2004.
- Yang SJ, Xiong YQ, Boyle-Vavra S, Daum R, Jones T, Bayer AS. 2010. Daptomycin-oxacillin combinations in treatment of experimental endocarditis caused by daptomycin-nonsusceptible strains of methicillin-resistant Staphylococcus aureus with evolving oxacillin susceptibility (the "seesaw effect"). Antimicrob Agents Chemother 54:3161–3169. https://doi.org/10.1128/AAC.00487-10.
- Dhand A, Bayer AS, Pogliano J, Yang SJ, Bolaris M, Nizet V, Wang G, Sakoulas G. 2011. Use of antistaphylococcal beta-lactams to increase daptomycin activity in eradicating persistent bacteremia due to methicillin-resistant Staphylococcus aureus: role of enhanced daptomycin binding. Clin Infect Dis 53:158–163. https://doi.org/10.1093/ cid/cir340.
- Moise PA, Amodio-Groton M, Rashid M, Lamp KC, Hoffman-Roberts HL, Sakoulas G, Yoon MJ, Schweitzer S, Rastogi A. 2013. Multicenter evaluation of the clinical outcomes of daptomycin with and without concomitant beta-lactams in patients with Staphylococcus aureus bacteremia and mild to moderate renal impairment. Antimicrob Agents Chemother 57:1192–1200. https://doi.org/10.1128/AAC.02192-12.
- Jousselin A, Manzano C, Biette A, Reed P, Pinho M, Rosato A, Kelley WL, Renzoni A. 2015. The Staphylococcus aureus chaperone PrsA is a new auxiliary factor of oxacillin resistance affecting penicillin-binding protein 2A. Antimicrob Agents Chemother 60:1656–1666. https://doi.org/ 10.1128/AAC.02333-15.
- 14. Jousselin A, Renzoni A, Andrey DO, Monod A, Lew DP, Kelley WL. 2012. The posttranslocational chaperone lipoprotein PrsA is involved in both glycopeptide and oxacillin resistance in Staphylococcus aureus. Antimi-

- crob Agents Chemother 56:3629-3640. https://doi.org/10.1128/ AAC.06264-11.
- 15. Pillai DR, Melano R, Rawte P, Lo S, Tijet N, Fuksa M, Roda N, Farrell DJ, Krajden S. 2009. Klebsiella pneumoniae carbapenemase, Canada. Emerg Infect Dis 15:827-829. https://doi.org/10.3201/eid1505.081536
- 16. Samra Z, Ofir O, Lishtzinsky Y, Madar-Shapiro L, Bishara J. 2007. Outbreak of carbapenem-resistant Klebsiella pneumoniae producing KPC-3 in a tertiary medical centre in Israel. Int J Antimicrob Agents 30:525-529. https://doi.org/10.1016/j.ijantimicag.2007.07.024.
- 17. Bowker KE, Holt HA, Lewis RJ, Reeves DS, MacGowan AP. 1998. Comparative pharmacodynamics of meropenem using an in-vitro model to simulate once, twice and three times daily dosing in humans. J Antimicrob Chemother 42:461-467. https://doi.org/10.1093/jac/42.4.461.
- 18. Cahoon LA, Freitag NE. 2014. Listeria monocytogenes virulence factor secretion: don't leave the cell without a chaperone. Front Cell Infect Microbiol 4:13. https://doi.org/10.3389/fcimb.2014.00013.
- 19. Hachmann AB, Angert ER, Helmann JD. 2009. Genetic analysis of factors affecting susceptibility of Bacillus subtilis to daptomycin. Antimicrob Agents Chemother 53:1598-1609. https://doi.org/ 10.1128/AAC.01329-08.
- 20. Pogliano J, Pogliano N, Silverman JA. 2012. Daptomycin-mediated reorganization of membrane architecture causes mislocalization of essential cell division proteins. J Bacteriol 194:4494-4504. https://doi.org/ 10.1128/JB.00011-12.
- 21. Berti AD, Sakoulas G, Nizet V, Tewhey R, Rose WE. 2013. β -Lactam antibiotics targeting PBP1 selectively enhance daptomycin activity against methicillin-resistant Staphylococcus aureus. Antimicrob Agents Chemother 57:5005-5012. https://doi.org/10.1128/AAC.00594-13.
- 22. Berti AD, Theisen E, Sauer JD, Nonejuie P, Olson J, Pogliano J, Sakoulas G, Nizet V, Proctor RA, Rose WE. 2015. Penicillin binding protein 1 is important in the compensatory response of Staphylococcus aureus to daptomycin-induced membrane damage and is a potential target for β-lactam-daptomycin synergy. Antimicrob Agents Chemother 60: 451-458. https://doi.org/10.1128/AAC.02071-15.
- 23. Turner RD, Hurd AF, Cadby A, Hobbs JK, Foster SJ. 2013. Cell wall elongation mode in Gram-negative bacteria is determined by peptidoglycan architecture. Nat Commun 4:1496. https://doi.org/10.1038/ ncomms2503.
- 24. Turner RD, Ratcliffe EC, Wheeler R, Golestanian R, Hobbs JK, Foster SJ. 2010. Peptidoglycan architecture can specify division planes in Staphylococcus aureus. Nat Commun 1:26. https://doi.org/10.1038/ ncomms1025.
- 25. Pinho MG, Errington J. 2005. Recruitment of penicillin-binding protein PBP2 to the division site of Staphylococcus aureus is dependent on its transpeptidation substrates. Mol Microbiol 55:799-807. https://doi.org/ 10.1111/j.1365-2958.2004.04420.x.
- 26. Hyyrylainen HL, Pietiainen M, Lunden T, Ekman A, Gardemeister M, Murtomaki-Repo S, Antelmann H, Hecker M, Valmu L, Sarvas M, Kontinen VP. 2007. The density of negative charge in the cell wall influences two-component signal transduction in Bacillus subtilis. Microbiology 153:2126-2136. https://doi.org/10.1099/mic.0.2007/008680-0.
- 27. Stoll H, Dengjel J, Nerz C, Gotz F. 2005. Staphylococcus aureus deficient in lipidation of prelipoproteins is attenuated in growth and immune activation. Infect Immun 73:2411-2423. https://doi.org/10.1128/ IAI.73.4.2411-2423.2005.
- 28. Dubrac S, Boneca IG, Poupel O, Msadek T. 2007. New insights into the WalK/WalR (YycG/YycF) essential signal transduction pathway reveal a major role in controlling cell wall metabolism and biofilm formation in Staphylococcus aureus. J Bacteriol 189:8257-8269. https://doi.org/ 10.1128/JB.00645-07.
- 29. Julian K, Kosowska-Shick K, Whitener C, Roos M, Labischinski H, Rubio A, Parent L, Ednie L, Koeth L, Bogdanovich T, Appelbaum PC. 2007. Characterization of a daptomycin-nonsusceptible vancomycinintermediate Staphylococcus aureus strain in a patient with endocarditis. Antimicrob Agents Chemother 51:3445-3448. https:// doi.org/10.1128/AAC.00559-07.
- 30. Mangili A, Bica I, Snydman DR, Hamer DH. 2005. Daptomycin-resistant, methicillin-resistant Staphylococcus aureus bacteremia. Clin Infect Dis 40:1058-1060. https://doi.org/10.1086/428616.
- 31. Sieradzki K, Leski T, Dick J, Borio L, Tomasz A. 2003. Evolution of a vancomycin-intermediate Staphylococcus aureus strain in vivo: multiple changes in the antibiotic resistance phenotypes of a single lineage of

- methicillin-resistant S. aureus under the impact of antibiotics administered for chemotherapy. J Clin Microbiol 41:1687-1693. https://doi.org/ 10.1128/JCM.41.4.1687-1693.2003.
- 32. Sieradzki K, Tomasz A. 1999. Gradual alterations in cell wall structure and metabolism in vancomycin-resistant mutants of Staphylococcus aureus. J Bacteriol 181:7566-7570.
- 33. Severin A, Wu SW, Tabei K, Tomasz A. 2004. Penicillin-binding protein 2 is essential for expression of high-level vancomycin resistance and cell wall synthesis in vancomycin-resistant Staphylococcus aureus carrying the enterococcal vanA gene complex. Antimicrob Agents Chemother 48:4566-4573. https://doi.org/10.1128/AAC.48.12.4566-4573.2004.
- 34. Reed P, Atilano ML, Alves R, Hoiczyk E, Sher X, Reichmann NT, Pereira PM, Roemer T. Filipe SR. Pereira-Leal JB. Ligoxygakis P. Pinho MG. 2015. Staphylococcus aureus survives with a minimal peptidoglycan synthesis machine but sacrifices virulence and antibiotic resistance. PLoS Pathog 11:e1004891. https://doi.org/10.1371/journal.ppat.1004891.
- 35. Bayer AS, Schneider T, Sahl HG. 2013. Mechanisms of daptomycin resistance in Staphylococcus aureus: role of the cell membrane and cell wall. Ann N Y Acad Sci 1277:139-158. https://doi.org/10.1111/j.1749 -6632.2012.06819.x.
- 36. Kuhn S, Slavetinsky CJ, Peschel A. 2015. Synthesis and function of phospholipids in Staphylococcus aureus. Int J Med Microbiol 305: 196-202. https://doi.org/10.1016/j.ijmm.2014.12.016.
- 37. Hutchings MI, Palmer T, Harrington DJ, Sutcliffe IC. 2009. Lipoprotein biogenesis in Gram-positive bacteria: knowing when to hold 'em, knowing when to fold 'em. Trends Microbiol 17:13-21. https://doi.org/ 10.1016/j.tim.2008.10.001.
- 38. Sankaran K, Wu HC. 1994. Lipid modification of bacterial prolipoprotein. Transfer of diacylglyceryl moiety from phosphatidylglycerol. J Biol Chem 269:19701-19706.
- 39. Qi HY, Sankaran K, Gan K, Wu HC. 1995. Structure-function relationship of bacterial prolipoprotein diacylglyceryl transferase: functionally significant conserved regions. J Bacteriol 177:6820-6824.
- 40. Mao G, Zhao Y, Kang X, Li Z, Zhang Y, Wang X, Sun F, Sankaran K, Zhang XC. 2016. Crystal structure of E. coli lipoprotein diacylglyceryl transferase. Nat Commun 7:10198. https://doi.org/10.1038/ncomms10198.
- 41. Dumoulin A, Grauschopf U, Bischoff M, Thony-Meyer L, Berger-Bachi B. 2005. Staphylococcus aureus DsbA is a membrane-bound lipoprotein with thiol-disulfide oxidoreductase activity. Arch Microbiol 184:117-128. https://doi.org/10.1007/s00203-005-0024-1.
- 42. Davlieva M, Shi Y, Leonard PG, Johnson TA, Zianni MR, Arias CA, Ladbury JE, Shamoo Y. 2015. A variable DNA recognition site organization establishes the LiaR-mediated cell envelope stress response of enterococci to daptomycin. Nucleic Acids Res 43:4758-4773. https://doi.org/10.1093/ nar/gkv321.
- 43. Munita JM, Panesso D, Diaz L, Tran TT, Reyes J, Wanger A, Murray BE, Arias CA. 2012. Correlation between mutations in liaFSR of Enterococcus faecium and MIC of daptomycin: revisiting daptomycin breakpoints. Antimicrob Agents Chemother 56:4354-4359. https://doi.org/10.1128/ AAC.00509-12.
- 44. Sakoulas G, Nonejuie P, Nizet V, Pogliano J, Crum-Cianflone N, Haddad F. 2013. Treatment of high-level gentamicin-resistant Enterococcus faecalis endocarditis with daptomycin plus ceftaroline. Antimicrob Agents Chemother 57:4042-4045. https://doi.org/10.1128/ AAC.02481-12.
- 45. Mascher T, Helmann JD, Unden G. 2006. Stimulus perception in bacterial signal-transducing histidine kinases. Microbiol Mol Biol Rev 70:910-938. https://doi.org/10.1128/MMBR.00020-06.
- 46. Clinical and Laboratory Standards Institute. 2007. Performance standards for antimicrobial disk susceptibility tests, 8th ed. Approved standard M2-A8. Clinical and Laboratory Standards Institute, Wayne, PA.
- 47. Hebert L, Courtin P, Torelli R, Sanguinetti M, Chapot-Chartier MP, Auffray Y, Benachour A. 2007. Enterococcus faecalis constitutes an unusual bacterial model in lysozyme resistance. Infect Immun 75:5390-5398. https://doi.org/10.1128/IAI.00571-07.
- 48. de Jonge BL, Chang YS, Gage D, Tomasz A. 1992. Peptidoglycan composition of a highly methicillin-resistant Staphylococcus aureus strain. The role of penicillin binding protein 2A. J Biol Chem 267:11248-11254.
- 49. Boyle-Vavra S, Yin S, Daum RS. 2006. The VraS/VraR two-component regulatory system required for oxacillin resistance in communityacquired methicillin-resistant Staphylococcus aureus. FEMS Microbiol Lett 262:163-171. https://doi.org/10.1111/j.1574-6968.2006.00384.x.

2.2 Understanding antibiotic-induced dormancy in Staphylococcus aureus

2.2.1 Insights into the global effect on *Staphylococcus aureus* growth arrest by induction of the endoribonuclease MazF toxin

(Nucleic Acids Research 2020 48:8545-8561)

The state of growth arrest plays a pivotal role in the bacterial survival strategy to avoid killing by antibiotics. Exposure to lethal concentrations of antibiotics reveals killing of growing bacterial cells, while highlighting the survival of a non-growing subpopulation, which remains genetically susceptible. The antibiotic tolerance observed in these non-growing survival cells is explained by the inactive state of antibiotic targets rather than by heritable genetic mutations. Following the removal of antibiotics, these non-growing cells resume growth, but upon re-exposure to antibiotics, the majority of the population faces again antibiotic killing. This ability of non-growing cells to survive antibiotics may explain the clinical occurrence of bacterial chronic and relapsing infections despite antibiotic treatment. Consequently, there is an urgent nned to understand the molecular pathways leading to emergence of this non-growing bacterial state.

In several bacterila species, the non-growing state has been associated to bacterial toxinantitoxins systems, such as MazEF. Under normal growth conditions, MazF toxin activity is inhibited by a stoichiometric complex formed with the MazE antitoxin. Upon stressed conditions, cellular proteases degrade MazE, thereby liberating MazF toxin endoribonucleolytic activity. This activity induces growth arrest by specifically cleaving single stranded RNA molecules (ssRNA). In *S. aureus*, overexpression of MazF induces stasis or non-growing state, although the precise mechanism behind this phenomenon remaisn elusive.

By genetic and cell cytometry analysis our study reveals that MazF overexpression in the absence of MazE antitoxin induces growth arrest, where bacteria remain alive but do not divide. Flow cytometry enables quantification of cell viability, demonstrating no difference in the percentage of live or dead bacteria after MazF induction, regardless of the presence or absence of MazE antitoxin. These measurements of live/dead are in sharp contrast with the absence of bacterial colony counts on agar plates (Figure 5). This analysis indicates that after MazF induction, bacteria continue to survive but are unable to divide, leading to a reduced colony growth on agar plates.

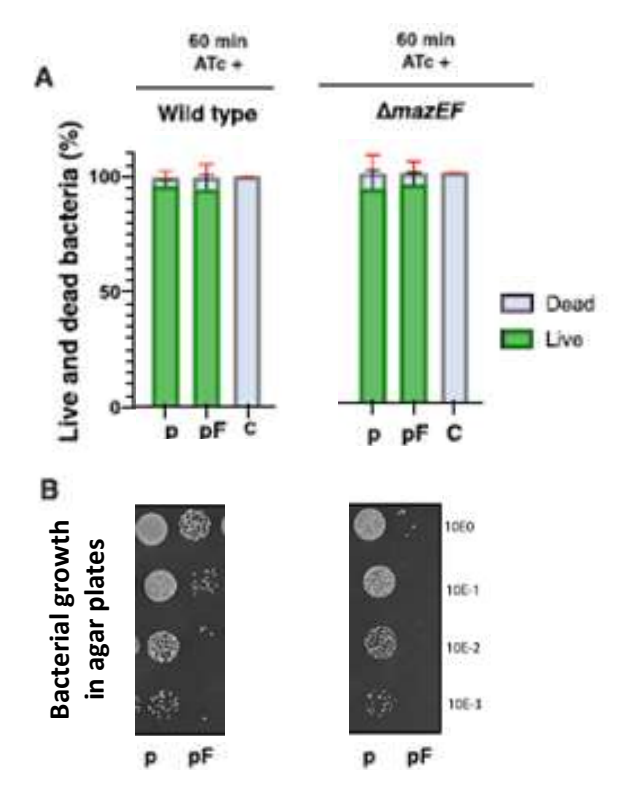


Figure 5. Details extracted from figure 2 of the manuscript, corresponding to cell cytometry analysis showing the percentage of live and dead bacteria present after mazF overexpression and the corresponding analysis of bacterial growth on agar plates. (A) S. aureus wild-type and mazEFdeleted strains carrying a control (p) or mazF (pF) plasmid were subject to ATc induction during 60 min, labeled using RedoxSensorGreen (specific marker for alive bacteria) and propidium iodide (specific marker for dead bacteria). Live and dead bacterial counts were determined fluorescence detection using cell cytometry. Fluorescence detection of heat-killed bacteria was used as a control (c). The percentage of live or dead bacteria from a total of 50 000 bacterial counts is reported. Data is represented as mean ± SD of three independent experiments. B) Bacterial growth of sorted live bacteria after mazF overexpression. Bacteria treated as in A, were sorted using the cell cytometer to obtain 8×10^5 live cells and were further serially diluted (top to bottom 10^0 to 10^{-3}), 10 ul of diluted bacteria were immediately spot-inoculated on Mueller-Hinton agar plates.

To determine the molecular link between *mazF* overexpression and growth arrest, we

initially identified MazF-cleaved targets on a genome-wide scale using nEMOTE technique (Figure 6). The nEMOTE procedure detects toxin endoribonuclease cleavages that produces 5'-OH transcript ends within the native host. The 5'-OH transcripts-ends and the resulting library was sequenced and analysed to identify the exact MazF cleavage motif and the ssRNA molecules subjected to MazF cleavage. Our findings revealed an extended and variable sequence recognized by MazF that goes beyond the canonical UACAU motif.

By RNA-seq we corroborate nEMOTE cleavage sites (**Figure 7**). Accordingly, an integrated analysis of transcriptomic regions containing MazF sites detected by nEMOTE, shows that 500 bp preciding the cleavage site, there is no discernible changes in read counts between strain expressing or not MazF. However, while approaching the MazF cleavage site (Figure 7, black line), a clear reduction in read counts are observed. In contrast, no decrease in read counts was observed in genomic regions lacking MazF cleavage sites (Figure 7, Blue line). The identification by nEMOTE of MazF cleaved targets allow us to propose the involvement of genes linked to ribosome biogenesis, cell wall synthesis, cell division and RNA turnover as MazF targets, providing a potential explanation to toxin-mediated growth arrest (**Figure 8**).

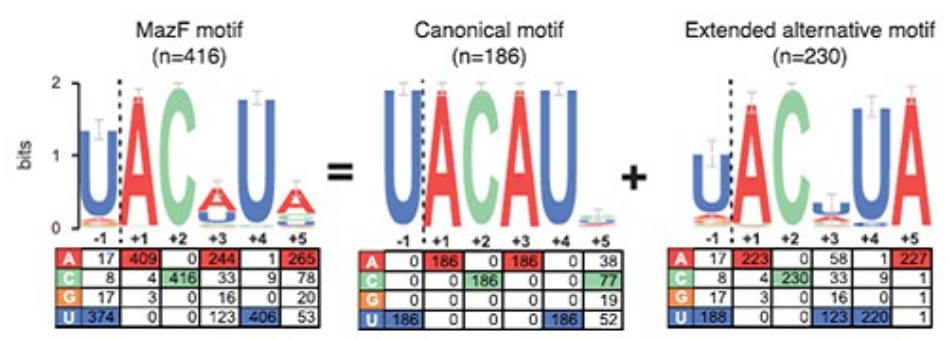


Figure 6. Logo plot showing MazF recognized abd cleaved RNA motif, obtained from the alignment of 416 MazF cleaved sites detected by nEMOTE. We propose this new MazF motif, based on a canonical sequence (N=186) previously proposed and an extended alternative motif (N=230). The base frequencies at each position are shown in tables below each logo plot.

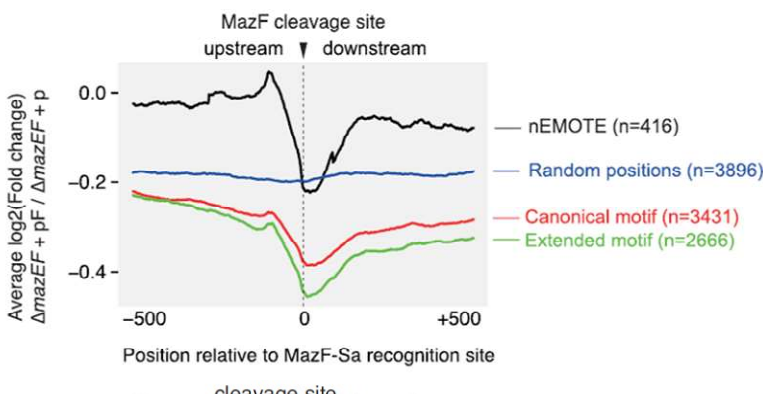
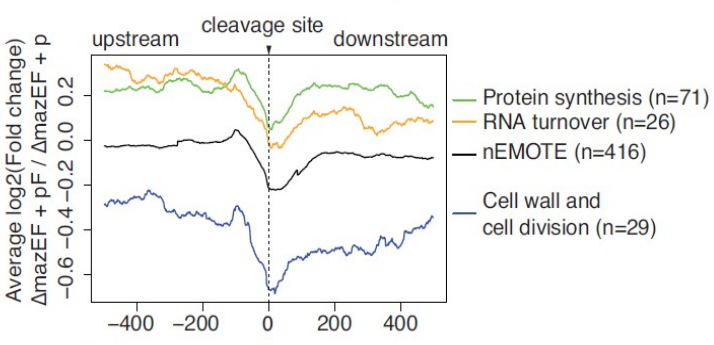


Figure 7. RNA-seq read coverage profiles 500bp before and after the nEMOTE-detected sites between mazEF-deleted strains overexpressing or not MazF toxin.



Position relative to MazF recognition site

Figure 8. RNA-seq read coverage profiles 500 bp before and after the nEMOTE-detected sites of genes involved in protein synthesis, RNA turnover, cell wall and cell division between MazEF-deleted strains overexpessing or not MazF toxin.

In Conclusion: we identified transcripts cleaved in vivo by MazF, establishing a direct association with growth stasis. We proposed a novel extended MazF cleavage site beyond the canonical known UACAU motif. The identification of numerous precise MazF cleavage sites now provides a snapshot of the extensive collection of genes impacted by the MazF endoribonuclease. This knowledge culminates in a more refined model elucidating the mechanism behind toxin-mediated growth arrest (Sierra, Viollier, and Renzoni 2018; Sierra et al. 2020).

Insights into the global effect on *Staphylococcus* aureus growth arrest by induction of the endoribonuclease MazF toxin

Roberto Sierra ^{1,2,*}, Julien Prados ², Olesya O. Panasenko ¹, Diego O. Andrey^{1,2}, Betty Fleuchot², Peter Redder³, William L. Kelley², Patrick H. Viollier ² and Adriana Renzoni^{1,2,*}

¹Service of Infectious Diseases, Department of Medical Specialties, Geneva University Hospitals and Medical School, Geneva 1211, Switzerland, ²Department of Microbiology and Molecular Medicine, University of Geneva, Geneva 1211, Switzerland and ³Centre de Biologie Intégrative, Université de Toulouse III, Toulouse 31400, France

Received February 18, 2020; Revised June 18, 2020; Editorial Decision July 09, 2020; Accepted July 27, 2020

ABSTRACT

A crucial bacterial strategy to avoid killing by antibiotics is to enter a growth arrested state, yet the molecular mechanisms behind this process remain elusive. The conditional overexpression of mazF, the endoribonuclease toxin of the MazEF toxin-antitoxin system in Staphylococcus aureus, is one approach to induce bacterial growth arrest, but its targets remain largely unknown. We used overexpression of mazF and high-throughput sequence analysis following the exact mapping of non-phosphorylated transcriptome ends (nEMOTE) technique to reveal in vivo toxin cleavage sites on a global scale. We obtained a catalogue of MazF cleavage sites and unearthed an extended MazF cleavage specificity that goes beyond the previously reported one. We correlated transcript cleavage and abundance in a global transcriptomic profiling during mazF overexpression. We observed that MazF affects RNA molecules involved in ribosome biogenesis, cell wall synthesis, cell division and RNA turnover and thus deliver a plausible explanation for how mazF overexpression induces stasis. We hypothesize that autoregulation of MazF occurs by directly modulating the MazEF operon, such as the rsbUVW genes that regulate the sigma factor SigB, including an observed cleavage site on the MazF mRNA that would ultimately play a role in entry and exit from bacterial stasis.

INTRODUCTION

The occurrence of antibiotic resistant bacteria is reaching worrying proportions and it is especially disturbing that the number of new antibiotics that reach the market is diminishing. Understanding how bacteria avoid killing by antibiotics will contribute to future development of new antimicrobial drugs. Notably, one mechanism that was observed decades ago and still remains poorly understood relates to avoidance of killing by antibiotics (1) wherein exposure to lethal concentrations of an antibiotic reveals the survival of a bacterial subpopulation which nevertheless remains genetically susceptible. Upon drug exposure, most of the growing cells in the bacterial population will be rapidly killed by the antibiotic and the remaining fraction of non-growing cells will survive because of a slowed-down metabolism within these cells (2).

Antibiotic tolerance in non-growing cells is explained by the inactive state of antibiotic targets and their associated biological processes and not by heritable genetic mutations of the bacterial population. In fact, upon antibiotic removal, non-growing cells regrow and re-exposure to antibiotics leads again to a rapid killing of the majority of the bacteria population (2–4). The antibiotic tolerance in nongrowing bacteria may explain the clinical occurrence of bacterial chronic and relapsing infections, which emphasizes the urgent need to better understand the molecular pathways leading to the development of this state (5).

The bacterial non-growing state has been linked in some studies to expression of toxin-antitoxin systems (TAS) in various organisms that interferes with replication (6,7), ribosomal activity (8), cell wall synthesis (9) and cell division (10). However, the role of TAS on antibiotic tolerance in non-growing bacteria is still debated (11). One of the best characterized TAS inducing bacterial growth ar-

^{*}To whom correspondence should be addressed. Tel: +41 22 372 40 79; Email: Adriana.Renzoni@hcuge.ch Correspondence may also be addressed to Roberto Sierra. Email: Roberto.Sierra@me.com

rest is MazEF. Homologs of this type II TAS operon are found in clinically important bacteria such as *Escherichia coli, Mycobacterium tuberculosis* and *Staphylococcus aureus*. MazF toxin activity is inhibited by a stoichiometric complex formed with the MazE antitoxin during normal growth conditions. Upon stressed conditions, MazE is degraded by cellular proteases, thereby liberating MazF toxin endoribonucleolytic activity that induces a growth arrest (11). In *E. coli* and *M. tuberculosis*, MazF specifically cleaves single-stranded RNA molecules and the identification of specific cleaved targets has led to a model, that MazF activity reduces overall translation and consequently inhibits bacterial growth (12–16). Unless otherwise stated, MazF in this study refers to the *S. aureus* toxin.

To understand the general function of MazEF in S. aureus, several studies first focused on the regulation of MazEF expression. The mazEF gene is chromosomally encoded and located upstream and co-transcribed with the sigB operon that encodes for the alternative stress sigma factor $B(\sigma^B)$ and its regulators RsbUVW. MazEF transcription is activated by sub-inhibitory concentrations of ervthromycin and tetracycline and it is regulated negatively and positively by the transcriptional regulator σ^B and SarA, respectively. Its cognate antitoxin MazE is regulated by proteolysis through ClpCP proteolytic complex primed with the adaptor protein TrfA (17,18) (Figure 5B). In vitro analysis of MazF cleavage activity on an exogeneous transcript, found that MazF toxin is a sequence-specific endoribonuclease that recognizes the pentad sequence U^ACAU (^ indicates MazF cleavage site) of mRNAs and cleaves independently of ribosomes (19,20). The MazF cleavage motif was further used to predict MazF target genes. A link between MazEF and virulence was proposed based on the identification and in vitro cleavage of selected virulence genes such as hla (α -hemolysin), spa (Protein A virulence factor), σ^B and sraP (adhesion factor) (19,21). MazF expression was also shown to inhibit biofilm formation and to increase antibiotic tolerance allowing transition of S. aureus from acute to chronic infections (22).

In *S. aureus*, stasis is induced upon overexpression of MazF toxin (21,23), yet whether transcripts are cleaved *in vivo* to prevent growth and which ones are targeted preferentially is still unknown. Bioinformatic prediction of targets based on the MazF pentad recognition sequence is not feasible since this motif is found across the genome. In this study, we have used a genome-wide high-throughput method to identify *bona fide* MazF targets *in vivo* and identified an extended and variable, but robust sequence recognition specificity beyond the canonical UACAU motif for MazF RNA cleavage. The identification of hundreds of precise cleavage sites now provides a snapshot of the extensive collection of genes affected by the MazF endoribonuclease and permits a refined model explaining toxin-mediated growth arrest.

MATERIALS AND METHODS

Induction of *mazF* and growth arrest

The pRAB11-mazF plasmid (AR1880), expressing mazF under control of an anhydrotetracycline (ATc) inducible promoter was constructed by amplification of *S. aureus*

HG003 *mazF* using primers carrying BgIII and EcoRI restriction sites (Supplementary Table S1). The amplified product was cut with BgIII and EcoRI and ligated the into pRAB11 (24). To induce the expression of MazF, ATc was added at a final concentration of 0.2 μM to the cell cultures and incubated for 10–60 min at 37°C with shaking. ATc was freshly prepared and aliquoted since aged ATc was found in pilot experiments to produce toxic breakdown products, which affected interpretation of viability assays.

S. aureus HG003 (RS123) and S. aureus HG003 ΔmazEF (RS125) were electroporated with ATc inducible pRAB11 (RS212, RS191) and pRAB11-mazF (RS124, RS126). Strains carrying pRAB11 were always grown in presence of chloramphenicol (15 μg/ml). Overnight cultures were diluted 1:1000 in 10 ml of Mueller–Hinton broth (Difco) and incubated at 37°C with shaking. At OD₆₀₀ 0.3, ATc was added at a final concentration of 0.2 μM. At each time point (0, 15, 30, 60 min post-induction) the samples were 10-fold serially diluted in 96-well plates using sterile saline solution (0.9% NaCl) and 10 μl aliquots were spot-inoculated in Mueller–Hinton agar plates and incubated at 37°C overnight. Colonies were then counted.

MazF antibody production

The mazE antitoxin gene fused to its cognate toxin gene (i.e. the *mazEF* genes) was PCR amplified using a synthetic fragment as template (IDT company; Supplementary Table S1). The resulting fragment was digested by NdeI/ScaI and ligated into the expression vector pCWR547 (25) digested by the same restriction enzymes. The resulting plasmids were used to transform competent E. coli strains. All the constructions were verified by PCR and validated by sequencing. His6-SUMO-MazEF proteins were expressed from pCWR547 in E. coli C41 (DE3) strain and purified under standard native conditions using nickel chelate chromatography. The proteins were then excised from a 15% SDS polyacrylamide gel to immunize rabbits (Josman LLC, Napa, CA, USA). Polyclonal antibodies were obtained and used for MazF western blot analysis at a dilution of 1:2500 and revealed by HRP-conjugated goat-anti-rabbit secondary antibodies.

Protein extraction

Cells cultures were grown until exponential phase (O.D₆₀₀ 0.4–0.8). The induction of the MazF expression by ATc was performed for 10-60 min, as needed. Cultures of 10 ml with OD₆₀₀ of 2-4 were collected and washed three times with 1 ml of phosphate-buffered saline (PBS). Cells were lysed in the presence of lysis buffer (LB) (PBS, 200 μg/ml lysostaphin, 200 μg/ml DNase I, protease inhibitors (Roche) 20 µl per 1 OD unit for 20 min at 37°C). Samples were chilled on ice, and sonicated 10 times with 30-s cycles using Cell Disrupter B-30 (Branson). Extracts were clarified by centrifugation for 10 min at $14\,000 \times g$ at 4° C. Total protein concentration was measured in supernatants by the Bradford protein assay. Samples were mixed with Laemmli sample buffer and analyzed by SDS polyacrylamide gel electrophoresis (SDS-PAGE) 16.5% tris-tricine peptide gels (BioRad). Gels were analyzed further by western blot using polyclonal antibodies described above.

RNA extractions for nEMOTE and RNA-seq

Overnight cultures were diluted 1:50 in 20 ml of Mueller–Hinton broth and incubated at 37°C without shaking until OD₆₀₀ 0.3. ATc was added to a final concentration of 0.2 μ M and incubated at 37°C during 10 min. Aliquots of 8 ml of bacterial culture were immediately transferred to 40 ml of ice-cold ethanol:acetone (1:1), and centrifugated at 5000 rpm and 4°C during 10 min. The supernatant was discarded, and pellet was washed with 1× TE. The pelleted cells were treated with lysostaphin (200 μ g/ml) and RNasin Plus (Promega) in a final volume of 100 μ l TE then placed in a heat block at 37°C during 10 min. RNA extractions were done on the same day using the ReliaPrep (Promega) following the manufacturer's instructions. Total RNA was frozen and kept at -80°C.

nEMOTE library preparation and sequencing

RNA was quantified using a Nanodrop 1000 and integrity was assessed with a Bioanalyzer (Agilent Technologies). The nEMOTE protocol was employed as in Kirkpatrick, 2016 (26–28). Briefly, mono-phosphorylated RNA was digested from 8 µg of high-quality total RNA with XRN-1 (New England Biolabs). XRN-1 was removed with a phenol-chloroform-isoamyl alcohol 25:24:1 (Sigma) extraction, and the aqueous phase was recovered using MaXtract High Density (Qiagen) tubes. The recovered RNA was split into two pools, one pool was treated with T4 polynucleotide kinase (+PNK) and the other was subject to the same treatment without PNK (-PNK) and used to establish a background signal. Rp6 RNA oligonucleotide was ligated with T4 RNAse ligase to the 5'phosphorylated RNA followed by an ethanol precipitation. Reverse transcription was carried out using semi-random primer DROAA and the cDNA was purified using Wizard SV Gel and PCR clean-up system (Supplementary Table S1) (Promega). Second-strand synthesis and barcode incorporation (D6A-D6O barcodes) were performed using O5 Hot Start High Fidelity DNA polymerase (New England Biolabs). The PCR products were purified (Oiagen PCR clean-up columns), mixed and size-selected between 300 and 1000 bp on agarose gels. The sample was then quantified by fluorometry using Qubit (Invitrogene) and sequenced in an Illumina HiSeq 2500 sequencer using 50 bp single-read cycle. Two independent replicates were performed.

RNA-seq library preparation and sequencing

Total RNA was quantified using Qubit (Life Technologies) and RNA integrity was assessed with a Bioanalyzer (Agilent Technologies). Total RNA (1 μ g) was ribo-depleted with the bacterial Ribo-Zero kit from Illumina. The Truseq total RNA stranded kit from Illumina was used for the library preparation. Library quantity was measured by the Qubit and quality was assessed with a Tapestation on a DNA High sensitivity chip (Agilent Technologies). Libraries were pooled at equimolarity for clustering. Single-read sequencing (100 bases) was performed using the SBS chemistry on an Illumina HiSeq 4000 sequencer.

Bioinformatic analysis of nEMOTE, RNA-seq and annotation of targets

The nEMOTE reads were processed with the R package EMOTE v0.2 (https://github.com/pradosj/EMOTE). This package checks the quality of reads and parses them to extract the mapping sequence as well as the unique molecular identifier (UMI) sequence; it then aligns the reads to the reference genome S. aureus NCTC 8325-4 (with Rbowtie package) and quantifies the number of reads with the unique UMI starting at each genomic position. The genomic positions with less than 4 UMI in both ΔmazEF pRAB11mazF+PNK replicates used, were not further considered. A beta-binomial model was then used to estimate the probability that +PNK condition is significantly enriched compared to the corresponding -PNK control condition (background noise removal). The P-values obtained for the two replicates are combined with Fisher's method, and the false discovery rate (FDR) computed to correct for multiple testing. To determine confident 5'-OH ends generated by MazF, each genomic position had to match the following criteria: an FDR <0.1 for $\triangle mazEF$ pRAB11-mazF condition, and an FDR >0.1 in $\triangle mazEF$ condition. Genomic positions mapping onto a rRNA feature were excluded. rRNA cleavage site analysis was performed separately with single rRNA sequences to avoid multiple mapping sites. The MazF cleavages were further annotated with genomic information (DNA sequence around the position, nearest gene), taken from both NCBI and Aureowiki (https://aureowiki. med.uni-greifwald.de/) (29).

The functional characteristics of the MazF-affected genes were obtained by mapping the cleavage sites to genes on the reference genome and performing gene ontology (GO) enrichment analysis using in-house scripts written in R programming language. The script retrieves GO terms annotations from Uniprot for the reference organism STAA8. Then, ancestors of the GO terms were inferred using « is_a » and « part_of » relationships of the ontology go-basic.obo available at http://geneontology.org. The analysis was corrected by identifying the GOs that are enriched in genes containing a MazF cleavage relatively to the 1000 most expressed genes on the genome. A hypergeometric test is performed to determine if a given GO term is enriched in the 260 MazF-affected genes out of the 1000 most expressed genes.

RNA-seq reads 500 bp before and after an nEMOTE-detected site were aligned on the reference genome with 'bwa mem' command and 'samtools' to generate files in BAM format. The BAM files are further processed to quantify the number of read in genes with the method 'summarizeOverlaps(mode = 'IntersectionStrict',inter.feature = FALSE)' from R package GenomicAlignments. Quantification around the cleavage sites were obtained with the method 'coverage()' of the R package 'GenomicAlignments'.

Flow cytometry to determine dead and alive bacterial cells

Cell preparation was as above for nEMOTE and RNA-seq protocols. At 10 min postinduction, the cultures were centrifuged, and the pellet was washed three times with 0.2

 μ m filtered 1× PBS. Cells were standardized to McFarland 0.5 (1.5 × 10⁸ CFU/ml) using a Densimat apparatus (bioMérieux) then diluted 1:100 in 1× PBS. The cells were stained using the *Bac*Light RedoxSensor Green Vitality Kit (Invitrogen) following the manufacturer's instructions. Dead (propidium iodide permeable) and alive cells (positive for bacterial reductase activity) were then counted on a Gallios flow cytometer (Beckman Coulter). Results were analyzed using FlowJo v. 10.6.1 software.

Cell sorting of living bacterial cells

To purify live cells, we used the same cell preparation as above but using a MoFlo Astrios (Beckman–Coulter) cell sorter. Purified live cells were spot inoculated on Mueller Hinton agar plates. In parallel, an equal volume of 2× Mueller-Hinton broth and 10× the ciprofloxacin minimum inhibitory concentration (5 μg/ml) was added to live sorted cells and incubated at 37°C overnight (18 h) without shaking. Cells were then centrifuged at 8000 rpm for 3 min, supernatant was discarded, and cells were washed three times using filtered $1 \times PBS$. Cells were stained again using the BacLight RedoxSensor Green Vitality Kit and dead and live cells were quantified on a Gallios flow cytometer. Results were analyzed using FlowJo v. 10.6.1 software. Significant difference between the strain carrying the empty plasmid (p) and the strain carrying the mazF-plasmid (pF) was analyzed using one-tailed, paired Student's t-test.

RNA extractions for qRT-PCR

Cells (1 ml) were collected at OD_{600} 0.3, centrifuged for 3 min at 8000 rpm, supernatant was discarded, and the pellet was washed with 1 ml 1× TE buffer. The pellet was resuspended in 100 μ l lysostaphin buffer composed of 200 μ g/ml lysostaphin, 200 μ g/ml DNase I, 40 U RNasin Plus Ribonuclease inhibitor (Promega) in 1× TE buffer and placed at 37°C for 10 min. RNA was then extracted using RNeasy Plus Mini Kit (Qiagen) following the manufacturer's instructions and adding two modifications: cell homogenization was performed with QIAshredder (Qiagen) columns after adding RTL Plus lysis buffer and DNase treatment using RNase-Free DNase Set (Qiagen) was applied after the first column wash.

Quantitative reverse transcription PCR (qRT-PCR)

Primers and probes were designed using PrimerExpress software (Applied Biosystems) and obtained from Eurogentec. Absence of DNA contamination in total RNA extractions was assessed by qPCR using $2\times$ Takyon probe assay (Eurogentec). Optimal concentration of primers and TaqMan® hydrolysis probes was assessed by using 4 ng of total RNA per well and a final concentration of primers of probes between 0.05 and 0.2 μ M to determine an efficiency of 100% (amplification factor of 2). mRNA levels of each gene were determined by quantitative reverse transcription PCR (qRT-PCR) using the Platinum qRT-PCR Thermo-Script One-Step system (Invitrogen). The mRNA levels of each gene were normalized to gyrB RNA levels, which were assayed in each round of qRT-PCR as internal controls.

To quantify qRT-PCR data the $2^{-\Delta\Delta Ct}$ method was used (30), where fold change of target gene expression in a target (treated) samples relative to a reference (non-treated) samples was normalized to the reference gene gyrB. Thus, the relative gene expression in non-treated samples was set to 1. The errors for the $\Delta\Delta Ct$ were obtained by least square error propagation of the standard deviation for the individual qRT-PCR measurements performed in triplicates. The statistical significance of strain-specific differences in normalized cycle threshold (C_T) values of each transcript was evaluated by paired Student's t-test, and data were considered significant when P was <0.05.

RESULTS

Effect of mazF overexpression on S. aureus growth

To identify sites targeted and cleaved by MazF endoribonuclease in vivo, we applied conditional overexpression of MazF toxin in S. aureus. We first confirmed that our MazF expression plasmid induces the characteristic growth defect observed upon mazF overexpression in S. aureus (21). Since MazF toxin activity is mitigated in the presence of MazE antitoxin, we analyzed the effect of mazF overexpression in the presence and absence of MazE antitoxin using wildtype, trfA-deleted (a condition previously shown to stabilize MazE antitoxin by reducing its proteolytic turnover (17)) or mazEF-deleted strains (20). All strains were transformed with a tightly regulated anhydrotetracycline (ATc) inducible plasmid carrying MazF toxin gene (pF) (Supplementary Table S2) and western blot analysis confirmed MazF protein (13.4 kDa) upon ATc induction (Figure 1A). In control strains lacking pF plasmid, MazF was not detected in the mazEF-deleted strain while MazF was detected at low levels in both the wild-type and trfA-deleted strain (as expected easily observed upon over-exposure of the immunoblot detection system, Supplementary Figure S1).

We observed a decrease in bacterial colony counts (efficiency of plating) at different time points after *mazF* overexpression (Figure 1B and C). This effect was enhanced in the absence of MazE antitoxin. Stabilization of MazE antitoxin through deletion of the ClpCP adaptor protein TrfA abolished the growth defect caused by the induction of MazF expression and restored colony formation comparable to wild-type control strain (Figure 1B and C). Collectively, these results show that MazF can be conditionally expressed and such cells show reduced ability to form colonies on agar plates in accordance with Fu *et al.* (21).

To further analyze the effect of *mazF* overexpression on growth, bacterial populations with and without *mazF* induction and in the presence (wild-type) and absence of MazE antitoxin (*mazEF*-deleted strain) were analyzed by flow cytometry to quantify cell viability. Interestingly, no difference in the percentage of live (RedoxSensorGreen labeled) or dead (propidium iodide labeled) bacteria was observed after 30 or 60 min of MazF induction in either the presence or absence of MazE antitoxin (Figure 2A). In all conditions tested, we counted 50 000 cells and detected overall 95% live and 5% dead bacteria. These live/dead measurements are in sharp contrast with the absence of detectable bacterial colony counts observed after 30 or 60 min

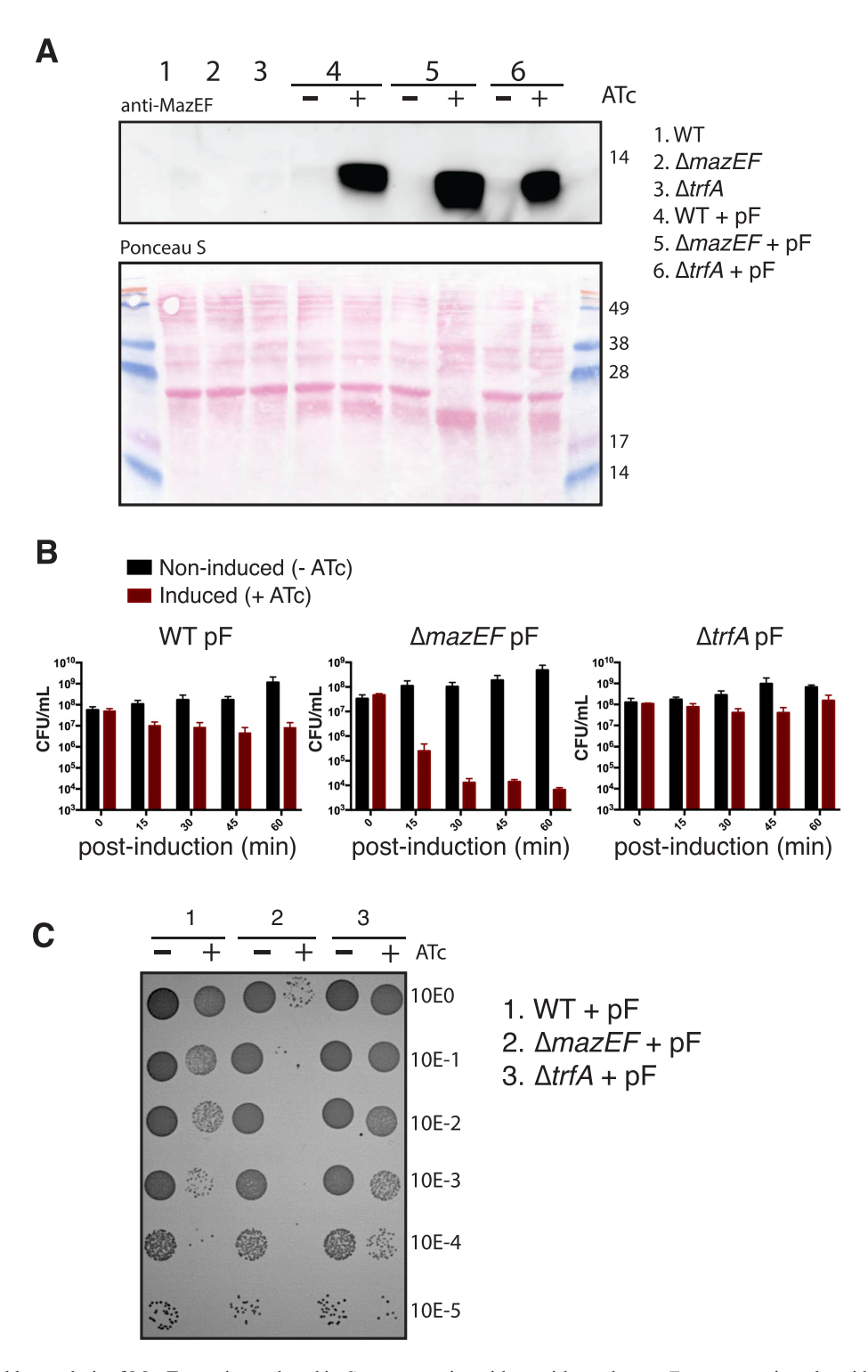


Figure 1. (A) Western blot analysis of MazF protein produced in *S. aureus* strains with or without the *mazF* overexpression plasmid (pF). After *mazF* gene induction with anhydrotetracycline (+ATc) or in non-induced cells (-ATc), total soluble protein extracts from *S. aureus* strains were loaded in SDS 16.5% polyacrylamide gels and MazF protein (13.4 kDa) was detected using a rabbit-polyclonal anti-MazEF antibody (top) and Ponceau S staining (bottom). A Coomassie Brilliant Blue stain on same samples loaded above is shown in Supplementary Figure S2. (B) Effect of *mazF* overexpression on *S. aureus* strains. Colony forming units (CFU) counts at five time points (between 0 and 60 min) after *mazF*-induced (+ATc) or uninduced (-ATc) *S. aureus* strains. Data are represented as mean ± SD of three independent experiments. (C) Representative image showing the spot (10 µl) serial dilutions of bacterial cultures on agar plates, after 60 min of *mazF*-induced (+ATc) and uninduced (-ATc) *S. aureus* strains. Serial dilutions are indicated at the right margin. CFU counts of *S. aureus* carrying an empty vector with and without ATc is shown in Supplementary Figure S3.

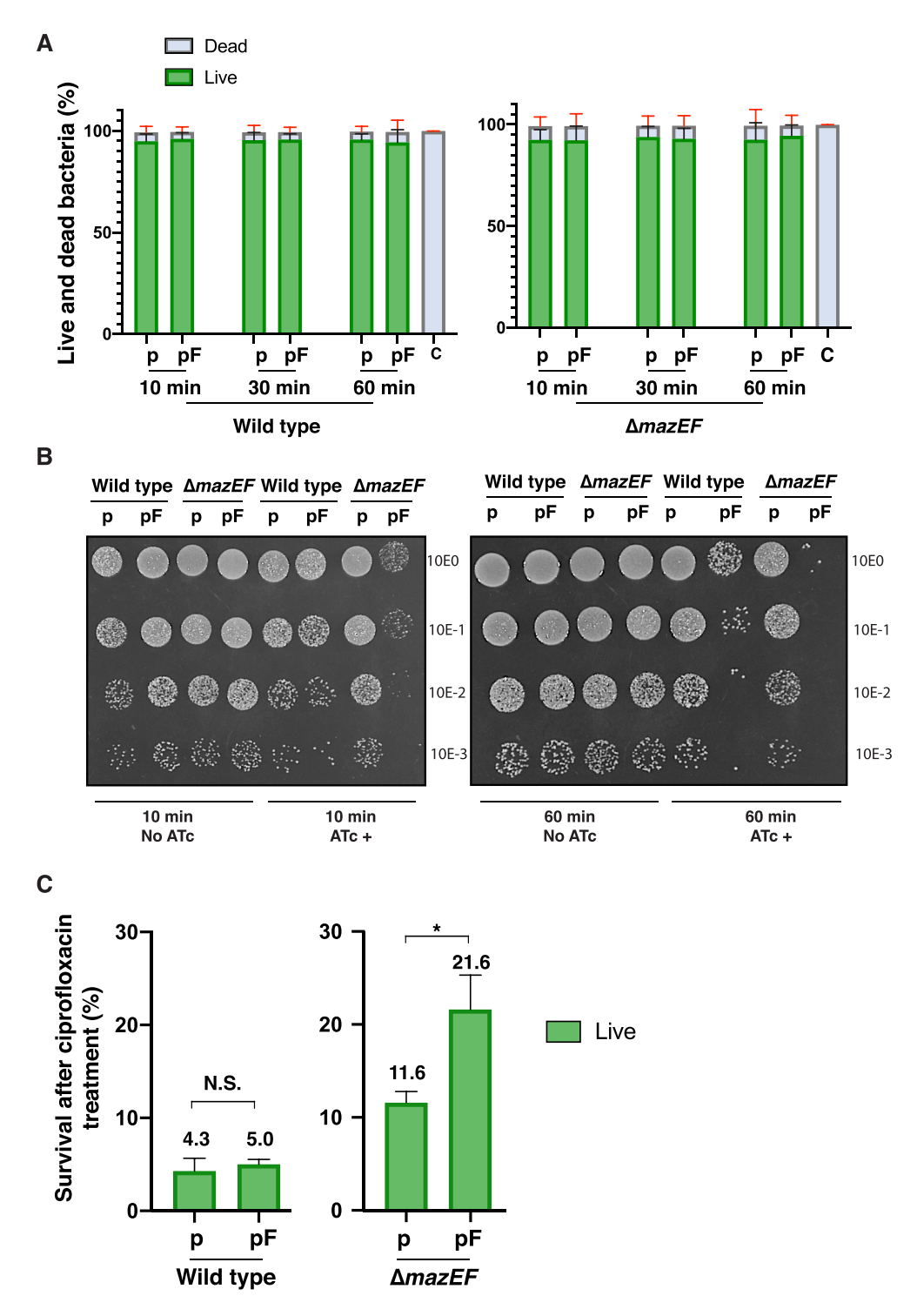


Figure 2. (A) Cell cytometry analysis showing the percentage of live and dead bacteria present after mazF overexpression. S. aureus wild-type and mazEF deleted strains carrying a control (p) or mazF (pF) plasmid were subject to ATc induction during time. Bacteria were subsequently labeled using RedoxSensorGreen and propidium iodide. Live and dead bacterial counts were determined by fluorescence detection using cell cytometry. Fluorescence detection of heat-killed bacteria was used as a control (c). The percentage of live or dead bacteria from a total of 50 000 bacterial counts is reported. Data is represented as mean \pm SD of three independent experiments. (B) Bacterial growth of sorted live bacteria after mazF overexpression. Wild-type and mazEF-deleted strains carrying a control plasmid (p) or a mazF plasmid (pF) were treated or not with ATc. After 10 min (left panel) or 60 min (right panel) of ATc treatment, bacteria were washed, labeled and sorted to obtain 8×10^5 live cells and were serially diluted (top to bottom 10^0 to 10^{-3}), 10 μ l of diluted bacteria were immediately spot-inoculated on Mueller–Hinton agar plates. (C) Wild-type and mazEF-deleted strains carrying a control (p) or a mazF (pF) plasmid were treated with ATc during 10 min. Cell were labeled and sorted and a purified live population of bacteria (8×10^5 cells) was exposed to ciprofloxacin overnight. The remaining bacteria were again labeled, and live cells were counted by cell cytometry. Results are presented as means \pm SD of three independent experiments; N.S. is not significant; * P < 0.05 significant differences between the strain carrying the empty (p) or mazF (pF) plasmid.

of MazF induction (Figure 1C). These observations suggest that after MazF induction, bacteria remain alive but cannot divide, resulting in reduced colony formation observed on agar plates.

To further confirm that after MazF induction bacteria were alive but unable to divide, a second analysis was performed by sorting a fixed number of live bacteria (8 \times 10⁵) from each condition: MazF induced or uninduced cultures in the presence or absence of MazE antitoxin. Sorted live bacteria were immediately spotted on agar plates (Figure 2B). In the absence of MazE antitoxin, induction of MazF in the $\triangle mazEF$ strain, we observed that despite viability measured by FACS analysis, bacteria were unable to divide to form visible bacterial colonies on agar plates. In contrast, live bacteria after MazF induction but carrying MazE antitoxin could divide and give rise to visible bacterial colonies on agar plates. We conclude from these analyses that under our conditions mazF overexpression induced bacterial growth arrest corroborating the characteristic mazF overexpression phenotype in S. aureus.

We next verified that under our conditions of MazF induction, bacteria were indeed in a growth arrested state by evaluating bacterial survival when challenged with the bactericidal antibiotic ciprofloxacin. As antibiotics targeting active growth processes kill less efficiently during growth arrest (31,32), we expect an increased survival to antibiotic treatment upon mazF overexpression. Wild-type and $\triangle mazEF$ cells carrying mazF-expression plasmids or control plasmids, were induced with ATc. Ten minutes post induction (mpi), cells were labeled, and the population was sorted to obtain 8×10^5 live bacteria. These live cells were exposed to 10X the ciprofloxacin minimum inhibitory concentration (MIC) overnight. After washing, the remaining bacteria were again labeled, and live and dead cells were determined by flow cytometry. In the presence of MazE antitoxin (wild-type strain background), we recovered ~5% of the original live population and no significant difference was found between the population carrying an empty plasmid or overexpressing mazF. In contrast, upon mazF overexpression in the absence of the antitoxin ($\Delta mazEF$ strain background), we recovered on average nearly twice as many cells (21.6%) of the original population than in the population carrying an empty plasmid (11.6%) (Figure 2C). These results suggest that induction of active MazF in the absence of MazE antitoxin increases bacterial survival towards the antibiotic ciprofloxacin. All together, these results confirm that MazF induction in our experimental conditions induces bacterial growth arrest.

MazF cleavage sequence recognition identified by nEMOTE

To determine the molecular link between mazF overexpression and the observed growth arrest, we identified MazF-cleaved targets on genome-wide scale using nEMOTE (non-phosphorylated exact mapping of transcriptome ends) coupled to high-throughput sequencing analysis. The nEMOTE procedure detects toxin endoribonuclease cleavages that produce 5'-OH transcript-ends in vivo and in the native host. Briefly, total RNA was isolated from mazEF-deleted strain carrying the overexpression plasmid with or without mazF gene following a 10 min treatment with ATc. The nEMOTE protocol was then applied to enrich for 5'-OH transcripts-ends and the resulting library was sequenced. MazF specific cleavage sites were identified by comparing 5'-ends enriched in mazF induced strain compared to the control condition after elimination of background noise using internal nEMOTE controls (see materials and methods).

Our nEMOTE analysis detected 416 different RNA sites cleaved by MazF toxin (Supplementary Table S3) that we have precisely mapped on the S. aureus NCTC 8325 genome. The sequence logo plot of the 416 RNA sequences around the detected cleavage sites is shown in Figure 3A. The experiment recovered the MazF canonical sequence recognition U^ACAU previously identified in vitro for coa and spa genes (20). This strict canonical motif explains only 44.7% (n = 186) of all detected MazF cleavages, leaving other cleavage sites showing a variation in the motif at +3 position. The remaining sequences display an alternative extended MazF recognition sequence (motif U^ACNUA). Compared to the canonical motif, the alternative extended motif shows a decrease in base conservation at positions -1 and +3 and concomitantly, a conserved +5 position emerges (Figure 3A). As shown in Figure 3B, this alternative motif overlaps with the canonical motif because the RNA sequence UACAUA (cleaved n = 38 times) matches both patterns (i.e. UACAU and UACNUA). The extended motif UACNUA was identified 168 times, although other variations were also detected (n = 62). To better understand the exact cleavage sites that compose the motifs and their overlap, we show in Figure 3C motifs with a single variable position (blue squares) linked to the cleavage site sequence, and the number of times observed (white circles), which explain the motif.

The MazF cleavage motifs determined by nEMOTE allow prediction of other potential MazF cleavage sites by bioinformatics. Transcriptome-wide scan of the S. aureus 2.4 MB genome for canonical and extended alternative motifs, predicted a total of 3584 and 2181 potential MazF cleavage sites (Figure 3D), but nEMOTE detected 186 and 230 cleaved sites, respectively (Figure 3B). Although potential cleavage sites are widespread throughout the transcriptome, we were able to positively identify just a small fraction of these sites. We did not expect all recognition sequences to be cleaved because other factors involved might impede or determine cleavage at these sites (33). They may be also localized in genes with low expression levels that would avoid capturing by the nEMOTE technique.

RNA-seq expression profile and cleavage sites

To further validate and evaluate the limits of detection of the nEMOTE technique in our experimental conditions, we correlated RNA-seq expression data with the identified cleavage sites. RNA-seq was conducted on $\Delta mazEF$ strains carrying *mazF* overexpression plasmid or the empty vector. A global comparison of gene expression between the two conditions indicates an overall decrease of expression when mazF is overexpressed in the cell (Figure 3E and Supplementary Table S4). By overlapping the expression levels and the 416 nEMOTE cleavage sites we observed that cleavages are mostly detectable for highly expressed genes.

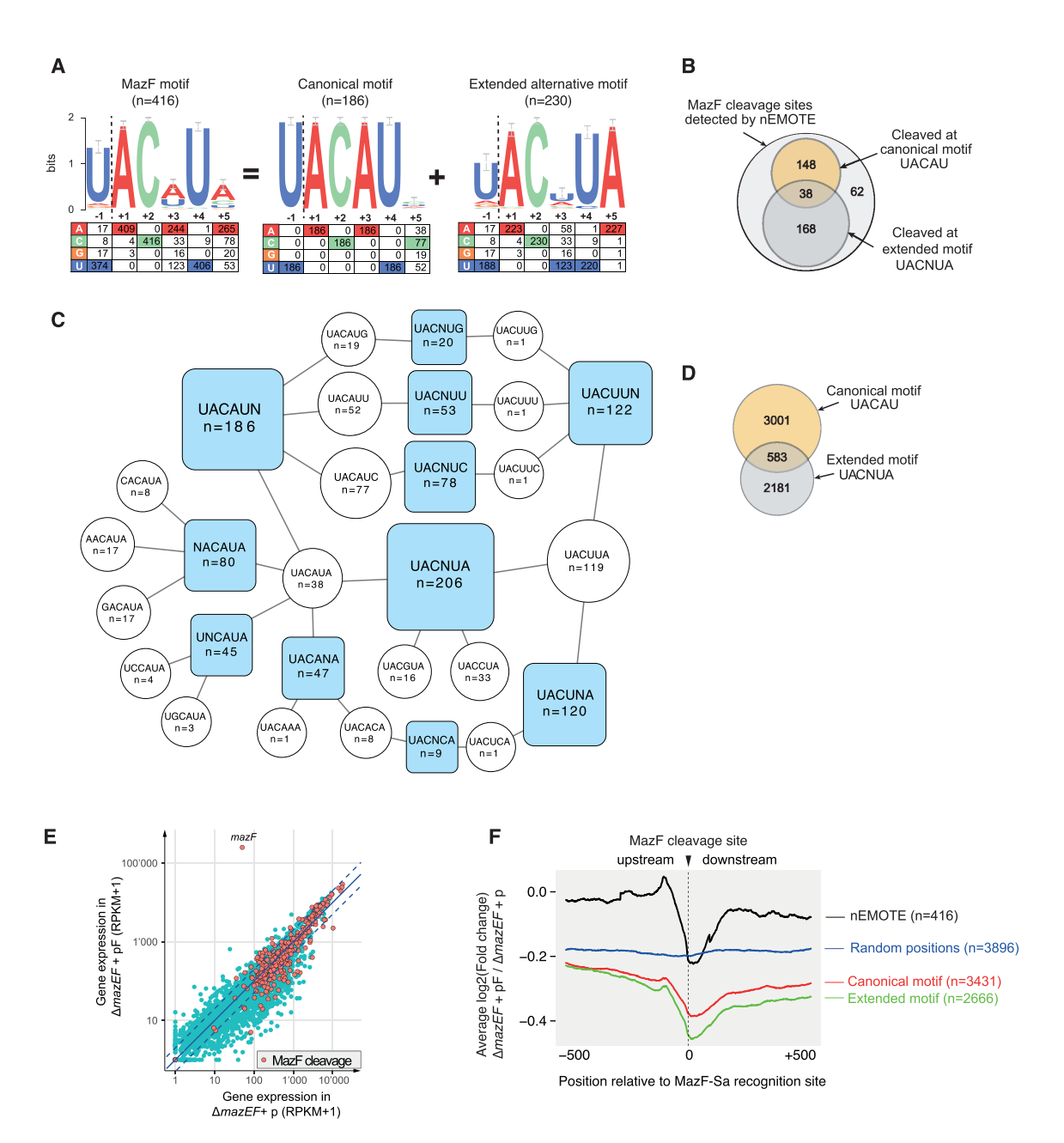


Figure 3. (**A**) Logo plot obtained from the alignment of the 416 MazF cleavage sites detected by nEMOTE and the base frequency at each position is indicated in the table below. A logo plot with the strict canonical motif (previously identified) was extracted from the 416 MazF cleavage sites revealing a second extended alternative motif. (**B**) Venn diagram showing the number of MazF cleavage sites detected by nEMOTE. (**C**) Diagram showing motifs with a single variable position (blue square) and the cleaved sequences composing each blue motif are shown in white circles. (**D**) Venn diagram showing the number of predicted canonical and extended alternative MazF recognition sequence along the *S. aureus* transcriptome based on the nEMOTE results. (**E**) Overlap of RNA-seq global expression profile (blue dots) of *mazEF*—deleted strain overexpressing *mazF* (pF) and control (p) and nEMOTE cleavage sites (orange dots). (**F**) RNA-seq read coverage profiles 500 bp before and after the nEMOTE-detected sites between *mazEF*-deleted strain overexpressing or not *mazF* (log₂ *mazEF*-pF/*mazEF*-p). Profiles obtained around the MazF cleaved sites detected by nEMOTE (black line), around nEMOTE predicted canonical (red line) and alternative extended (green line) sites and around random genome positions (blue line). The y-axis positioning of the curves reflects the average impact of MazF activity on the genes.

We reasoned that we would detect fewer reads across a MazF cleavage site in the presence of MazF than in its absence. We analyzed the RNA-seq read coverage profiles 500 bp before and after a nEMOTE-detected site between *mazEF* deleted strain carrying or not *mazF* overexpression plasmid (log₂ *mazEF*-pF/*mazEF*-p) (see Material and Methods). Aggregated analysis of transcriptomic regions

containing MazF sites detected by nEMOTE shows that 500 bp before the cleavage site there is no discernible read count changes between the strain carrying or not the MazF toxin, while a decrease in read counts is observed approaching nEMOTE MazF cleavage site (black line, Figure 3F). In contrast, no decrease was observed in genomic regions without detected cleavage by MazF or lacking predicted

MazF cleavage motifs (blue line, Figure 3F). The analysis of regions containing the predicted canonical (red line, Figure 3F) or alternative MazF motifs (green line, Figure 3F) similarly shows a decrease in fragment ratios approaching nEMOTE MazF cleavage site. These results suggest that MazF is also cleaving sites we did not detect by nEMOTE because the expression level was too low or because of biases in labeling the 5'-OH ends in the nEMOTE procedure. RNA-seg data corroborated the identified nEMOTE cleavage sites by clearly showing a marked decrease in number of reads crossing MazF cleavage sites.

MazF cleaves motifs present in coding and non-coding regions

To further characterize MazF toxin cleavage sites, we analyzed the position of nEMOTE-detected cleavages relative to coding sequences (CDSs). As shown in Supplementary Figure S4A, MazF recognizes RNA sequences present in coding (n = 372) or non-coding (n = 44) regions with a higher frequency in coding regions. From the 44 cleavages in non-coding regions, 31 and 13 are located in 5' promoter or 3' regions, respectively. Moreover, MazF cleaves both canonical and alternative sites in all three reading frames (In-frame or 0, frame +1 or frame +2). As shown in Supplementary Figure S4B, no preference of cleavage was observed taking into account the relative position of the motif inside a gene. This analysis shows that MazF cleaves inside and outside open reading frames and does not show a reading frame preference.

Global MazF target cleavage and its correlation with S. aureus growth arrest

To understand the molecular link between mazF overexpression and the observed growth defect, we analyzed MazF targets according to their global functional role. An overview of nEMOTE MazF cleaved targets highlights the effect on different mRNAs that are transcribed from essential or non-essential genes corresponding to several metabolic pathways involved in mRNA turnover, translation, transcription, replication, cell division, cell wall metabolism among others (Supplementary Table S3).

The functional characteristics of the MazF-affected genes were obtained by performing gene ontology (GO) enrichment analysis. To avoid the functional analysis to reflect the function of highly expressed genes instead of MazFaffected genes, we limited the analysis to the 1000 most expressed genes, according to the gene-expression given by the $\triangle mazEF$ RNA-seq data (measured as read per kilobase pair per million), and assume that the presence of a cleavage is equally likely to be detected in each of them. Out of the 315 genes affected by a MazF cleavage (Supplementary Table S3), 260 (82%) are in the top 1000 most expressed genes. The analysis using gene ontology biological process classifications showed that the most commonly found annotations were metabolic process resulting in cell growth (GO:0008152) and related categories such as generation of precursor metabolites and energy (GO:00006091), ADP metabolic process (GO:0046031) and ATP generation from ADP (GO:0006757). Similarly, molecular function classifications identified affected categories such as RNA binding (GO:0003723), translation factor activity, RNA binding

(GO:0008135), endoribonuclease activity (GO:00004521) and translation elongation factor activity (GO:00003746). among others. The complete set of GO enriched categories can be found in Supplementary Table S6.

The increased interest to understand bacterial growth has also pinpointed protein synthesis as an important metabolic pathway to regulate growth (34–36). Interestingly, MazF is known to affect translation-related genes in other species (16). Accordingly, we observed by nEMOTE (Table 1) that in our conditions, MazF cleaves several transcripts involved in protein synthesis. We found transcripts cleaved by MazF at canonical or alternative sequence recognition sites that are present once or multiple times per transcript (Table 1). RNA-seq confirmed the MazF cleavage of translation-related transcripts. Fragment counts between $\triangle mazEF$ strain carrying or not mazF overexpression plasmid (log₂ mazEF-pF/mazEF p), show a clear decrease in fragment ratios detected at or near nEMOTE MazF cleavage sites (Figure 4). More specifically, MazF cleaves transcripts encoding translation initiation factors (IF-1 and IF-2), translation elongation factors (Ts, P, Tu, G), termination factors (peptide release factors 2 and 3), several tRNA synthetases required for amino acid loading on tRNAs, an uracil tRNA methyltransferase required for tRNA maturation and a rlmB methyltransferase affecting the posttranscriptional modification of 23S rRNA essential for peptidyltRNA ribosomal recognition. Moreover, as recently observed for E. coli (16), we observed MazF cleavage on several ribosomal protein-related mRNAs (Table 1) that predict altered ribosomal protein production that will disrupt ribosome biogenesis. We identified canonical and alternative cleavage sites in 5S, 16S and 23S rRNAs that would also predict to affect ribosome biogenesis (Supplementary Table

Another set of important transcripts that we identified in our nEMOTE analysis and confirmed by RNA-seq data are those encoding cell division and cell wall synthesis genes. These two cellular processes drive growth of the cell envelope and thus reproduction. As such, defects in these pathways may lead to growth arrest and a reduction in colony formation. As shown in Table 2 and Figure 4, divisionrelated transcripts of ftsA and ftsZ that are required for Z-ring formation, the pbp1 and pbp2 transcripts, the divIC late division transcript, the mraZ transcript encoding and transcriptional regulator of cell division, the sle1 transcript encoding an autolysin and lytM transcript encoding a cell wall hydrolase are detected as MazF-cleaved messages. Peptidoglycan synthesis or teichoic acid-related transcripts including fmhB, uppS, glmM, femAB, murE and murA2, murI, mprF (fmtC), dltA, oatA, tagB and tagG are detected (37– 40). Cell morphology-related mRNAs such as ssaA and alr and the division localized mreD transcripts were found to be cleaved by MazF. The link of mreD cleavage and cell division is unknown as recently it has been shown that mreD has no effect on cell morphology, cell volume or peptidoglycan composition (41).

The regulation of mRNA turnover can be an important pathway to modulate the transcriptional demand that must be imposed to establish a bacterial growth stasis. Deletion of mRNA degradation genes has been shown to reduce growth, suggesting that mRNA turnover is an essential pro-

Table 1. nEMOTE detected cleavage sites in genes involved in protein synthesis

Gene	Gene number	Gene description ^a	MazF motif and localization ^b	GO category ^c
rlmB	SAOUHSC_00513	23S rRNA (guanosine(2251)-2'-O)- methyltransferase RlmB	[290/UACUUA]	RNA methylation [GO:0001510]
rplK	SAOUHSC_00518	50S ribosomal protein L11	[233/UACUUA]	Structural constituent of ribosome [GO:0003735]
rplA	SAOUHSC_00519	50S ribosomal protein L1	[]104/UACCUA	Structural constituent of ribosome [GO:0003735]
rpsG	SAOUHSC_00528	30S ribosomal protein S7	5/UACAUU[]	Structural constituent of ribosome [GO:0003735]
SAOUHSC_00580	SAOUHSC_00580	Hypothetical protein	[9/UACAUU]	n/a
prfB	SAOUHSC_00771	Peptide chain release factor 2	[492/UACAUU]	n/a
trpS	SAOUHSC_00933	Tryptophanyl-tRNA synthetase	[372/AACAUA]	tRNA aminoacylation for protein Translation [GO:0006418]
prfC	SAOUHSC_00956	Peptide chain release factor 3	[590/UACAUU]	Regulation of translational Termination [GO:0006449]
pheS	SAOUHSC_01092	Phenylalanyl-tRNA synthetase subunit alpha	[100/UACUUA]	Phenylalanyl-tRNA aminoacylation [GO:0006432]
ileS	SAOUHSC_01159	Isoleucyl-tRNA synthetase	[188/UACAUA]	n/a
rpsP	SAOUHSC_01208	30S ribosomal protein S16	[114/UACUUA]	Ribosome [GO:0005840]
Gid	SAOUHSC_01223	tRNA (uracil-5-)-methyltransferase Gid	[526/UACUUA]	tRNA wobble uridine modification [GO:0002098]
infB	SAOUHSC_01246	Translation initiation factor IF-2	[1257/UACUUA]	Translational initiation [GO:0006413]
rpsA	SAOUHSC_01493	30S ribosomal protein S1	[253/UACAUC]	Structural constituent of ribosome [GO:0003735]
Efp	SAOUHSC_01625	Elongation factor P	[310/UACUUA]	translation elongation factor activity [GO:0003746]
aspS	SAOUHSC_01737	Aspartyl-tRNA synthetase	[1362/UACAUC]	Aspartyl-tRNA aminoacylation [GO:0006422]
queA	SAOUHSC_01749	S-adenosylmethionine:tRNA ribosyltransferase-isomerase	[457/UACAUC]	n/a
valS	SAOUHSC_01767	valyl-tRNA synthetase	[229/UACUUA]	Valyl-tRNA aminoacylation [GO:0006438]
rpsD	SAOUHSC_01829	30S ribosomal protein S4	[175/UACUUA]	Structural constituent of ribosome [GO:0003735]
leuS	SAOUHSC_01875	Leucyl-tRNA synthetase	[575/UACUUA]	Aminoacyl-tRNA editing activity [GO:0002161]
SAOUHSC_02248	SAOUHSC_02248	Hypothetical protein	[417/UACAUC]	n/a
SAOUHSC_02297	SAOUHSC_02297	S1 RNA-binding	[1662/UACAUC]	Structural constituent of
		domain-containing protein		ribosome [GO:0003735]
rpsI	SAOUHSC_02477	30S ribosomal protein S9	[314/UACUUA]	Structural constituent of ribosome [GO:0003735]
rpsE	SAOUHSC_02494	30S ribosomal protein S5	2/UACAUG[]	Structural constituent of ribosome [GO:0003735]
rplX	SAOUHSC_02501	50S ribosomal protein L24	[2/UGCAUA]	Structural constituent of ribosome [GO:0003735]
rplP	SAOUHSC_02505	50S ribosomal protein L16	[169/UACAUG]	Structural constituent of ribosome [GO:0003735]
rpsC	SAOUHSC_02506	30S ribosomal protein S3	[570/UACUUA]	Structural constituent of ribosome [GO:0003735]
SAOUHSC_02512a	SAOUHSC_02512a	30S ribosomal protein S10	[145/UACACA]	n/a
SAOUHSC_02519	SAOUHSC_02519	Hypothetical protein	[406/UACAUA]	n/a
SAOUHSC_02827	SAOUHSC_02827	Hypothetical protein	[167/UACUUA]	n/a
rpmH	SAOUHSC_03055	50S ribosomal protein L34	[12/UACUUA]	Structural constituent of ribosome [GO:0003735]
rpsF	SAOUHSC_00348	30S ribosomal protein S6	[6/AACAUA] [22/UACAUC]	Structural constituent of ribosome [GO:0003735]
fusA	SAOUHSC_00529	Elongation factor G	2/UACAUG[] [829/UACUUA]	GTPase activity [GO:0003924]
SAOUHSC_01091	SAOUHSC_01091	SpoU rRNA Methylase family protein	[665/UACCUA] []186/UACUUA	n/a
Tsf	SAOUHSC_01234	Elongation factor Ts	[466/UACUUA] [548/UGCAUA]	Translational elongation [GO:0006414]
asnC	SAOUHSC_01471	Asparaginyl-tRNA synthetase	[789/UACAUC] [559/UACUUA]	Asparaginyl-tRNA aminoacylation [GO:0006421]
queG	SAOUHSC_01989	Hypothetical protein	[867/AACAUA] [839/UACGUA]	Epoxyqueuosine reductase activity [GO:0052693]

Table 1. Continued

Gene	Gene number	Gene description ^a	MazF motif and localization ^b	GO category ^c
infA	SAOUHSC_02489	Translation initiation factor IF-1	[201/UACUUA]	Translation initiation factor
			[130/UACAUU]	activity [GO:0003743]
rplN	SAOUHSC_02502	50S ribosomal protein L14	[]15/UACAAA	Structural constituent of
			[226/UACAUC]	ribosome [GO:0003735]
cysS	SAOUHSC_00511	Cysteinyl-tRNA synthetase	[540/UACAUU]	Cysteinyl-tRNA aminoacylation
			[665/UACAUG]	[GO:0006423]
			[1017/GACAUA]	
rpsL	SAOUHSC_00527	30S ribosomal protein S12	[185/UACGUA]	Structural constituent of
			[235/UACAUC]	ribosome [GO:0003735]
			[251/GACAUA]	
rpsS	SAOUHSC_02508	30S ribosomal protein S19	[234/UACAUU]	Structural constituent of
			[137/GACAUA]	ribosome [GO:0003735]
			25/CACAUA[]	
Tuf	SAOUHSC_00530	Elongation factor Tu	[591/UACUUA]	Translational elongation
			[595/UACAUU]	[GO:0006414]
			[743/UACAUG]	
			[928/UACGUA]	
rplC	SAOUHSC_02512	50S ribosomal protein L3	[324/UACUUU]	Structural constituent of ribosome [GO:0003735]
tadA	SAOUHSC_00541	Hypothetical protein	[]8/UACAUA	n/a
trnaT	SAOUHSC_T00055	tRNA-Thr	7/UACAUA∏	n/a
hemA	SAOUHSC_01776	Glutamyl-tRNA reductase	[455/CACAUA]	Glutamyl-tRNA reductase
				activity [GO:0008883]
SAOUHSC_00526	SAOUHSC_00526	50S ribosomal protein L7Ae-like	[90/UACAUC]	Ribosome [GO:0005840]
		protein		
ychF	SAOUHSC_00346	GTP-dependent nucleic	[152/UACUUA]	Ribosome binding
-		acid-binding protein EngD	[846/AACAUA]	[GO:0043022]
hflX	SAOUHSC_01283	Hypothetical protein HflX	[422/UACCUA]	Ribosome binding
				[GO:0043022]

^aGene product as annotated in Aureowiki for NCTC8325 genome

cess for growth (42–44). From the 31 genes annotated as involved in transcription, MazF was found to cleave 12 important mRNAs coding for both RNA polymerase subunits B and B' (rpoB and rpoC), termination factor rho together with endo and exoribonucleases such as RNase III (mrnc) and RNase R (rnr) respectively, mRNAs coding for CshA, J1, J2 and RNase Y proteins that are part of the S. aureus RNA degradation machinery (cshA, rnjA, rnjB and rny genes), regulating RNA decay in bacteria (Table 3). We found canonical or alternative sequence recognition sites and the majority are found cleaved inside open reading frames. To visualize the MazF-dependent cleavage of mRNA turnover transcripts, we again used RNA-seq technique as described above. As shown in Figure 4, a decrease in the number of sequenced reads across the MazF cleavage site is observed in cells expressing MazF compared to cells in which MazF is not expressed, showing a MazFdependent cleavage of selected mRNA turnover genes.

MazF-dependent cleavage of candidate genes potentially modulating MazF toxin

To clarify if MazF can also modulate its own production or activity, we searched for MazF cleavage sites present on transcripts spanning the mazEF locus or that may modulate MazF activity (Table 4 and Figure 5). Transcription of the mazEF locus was previously shown to be negatively and

positively regulated by σ^B and SarA transcriptional regulators, respectively (45). We therefore analyzed in detail the MazF sequence recognition and cleavage in the transcriptomic product of σ^B operon and sarA genomic regions (Figure 5A). MazF recognition sequences were detected or predicted in sarA, in $\sigma^B/rsbV/rsbW$ operon and mazF transcripts while no motif sequence was present in mazE or rsbUtranscripts. qRT-PCR was used to confirm MazF cleavage of selected transcripts, using TaqMan® hydrolysis probes hybridizing exactly over the selected MazF recognition sequence. We expected a reduced target-probe hybridization and detection of mRNA levels present upon mazF overexpression due to MazF cleavage. qRT-PCR analyses were normalized using gyrB, which does not have a MazF recognition sequence (21).

The mRNA levels of selected genes were analyzed upon mazF overexpression in the presence (wild type strain background) or absence ($\triangle mazEF$ strain background) of MazE antitoxin (Figure 5A). As expected, mazF overexpression did not affect mRNA levels of mazE gene lacking a MazF recognition sequence. However, >2-fold reduction in mRNA levels was observed upon induction of MazF toxin in the presence or absence of MazE antitoxin for the rsbV, rsbW and sigB transcripts. As previously observed, despite the presence of a canonical motif in sarA mRNA (UACAU motif at position 124), no decrease of sarA mRNA level was

^bBrackets represent the ORF; number inside brackets indicate The MazF cleavage position relative to the ATG codon; while brackets before or after the cleavage position indicates cleavage outside the ORF, downstream or upstream respectively.

^cComplete gene ontology enrichment analysis in Supplementary Table S6.

Table 2. nEMOTE detected cleavage sites in genes involved in cell wall and cell division

Gene	Gene number	Gene description ^a	MazF motif and localization ^b	GO category ^c
Alr	SAOUHSC_02305	Alanine racemase	[839/UACCUA]	Alanine racemase activity [GO:0008784]
capF	SAOUHSC_00119	Capsular polysaccharide biosynthesis protein Cap8F	[988/GACAUA]	Catalytic activity [GO:0003824]
capJ	SAOUHSC_00123	Capsular polysaccharide biosynthesis protein Cap5J	[434/UACCUA]	n/a
divIC	SAOUHSC_00482	Hypothetical protein	[313/UACUUA]	n/a
dltA	SAOUHSC_00869	D-Alanine–poly(phosphoribitol) ligase subunit 1	[1077/UACAUA]	Cell wall organization or biogenesis [GO:0071554]
femA	SAOUHSC_01373	Methicillin resistance factor FemA	[993/UACAUC]	n/a
femB	SAOUHSC_01374	Methicillin resistance factor	[453/UACAUC]	Cell wall organization or biogenesis [GO:0071554]
fmhB	SAOUHSC_02527	Peptidoglycan pentaglycine interpeptide biosynthesis protein FmhB	[952/UACUUA]	Cell wall organization or biogenesis [GO:0071554]
fmtC	SAOUHSC_01359	Hypothetical protein	[2089/UACUUA]	Lysyltransferase activity [GO:0050071]
ftsA	SAOUHSC_01149	Cell division protein	[1257/UACUCA] [1322/AACAUA]	Cell division site [GO:0032153]
ftsZ	SAOUHSC_01150	Cell division protein FtsZ	[477/UACAUU]	Cell division site [GO:0032153]
glmM	SAOUHSC_02405	Phosphoglucosamine mutase	[446/UACAUU]	Cell wall organization or biogenesis [GO:0071554]
lytM	SAOUHSC_00248	Peptidoglycan hydrolase	[237/UACAUU]	Cell wall organization or biogenesis [GO:0071554]
mraZ	SAOUHSC_01142	Cell division protein MraZ transcriptional regulator	[173/UACCUA]	Regulation of biosynthetic process [GO:0009889]
mreD	SAOUHSC_01758	Cell-wall related protein	[]30/UACAUA	n/a
murA2	SAOUHSC_02365	UDP-N-acetylglucosamine 1-carboxyvinyltransferase	[470/CACAUA]	Cell wall organization or biogenesis [GO:0071554]
murE	SAOUHSC_00954	UDP- <i>N</i> -acetylmuramoylalanyl-D- glutamate-L-lysine ligase	[1330/GACAUA]	Cell wall organization or biogenesis [GO:0071554]
murI	SAOUHSC_01106	Glutamate racemase	[94/UACUUA]	Cell wall organization or biogenesis [GO:0071554]
oatA	SAOUHSC_02885	O-Acetylation of cell-wall peptidoglycan	[49/UACUUA]	Integral component of membrane [GO:0016021]
pbp1	SAOUHSC_01145	Penicillin-binding protein 1	[1095/UACUUA]	Cell wall organization or biogenesis [GO:0071554]
pbp2	SAOUHSC_01467	Penicillin-binding protein 2	[1660/UACAUG] [1761/UACUUA]	Cell wall organization or biogenesis [GO:0071554]
sle1	SAOUHSC_00427	Autolysin	[753/UACUUA]	Cell wall organization or biogenesis [GO:0071554]
ssaA	SAOUHSC_02576	Secretory antigen SsaA, autolysin	[159/UACAUC]	n/a
tagB	SAOUHSC_00643	Teichoic acid biosynthesis protein TagB	[304/UACCUA] [469/UACUUA]	n/a
agG	SAOUHSC_00642	Teichoic acid biosynthesis protein	[431/UACAUA]	n/a
uppS	SAOUHSC_01237	Undecaprenyl pyrophosphate synthase	[211/UACUUA]	Isoprenoid biosynthetic process [GO:0008299]

^aGene product as annotated in Aureowiki for NCTC8325 genome

observed upon *mazF* overexpression in either wild type or *mazEF*-deleted strain backgrounds (21).

The *sarA* sequence recognition site may potentially be protected by RNA-binding proteins such as CshA or forming a double strand RNA structure precluding its cleavage as previously proposed (33). The nEMOTE detected cleavage of *mazF* mRNA at the alternative sequence recognition U^ACUUA at position 277, showing that MazF in *S. aureus* is prone to autoregulation as recently shown for MazF in *E. coli* (46). As the same *mazF* alternative recognition sequence (UACUUA) is found in *sarS* mRNA at position 273, we predicted a MazF-dependent cleavage of *sarS*. Both nEMOTE and TaqMan® qRT-PCR analyses show a MazF-dependent cleavage of *sarS* mRNA (Figure 5A).

MazF toxic activity can be modulated by activation of antitoxin production or stabilization, as antitoxins inherently block toxin activity (47–49). We further hypothesized that production or stabilization of the MazE antitoxin can be achieved through cleavage of trfA, clpP, clpC and spx transcripts. These transcripts encode factors promoting the proteolytic degradation of the MazE antitoxin (Figure 5B and Table 4) and they carry predicted MazF recognition sequence. However, qRT-PCR shows only a decrease of clpC mRNA levels upon mazF overexpression in both strain backgrounds. All together these results show that under our growth conditions of mazF overexpression, transcripts of the σ^B operon, clpC and mazF itself are targets of MazF cleavage.

^bBrackets represent the ORF; number inside brackets indicate the MazF cleavage position relative to the ATG codon; brackets before or after the cleavage position indicates cleavage outside the ORF, downstream or upstream respectively.

^cComplete gene ontology enrichment analysis in Supplementary Table S6.

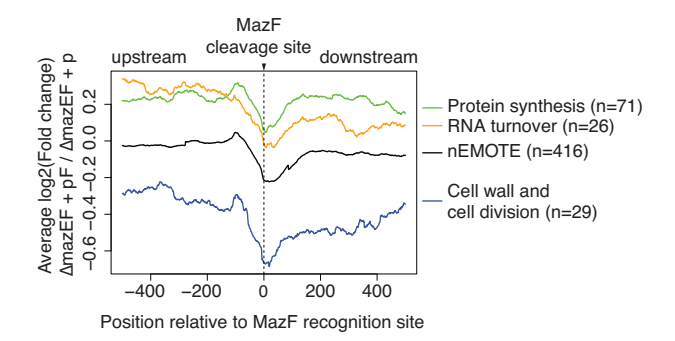


Figure 4. RNA-seq reads coverage profiles 500 bp before and after an nEMOTE-detected cleavage site between mazEF-deleted strain overexpressing or not mazF (log2 mazEF-pF/mazEF-p). Profiles obtained around MazF cleaved sites on protein synthesis genes (green line), RNA turnover genes (vellow line), cell wall and cell division-related genes (blue line). The complete set of nEMOTE-detected sites are shown for comparison (black line).

DISCUSSION

Controlled overexpression of some toxins in TAS, is one of the experimental tools used to induce a non-growing state and to identify key metabolic pathways potentially involved. This strategy has yielded important insights in several model organisms despite the artificial nature of the toxin induction (14,48,50). In this study, we used conditional overexpression of mazF endoribonuclease toxin to facilitate a global in vivo identification of genes involved in S. aureus growth arrest. Using the nEMOTE transcriptomewide mapping technique, we provide an extensive catalog of targets, including its own transcript, identified an extended MazF recognition sequence and revealed insights into the MazF cleavage mechanism.

MazF cleavage mechanism

MazF is a toxin present across phylogenetically distant bacterial species including E. coli, M. tuberculosis and S. aureus. In general, MazF was described as a ribosome-independent and sequence specific endoribonuclease recognizing a specific sequence in RNA molecules such as mRNA, tRNA and rRNA (14-16,51-54). The ACA RNA sequence is recognized by E. coli MazF toxin while in M. tuberculosis MazF toxin recognizes sequences such as UGGCU or UUCCU.

In this study, the nEMOTE technique detected the previously recognized MazF sequence specificity (U^ACAU), showing that nEMOTE is a reliable technique to detect global toxin cleavage sites in vivo. The massive quantity of RNAs analyzed in parallel and in vivo by the nEMOTE procedure has proven advantageous in also identifying a new extended alternative recognition sequence, previously unrecognized by in vitro studies that used single-molecule testing. We could detect that cleavages outside the canonical U^ACAU sequence have an extended recognition specificity. It is interesting to point out that E. coli MazF has also been found to have extended recognition beyond its canonical ACA motif (16). As for E. coli, we found MazF cleavage on transcripts within the coding sequence, but also in the untranslated regions.

Our finding that MazF has different sequence recognition sites might have implications related to cleavage preferences or the need of other factors for full functionality, such as structural or protein factors helping MazF sequence recognition and/or cleavage, as recently suggested in other bacterial species. Indeed, whole-genome studies on E. coli MazF activity have shown that not all ACA sites are cleaved. While reasons for uncleaved E. coli ACA sites remain unknown, studies concerning MazF-mt9 of M. tuberculosis show that the RNA structure is a key element that can determine MazF toxin cleavage, as MazF-mt9 preferentially cleaves tRNA carrying a MazF specific sequence and structure (14). In S. aureus, MazF recognition sites may also be targets of other RNA binding proteins that can promote or inhibit MazF cleavage. We observed that not all MazF recognition sites in highly expressed genes are cleaved and accordingly, S. aureus CshA RNA helicase has been proposed to confer protection to specific mRNAs from MazF cleavage (33). Interestingly, despite the *in vivo* MazF activity measurement using nEMOTE, this technique identifies the same canonical MazF motif previously observed with classical in vitro techniques, suggesting that at least for cleavage at the MazF canonical recognition site no other factors are apparently required. We do not exclude the possibility of the activation of a second mazF-dependent TAS that could be cleaving RNA, although we do not have evidence that other S. aureus TAS are induced transcriptionally upon mazF overexpression. Further studies will decipher whether structural and/or other proteins and/or RNA post-transcriptional modifications are involved in MazF endoribonuclease activity in S. aureus.

Analysis of the S. aureus genome shows that 700 genes do not carry any MazF cleavage site and that they are essentially short genes (414 bp average length). These genes might have evolved to avoid being cleaved by MazF, and they might be indicative of the core functions that allow the cell to survive in a non-growing state triggered by MazF toxin and/or necessary for regrowth. The functional analysis of the 100 longest genes that do not carry MazF recognition sequence reveals that these genes are implicated in oxidoreductase activity [GO:0016491] and tRNA methylation [GO:0032259]. Whether oxidoreductase and methylation activity are necessary for S. aureus survival during growth arrest remains to be studied. However, defects in methylation-related genes in other bacteria are related to growth defects or shown to be essential for life (55-57).

Identified MazF targets and correlation with growth stasis

The overexpression of MazF used in this study allowed the identification of a thorough set of MazF target transcripts, but currently we can only speculate about the correlation between them and the observed MazF-induced growth stasis phenotype. However, it is worth mentioning that several other studies observed defects in growth upon deletion of gene targets that we also found cleaved by MazF: such as spa (protein A) or the sigB transcriptional regulator using other technical methods (21). We also found transcripts previously related to MazF function such as CshA (33) and others that can be intuitively linked to the MazF induced

Table 3. nEMOTE detected cleavage sites in genes involved in RNA turnover

Gene	Gene number	Gene description ^a	MazF motif and localization ^b	GO category ^c
nusG	SAOUHSC_00517	Transcription antitermination protein	[42/UACAUA]	Regulation of transcription, DNA-templated [GO:0006355]
rnr	SAOUHSC_00803	Ribonuclease R	[1677/UACAUC]	3'-5' exonuclease activity [GO:0008408]
nusA	SAOUHSC_01243	Transcription elongation factor NusA	[413/UACUUA]	Transcription regulator activity [GO:0140110]
rnjB	SAOUHSC_01252	RNAse J2	[936/UACAUU]	Exonuclease activity [GO:0004527]
rpoB	SAOUHSC_00524	DNA-directed RNA polymerase subunit	[2697/UACAUU]	5'-3' RNA polymerase activity
		beta	[2836/UACUUA]	[GO:0034062]
rnjA	SAOUHSC_01035	RNAse J1	[1160/UACCUA] [275/UACCUA]	exonuclease activity [GO:0004527]
rho	SAOUHSC_02362	Transcription termination factor Rho	[18/UACAUC] 39/UACUUA[]	DNA-templated transcription, termination [GO:0006353]
rny/cvfA	SAOUHSC_01263	RNAse Y phosphodiesterase	[1004/UACUUA] [1097/UACAUG] [1233/UACAUC]	Hydrolase activity, acting on ester bonds [GO:0016788]
rpoC	SAOUHSC_00525	DNA-directed RNA polymerase subunit beta'	[1205/UACUUA] [1286/UACAUC] [2801/UCCAUA] [3209/UACGUA]	5'-3' RNA polymerase activity [GO:0034062]
mrnC	SAOUHSC_00512	Hypothetical protein RNAse III	[131/UACAUC]	Ribonuclease III activity [GO:0004525]
cshA	SAOUHSC_02316	DEAD-box ATP dependent DNA helicase	[972/UACACA]	RNA helicase activity [GO:0003724]
chsB	SAOUHSC_01659	DEAD-box helicase-magnesium homeostasis	[730/UACUUA]	RNA helicase activity [GO:0003724]

^aGene product as annotated in Aureowiki for NCTC8325 genome

Table 4. MazF cleavage on potential MazEF TAS regulatory circuit

Gene	Gene number	Gene description ^a	MazF motif and localization ^b	Detection method
sigB	SAOUHSC_02298	RNA polymerase sigma factor SigB	[317/UACAUG]	Predicted, probe
rsbW	SAOUHSC 02299	Serine–protein kinase RsbW	[135/UACAUA]	Predicted, probe
rsbV	SAOUHSC 02299	STAS domain-containing protein	[232/UACAUU]	Probe, nEMOTE
rsbU	SAOUHSC_02301	Phosphatase RsbU	No motif	=
mazF	SAOUHSC_02303	Hypothetical protein	[277/UACUUA]	nEMOTE
mazE	SAOUHSC_02304	Hypothetical protein	No motif	_
clpC	SAOUHSC_00505	Endopeptidase	[293/UACAUC]	Probe, nEMOTE
clpP	SAOUHSC_00790	ATP-dependent Clp protease proteolytic subunit	[187/UACAUU]	Predicted, No experimental detection
spxA	SAOUHSC_00934	Transcriptional regulator Spx	[341/UACCUA]	nEMOTE
trfA	SAOUHSC_00935	Adaptor protein MecA	[191/UACAUG]	Predicted, no experimental detection
sarA	SAOUHSC_00620	Accessory regulator A	[124/UACAUC]	Predicted, no experimental detection
sarS	SAOUHSC_00070	Accessory regulator-like protein	[273/UACUUA]	Probe, nEMOTE

^aGene product as annotated in Aureowiki for NCTC8325 genome

non-growing state (e.g., cell wall, division or protein translation genes).

As shown by Culviner *et al.* in *E. coli*, our analysis identified some MazF targets affecting ribosome biogenesis, however we also observed cleavage of mRNAs involved in protein translation (see Table 1). Intriguingly, we observed cleavage of RNA encoding the HflX GTPase, a factor shown in *S. aureus* to be involved in disassembly of 100S ribosomes (70S homodimeric) (58). The 100S ribosomes are assembled upon stress conditions and promote bacterial survival by sequestering ribosomes, protecting them from degradation and preventing their use for translation. The 100S ribosome assembly and disassembly is reversible

(58,59). Based on our data, the predicted GTPase HflX cleavage by MazF argues for the role of MazF to maintain ribosome dimers, decreasing translation and contributing to growth stasis. This hypothesis is in agreement with our unpublished results, showing that upon *mazF* overexpression formation of S100 ribosomes is observed.

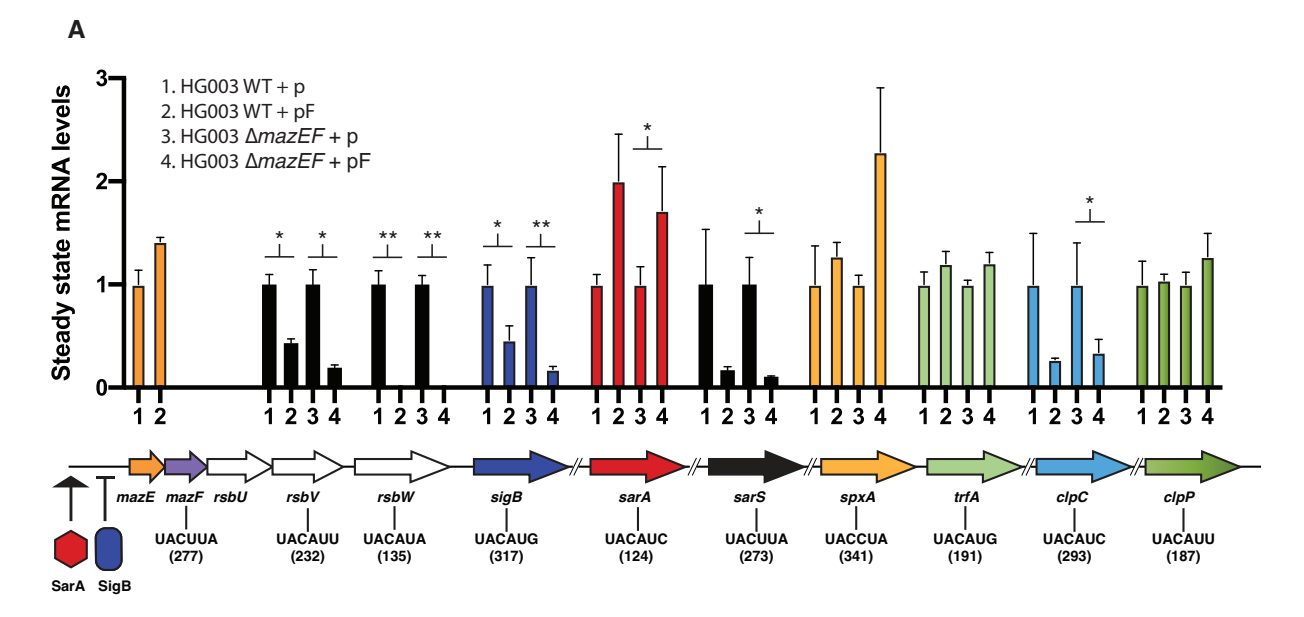
Identified MazF targets and correlation with regrowth

Genes non-targeted by MazF may be essential for survival under growth arrest and others may be essential to promote regrowth (60–64). Interestingly, among the transcripts not targeted by MazF are the antitoxin *mazE* (171bp) and the

^bBrackets represent the ORF; number inside brackets indicate the MazF cleavage position relative to the ATG codon; brackets before or after the cleavage position indicates cleavage outside the ORF, downstream or upstream respectively.

^cComplete gene ontology enrichment analysis in Supplementary Table S6.

^bBrackets represent the ORF; number inside brackets indicate the MazF cleavage position relative to the ATG codon; brackets before or after the cleavage position indicates cleavage outside the ORF, downstream or upstream respectively.



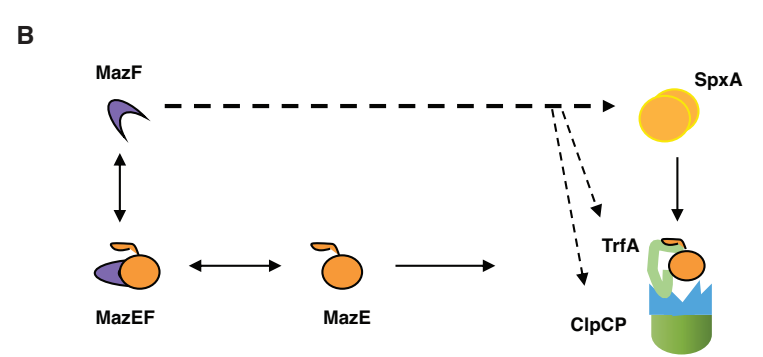


Figure 5. (A) Steady state transcript levels recorded by qRT-PCR for ten genes in wild-type or mazEF-deleted strains carrying the empty plasmid (p) compared to mazF-plasmid (pF) 10 mpi with ATc. Results are presented as means \pm SD of three independent experiments; ** P < 0.01; * P < 0.05 significant differences between the strain carrying the empty plasmid (p) and the strain carrying the mazF-plasmid (pF). The gyrB gene was used to normalize for RNA content. Gene hydrolysis probes hybridize specifically onto the MazF detected site. The MazF recognition sequence and position within the gene is indicated in the gene diagram below. (B) Diagram showing MazF effect on proteins involved in MazE antitoxin proteolysis and containing MazF cleavage motifs. MazF can potentially cleave spxA, trfA, clpC and clpP transcripts (denoted by dashed arrows). SpxA regulates transcription of TrfA adaptor protein, TrfA adaptor in turn is responsible of presenting MazE substrate for degradation to the ClpCP proteolytic system.

sigB-related rsbU (991bp) transcripts. MazE and RsbU may be seen as key proteins to decrease MazF activity and to promote exit from the MazF-induced growth stasis. RsbU may be necessary to ensure production of MazE antitoxin by affecting the negative regulator SigB. Indeed, SigB is a negative transcriptional regulator of mazEF transcription whose activity is modulated by an upstream pathway involving the RsbU phosphatase (65). RsbU inactivation will result in SigB sequestration by its anti-sigma factor RsbW and predicting a decrease amount of SigB and de-repression of mazEF transcription. The exact mechanism of RsbUdependent control of mazEF transcription to restore regrowth remains to be determined.

Besides guaranteeing production of MazE antitoxin by maintaining its transcription and avoiding cleavage, antitoxin stabilization or an induced imbalance between MazE and MazF concentrations may be another mechanism to restore growth (47–49). While antitoxin stabilization is modulated by affecting proteolytic systems involved in anti-

toxin degradation, toxin-antitoxin equilibrium is modulated through autoregulation of mazEF gene expression by transcriptional and post-transcriptional mechanisms as shown in E. coli (46,66). Recently, a mazF gene posttranscriptional autoregulation has been observed, where MazF cleaves its own transcript, producing pulsed MazF levels and affecting bacterial division and a higher antitoxin protein synthesis (46,66).

In S. aureus, ClpCP proteolytic system degrades MazE antitoxin, and interestingly, we identified a MazF motif present and cleaved in clpC transcript. This will predict an increase in stability of MazE antitoxin through disruption of ClpC chaperone. Moreover, our nEMOTE and qRT-PCR techniques detected an alternative extended MazF recognition site cleaved inside the *mazF* coding sequence. This observation suggests a possible post-transcriptional MazF autoregulation in S. aureus through cleavage of mazF transcript, similar to E. coli. We can propose that decreased mazF transcript and protein levels will produce a

toxin-antitoxin imbalance favoring antitoxin concentration needed for regrowth.

The small subset of transcripts lacking a MazF sequence recognition motif argue for their importance for survival and regrowth during and after stasis. A major future task is to identify whether precise targets are linked to the induction of stasis and whether this is entirely stochastic. Evolution must have led to fine tuning to not compromise all cells in order to support the re-establishment of the population.

DATA AVAILABILITY

The data associated with our analyses are available in the GEO data repository accession GSE141855.

SUPPLEMENTARY DATA

Supplementary Data are available at NAR Online.

ACKNOWLEDGEMENTS

We thank Prof. Friedrich Götz (Universität Tübingen, Tübingen, Germany) for HG003 *mazEF*-deleted strain.

FUNDING

Swiss National Science Foundation [310030-169404, 310030-166611, CRSII3_160703 to A.R., W.K., P.V.]; Foundation privée [HUG RS1-27 to A.R., P.V.]. Funding for open access charge: Schweizerischer Nationalfonds zur Förderung der Wissenschaftlichen Forschung. *Conflict of interest statement.* None declared.

REFERENCES

- 1. Bigger, J.W. (1944) Treatment of staphylococcal infections with penicillin by intermittent sterilisation. *Lancet.*, **244**, 497–500.
- Dorr, T., Vulic, M. and Lewis, K. (2010) Ciprofloxacin causes persister formation by inducing the TisB toxin in Escherichia coli. *PLoS Biol.*, 8, e1000317.
- 3. Claudi, B., Sprote, P., Chirkova, A., Personnic, N., Zankl, J., Schurmann, N., Schmidt, A. and Bumann, D. (2014) Phenotypic variation of Salmonella in host tissues delays eradication by antimicrobial chemotherapy. *Cell*, **158**, 722–733.
- Moyed, H.S. and Bertrand, K.P. (1983) hipA, a newly recognized gene of Escherichia coli K-12 that affects frequency of persistence after inhibition of murein synthesis. *J. Bacteriol.*, 155, 768–775.
- Balaban, N.Q., Helaine, S., Lewis, K., Ackermann, M., Aldridge, B., Andersson, D.I., Brynildsen, M.P., Bumann, D., Camilli, A., Collins, J.J et al. (2019) Definitions and guidelines for research on antibiotic persistence. Nat. Rev. Microbiol., 17, 441–448.
- Harms, A., Stanger, F.V., Scheu, P.D., de Jong, I.G., Goepfert, A., Glatter, T., Gerdes, K., Schirmer, T. and Dehio, C. (2015) Adenylylation of gyrase and Topo IV by FicT toxins disrupts bacterial DNA topology. *Cell Rep.*, 12, 1497–1507.
- Aakre, C.D., Phung, T.N., Huang, D. and Laub, M.T. (2013) A bacterial toxin inhibits DNA replication elongation through a direct interaction with the beta sliding clamp. *Mol. Cell.*, 52, 617–628.
- Castro-Roa, D., Garcia-Pino, A., De Gieter, S., van Nuland, N.A.J., Loris, R. and Zenkin, N. (2013) The Fic protein Doc uses an inverted substrate to phosphorylate and inactivate EF-Tu. *Nat. Chem. Biol.*, 9, 811–817.
- 9. Mutschler, H., Gebhardt, M., Shoeman, R.L. and Meinhart, A. (2011) A novel mechanism of programmed cell death in bacteria by toxin–antitoxin systems corrupts peptidoglycan synthesis. *PLoS Biol.*, **9**, e1001033.

- Masuda, H., Tan, Q., Awano, N., Wu, K.P. and Inouye, M. (2012) YeeU enhances the bundling of cytoskeletal polymers of MreB and FtsZ, antagonizing the CbtA (YeeV) toxicity in Escherichia coli. *Mol. Microbiol.*, 84, 979–989.
- 11. Harms, A., Brodersen, D.E., Mitarai, N. and Gerdes, K. (2018) Toxins, targets, and triggers: an overview of toxin-antitoxin biology. *Mol. Cell.*, **70**, 768–784.
- 12. Yamaguchi, Y., Park, J.H. and Inouye, M. (2011) Toxin-antitoxin systems in bacteria and archaea. *Annu. Rev. Genet.*, **45**, 61–79.
- 13. Vesper,O., Amitai,S., Belitsky,M., Byrgazov,K., Kaberdina,A.C., Engelberg-Kulka,H. and Moll,I. (2011) Selective translation of leaderless mRNAs by specialized ribosomes generated by MazF in Escherichia coli. *Cell*, **147**, 147–157.
- Schifano, J.M., Cruz, J.W., Vvedenskaya, I.O., Edifor, R., Ouyang, M., Husson, R.N., Nickels, B.E. and Woychik, N.A. (2016) tRNA is a new target for cleavage by a MazF toxin. *Nucleic Acids Res.*, 44, 1256–1270.
- Schifano, J.M., Vvedenskaya, I.O., Knoblauch, J.G., Ouyang, M., Nickels, B.E. and Woychik, N.A. (2014) An RNA-seq method for defining endoribonuclease cleavage specificity identifies dual rRNA substrates for toxin MazF-mt3. *Nat. Commun.*, 5, 3538.
- Culviner,P.H. and Laub,M.T. (2018) Global analysis of the E. coli toxin MazF reveals widespread cleavage of mRNA and the inhibition of rRNA maturation and ribosome biogenesis. *Mol. Cell.*, 70, 868–880
- Donegan, N.P., Marvin, J.S. and Cheung, A.L. (2014) Role of adaptor TrfA and ClpPC in controlling levels of SsrA-tagged proteins and antitoxins in Staphylococcus aureus. *J. Bacteriol.*, 196, 4140–4151.
- 18. Donegan, N.P., Thompson, E.T., Fu, Z. and Cheung, A.L. (2010) Proteolytic regulation of toxin–antitoxin systems by ClpPC in Staphylococcus aureus. *J. Bacteriol.*, **192**, 1416–1422.
- Zhu, L., Inoue, K., Yoshizumi, S., Kobayashi, H., Zhang, Y., Ouyang, M., Kato, F., Sugai, M. and Inouye, M. (2009) Staphylococcus aureus MazF specifically cleaves a pentad sequence, UACAU, which is unusually abundant in the mRNA for pathogenic adhesive factor SraP. J. Bacteriol., 191, 3248–3255.
- Schuster, C.F., Mechler, L., Nolle, N., Krismer, B., Zelder, M.E., Gotz, F. and Bertram, R. (2015) The MazEF toxin-antitoxin system alters the beta-lactam susceptibility of Staphylococcus aureus. *PLoS One.*, 10, e0126118.
- Fu,Z., Tamber,S., Memmi,G., Donegan,N.P. and Cheung,A.L. (2009) Overexpression of MazFsa in Staphylococcus aureus induces bacteriostasis by selectively targeting mRNAs for cleavage. *J. Bacteriol.*, 191, 2051–2059.
- Ma, D., Mandell, J.B., Donegan, N.P., Cheung, A.L., Ma, W., Rothenberger, S., Shanks, R.M.Q., Richardson, A.R. and Urish, K.L. (2019) The toxin-antitoxin MazEF drives Staphylococcus aureus biofilm formation, antibiotic tolerance, and chronic infection. *mBio.*, 10. e01658-19.
- 23. Sierra, R., Viollier, P. and Renzoni, A. (2019) Linking toxin–antitoxin systems with phenotypes: a Staphylococcus aureus viewpoint. *Biochim. Biophys. Acta. Gene. Regul. Mech.* **1862**, 742–751.
- Helle, L., Kull, M., Mayer, S., Marincola, G., Zelder, M.E., Goerke, C., Wolz, C. and Bertram, R. (2011) Vectors for improved Tet repressor-dependent gradual gene induction or silencing in Staphylococcus aureus. *Microbiology*, 157, 3314–3323.
- Radhakrishnan, S.K., Pritchard, S. and Viollier, P.H. (2010) Coupling prokaryotic cell fate and division control with a bifunctional and oscillating oxidoreductase homolog. *Dev. Cell.* 18, 90–101.
- Kirkpatrick, C.L., Martins, D., Redder, P., Frandi, A., Mignolet, J., Chapalay, J.B., Chambon, M., Turcatti, G. and Viollier, P.H. (2016) Growth control switch by a DNA-damage-inducible toxin-antitoxin system in Caulobacter crescentus. *Nat. Microbiol.*, 1, 16008.
- 27. Redder,P. (2015) Using EMOTE to map the exact 5'-ends of processed RNA on a transcriptome-wide scale. *Methods Mol. Biol.*, **1259**, 69–85.
- 28. Redder,P. (2018) Mapping 5'-ends and their phosphorylation state with EMOTE, TSS-EMOTE, and nEMOTE. *Methods Enzymol.*, **612**, 361–391.
- Fuchs,S., Mehlan,H., Bernhardt,J., Hennig,A., Michalik,S., Surmann,K., Pane-Farre,J., Giese,A., Weiss,S., Backert,L. et al. (2018) AureoWiki the repository of the Staphylococcus aureus research and annotation community. Int. J. Med. Microbiol., 308, 558–568.

- 30. Rao, X., Huang, X., Zhou, Z. and Lin, X. (2013) An improvement of the 2⁽¹⁾-(delta delta CT) method for quantitative real-time polymerase chain reaction data analysis. *Biostat. Bioinforma. Biomath.*, 3, 71–85.
- 31. Gefen, O., Chekol, B., Strahilevitz, J. and Balaban, N.Q. (2017) TDtest: easy detection of bacterial tolerance and persistence in clinical isolates by a modified disk-diffusion assay. *Sci. Rep.*, 7, 41284.
- Brauner, A., Fridman, O., Gefen, O. and Balaban, N.Q. (2016)
 Distinguishing between resistance, tolerance and persistence to antibiotic treatment. *Nat. Rev. Microbiol.*, 14, 320–330.
- 33. Kim,S., Corvaglia,A.R., Leo,S., Cheung,A. and Francois,P. (2016) Characterization of RNA Helicase CshA and its role in protecting mRNAs and small RNAs of Staphylococcus aureus strain Newman. *Infect. Immun.*, **84**, 833–844.
- Zhu, M. and Dai, X. (2018) On the intrinsic constraint of bacterial growth rate: M. tuberculosis's view of the protein translation capacity. Crit. Rev. Microbiol., 44, 455–464.
- Deris, J.B., Kim, M., Zhang, Z., Okano, H., Hermsen, R., Groisman, A. and Hwa, T. (2013) The innate growth bistability and fitness landscapes of antibiotic-resistant bacteria. *Science*, 342, 1237435.
- Shahrezaei, V. and Marguerat, S. (2015) Connecting growth with gene expression: of noise and numbers. *Curr. Opin. Microbiol.*, 25, 127–135.
- Lund, V.A., Wacnik, K., Turner, R.D., Cotterell, B.E., Walther, C.G., Fenn, S.J., Grein, F., Wollman, A.J., Leake, M.C., Olivier, N. et al. (2018) Molecular coordination of Staphylococcus aureus cell division. Elife., 7, e32057.
- Monteiro, J.M., Fernandes, P.B., Vaz, F., Pereira, A.R., Tavares, A.C., Ferreira, M.T., Pereira, P.M., Veiga, H., Kuru, E., Van Nieuwenhze, M.S. et al. (2015) Cell shape dynamics during the staphylococcal cell cycle. *Nat. Commun.*, 6, 8055.
- 39. Yu, W., Missiakas, D. and Schneewind, O. (2018) Septal secretion of protein A in Staphylococcus aureus requires SecA and lipoteichoic acid synthesis. *Elife.*, 7, e34092.
- Rohrer, S., Ehlert, K., Tschierske, M., Labischinski, H. and Berger-Bachi, B. (1999) The essential Staphylococcus aureus gene fmhB is involved in the first step of peptidoglycan pentaglycine interpeptide formation. *Proc. Natl. Acad. Sci. U.S.A.*, 96, 9351–9356.
- Tavares, A.C., Fernandes, P.B., Carballido-Lopez, R. and Pinho, M.G. (2015) MreC and MreD proteins are not required for growth of Staphylococcus aureus. *PLoS One.*, 10, e0140523.
- 42. Cho, K.H. (2017) The structure and function of the Gram-positive bacterial RNA degradosome. *Front. Microbiol.*, **8**, 154.
- Morrison, J.M. and Dunman, P.M. (2011) The modulation of Staphylococcus aureus mRNA turnover. *Future Microbiol.*, 6, 1141–1150.
- Linder, P., Lemeille, S. and Redder, P. (2014) Transcriptome-wide analyses of 5'-ends in RNase J mutants of a gram-positive pathogen reveal a role in RNA maturation, regulation and degradation. *PLoS Genet.*, 10, e1004207.
- 45. Donegan, N.P. and Cheung, A.L. (2009) Regulation of the mazEF toxin–antitoxin module in Staphylococcus aureus and its impact on sigB expression. *J. Bacteriol.*, **191**, 2795–2805.
- Nikolic, N., Bergmiller, T., Vandervelde, A., Albanese, T.G., Gelens, L. and Moll, I. (2018) Autoregulation of mazEF expression underlies growth heterogeneity in bacterial populations. *Nucleic Acids Res.*, 46, 2918–2931.
- Amitai, S., Yassin, Y. and Engelberg-Kulka, H. (2004) MazF-mediated cell death in Escherichia coli: a point of no return. *J. Bacteriol.*, 186, 8295–8300.
- Cho, J., Carr, A.N., Whitworth, L., Johnson, B. and Wilson, K.S. (2017)
 MazEF toxin–antitoxin proteins alter Escherichia coli cell

- morphology and infrastructure during persister formation and regrowth. *Microbiology*, **163**, 308–321.
- Pedersen, K., Christensen, S.K. and Gerdes, K. (2002) Rapid induction and reversal of a bacteriostatic condition by controlled expression of toxins and antitoxins. *Mol. Microbiol.*, 45, 501–510.
- Mok, W.W., Park, J.O., Rabinowitz, J.D. and Brynildsen, M.P. (2015) RNA futile cycling in model persisters derived from MazF accumulation. *MBio.*, 6, e01588-15.
- Zhang, Y., Zhang, J., Hoeflich, K.P., Ikura, M., Qing, G. and Inouye, M. (2003) MazF cleaves cellular mRNAs specifically at ACA to block protein synthesis in Escherichia coli. *Mol. Cell.*, 12, 913–923.
- Schifano, J.M., Edifor, R., Sharp, J.D., Ouyang, M., Konkimalla, A., Husson, R.N. and Woychik, N.A. (2013) Mycobacterial toxin MazF-mt6 inhibits translation through cleavage of 23S rRNA at the ribosomal A site. *Proc. Natl. Acad. Sci. U.S.A.*, 110, 8501–8506.
- 53. Schifano, J.M. and Woychik, N.A. (2014) 23S rRNA as an a-Maz-ing new bacterial toxin target. *RNA Biol.*, 11, 101–105.
- Mets, T., Lippus, M., Schryer, D., Liiv, A., Kasari, V., Paier, A., Maivali, U., Remme, J., Tenson, T. and Kaldalu, N. (2017) Toxins MazF and MqsR cleave Escherichia coli rRNA precursors at multiple sites. RNA Biol., 14, 124–135.
- Bjork, G.R., Jacobsson, K., Nilsson, K., Johansson, M.J., Bystrom, A.S. and Persson, O.P. (2001) A primordial tRNA modification required for the evolution of life? *EMBO J.*, 20, 231–239.
- Gamper, H.B., Masuda, I., Frenkel-Morgenstern, M. and Hou, Y.M. (2015) Maintenance of protein synthesis reading frame by EF-P and m(1)G37-tRNA. *Nat. Commun.*, 6, 7226.
- Graille, M., Figaro, S., Kervestin, S., Buckingham, R.H., Liger, D. and Heurgue-Hamard, V. (2012) Methylation of class I translation termination factors: structural and functional aspects. *Biochimie.*, 94, 1533–1543.
- Basu,A. and Yap,M.N. (2017) Disassembly of the Staphylococcus aureus hibernating 100S ribosome by an evolutionarily conserved GTPase. *Proc. Natl. Acad. Sci. U.S.A.*, 114, E8165–E8173.
- Gohara, D. W. and Yap, M.F. (2018) Survival of the drowsiest: the hibernating 100S ribosome in bacterial stress management. *Curr. Genet.*, 64, 753–760.
- 60. Joers, A., Kaldalu, N. and Tenson, T. (2010) The frequency of persisters in Escherichia coli reflects the kinetics of awakening from dormancy. *J. Bacteriol.*, **192**, 3379–3384.
- Mukamolova, G.V., Turapov, O., Malkin, J., Woltmann, G. and Barer, M.R. (2010) Resuscitation-promoting factors reveal an occult population of tubercle Bacilli in Sputum. Am. J. Respir. Crit. Care. Med., 181, 174–180.
- 62. Pinto, D., Sao-Jose, C., Santos, M.A. and Chambel, L. (2013) Characterization of two resuscitation promoting factors of Listeria monocytogenes. *Microbiology*, **159**, 1390–1401.
- 63. Rosser, A., Stover, C., Pareek, M. and Mukamolova, G.V. (2017) Resuscitation-promoting factors are important determinants of the pathophysiology in Mycobacterium tuberculosis infection. *Crit. Rev. Microbiol.*, 43, 621–630.
- Pascoe, B., Dams, L., Wilkinson, T.S., Harris, L.G., Bodger, O., Mack, D. and Davies, A.P. (2014) Dormant cells of Staphylococcus aureus are resuscitated by spent culture supernatant. *PLoS One.*, 9, e85998.
- Giachino, P., Engelmann, S. and Bischoff, M. (2001) Sigma(B) activity depends on RsbU in Staphylococcus aureus. *J. Bacteriol.*, 183, 1843–1852.
- Nikolic, N. (2019) Autoregulation of bacterial gene expression: lessons from the MazEF toxin–antitoxin system. Curr. Genet., 65, 133–138.

2.2.2 YjbH solubility controls Spx in *Staphylococcus aureus*: Implication for MazEF toxinantitoxin system regulation.

Frontiers in Microbiology 2020, https://doi.org/10.3389/fmicb.2020.00113

As stated above, one strategy used by bacteria to avoid killing by antibiotics involves their transition into a dormant state. While exposure to antibiotics kills growing bacterial cells, a subset of the bacterial population enters a dormant state, enabling them to survive. Dormant bacteria are not genetically resistant. In fact, upon removal of antibiotics, dormant bacteria resume growth and revert to a susceptible population, indicating the presence of a reversible molecular mechanism governing to entry and exit from a dormancy. Interestingly, the toxinantitoxin systems (TAS), such as MazEF, emerge as potential candidates for contributing to this reversible phenomenon. Indeed, MazEF is a stress-inducible functional complex in which the activity of MazF toxin is suppressed through stoichiometric binding to the antitoxin (Park, Yamaguchi, and Inouye 2011; Page and Peti 2016). Upon proteolytic degradation of the antitoxin, the toxin is liberated, becoming active and able to cleave its targets to initiate bacterial dormancy (Coussens and Daines 2016). A subsequent stabilization of the antitoxin will restore formation of the toxin-antitoxin complex and will induce exit from dormancy (Figure 9C). We previously showed that the endoribonucleolytic activity of free MazF toxin, allows entry into a dormant state. However, intricate molecular regulation governing the potential reversibility of the MazEF TAS remains to be determined. In this study, we contribute to decipher this mechanism, and analysed which environmental conditions, sensing mechanisms, and signal transmission pathways that facilitate the activation and release of active MazF toxin.

In S. aureus, MazEF complex is composed of MazF toxin and MazE antitoxin, which binds MazF and neutralizes MazF activity. MazE undergoes cleavage through the ClpCP degradation module, wherein ClpC acts as a chaperone with unfolding capabilities, and ClpP function as a protease. This process is facilitated by the adaptor protein TrfA, which enables ClpCP protease to recognize MazE as a substrate for degradation. TrfA transcription is regulated by the redox sensitive transcriptional factor, Spx. In turn, Spx proteolysis is controlled by ClpXP proteolytic system and requires the involvement of YjbH as adaptor protein for proteolysis. We hypothesize that in *S. aureus* YjbH forms aggregates and its modulation impacts the MazEF TAS through the YjbH-Spx-TrfA cascade in response to environmental stresses (Figure 9).

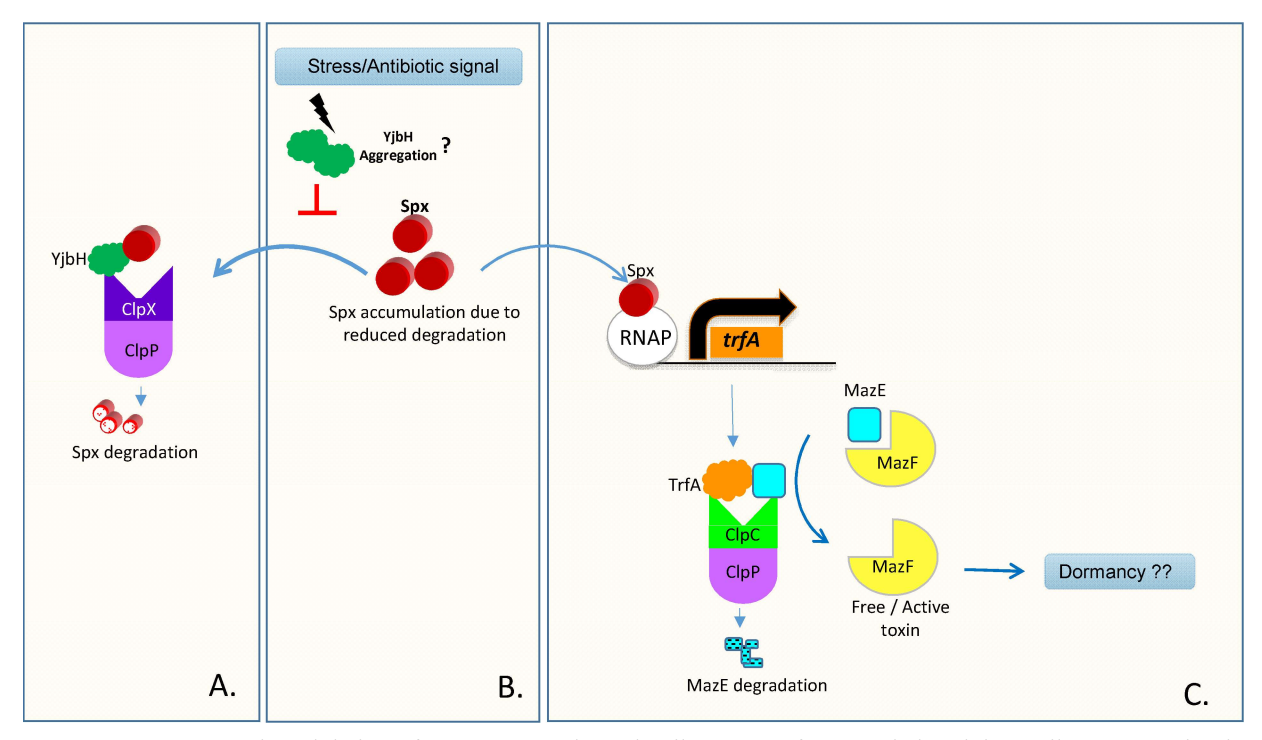


Figure 9. Proposed modulation of MazEF TAS through YjbH-Spx-TrfA cascade involving YjbH aggregation in response to environmental stress. **A)** Spx proteolysis is controlled by ClpPX proteolytic systems that requires YjbH adaptor protein. **B)** We hypothesized that, under certain environmental stresses, YjbH aggregates, reducing SpX proteolysis. **C)** The *trfA* transcription is regulated by Spx. In turn, TrfA adaptor protein is involved, together with the ClpCP proteolytic systems, in proteolysis of MazE antitoxin. MazE proteolysis will free MazF toxin resulting in bacterial dormancy.

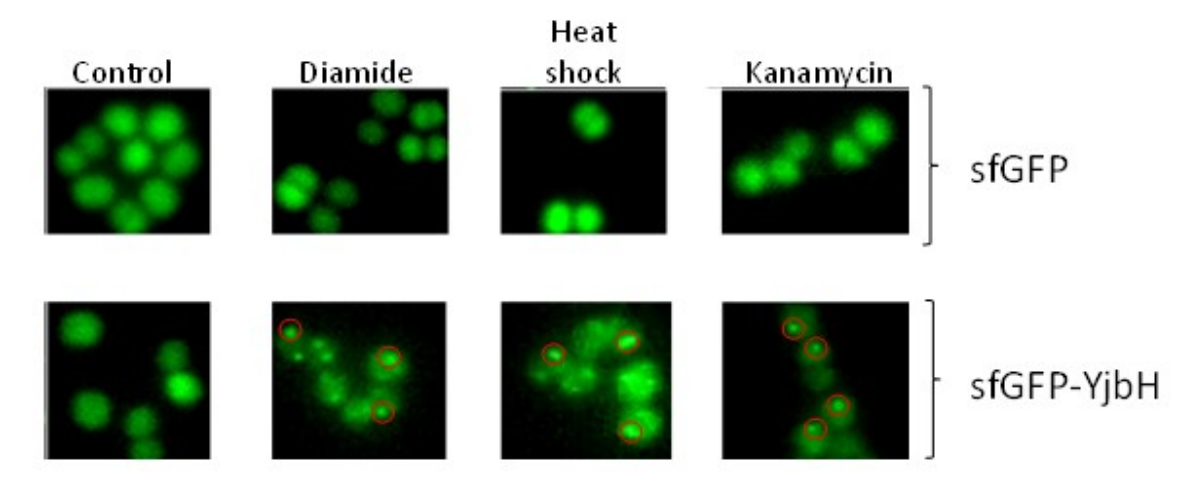


Figure 10. YjbH induced aggregation. Cells expressing sfGFP or sfGFP-YjbH were treated with high temperature (53°C) or 5Mm of diamide or 400ug/ml of ribosome-targeting antibiotic, kanamycin Kan) and analysed and compared to untreated cells using fluorescence microscopy. Fluorescent signal is distributed homogeneously in non-treated cells while distinct foci are observed in treated cells (foci are highlighted in red circles).

By fluorescence microscopy we demonstrated that **YjbH protein is prone to aggregation in response to environmental stresses, including exposure to antibiotics. Remarkably,** *S. aureus* uses this aggregation phenomenon as a mechanism to modulate specific environmental responses (Figure 10). The YjbH aggregation was further validated by western blot analysis, using soluble and insoluble protein fractions. Under non-stressed conditions, YjbH remains mainly in the soluble fraction. However, upon heat shock, ethanol, diamide, kanamycin, tetracyclin and erythromycin treatments, YjbH becomes insoluble (aggregation state) (Figure 3C of the manuscript).

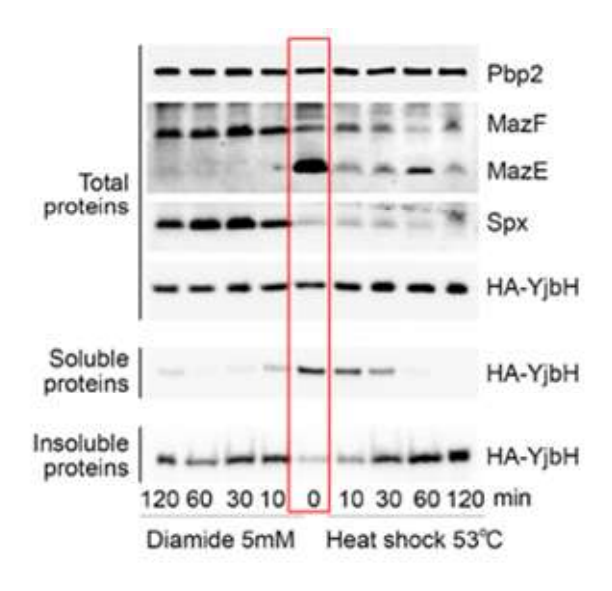


Figure 11. Upon heat shock and diamide stresses MazE antitoxin levels correlate with YjbH aggregation and Spx solubility. *YjbH* mutant bacteria expressing HA-YjbH were treated with high temperature and diamide for different times. Non-treated cells are marked in time 0. Total proteins were adjusted to the same protein concentration and soluble and insoluble proteins were isolated. Samples were run and analysed by western blot using anti YjbH, Spx, MazE and MazF antibodies. PBP2 was used as control for equal amount loading in whole cell extracts.

YjbH aggregation will compromise its function as an adaptor for ClpXP protease) and predict accumulation of Spx transcriptional regulator (see model Figure 9A-B). However, we

showed that not all conditions inducing YjbH aggregation result in accumulation or increased levels of Spx (Figure 3C of the manuscript). We further showed that Spx can also be found in the insoluble or soluble fractions and solubility governs its activity as a transcriptional regulator of *trfA* (Figure 4 of the manuscript).

We further analyse the potential molecular cascade governing MazF activity. By examining the correlation between YjbH aggregation, levels of active/inactive Spx protein, and trfA transcription in response to heat shock or diamide stress, we predicted an ultimate impact on MazE and MazF activity. (Figure 9). We therefore choose heat shock and diamide stress, as conditions triggering YjbH aggregation or not, respectively. We analysed the effects of these conditions on YjbH, Spx, MazE and MazF protein levels in both soluble and insoluble fractions (Figure 11). Diamide induces YjbH aggregation and follows, as expected, our hypothesis, leading

to Spx stabilization, decreased levels of MazE due to enhanced ClpCP degradation. However, we encounter unexpected findings under heat shock conditions, other factors must be involved.

In Conclusion: We provide evidence that in *S. aureus* YjbH undergoes aggregation in response to diverse environmental stresses. YjbH aggregation along with the stress conditions, impacts the levels, solubility, and functional status of the transcriptional factor Spx and, consequently, its downstream targets, such as TrfA (Panasenko et al. 2020). We propose a model where YjbH acts as an environmental stress sensor, exerting downstream regulation over MazEF activity. Through coordinated control of YjbH aggregation, soluble Spx, and TrfA, a modulation of MazE antitoxin levels and consequently MazF toxin activity is achieved. This model implies that specific stress conditions can lead to the modulation of MazF activity, ultimately resulting in growth stasis during in vivo infections.





YjbH Solubility Controls Spx in Staphylococcus aureus: Implication for MazEF Toxin-Antitoxin System Regulation

Olesya O. Panasenko^{1,2*}, Fedor Bezrukov³, Olga Komarynets⁴ and Adriana Renzoni^{1,2*}

¹ Service of Infectious Diseases, Department of Medical Specialties, University Hospital and Medical School of Geneva, Geneva, Switzerland, ² Department of Microbiology and Molecular Medicine, Faculty of Medicine, University of Geneva, Geneva, Switzerland, ³ Department of Physics and Astronomy, The University of Manchester, Manchester, United Kingdom, ⁴ Department of Cell Physiology and Metabolism, Faculty of Medicine, University of Geneva, Geneva, Switzerland

OPEN ACCESS

Edited by:

Satoshi Tsuneda, Waseda University, Japan

Reviewed by:

Dorte Frees,
University of Copenhagen, Denmark
Jung-Ho Park,
Korea Research Institute
of Bioscience and Biotechnology
(KRIBB), South Korea

*Correspondence:

Olesya O. Panasenko olesya.panasenko@unige.ch Adriana Renzoni adriana.renzoni@hcuge.ch

Specialty section:

This article was submitted to Microbial Physiology and Metabolism, a section of the journal Frontiers in Microbiology

> Received: 26 August 2019 Accepted: 17 January 2020 Published: 06 February 2020

Citation

Panasenko OO, Bezrukov F, Komarynets O and Renzoni A (2020) YjbH Solubility Controls Spx in Staphylococcus aureus: Implication for MazEF Toxin-Antitoxin System Regulation. Front. Microbiol. 11:113. doi: 10.3389/fmicb.2020.00113 Bacterial cells respond to environmental stresses by modulating their gene expression and adjusting their proteome. In Staphylococcus aureus, selective degradation by ClpP protease eliminates damaged proteins and regulates the abundance of functional proteins such as many important stress-induced transcriptional regulators. Degradation by ClpP requires the unfolding activity of partner Clp ATPases, such as ClpX and ClpC, and assistance of substrate-specific adaptor proteins such as YibH and TrfA. Herein, we demonstrated that YibH is aggregated in response to growth stress stimuli, such as oxidative and antibiotic stresses. In consequence, its function as an adaptor protein is compromised. YjbH controls the degradation of the stress-induced transcriptional regulator, Spx. Aggregated YibH cannot assist Spx degradation, which results in Spx accumulation. We discovered that depending on the stress stimulus, Spx can be soluble or insoluble, and, consequently, transcriptionally active or inactive. Therefore, Spx accumulation and solubility are key components governing activation of Spxdependent genes. Spx positively regulates expression of a ClpCP adaptor protein TrfA. TrfA in turn is required for degradation of MazE antitoxin, the unstable component of the MazEF toxin-antitoxin system, that neutralizes the endoribonuclease activity of MazF toxin. Bacterial toxin-antitoxin systems are associated with dormancy and tolerance to antibiotics that are related to chronic and relapsing infections, and it is at present a key unresolved problem in medicine. MazF activity was linked to growth stasis, yet the precise environmental signals that trigger MazE degradation and MazF activation are poorly understood. Here we propose a model where YibH serves as a sensor of environmental stresses for downstream regulation of MazEF activity. YibH aggregation, soluble Spx, and TrfA, coordinately control MazE antitoxin levels and consequently MazF toxin activity. This model implies that certain stress conditions culminate in modulation of MazF activity resulting in growth stasis during in vivo infections.

Keywords: YjbH, aggregation, Staphylococcus aureus, Spx, MazEF, toxin-antitoxin system, dormancy, antibiotic resistance

1

INTRODUCTION

Bacterial antibiotic resistance has been recognized as a worldwide problem with still few solutions. It may occur as a result of mutations in bacterial populations selected during antibiotic treatment. However, another important aspect of antimicrobial resistance is bacterial dormancy.

The first type of dormant bacteria tolerant to antibiotics was described in *Staphylococcus aureus* strains long ago (Bigger, 1944). Antibiotic treatment of a susceptible bacterial population kills the majority of the cells but induces the formation of non-dividing dormant bacteria that survive antibiotic challenge. Dormant bacteria are not genetically resistant and after removal of antibiotics, they can regrow and evolve into a susceptible population. The mechanism of entry into antibiotic tolerant state with later regrowth after antibiotic removal, may explain the clinical chronic and relapsing infections. This emphasizes the urgent need to understand the molecular pathways that lead to bacterial dormancy.

Toxin-antitoxin systems (TAS) are stress-inducible functional complexes where toxin component binds an antitoxin (Yamaguchi et al., 2011; Page and Peti, 2016). Toxin activity is inhibited by the antitoxin, that is typically an unstable protein susceptible to degradation by proteases. Antitoxin degradation leads to toxin activation that down-regulates central processes in the cell and may result in cell dormancy (Coussens and Daines, 2016). Different bacterial species enter into dormancy through activation of TAS that will interfere with replication (Maki et al., 1992; Aakre et al., 2013; Harms et al., 2015), inhibition of ribosomes (Castro-Roa et al., 2013; Van Melderen and Wood, 2017), cell wall synthesis (Mutschler et al., 2011), and cell division (Masuda et al., 2012; Mok et al., 2015).

One of the best characterized TAS in S. aureus is MazEF, a type II TAS (Schuster and Bertram, 2016). It is found also in other clinically important bacteria (Mittenhuber, 1999; Nguyen et al., 2011; Schifano et al., 2013; Cho et al., 2017). Several studies were conducted to characterize the MazEF locus by studying its transcriptional activation and function (Donegan and Cheung, 2009; Fu et al., 2009; Zhu et al., 2009; Zorzini et al., 2011, 2014; Miyamoto et al., 2018). MazEF is composed of MazF toxin and its activity is modulated by the MazE antitoxin (Figure 1). Under normal growth conditions, high MazE level ensures formation of toxin-antitoxin complex and consequently, MazF inactivity (Fu et al., 2007). MazE is cleaved by the ClpCP degradation module, where ClpC is a chaperone with unfolding activity and ClpP is a protease. MazE degradation is assisted by the adaptor protein TrfA, providing ClpCP specificity and facilitating MazE recognition (Donegan et al., 2010, 2014). We previously showed that transcription of trfA is positively regulated by the transcriptional activator Spx (Jousselin et al., 2013). In Bacillus subtilis, Spx is a central regulator of the stress response. It binds to the alpha subunits of RNA polymerase, and regulates positively and negatively expression of many genes (Schafer et al., 2019). Spx protein levels are regulated by the proteolytic system ClpXP and assisted by the adaptor protein YjbH (Garg et al., 2009; Renzoni et al., 2011; Engman et al., 2012) (Figure 1). It has been reported that Geobacillus thermodenitrificans YjbH directly interacts with C-terminal end of *B. subtilis* Spx to accelerate Spx proteolysis by ClpX (Chan et al., 2012, 2014). Later the crystal structure of YjbH from *Geobacillus kaustrophilus*, a functional homologs of YjbH from *S. aureus*, bound to *B. subtilis* Spx was published (Awad et al., 2019). In *B. subtilis* it was demonstrated that YjbH is aggregated in response to environmental stresses, and it was proposed that via aggregation YjbH may control Spx levels (Engman and von Wachenfeldt, 2015). However, in *S. aureus* the regulation and properties of Spx and YjbH are poorly understood.

It has been reported that MazF toxin overexpression in *S. aureus* leads to growth stasis or growth arrest (Fu et al., 2009), raising the question whether MazF may be a potential regulator of bacterial dormancy and antibiotic tolerance. Several studies identified genome-wide targets of MazF trying to clarify its role in growth stasis (Fu et al., 2009; Zhu et al., 2009; Schuster et al., 2015; Culviner and Laub, 2018; Sierra et al., 2019). However, the link of MazEF to bacterial dormancy is still to be determined. The described metabolic effects of MazF have been observed under artificial overexpression of MazF. Presently, it is still unknown which environmental conditions, mechanism of sensing, and signal transmission lead to active and free MazF toxin.

We provide evidences that in *S. aureus* YjbH aggregates in response to different environmental stresses. Both YjbH aggregation and the stress conditions affect the levels, solubility, and functional state of transcriptional factor Spx and consequently its downstream targets, such as TrfA. We hypothesized the different environmental stimuli may regulated MazEF TAS through YjbH aggregation, soluble Spx, and TrfA (**Figure 1**).

MATERIALS AND METHODS

Bacteria Cultures, Strains, and Plasmids

All bacteria strains and plasmids used in this work are listed in **Table 1**. Most *S. aureus* genetic constructs were created in HG003 strain background (Herbert et al., 2010; Sassi et al., 2014). *S. aureus* bacterial cultures were grown on Mueller Hinton Broth (MHB) media until OD₆₀₀ of 0.5–0.7 at 37°C with shaking. Bacteria containing plasmids with chloramphenicol or tetracycline resistance were grown in the presence of 15 μ g/ml of chloramphenicol and 3 μ g/ml of tetracycline, respectively.

Plasmid pOP172 was obtained from GENEWIZ. Synthetic codon optimized *S. aureus* YjbH gene with HA₃ tag (HA₃-YjbH) was synthesized and cloned into pUC57 vector resulting in pOP172. To create pOP173 plasmid, HA₃-YjbH fragment was *KpnI/PstI* digested from pOP172 and cloned into pMK4-pHU vector (Andrey et al., 2010). *S. aureus* strains carrying sfGFP alone or sfGFP-YjbH under control of IPTG inducible promoter were kindly provided by Claes von Wachenfeld (Lund University). The pRAB11-MazF plasmid (pAR1884), expressing *mazF* gene under control of anhydrotetracycline (ATc) inducible promoter was constructed by amplification of HG003 *mazF* gene using primers carrying Bgl2 and EcoR1 restriction sites. Amplified product was cut with Bgl2 and

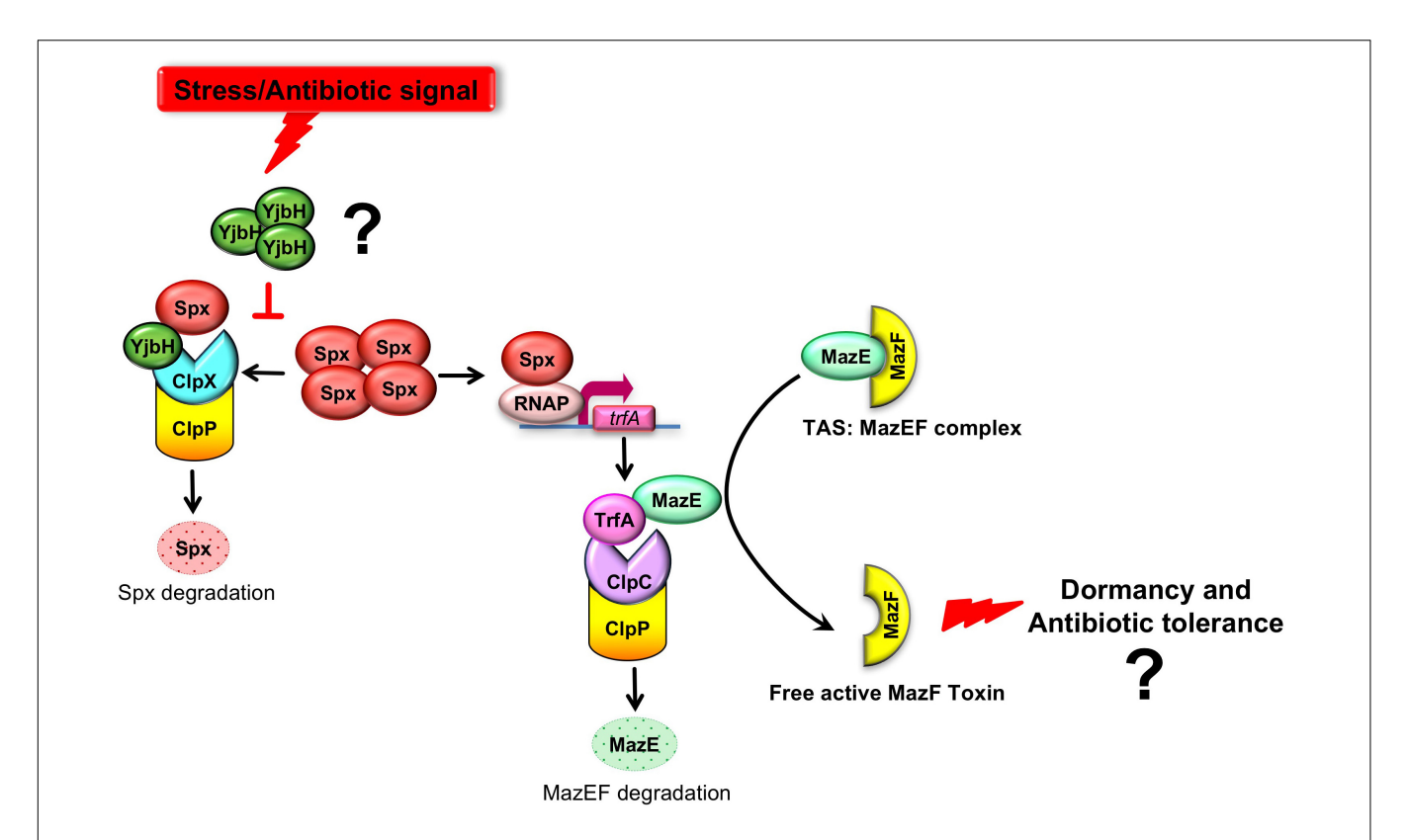


FIGURE 1 | A model where YjbH serves as a sensor of environmental stress and downstream regulation MazEF activity. MazEF complex is composed of MazF toxin and MazE antitoxin which binds MazF and neutralizes MazF activity. MazE is cleaved by the ClpCP degradation module, where ClpC is a chaperone with unfolding activity and ClpP is a protease. MazE degradation is assisted by the adaptor protein TrfA, providing ClpCP specificity and facilitating MazE recognition. The trfA transcription is regulated by the redox sensitive transcriptional factor, Spx. In turn, Spx proteolysis is controlled by ClpXP proteolytic system and requires YjbH adaptor protein. We hypothesized (indicated by question mark) that in S. aureus YjbH aggregates and modulation of YjbH aggregation affects MazEF TAS through the YjbH-Spx-TrfA cascade in response to environmental stresses.

TABLE 1 | Bacteria strains and plasmids.

C	211	raire	· ctr	ains

Strain	Background	Strain resistance	Plasmid	Plasmid resistance	Source
HG003 wt	HG003				(Herbert et al., 2010)
HG003 + pOP173	HG003		pOP173	Cm, Amp	This work
HG003, yjbH:ery 5	HG003	Ery			This work
HG003, yjbH:ery 5 + pOP173	HG003	Ery	pOP173	Cm, Amp	This work
NEWMAN + pCL25-sfGFP	NEWMAN		pCL25-sfGFP	Tet	Gift from Claes von Wachenfeld
NEWMAN + pCL25-sfGFP SAYjbH	NEWMAN		pCL25-sfGFP SAYjbH	Tet	Gift from Claes von Wachenfeld
HG003, ∆trfA:tet	HG003	Tet			This work
HG003, ∆mazEF	HG003				(Schuster et al., 2015)
HG003, Δ <i>mazEF</i> + pAR1884	HG003		pRAB11-MazF	Cm, Amp	This study
HG003, ∆mazEF + pOP174	HG003		pOP174	Cm, Amp	This study

Plasmids

Plasmid name	Gene	Vector	S. aureus marker	E. coli marker	Source
pOP172 (pUC57-HA3-YjbH)	HA3-YjbH	pUC57		Amp	This work
pOP173 (pMK4-pHU-HA3-YjbH)	HA3-YjbH	pMK4	Cm	Amp	This work
pOP174 (pRAB11)		pRAB11	Cm	Amp	(Helle et al., 2011)
pAR1884 (pRAB11-MazF)	MazF	pRAB11	Cm	Amp	This study

EcoR1 and ligated the into pRAB11 vector (Helle et al., 2011). To induce the expression of MazF, 0.2 μ M of ATc was added to the cell cultures and incubated for 10–180 min at 37°C with shaking.

Protein Extraction

Cultures of 25 ml with OD $_{600}$ of 0.7 were collected and washed three times with 1 ml of Phosphate-buffered saline (PBS) buffer. Cells were lysed in the presence of 400 μ l of lysis buffer 1 (LB 1) [PBS, 200 μ g/ml lysostaphin, 200 μ g/ml DNAse I, protease inhibitors (Roche)] for 20 min at 37°C, chilled on ice, and sonicated 10 times with 30-s cycles using Cell Disrupter B-30 (Branson). Extracts were clarified by centrifugation for 10 min at 14000 \times g 4°C. Total protein concentration was measured in supernatants (SN) by the Bradford protein assay. This method permitted to obtain of about 1 mg of total protein with a concentration of about 2.5–3.0 mg/ml. Samples were mixed with Laemmli Sample Buffer (SB) and analyzed by SDS polyacrylamide gel electrophoresis (SDS-PAGE) with following Coomassie Blue staining or western blot.

Isolation of Aggregated Proteins

The protocol for isolation of aggregated proteins from S. aureus was developed on the base of method described for yeast (Panasenko and Collart, 2012). Cells were grown on MHB until OD₆₀₀ of 0.5-0.8. Control bacterial culture was left at 37°C without treatment. Other cultures were incubated at 37°C for 30 min with 5 mM of diamide, 10% ethanol or with antibiotics [oxacillin (10-40 µg/ml), vancomycin (10-40 μ g/ml), kanamycin (50–400 μ g/ml), tetracycline (60 μ g/ml), erythromycin (20 µg/ml)]. For heat shock (HS), cells were incubated at 53°C for 30 min. After cultures treatment, 15 OD₆₀₀ units were harvested at 4000 g for 5 min, and washed with 1 ml of PBS. Pellets were resuspended in 0.3 ml (20 µl per 1 OD unit) of lysis buffer 2 (LB2) [20 mM Na-phosphate, pH 7.6, 10 mM DTT, 1 mM EDTA, 0.1% Tween 20, 1 mM PMSF, protease inhibitor cocktail (Roche), 200 µg/ml DNAse, 200 μg/ml lysostaphin] and incubated at 37°C for 20 min. Chilled samples were sonicated 10 times with 40-s cycles, using Cell Disrupter B-30 (Branson), and centrifuged for 20 min at 200 × g at 4°C. Total protein concentration was measured in supernatants by the Bradford protein assay. Whole cell extracts were adjusted to identical protein concentration of 1.0 mg/ml. 30 μ l of supernatants were boiled with 10 μ l of 4× SB (total proteins). Anti-Pbp2 antibody was used as a control for the equal protein amount in whole cell extracts. Equal amount of whole cell extracts (200 μ l) were centrifuged at 16000 \times g for 20 min at 4°C to pellet the aggregated proteins. After removing supernatants (soluble fractions), insoluble proteins were washed twice with washing buffer (20 mM Na-phosphate, pH 7.6, 2% of NP-40, 1 mM PMSF, protease inhibitor cocktail (Roche), sonicated (10 s at duty cycle 40%), and centrifuged at $16000 \times g$ for 20 min at 4°C. Insoluble (aggregated) proteins were boiled in 50 μl of SB. 60 μ l of soluble fractions were boiled with 20 μ l of 4× SB. 15 μ l of samples were separated by gradient (4-12%) SDS-PAGE, and analyzed by Coomassie Blue staining or western blot.

Fluorescent Microscopy of sfGFP-YjbH Aggregates

Cells expressing either sfGFP-YjbH or only sfGFP under IPTG inducible promoter were grown on MHB with 3 $\mu g/ml$ of tetracycline overnight. Cultures were diluted 1/100 in MHB with 3 $\mu g/ml$ of tetracycline and with 1 mM of IPTG and grown 37°C for 5 h. Cells were incubated at 37°C for 30 min with 5 mM of diamide, or with antibiotics [oxacillin (20–40 $\mu g/ml$), tetracycline (20–60 $\mu g/ml$), kanamycin (200–400 $\mu g/ml$)]. For heat shock (HS) cells were incubated at 53°C for 30 min. Control culture was left at 37°C without treatment. 1.5 ml of cultures were chilled and centrifuged at 4°C 10000 \times g for 1 min. Pellets were resuspended in 30 μl of PBS and 7 μl of cell suspension was loaded on 1% agar, and analyzed with fluorescent microscope.

RTqPCR

RNAs were purified using RNeasy Plus Mini Kit (Qiagen) and QIAshredder Kit (Qiagen). DNA was removed using QIAGEN DNase Kit (Qiagen). TaqMan real-time quantitative polymerase chain reaction (RTqPCR) was performed with Platinum Quantitative RT-PCR ThermoScript One-Step System (Invitrogen). All RNAs were tested for the absence of DNA contaminations. Primers and MGB Double-Dye probes for trfA, rsbW, 16S RNA, and gyrB (Table 2) were designed using Primer Express software (version 1.5; Applied Biosystems), obtained from Eurogentec and used in a concentration 0.05-0.1 µM. For each pair of primers, primer efficiency was calculated and primers and probes were used in concentrations that give the same primer efficiency with housekeeping gene (16S RNA or gyrB). To quantify RTqPCR data the $2^{-}(-\Delta \Delta CT)$ method has been used (Rao et al., 2013), where fold change of target gene expression in a target (treated) samples relative to a reference (non-treated) samples was normalized to a reference gene (16S RNA or gyrB). Thus, the relative gene expression in non-treated samples was set to 1. The errors for the $\Delta \Delta CT$ were obtained by least square error propagation of the standard deviation for the individual RTqPCR measurements performed in triplicates.

RNA-Seq Analysis

The induction of the MazF expression by ATc was performed for 10 min. Total RNAs were purified as described above in biological duplicates. Ribosomal RNAs were depleted with RiboZero kit (Illumina). Libraries were created using the Illumina TruSeq stranded mRNA kit. 1st strand cDNAs were synthesized with random primer. Libraries were sequenced at Fasteris SA. Results of RNA-seq were normalized for sequencing depth [normalization estimated by edgeR (Robinson and Oshlack, 2010; Robinson et al., 2010)], and by the length of the gene, in kilobases and presented in RPKM (Reads Per Kilobase Million).

Antibodies

Anti-HA (anti-influenza hemagglutinin; Sigma) antibodies were used at the dilution 1:3000. Anti-Spx was a gift from Dorte Frees (University of Copenhagen) (Stahlhut et al., 2017) and used in dilution 1:3000. Anti-MazE and anti-MazF antibodies were a gift from Patrick Viollier (University of Geneva) and used in

TABLE 2 | RTgPCR primers and probes.

Gene	Туре	Name	Sequence
gyrB	Forward primer	gyrB-118F	TCAGAGAGAGGTTTGCACCATTT
gyrB	Reverse primer	gyrB-185R	CCAGCTAATGCTTCATCGATACTATT
gyrB	MGB Double-Dye Probes	gyrB-143P	FAM – TGTGGGAAATTGTCG – MGB Eclipse
rRNA16S	Forward primer	rRNA16S-1024F	GATAGAGCCTTCCCCTTCGG
rRNA16S	Reverse primer	rRNA16S-1147R	CCGGCAGTCAACTTAGAGTGC
rRNA16S	Probe	rRNA16S-1071T	FAM - ACATCTCACGACACGAGCTGACGACA - MGB Eclipse
rsbW	Forward primer	rsbW-104F	CACTITCTGGCGTTTTTTCGA
rsbW	Reverse primer	rsbW-167R	GCAATCTTGGCATCTTCAATATCA
rsbW	MGB Double-Dye Probes	rsbW-126P	FAM – AGCTGGTGCTACATATG – MGB Eclipse
trfA	Forward primer	trfA-314F	AAACATTAGAAGGTGAAGATCAATTAGAAG
trfA	Reverse primer	trfA-409R	GTGCTGAAGACTTTTGACGTTT
trfA	MGB Double-Dye Probes	trfA-355P	FAM - CAACGAACAAAAGAAAAAGAAGCTCAA - MGB Eclipse

dilution 1:500. Anti-Pbp2 antibodies were a gift from Mariana Gomes de Pinho (ITQB NOVA, University of Lisbon) and used in dilution 1:8000.

(5 mM), and different antibiotics. Whole cell extracts were adjusted to the same protein concentration. Equal amounts of total protein were separated into soluble and insoluble fractions by centrifugation. Precipitated proteins were washed twice by

RESULTS

Environmental Stimuli Lead to Aggregation of the Adaptor Protein YjbH

MazE antitoxin is regulated by an upstream pathway activated by yet unknown stimuli and unknown mechanisms (Figure 1). We hypothesized that YibH adaptor protein may be involved in stimulus sensing. In B. subtilis it was demonstrated that YjbH is aggregated upon heat shock and diamide-induced oxidative stress, and this aggregation is accompanied by an increase in level of transcriptional regulator Spx (Larsson et al., 2007; Engman and von Wachenfeldt, 2015). We first asked whether YjbH in S. aureus is also prone to aggregation and if so, in which conditions. We used cells expressing IPTG inducible sfGFP alone or sfGFP fused to YjbH (sfGFP-YjbH). After IPTG-induction of sfGFP constructs, bacterial cells were subject to treatment with heat shock, diamide and ribosome-targeting antibiotic, kanamycin, and observed with the fluorescent microscopy (Figure 2). A bacterial strain carrying sfGFP alone show a fluorescent signal distributed homogeneously in all cells before and after tested conditions (Figure 2, upper panel, GFP). In non-treated cells, expressing sfGFP-YjbH fusion, fluorescent signal was also distributed homogeneously. In contrast, distinct fluorescent foci were visible after 30 min of treatment with diamide, heat shock, and kanamycin (Figure 2, lower panel, GFP-YjbH). The same foci were detected after treatment with the cell wall antibiotic, oxacillin, and ribosome-targeting antibiotic, tetracycline (data are not shown).

We speculate that visible foci appeared after stress treatment are aggregated sfGFP-YjbH protein, as was described for *B. subtilis* (Engman and von Wachenfeldt, 2015). To verify this hypothesis, we developed a method to isolate insoluble proteins in *S. aureus*. We treated wild-type cells with different stress conditions, such as heat shock (53°C), ethanol (10%), diamide

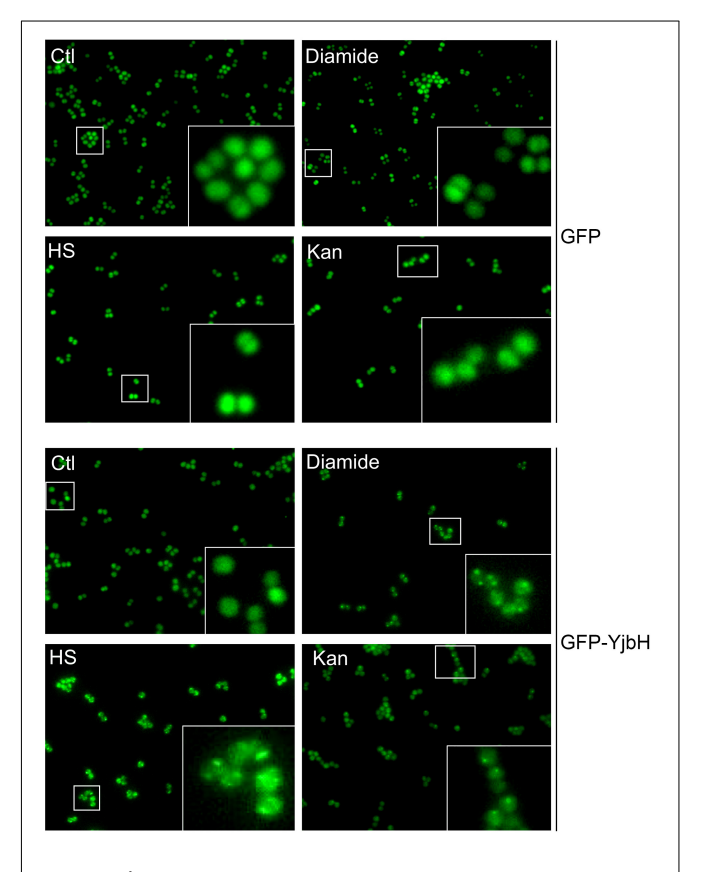


FIGURE 2 | sfGFP-YjbH is accumulated in foci upon heat shock, oxidative stress, and antibiotic treatment. Cells, expressing sfGFP-YjbH were not treated (CtI), or treated with high temperature (53°C, HS), 5 mM of diamide or 400 μ g/ml of ribosome-targeting antibiotic, kanamycin (Kan) and analyzed by fluorescence microscopy (lower panel, GFP-YjbH). Cells, expressing only sfGFP were used as a control and treated in the same manner (upper panel, GFP).

sonication in buffer containing 2% of non-ionic detergent NP-40 to disrupt the membranes. Proteins remained insoluble after that treatment, are likely to be aggregated proteins (Engman and von Wachenfeldt, 2015), therefore we use the term aggregates for them. Insoluble proteins were resuspended in the sample buffer containing 2% of SDS and analyzed by SDS-PAGE and Coomassie Blue staining.

No difference was observed in soluble protein fractions from non-stress or stress conditions (**Figure 3A**). However, significant difference was in insoluble fractions. Heat shock, ethanol and kanamycin, induced massive protein aggregation compared to non-stressed conditions, suggesting that under these conditions many proteins are altered and prone to aggregation. Oxidative stress induced by diamide, and treatment with cell wall antibiotics oxacillin and vancomycin, did not lead to notable protein aggregation.

To prove that visible foci at Figure 2 are indeed insoluble sfGFP-YjbH, we constructed a plasmid expressing HA-tagged

YjbH protein expressed from a constitutive HU promoter. The plasmid was transformed into either wild-type cells or cells deleted for yjbH ($\Delta yjbH$). HA-YjbH expression was detected in both strains (**Figure 3B**). Spx accumulation was observed upon yjbH deletion, as previously described in B. subtilis (Larsson et al., 2007) and in S. aureus (Renzoni et al., 2011). Spx level was decreased upon YjbH plasmid overexpression (**Figure 3B**). Thus, HA-tagged YjbH protein was indeed functional and compensated the yjbH deletion.

The effect of different environmental stresses on YjbH protein levels was then analyzed. Exponentially growing $\Delta yjbH$ bacteria expressing HA-YjbH were subjected to the different stresses, such as heat, ethanol, diamide and antibiotics. Total protein extracts were adjusted to the same protein concentration and fractionated. Fractions of soluble and insoluble proteins were analyzed by SDS-PAGE and western blot for the presence of YjbH and Spx.

In total protein extracts the levels of YjbH were not changed under stress to non-stress conditions (Figure 3C

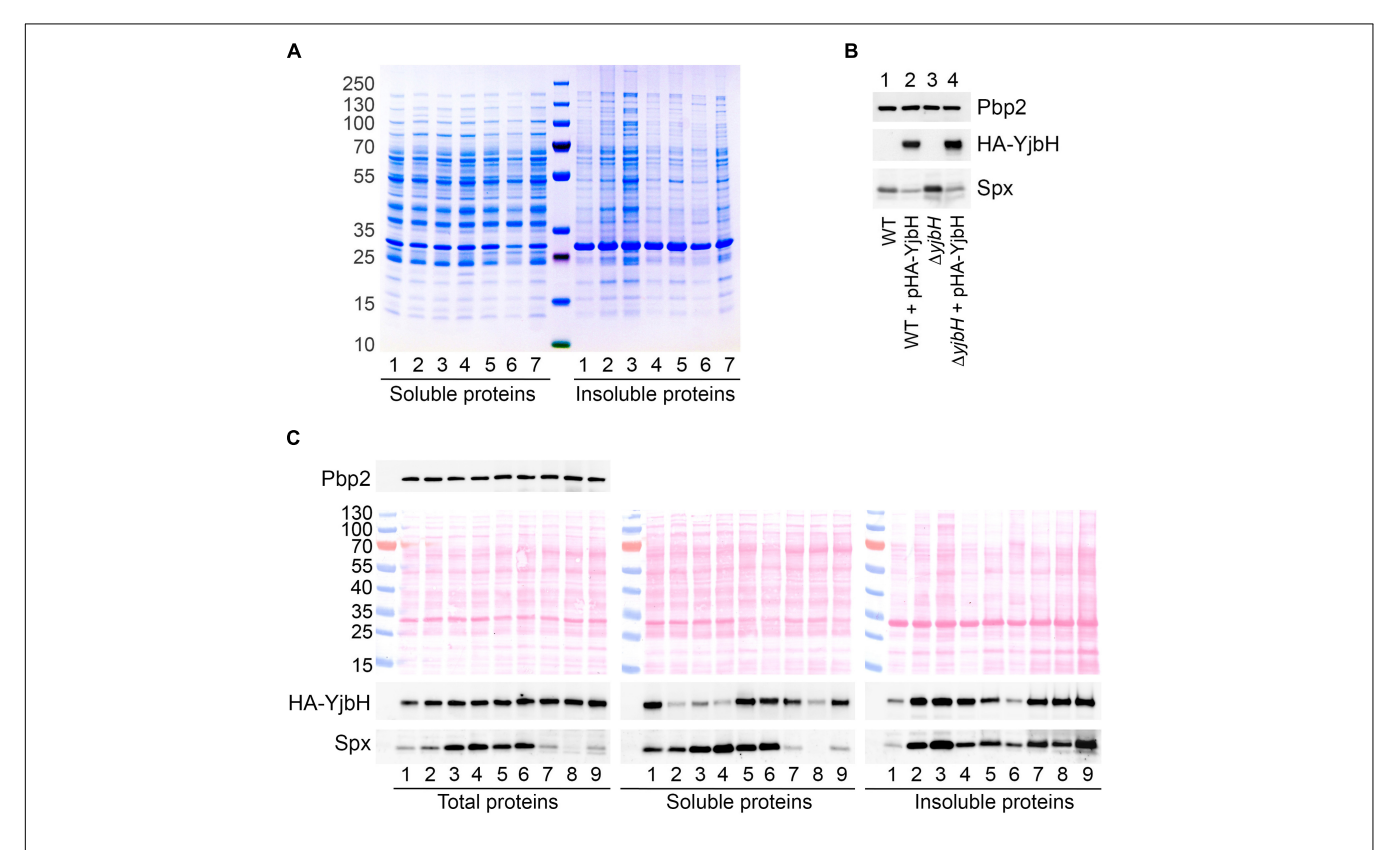


FIGURE 3 | HA-YjbH is aggregated upon heat shock, oxidative stress and antibiotic treatment. (A) Exponentially growing cells (1) were treated with high temperature of 53°C (2), 10% of ethanol (3), 5 mM of diamide (4), 10 μg/ml of oxacillin (5), 10 μg/ml of vancomycin (6), and 50 μg/ml of kanamycin (7). Whole cell extracts were adjusted to the same total protein concentration and fractionated into the soluble and insoluble fractions. Samples were separated by gradient (4–12%) SDS-PAGE, and analyzed by Coomassie Blue staining. (B) Cells, either wild type (WT) or ΔyjbH were transformed with plasmid expressing HA-tagged YjbH (HA-YjbH). Whole cell extracts were prepared and the levels of HA-YjbH and Spx were estimated by western blot with anti-HA and anti-Spx antibodies. Penicillin binding protein 2, Pbp2, was used as a control for equal loading. (C) ΔyjbH cells expressing HA-YjbH were not treated (1) or treated with high temperature (53°C) (2), 10% of ethanol (3), 5 mM of diamide (4), 40 μg/ml of oxacillin (5), 40 μg/ml of vancomycin (6), 400 μg/ml of kanamycin (7), 60 μg/ml of tetracycline (8), and 20 μg/ml of erythromycin (9). Whole cell extracts were adjusted to the equal protein concentration and fractionated into the soluble and insoluble fractions. Proteins were separated by gradient (4–12%) SDS-PAGE and transferred to the nitrocellulose membranes. Membranes were stained with Ponceau S for detection of protein bands and control of loading, and analyzed by western blot with anti-HA, anti-Spx, and anti-Pbp2 antibodies. Pbp2 was used as a control for the equal protein amount in whole cell extracts. Western blots were quantified with ImageJ program and normalized to the signal in untreated control (Supplementary Figure S1).

and Supplementary Figure S1, Total proteins). However, the distribution of YjbH in soluble and insoluble fraction was affected (Figure 3C and Supplementary Figure S1, Soluble and Insoluble proteins). In non-stressed conditions YjbH mainly remained soluble (Figure 3C, lane 1). Only a minor fraction of YibH was insoluble. In contrast, a significant amount of YjbH was insoluble after exposure to heat shock, ethanol, diamide, and ribosome-targeting antibiotics, such as kanamycin, tetracycline, and erythromycin (Figure 3C, lanes 2-4, 7-9). At the same time, less YjbH remained in soluble fraction under these conditions. It was shown earlier, that insoluble YibH is not membrane associated but rather an aggregate (Engman and von Wachenfeldt, 2015). Cell wall antibiotics, oxacillin and vancomycin, did not cause significant YjbH aggregation and it remained mainly soluble (Figure 3C, lanes 5-6). Taken together, these observations suggest that in S. aureus YjbH is prone to aggregation upon environmental stimuli like it does in B. subtilis. However, not all tested stress conditions induced similar YjbH aggregation. Importantly, YjbH aggregation was observe under oxidative stress caused by diamide that did not result in dramatic increase of general protein aggregation and looked similar to untreated conditions (Figure 3A, right, lanes 1 and 4). Thus, YjbH aggregation may be selective and exploited to regulate certain environmental responses.

Transcription of *trfA* Depends Not Only on YjbH Solubility but Also on Functional State of Spx

In B. subtilis heat and diamide induced YjbH aggregation and consequent Spx stabilization was observed due to decreased proteolysis of Spx by ClpXP (Garg et al., 2009; Engman and von Wachenfeldt, 2015). To analyze if stress conditions resulting in YjbH aggregation in S. aureus leads to accumulation of Spx protein, we followed steady state Spx protein levels by western blot. We observed increased levels of Spx in case of ethanol and diamide treatment (Figure 3C, Total proteins, lanes 3 and 4), when YjbH was aggregated (Figure 3C, Insoluble proteins, lanes 3 and 4). However, upon oxacillin and vancomycin treatment we also observed increased levels of Spx (Figure 3C, Total proteins, lanes 5 and 6) while YjbH remains mainly soluble in these conditions (Figure 3C, Soluble proteins, lanes 5 and 6). At the same time, heat shock and ribosome-targeting antibiotics, that caused aggregation of YjbH, did not lead to increased levels of Spx in total extracts (Figure 3C, Total proteins, lanes 2, 7-9). Thus, not all stress conditions leading to YjbH aggregation, resulted in Spx increased levels. This observation suggests that Spx steady state levels are not exclusively modulated by YjbH.

To understand better the link between YjbH solubility and Spx levels we next analyzed the distribution of Spx between soluble and insoluble fractions during various stresses. We found that even if the total amount of Spx was not induced upon heat shock or ribosome-targeting antibiotics, the majority of protein was found in aggregates and a very low amount was detected in soluble fractions [Figure 3C, compare Soluble and Insoluble fractions (lanes 2, 7–9)]. Under diamide, oxacillin or vancomycin stresses, where increased Spx levels were observed in the total

extracts, also higher amounts were found in the soluble fraction compared to the aggregated fraction [Figure 3C, compare Soluble and Insoluble fractions (lanes 4–6)]. These results demonstrate that diamide and cell wall antibiotics, oxacillin and vancomycin, increase the total levels of Spx. Spx mostly remains soluble and, thus, probably functional under these stress conditions. Heat shock and ribosome-targeting antibiotics, kanamycin, tetracycline, and erythromycin, treatments did not increase total levels of Spx, and Spx was found aggregated in probably an inactive form.

Spx is a transcriptional factor, which interacts with the alpha—subunit of the RNA polymerase and induces transcription of many genes, including trfA (Jousselin et al., 2013). In B. subtilis it was shown that oxidation of Spx molecule leads to formation of intramolecular S-S bond between Cys10 and Cys13, that modulates the activity of Spx (Antelmann and Helmann, 2011; Rojas-Tapias and Helmann, 2018). These amino acid residues are conserved in S. aureus. However, it is unknown how Spx oxidation or aggregation may affect its activity in S. aureus. To determine how functional was Spx upon stress conditions we followed its activity by analyzing trfA transcription using RTqPCR. We analyzed expression of *trfA* transcript in conditions that cause increased Spx protein levels, such as yjbH deletion, and probably modulate Spx activity, such as diamide. RNAs were purified from diamide treated and non-treated cells, and trfA mRNA levels were measured by RTqPCR. In non-treated conditions we observed an increase of trfA transcript levels in the *yjbH* deletion mutant compared to the wild-type cells (about three times) (Figure 4A). Diamide treatment increases trfA transcription in both wild-type and yjbH deleted strains. However, the difference in trfA transcription in wild type and yjbH deletion mutant on diamide was less, that in untreated conditions (4.2 and 6.2 compare to 3 and 1). Diamide treatment led to higher induction of trfA in wild-type cells compare to $\Delta yjbH$ cells (Figure 4A, blue columns 1 and 4.2 compare to orange columns 3 and 6.2). These data are expected, because deletion of yjbH results only in increase of Spx protein levels, while, diamide treatment results in both, increase of Spx protein levels and oxidation of Spx protein, leading to higher levels of active Spx and consequently, higher *trfA* transcription.

Next, we tested if solubility affects functional state of Spx. We analyzed expression of *trfA* under heat and oxidative stress, where we observed different solubility of Spx. We found, that *trfA* mRNA levels were decreased upon heat shock stress while increased upon oxidative stress (**Figure 4B**). These observations corroborate our hypothesis that Spx is aggregated and less functional after heat shock, but not after diamide treatment where Spx was found soluble.

Oxidative Stress Decreases MazE Levels and Increases MazF Activity That Correlates With Solubility of YjbH and Spx

The correlations between YjbH aggregation, protein levels of active/inactive Spx and *trfA* transcription after heat or oxidative stresses, predict a different end-point effect on MazE antitoxin

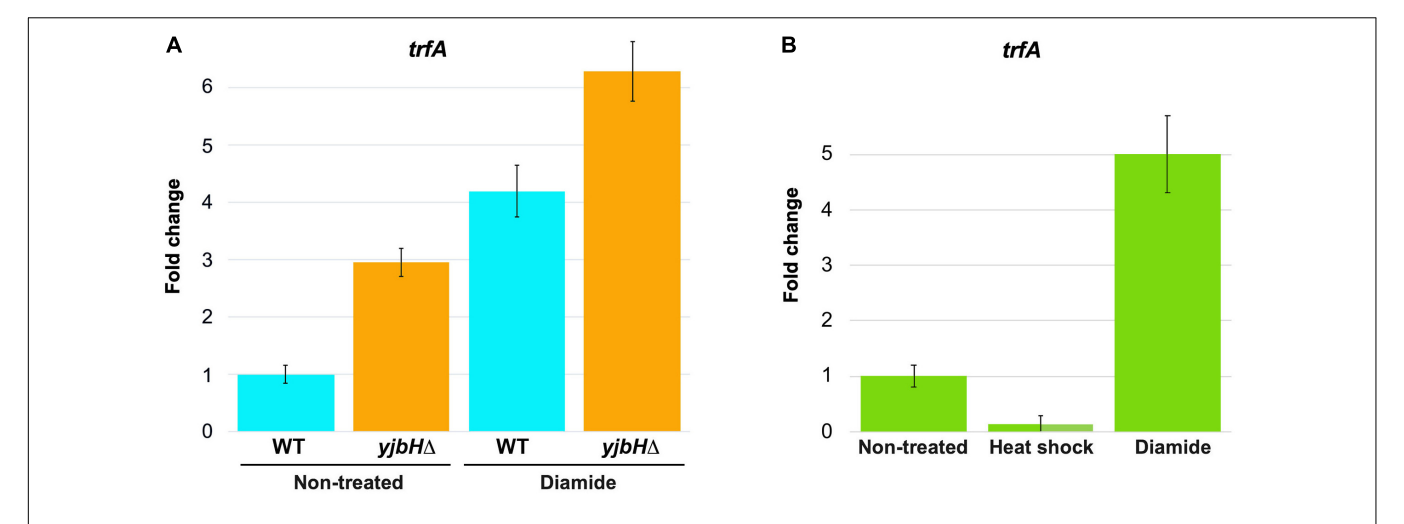


FIGURE 4 | Transcription of *trfA* correspond to the high protein levels and solubility of Spx. RNAs were purified from cells described in **Figures 3B,C**. The level of *trfA* RNA was measured by RTqPCR in non-treated cells and in cells treated for 30 min with either heat shock or oxidative stress induced by diamide. *16S RNA* was used as a reference normalizing housekeeping gene. Fold change of *trfA* gene expression in treated samples relative to non-treated samples was normalized to a reference gene (*16S RNA*). The relative gene expression in non-treated cells was set to 1. **(A)** The levels of *trfA* were increased in the *yjbH* deletion mutant, where the levels of Spx were increased. **(B)** Transcription of *trfA* is decreased after heat shock and increased after oxidative stress, that correspond to solubility of Spx.

levels and MazF toxin activity. We, therefore, analyzed YjbH, Spx and MazE protein levels after diamide or heat shock treatment at different time points. Soluble and insoluble proteins were isolated from cell extracts adjusted to the same total protein concentrations.

In total protein extracts the levels of YjbH were similar before and after both stress conditions (**Figure 5**, Total proteins). YjbH was mostly found in the soluble fractions before stress (time 0). After 10 min of diamide treatment YjbH aggregated and, concomitantly, Spx was stabilized (**Figure 5**, left panel, diamide, Spx in Total proteins). As diamide treatment induces *trfA* transcription through increased amounts of functional Spx (**Figure 4B**), we expected an increase of MazE proteolysis. Indeed, after 10 min of diamide treatment we observed a dramatic reduction of MazE proteolysis by ClpCP (**Figure 5**, left panel, diamide, MazE in Total proteins). At the same time upon diamide treatment the level of MazF was increased, compared to untreated cells (**Figure 5**, left panel, diamide, MazF in Total proteins).

After heat shock YjbH remained soluble for longer than upon diamide stress, but finally aggregated after 60 min of treatment (**Figure 5**, right panel, YjbH in Soluble and Insoluble proteins). Despite YjbH aggregation, Spx levels remained low and unchanged during all times of heat shock treatment compared to non-stressed conditions (**Figure 5**, right panel, heat shock, Spx in Total proteins). In agreement with inactive Spx that was found mostly aggregated after heat shock (**Figure 3C**), we observed a consequent reduced transcription of *trfA* gene (**Figure 4B**). A decreased *trfA* transcription suggests stabilization of MazE antitoxin, as reduction of TrfA will reduce MazE proteolysis. However, we did not observe stabilization of MazE proteolysis after heat shock. Levels of MazE protein were reduced compared to non-stress conditions, but not as much as after diamide treatment (**Figure 5**, right panel, MazE in Total proteins). These

observations suggest that other potential factors must therefore be affected by heat shock and that could explain reduced MazE protein levels without an increase of TrfA.

The decreased MazE levels upon diamide or heat shock stress predict not only stabilized MazF, but also a higher MazF endoribonuclease activity compared to non-stressed condition. To investigate MazF activity we created a plasmid expressing MazF under control of inducible promoter. We transformed

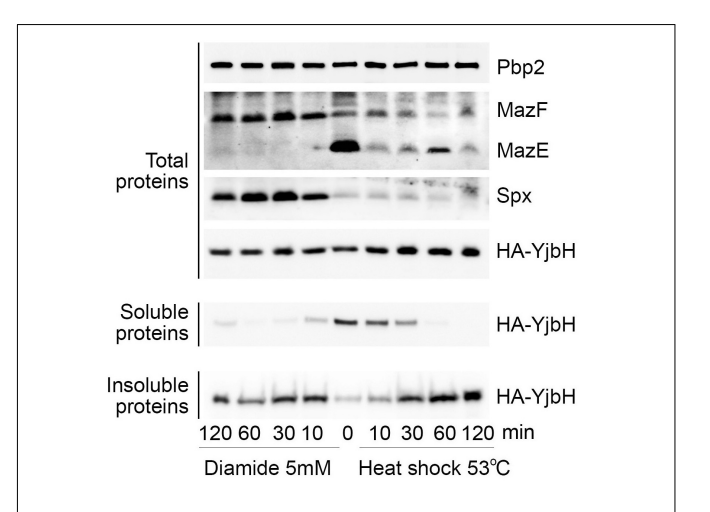


FIGURE 5 | Upon heat shock and oxidative stresses MazE levels correlate with YjbH aggregation and Spx solubility. $\Delta yjbH$ cells expressing HA-YjbH were treated with high temperature (53°C, right), or with 5 mM of diamide (left) for different times, as indicated. Non-treated cells are marked by time 0. Whole cell extracts (Total protein) were adjusted to the same protein concentration and soluble and insoluble proteins were isolated. Samples were separated by gradient (4–12%) SDS-PAGE and analyzed by western blot with anti-HA, anti-Spx, anti-MazE, and anti-MazF antibodies. Pbp2 was used as a control for the equal protein amount in whole cell extracts.

this plasmid in the strain deleted for *mazEF* TAS to model the situation when MazF is not inhibited by MazE. MazF protein was visible after 10 min of induction (**Figure 6A**). To investigate MazF endoribonuclease activity we analyzed mRNA levels of *rsbW* gene, one of the previously described MazF endoribonuclease targets (Schuster et al., 2015). We expect a higher cleavage or

decreased mRNA levels of rsbW upon MazF toxin expression or conditions increasing MazF activity. The level of rsbW transcript was slightly increased in $\Delta mazEF$ cells compared to wild-type cells, and it was dramatically decreased when mazF transcription was induced in $\Delta mazEF$ cells (**Figure 6B**). In-depth analysis of reads covering rsbW transcript, clearly showed a reduction

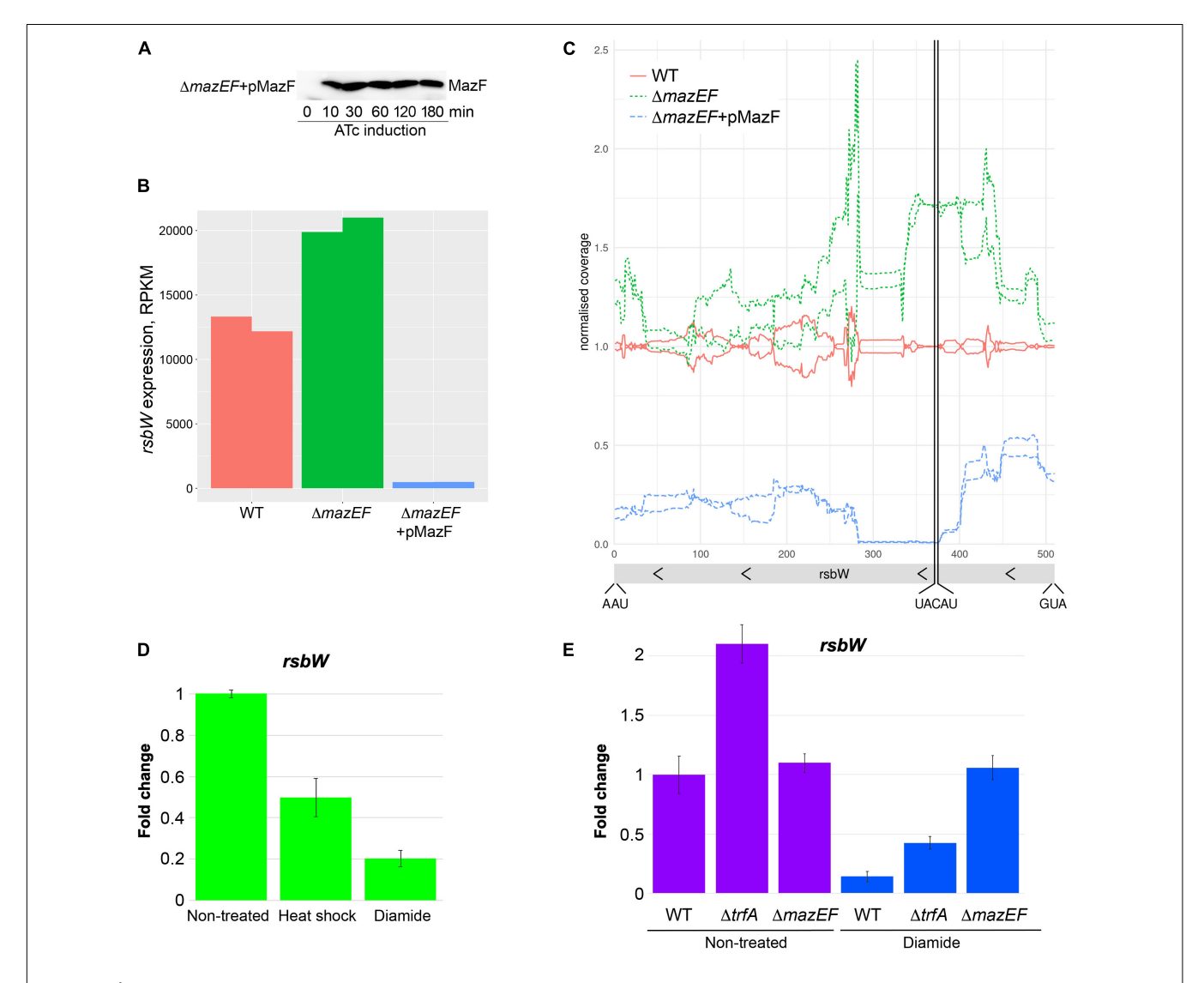


FIGURE 6 | MazF cleaves rsbW at UACAU cleavage site and MazF activity correlates with YjbH aggregation and Spx solubility. (A) Western blot analysis of MazF protein produced after anhydrotetracycline (ATc) induction. The mazEF deleted strain was transformed with the pRAB11-MazF plasmid (indicated as pMazF), expressing mazF gene under control of ATc inducible promoter. Cultures were collected before ATc induction (time 0). Then ATc was added and cultures were collected after 10, 30, 60, 120, and 180 min. Protein were extracted and analyzed by SDS-PAGE and western blot with anti-MazF antibody. (B) Effect of MazF on rsbW level. Wild-type or ΔmazEF cells expressing either empty vector (WT and ΔmazEF) or mazF gene under control of ATc promoter (ΔmazEF + pMazF) were collected after 10 min of ATc induction. Total RNAs were purified and analyzed by RNA-seq. The RPKM values (Reads Per Kilobase Million) normalized by edgeR after excluding plasmid genes are show in duplicates. (C) In-depth analysis of rsbW gene expression by RNA-seq. Cells were treated as in panel (B). RNA-seq coverage along the rsbW region relative to the average wild type is shown. The raw RNASeq coverage was normalized to the total number of reads over the chromosome region and then divided by the coverage of the wild-type samples. The start codon, stop codon and, MazF cleavage site are indicated. (D) RNAs were purified from cells described in Figure 5. The level of rsbW RNA was measured by RTqPCR in non-treated cells and in cells treated for 30 min with either heat shock or oxidative stress induced by diamide. gyrB was used as a reference normalizing housekeeping gene. Fold change of rsbW gene expression in treated samples relative to non-treated samples was normalized to a reference gene (gyrB). The relative gene expression in non-treated cells was set to 1. (E) The level of rsbW RNA was measured by RTqPCR in wild-type, ΔtrfA or ΔmazEF cells treated or not with diamide for 30 min, as described in panel (D). The relative gene expression in non-treate

of reads mapping the identified MazF cleavage motif (UACAU) present in rsbW gene (**Figure 6C**). These results corroborate previous observations that rsbW mRNA is a target of MazF toxin (Schuster et al., 2015) and show that rsbW transcript levels are decreased upon MazF overexpression.

To analyze if diamide or heat shock stress affect MazF endoribonuclease activity, we measure levels of *rsbW* mRNA target by RTqPCR using a probe hybridizing exactly on the MazF cleavage motif. For control and normalization, we used *gyrB* gene that was previously shown to be a non-target of MazF (Fu et al., 2009). We observed two-fold and a five-fold reduction of *rsbW* mRNA levels upon heat shock or diamide treatment, respectively (**Figure 6D**).

Taken together, these results show that decreased levels of MazE antitoxin upon diamide and heat shock resulted in modulation of MazF toxin activity. The slight decrease of *rsbW* mRNA cleavage, despite the reduced levels of MazE upon heat shock, can be explained by residual MazE sufficient to maintain MazF inactive. In contrast, MazE levels upon diamide are absent or highly reduced thus resulting in liberated highly active MazF toxin.

To show that decreased levels of MazE protein upon diamide treatment (Figure 5), affecting MazF activity, is dependent on trfA adaptor, we analyzed rsbW levels in trfA deleted strain with or without diamide treatment (Figure 6E). As expected, the deletion of trfA resulted in increased levels of rsbW in both conditions, confirming the role of TrfA in MazE degradation and, consequently, MazF activation. We further analyzed whether the deletion of mazEF affects rsbW levels in cells treated or not with diamide. Deletion of mazEF in non-treated conditions did not dramatically change rsbW levels, being in agreement with data obtained by RNA-seq (Figure 6B). These results were expected as MazF activity is inhibited by MazE in wild type or not present in $\Delta mazEF$ mutant. However, upon diamide treatment we observed strong stabilization of rsbW in $\Delta mazEF$ mutant, that may be explained by some additional effects of diamide on rsbW expression by unknown mechanisms.

DISCUSSION

MazE antitoxin level ensures formation of at least a stoichiometric toxin-antitoxin complex and consequently, MazF inactivity. Under unknown conditions, the MazF endoribonuclease activity can increase and result in destruction of mRNA molecules leading to growth stasis (reviewed in Sierra et al., 2019). The clinical importance of MazF was recently highlighted by studies showing the role of MazF expression in chronic S. aureus infections (Ma et al., 2019). Using a murine abscess model of infection, MazF expression was shown to inhibit biofilm formation and to increase antibiotic tolerance allowing transition of S. aureus from acute to chronic infections (Ma et al., 2019). However, it is still unknown how S. aureus induces MazF expression and activity under in vivo infection conditions. To understand the possible mechanisms of MazF-activation, we investigated how MazF is regulated under different growth conditions.

In S. aureus, evidence suggests that the dormancy-related MazEF TAS is controlled by two different upstream proteolytic systems (ClpCP and ClpXP) involving two adaptor proteins, TrfA and YjbH, respectively. As YjbH adaptor was shown in B. subtilis to be prone to aggregation (Engman and von Wachenfeldt, 2015), we postulated that modulation of YibH activity through aggregation can be a key step to control MazEF-dependent hdormancy (Figure 1). Indeed, we showed that upon various environmental stress stimulus S. aureus YjbH also aggregates and induces downstream effects regulating MazEF TAS through Spx/TrfA pathway. We showed that diamide induced oxidative stress, causes an increase of MazF toxin activity. Specifically, we uncovered a diamide-stress modulation of MazF activity through an upstream pathway that involves YjbH aggregation, accumulation of active/soluble Spx and increase transcription of the ClpCP adaptor protein TrfA. Increase of trfA transcription upon antibiotic treatment is accompanied by an increase of TrfA protein levels (Jousselin et al., 2013). And the decreased protein levels of TrfA are correlated with the increased protein levels of MazE (Donegan et al., 2014). In agreement with these previous studies, we showed, that the TrfA increase leads to decreased levels of MazE antitoxin and higher amounts of active MazF toxin. These results show that at least oxidative stress increases MazF activity, a stress condition certainly found during S. aureus eukaryotic cell infection.

Despite a decrease in MazE antitoxin levels upon heat shock there was only a slight decrease in MazF activity. Since, the level of MazF was also decreased upon heat shock, we suggested that the low amount of MazE antitoxin present was sufficient to maintain low level of MazF inactive. Interestingly, heat shock reduction of MazE levels was achieved by upstream changes that do not affect Spx accumulation in contrast to diamide stress. Heat shock did not induce accumulation of Spx protein but instead resulted in higher amounts of aggregated and inactive Spx, in accordance with decreased transcription of *trfA*. A potential decreased activity of ClpCP proteolytic systems at heat shock may explain TrfA stabilization that assists MazE degradation.

We observed that not all conditions leading to YjbH aggregation resulted in Spx accumulation. This finding can be explained by stimuli-specific changes in other proteolytic partners involved in Spx degradation. Indeed, Spx accumulation upon diamide stress in *B. subtilis* is dependent on decreased activity of ClpP protease and aggregation of both ClpX and YjbH proteins (Garg et al., 2009; Engman and von Wachenfeldt, 2015). Moreover, it has recently been observed that depending on the stimuli, different regulatory events occur to increase and activate Spx (Rojas-Tapias and Helmann, 2018). While activation of *Spx* regulon under oxidative stress is accompanied by decreased proteolysis and decreased oxidation state of Spx itself, activation of *Spx* regulon under cell wall stress requires *Spx* transcriptional increase and Spx reduced state (Rojas-Tapias and Helmann, 2018).

Our observations suggest that a similar stimuli-dependent effect is present in *S. aureus*. We observed an increased accumulation of Spx protein both under diamide and vancomycin stress, however, achieved through different regulatory events. Diamide induces YjbH aggregation and no

effect on *Spx* transcription was observed (our unpublished observation). In contrast, vancomycin does not induce YjbH aggregation but induces *Spx* transcription (our unpublished observation). Interestingly, both conditions result in production of an active Spx because transcription of Spx targets, such as *trfA*, is increased (Jousselin et al., 2013).

We argue that adaptor proteins YjbH and TrfA, proteolytic systems ClpXP and ClpCP and, finally, Spx transcriptional regulator are involved in upstream control of MazEF TAS. However, expression and activity of YjbH and TrfA, ClpXP and ClpCP, and Spx can be differently modulated, as it was observed previously upon diamide and heat shock in B. subtilis and S. aureus (Frees et al., 2003, 2004; Zhang and Zuber, 2007; Garg et al., 2009). YjbH can be controlled at both transcriptional and/or post-transcriptional levels. Oxidative stress induced by diamide, activated transcription of yjbH in S. aureus (Engman et al., 2012). However, no other stress stimuli have been tested. At the post-transcriptional level, YjbH activity can be modulated by aggregation and/or through anti-adaptor proteins and/or phosphorylation following different stimuli, as shown in B. subtilis and other bacteria (Kirstein et al., 2007; Elsholz et al., 2011; Engman and von Wachenfeldt, 2015; Rojas-Tapias and Helmann, 2018). Our results show that in S. aureus, YjbH can also aggregate, however, the identification of YjbH anti-adaptors such as YirB in B. subtilis, or adaptor phosphorylation remains to be investigated. Also, no studies have been conducted to investigate potential anti-adaptors or phosphorylation of TrfA, the second adaptor protein governing MazEF TAS.

Finally, some studies have analyzed the effect of different stress stimuli on Spx. First, *Spx* is transcribed from at least two different promoters and affected by mutation of *clpP* and *clpX* genes (Pamp et al., 2006; Jousselin et al., 2013). Conditions inducing Spx protein accumulation reduced Spx transcription, thus, Spx was proposed to be a repressor of its own expression (Pamp et al., 2006; Donegan et al., 2019). Interestingly, Spx transcription is induced by anaerobiosis and not affected by high temperature, diamide or NaCl (Pamp et al., 2006). In agreement with these observations, we did not observe increased Spx transcription under diamide, heat shock, oxacillin or kanamycin stress while a two-fold induction was observed upon vancomycin stress [(Jousselin et al., 2013) (and our unpublished observation)]. Secondly, Spx is not regulated only at the transcriptional level. As no correlation between transcription and Spx protein levels was observed, Spx post-transcriptional regulation was postulated. Indeed, Spx levels can be modulated by proteolysis through ClpXP, and Spx activity can be modulated by its redox state that differs upon different stimuli in B. subtilis (Rojas-Tapias and Helmann, 2018). We observed a stimuli dependent Spx protein aggregation that affected Spx activity, and could conceivably be responsible for downstream effects, such as regulation of MazEF TAS.

CONCLUSION

In conclusion, the exact mechanisms of sensing and signal transmission that culminate in MazEF TAS activation remain

to be elucidated. Our work demonstrates YjbH aggregation in *S. aureus* in response to different environmental stresses, may presumably lead to modulation of MazF activity. We found oxidative stress as one potential *in vivo* growth condition regulating MazF activity. Our observation supports the hypothesis that oxidative stress, found upon *in vivo* infection in *Escherichia coli*, can trigger activation of MazF endonuclease leading to a reduced metabolic state and, consequently, entry into persistence state (Mok et al., 2015). Our hypothesis was strongly supported by the very interesting recent study where the persister-like phenotype in *B. subtilis* was connected to increased levels of Spx at specific environmental conditions, such as stationary phase (Schafer et al., 2019).

DATA AVAILABILITY STATEMENT

The datasets generated for this study are available on request to the corresponding author.

AUTHOR CONTRIBUTIONS

OP designed and performed the experiments, constructed the plasmids and strains, and participated in the writing of the manuscript and conception of the work. OK did the fluorescent microscopy. AR participated in the writing of the manuscript and conception of the work. FB did all the RNAseq analysis and the analysis of MazF cleavage site, and participated in the discussion of the results, revision of the manuscript, writing of the revised manuscript, and conception of the work.

FUNDING

This work was supported by the Swiss National Science Foundation grants 310030-169404 awarded to AR, and grants from Helmut Horten Stiftung and from Ernst and Lucie Schmidheiny Foundation awarded to OP.

ACKNOWLEDGMENTS

We kindly thank Claes von Wachenfeld (Lund University) for sfGFP-YjbH plasmids and strains, Dorte Frees for anti-Spx antibody, Patrick Viollier for anti-MazE and anti-MazF antibodies, Friedrich Götz for HG003 *mazEF* deleted strain, Mariana Gomes de Pinho for anti-Pbp2 antibodies, and William Kelley for critical reading of the manuscript.

SUPPLEMENTARY MATERIAL

The Supplementary Material for this article can be found online at: https://www.frontiersin.org/articles/10.3389/fmicb.2020. 00113/full#supplementary-material

REFERENCES

- Aakre, C. D., Phung, T. N., Huang, D., and Laub, M. T. (2013). A bacterial toxin inhibits DNA replication elongation through a direct interaction with the beta sliding clamp. Mol. Cell 52, 617–628. doi: 10.1016/j.molcel.2013.10.014
- Andrey, D. O., Renzoni, A., Monod, A., Lew, D. P., Cheung, A. L., and Kelley, W. L. (2010). Control of the Staphylococcus aureus toxic shock tst promoter by the global regulator SarA. J. Bacteriol. 192, 6077–6085. doi: 10.1128/JB.00146-10
- Antelmann, H., and Helmann, J. D. (2011). Thiol-based redox switches and gene regulation. *Antioxid. Redox Signal.* 14, 1049–1063. doi: 10.1089/ars.2010.3400
- Awad, W., Al-Eryani, Y., Ekstrom, S., Logan, D. T., and von Wachenfeldt, C. (2019). Structural basis for YjbH adaptor-mediated recognition of transcription factor spx. Structure 27, 923–936.e926. doi: 10.1016/j.str.2019.03.009
- Bigger, J. W. (1944). Treatment of staphylococcal infections with penicillin by intermittent sterilisation. *Lancet* 244, 497–500. doi: 10.1016/S0140-6736(00) 74210-3
- Castro-Roa, D., Garcia-Pino, A., De Gieter, S., van Nuland, N. A. J., Loris, R., and Zenkin, N. (2013). The Fic protein Doc uses an inverted substrate to phosphorylate and inactivate EF-Tu. Nat. Chem. Biol. 9, 811–817. doi: 10.1038/nchembio.1364
- Chan, C. M., Garg, S., Lin, A. A., and Zuber, P. (2012). Geobacillus thermodenitrificans YjbH recognizes the C-terminal end of *Bacillus subtilis* Spx to accelerate Spx proteolysis by ClpXP. *Microbiology* 158(Pt 5), 1268–1278. doi: 10.1099/mic.0.057661-0
- Chan, C. M., Hahn, E., and Zuber, P. (2014). Adaptor bypass mutations of *Bacillus subtilis* spx suggest a mechanism for YjbH-enhanced proteolysis of the regulator Spx by ClpXP. *Mol. Microbiol.* 93, 426–438. doi: 10.1111/mmi.12671
- Cho, J., Carr, A. N., Whitworth, L., Johnson, B., and Wilson, K. S. (2017). MazEF toxin-antitoxin proteins alter *Escherichia coli* cell morphology and infrastructure during persister formation and regrowth. *Microbiology* 163, 308–321. doi: 10.1099/mic.0.000436
- Coussens, N. P., and Daines, D. A. (2016). Wake me when it's over bacterial toxin-antitoxin proteins and induced dormancy. *Exp. Biol. Med. (Maywood)* 241, 1332–1342. doi: 10.1177/1535370216651938
- Culviner, P. H., and Laub, M. T. (2018). Global analysis of the *E. coli* toxin MazF reveals widespread cleavage of mRNA and the Inhibition of rRNA maturation and ribosome biogenesis. *Mol. Cell* 70, 868–880.e10. doi: 10.1016/j.molcel.2018. 04.026
- Donegan, N. P., and Cheung, A. L. (2009). Regulation of the mazEF toxin-antitoxin module in *Staphylococcus aureus* and its impact on sigB expression. *J. Bacteriol*. 191, 2795–2805. doi: 10.1128/JB.01713-08
- Donegan, N. P., Manna, A. C., Tseng, C. W., Liu, G. Y., and Cheung, A. L. (2019).
 CspA regulation of Staphylococcus aureus carotenoid levels and sigma(B) activity is controlled by YjbH and Spx. Mol. Microbiol. 112, 532–551. doi: 10.1111/mmi.14273
- Donegan, N. P., Marvin, J. S., and Cheung, A. L. (2014). Role of adaptor TrfA and ClpPC in controlling levels of SsrA-tagged proteins and antitoxins in Staphylococcus aureus. J. Bacteriol. 196, 4140–4151. doi: 10.1128/JB.02222-14
- Donegan, N. P., Thompson, E. T., Fu, Z., and Cheung, A. L. (2010). Proteolytic regulation of toxin-antitoxin systems by ClpPC in *Staphylococcus aureus*. *J. Bacteriol.* 192, 1416–1422. doi: 10.1128/JB.00233-09
- Elsholz, A. K., Hempel, K., Michalik, S., Gronau, K., Becher, D., Hecker, M., et al. (2011). Activity control of the ClpC adaptor McsB in *Bacillus subtilis*. *J. Bacteriol.* 193, 3887–3893. doi: 10.1128/JB.00079-11
- Engman, J., Rogstam, A., Frees, D., Ingmer, H., and von Wachenfeldt, C. (2012). The YjbH adaptor protein enhances proteolysis of the transcriptional regulator Spx in *Staphylococcus aureus*. J. Bacteriol. 194, 1186–1194. doi: 10.1128/JB. 06414-11
- Engman, J., and von Wachenfeldt, C. (2015). Regulated protein aggregation: a mechanism to control the activity of the ClpXP adaptor protein YjbH. Mol. Microbiol. 95, 51–63. doi: 10.1111/mmi.12842
- Frees, D., Chastanet, A., Qazi, S., Sorensen, K., Hill, P., Msadek, T., et al. (2004). Clp ATPases are required for stress tolerance, intracellular replication and biofilm formation in *Staphylococcus aureus*. *Mol. Microbiol.* 54, 1445–1462. doi: 10.1111/j.1365-2958.2004.04368.x
- Frees, D., Qazi, S. N., Hill, P. J., and Ingmer, H. (2003). Alternative roles of ClpX and ClpP in Staphylococcus aureus stress tolerance and virulence. Mol. Microbiol. 48, 1565–1578. doi: 10.1046/j.1365-2958.2003.03524.x

- Fu, Z., Donegan, N. P., Memmi, G., and Cheung, A. L. (2007). Characterization of MazFSa, an endoribonuclease from *Staphylococcus aureus*. J. Bacteriol. 189, 8871–8879. doi: 10.1128/JB.01272-07
- Fu, Z., Tamber, S., Memmi, G., Donegan, N. P., and Cheung, A. L. (2009). Overexpression of MazFsa in *Staphylococcus aureus* induces bacteriostasis by selectively targeting mRNAs for cleavage. *J. Bacteriol.* 191, 2051–2059. doi: 10.1128/JB.00907-08
- Garg, S. K., Kommineni, S., Henslee, L., Zhang, Y., and Zuber, P. (2009). The YjbH protein of *Bacillus subtilis* enhances ClpXP-catalyzed proteolysis of Spx. *J. Bacteriol.* 191, 1268–1277. doi: 10.1128/JB.01289-08
- Harms, A., Stanger, F. V., Scheu, P. D., de Jong, I. G., Goepfert, A., Glatter, T., et al. (2015). Adenylylation of Gyrase and Topo IV by FicT toxins disrupts bacterial DNA topology. *Cell Rep.* 12, 1497–1507. doi: 10.1016/j.celrep.2015.07.056
- Helle, L., Kull, M., Mayer, S., Marincola, G., Zelder, M. E., Goerke, C., et al. (2011). Vectors for improved Tet repressor-dependent gradual gene induction or silencing in *Staphylococcus aureus*. *Microbiology* 157(Pt 12), 3314–3323. doi: 10.1099/mic.0.052548-0
- Herbert, S., Ziebandt, A. K., Ohlsen, K., Schafer, T., Hecker, M., Albrecht, D., et al. (2010). Repair of global regulators in *Staphylococcus aureus* 8325 and comparative analysis with other clinical isolates. *Infect. Immun.* 78, 2877–2889. doi: 10.1128/IAI.00088-10
- Jousselin, A., Kelley, W. L., Barras, C., Lew, D. P., and Renzoni, A. (2013). The Staphylococcus aureus thiol/oxidative stress global regulator Spx controls trfA, a gene implicated in cell wall antibiotic resistance. Antimicrob. Agents Chemother. 57, 3283–3292. doi: 10.1128/AAC.00220-13
- Kirstein, J., Dougan, D. A., Gerth, U., Hecker, M., and Turgay, K. (2007). The tyrosine kinase McsB is a regulated adaptor protein for ClpCP. EMBO J. 26, 2061–2070. doi: 10.1038/sj.emboj.7601655
- Larsson, J. T., Rogstam, A., and von Wachenfeldt, C. (2007). YjbH is a novel negative effector of the disulphide stress regulator, Spx, in *Bacillus subtilis*. Mol. Microbiol. 66, 669–684. doi: 10.1111/j.1365-2958.2007.05949.x
- Ma, D., Mandell, J. B., Donegan, N. P., Cheung, A. L., Ma, W., Rothenberger, S., et al. (2019). The toxin-antitoxin MazEF drives *Staphylococcus aureus* biofilm formation, antibiotic tolerance, and chronic infection. *mBio* 10:e01658-19. doi: 10.1128/mBio.01658-19
- Maki, S., Takiguchi, S., Miki, T., and Horiuchi, T. (1992). Modulation of DNA supercoiling activity of *Escherichia coli* DNA gyrase by F plasmid proteins. Antagonistic actions of LetA (CcdA) and LetD (CcdB) proteins. *J. Biol. Chem.* 267, 12244–12251.
- Masuda, H., Tan, Q., Awano, N., Wu, K. P., and Inouye, M. (2012). YeeU enhances the bundling of cytoskeletal polymers of MreB and FtsZ, antagonizing the CbtA (YeeV) toxicity in *Escherichia coli. Mol. Microbiol.* 84, 979–989. doi: 10.1111/j. 1365-2958.2012.08068.x
- Mittenhuber, G. (1999). Occurrence of mazEF-like antitoxin/toxin systems in bacteria. *J. Mol. Microbiol. Biotechnol.* 1, 295–302.
- Miyamoto, T., Yokota, A., Ota, Y., Tsuruga, M., Aoi, R., Tsuneda, S., et al. (2018). Nitrosomonas europaea MazF specifically recognises the UGG motif and promotes selective RNA degradation. Front. Microbiol. 9:2386. doi: 10. 3389/fmicb.2018.02386
- Mok, W. W., Park, J. O., Rabinowitz, J. D., and Brynildsen, M. P. (2015). RNA futile cycling in model persisters derived from MazF accumulation. MBio 6:e01588-15. doi: 10.1128/mBio.01588-15
- Mutschler, H., Gebhardt, M., Shoeman, R. L., and Meinhart, A. (2011). A novel mechanism of programmed cell death in bacteria by toxin-antitoxin systems corrupts peptidoglycan synthesis. *PLoS Biol.* 9:e1001033. doi: 10.1371/journal. pbio.1001033
- Nguyen, D., Joshi-Datar, A., Lepine, F., Bauerle, E., Olakanmi, O., Beer, K., et al. (2011). Active starvation responses mediate antibiotic tolerance in biofilms and nutrient-limited bacteria. Science 334, 982–986. doi: 10.1126/science.1211037
- Page, R., and Peti, W. (2016). Toxin-antitoxin systems in bacterial growth arrest and persistence. Nat. Chem. Biol. 12, 208–214. doi: 10.1038/nchembio.2044
- Pamp, S. J., Frees, D., Engelmann, S., Hecker, M., and Ingmer, H. (2006). Spx is a global effector impacting stress tolerance and biofilm formation in *Staphylococcus aureus*. *J. Bacteriol.* 188, 4861–4870. doi: 10.1128/JB.001 94.06
- Panasenko, O. O., and Collart, M. A. (2012). Presence of Not5 and ubiquitinated Rps7A in polysome fractions depends upon the Not4 E3 ligase. *Mol. Microbiol.* 83, 640–653. doi: 10.1111/j.1365-2958.2011.07957.x

- Rao, X., Huang, X., Zhou, Z., and Lin, X. (2013). An improvement of the 2´(delta delta CT) method for quantitative real-time polymerase chain reaction data analysis. *Biostat. Bioinforma. Biomath.* 3, 71–85.
- Renzoni, A., Andrey, D. O., Jousselin, A., Barras, C., Monod, A., Vaudaux, P., et al. (2011). Whole genome sequencing and complete genetic analysis reveals novel pathways to glycopeptide resistance in *Staphylococcus aureus*. *PLoS One* 6:e21577. doi: 10.1371/journal.pone.0021577
- Robinson, M. D., McCarthy, D. J., and Smyth, G. K. (2010). edgeR: a Bioconductor package for differential expression analysis of digital gene expression data. *Bioinformatics* 26, 139–140. doi: 10.1093/bioinformatics/btp616
- Robinson, M. D., and Oshlack, A. (2010). A scaling normalization method for differential expression analysis of RNA-seq data. *Genome Biol.* 11:R25. doi: 10.1186/gb-2010-11-3-r25
- Rojas-Tapias, D. F., and Helmann, J. D. (2018). Induction of the Spx regulon by cell wall stress reveals novel regulatory mechanisms in *Bacillus subtilis*. *Mol. Microbiol*. 107, 659–674. doi: 10.1111/mmi.13906
- Sassi, M., Felden, B., and Augagneur, Y. (2014). Draft genome sequence of Staphylococcus aureus subsp. aureus strain HG003, an NCTC8325 derivative. Genome Announc. 2:e00855-14. doi: 10.1128/genomeA.00855-14
- Schafer, H., Heinz, A., Sudzinova, P., Voss, M., Hantke, I., Krasny, L., et al. (2019). Spx, the central regulator of the heat and oxidative stress response in B. subtilis, can repress transcription of translation-related genes. Mol. Microbiol. 111, 514–533. doi: 10.1111/mmi.14171
- Schifano, J. M., Edifor, R., Sharp, J. D., Ouyang, M., Konkimalla, A., Husson, R. N., et al. (2013). Mycobacterial toxin MazF-mt6 inhibits translation through cleavage of 23S rRNA at the ribosomal a site. *Proc. Natl. Acad. Sci. U.S.A.* 110, 8501–8506. doi: 10.1073/pnas.1222031110
- Schuster, C. F., and Bertram, R. (2016). Toxin-antitoxin systems of Staphylococcus aureus. Toxins (Basel) 8:140. doi: 10.3390/toxins805 0140
- Schuster, C. F., Mechler, L., Nolle, N., Krismer, B., Zelder, M. E., Gotz, F., et al. (2015). The mazEF toxin-antitoxin system alters the beta-lactam susceptibility of Staphylococcus aureus. PLoS One 10:e0126118. doi: 10.1371/journal.pone. 0126118
- Sierra, R., Viollier, P., and Renzoni, A. (2019). Linking toxin-antitoxin systems with phenotypes: a Staphylococcus aureus viewpoint. Biochim. Biophys. Acta Gene Regul. Mech. 1862, 742–751. doi: 10.1016/j.bbagrm.2018.07.009

- Stahlhut, S. G., Alqarzaee, A. A., Jensen, C., Fisker, N. S., Pereira, A. R., Pinho, M. G., et al. (2017). The ClpXP protease is dispensable for degradation of unfolded proteins in *Staphylococcus aureus*. Sci. Rep. 7:11739. doi: 10.1038/s41598-017-12122-v
- Van Melderen, L., and Wood, T. K. (2017). Commentary: what is the link between stringent response, endoribonuclease encoding type II toxin-antitoxin systems and persistence? *Front. Microbiol.* 8:191. doi: 10.3389/fmicb.2017.00191
- Yamaguchi, Y., Park, J. H., and Inouye, M. (2011). Toxin-antitoxin systems in bacteria and archaea. Annu. Rev. Genet. 45, 61–79. doi: 10.1146/annurev-genet-110410-132412
- Zhang, Y., and Zuber, P. (2007). Requirement of the zinc-binding domain of ClpX for Spx proteolysis in *Bacillus subtilis* and effects of disulfide stress on ClpXP activity. *J. Bacteriol.* 189, 7669–7680. doi: 10.1128/JB.00745-07
- Zhu, L., Inoue, K., Yoshizumi, S., Kobayashi, H., Zhang, Y., Ouyang, M., et al. (2009). Staphylococcus aureus MazF specifically cleaves a pentad sequence, UACAU, which is unusually abundant in the mRNA for pathogenic adhesive factor SraP. J. Bacteriol. 191, 3248–3255. doi: 10.1128/JB.01815-08
- Zorzini, V., Buts, L., Sleutel, M., Garcia-Pino, A., Talavera, A., Haesaerts, S., et al. (2014). Structural and biophysical characterization of *Staphylococcus aureus* SaMazF shows conservation of functional dynamics. *Nucleic Acids Res.* 42, 6709–6725. doi: 10.1093/nar/gku266
- Zorzini, V., Haesaerts, S., Donegan, N. P., Fu, Z., Cheung, A. L., van Nuland, N. A., et al. (2011). Crystallization of the Staphylococcus aureus MazF mRNA interferase. Acta Crystallogr. Sect. F Struct. Biol. Cryst. Commun. 67(Pt 3), 386–389. doi: 10.1107/S1744309111000571

Conflict of Interest: The authors declare that the research was conducted in the absence of any commercial or financial relationships that could be construed as a potential conflict of interest.

Copyright © 2020 Panasenko, Bezrukov, Komarynets and Renzoni. This is an openaccess article distributed under the terms of the Creative Commons Attribution License (CC BY). The use, distribution or reproduction in other forums is permitted, provided the original author(s) and the copyright owner(s) are credited and that the original publication in this journal is cited, in accordance with accepted academic practice. No use, distribution or reproduction is permitted which does not comply with these terms.

2.2.3 MazF toxin causes alterations in *Staphylococcus aureus* transcriptome, translatome and proteome that underlie bacterial dormancy.

Nucleic Acid Research 2021, https://doi.org/10.1093/nar/gkaa1292

In our previous manuscript, we postulated a link between MazF and growth stasis by affecting protein synthesis, among other pathways. Specifically, it predicted the cleavage of the GTPase HflX, a protein involved in disassemble of 100S ribosomes (or ribosome dimers). Interestingly, 100S ribosomes are assembled during stress conditions and promote bacterial survival by sequestering ribosomes and protecting them from degradation. This action prevents their utilization for translation during stressful conditions. The assembly and disassembly of 100S ribosomes is a reversible process. The predicted MazF cleavage of HlfX argues for the role of MazF to maintain formation of 100S ribosomes and decreased translation during growth stasis. This interesting observation prompt us to study more in detail the exact effect of MazF overexpression on the global translation in vivo.

MazF endoribonuclease activity would predict changes in gene expression which can be measured through RNA sequencing (RNA-seq). However, mRNA levels only partially explain protein levels (Figure 12A). To analyse more precisely MazF effect on translation, we extended our approach beyond RNA-sequend incorporated ribosome sequencing (Ribo-seq) and quantitative proteomics to our analysis. Ribo-seq captures only those mRNAs that are actively translated given more precise information on which proteins are being translated and estimates their abundance (Figure 12B). By integrating these datasets we can provide a more comprehensive picture of gene expression dynamics.

Our initial step was to analyse *S. aureus* transcriptome using conditional expression of *mazF* employing **RNA-seq**. Our findings validate previous observations by demonstrating that MazF cleavage predominantly occurs on UACAU sequence motif, while also uncovering new genes that were not previously identified by nEMOTE. In general, MazF caused considerable perturbation on the transcriptome. **Ribo-seq** allow several and very interesting observations: 1-Ribosomes profiles clearly revealed that MazF overexpression led to reduced polysome formation, accompanied by the appearance of 100S ribosome peaks or ribosome dimers (Figure 13A), indicative of translationally inactive ribosomes. 2- Our analysis facilitated the first determination of the ribosomal P-site position in *S. aureus*. This was achieved through examination of RNA fragments protected by ribosome binding, resulting in a distinct peak at 27

nt and a defined 3-nucleotide periodicity. 3- We encovered that MazF cleavage triggers ribosome stalling when reaching the end of truncated mRNA, precisely before UACAU sequences. Remarkably, this aligns with the activation of the SsrA-tagging system, which play a role in rescuing stalled ribosomes (Figure 13B). 4- Overall, a substantial reduction in translation was observed following MazF induction. To further refine our analysis, we estimated protein abundance by **TMT-MS2**, and integrated this data with Ribo-seq and RNA-seq. However, we observed that while changes in transcription correlated with changes in translation (Ribo-seq vs RNA-seq), establishing a direct correlation bewtween protein levels Ribo-seq or RNA-seq proved challenging. The experimental conditions of 10 min may have been insufficient for protein expression to be reach observable levels and thus be fully aligned with RNA levels.

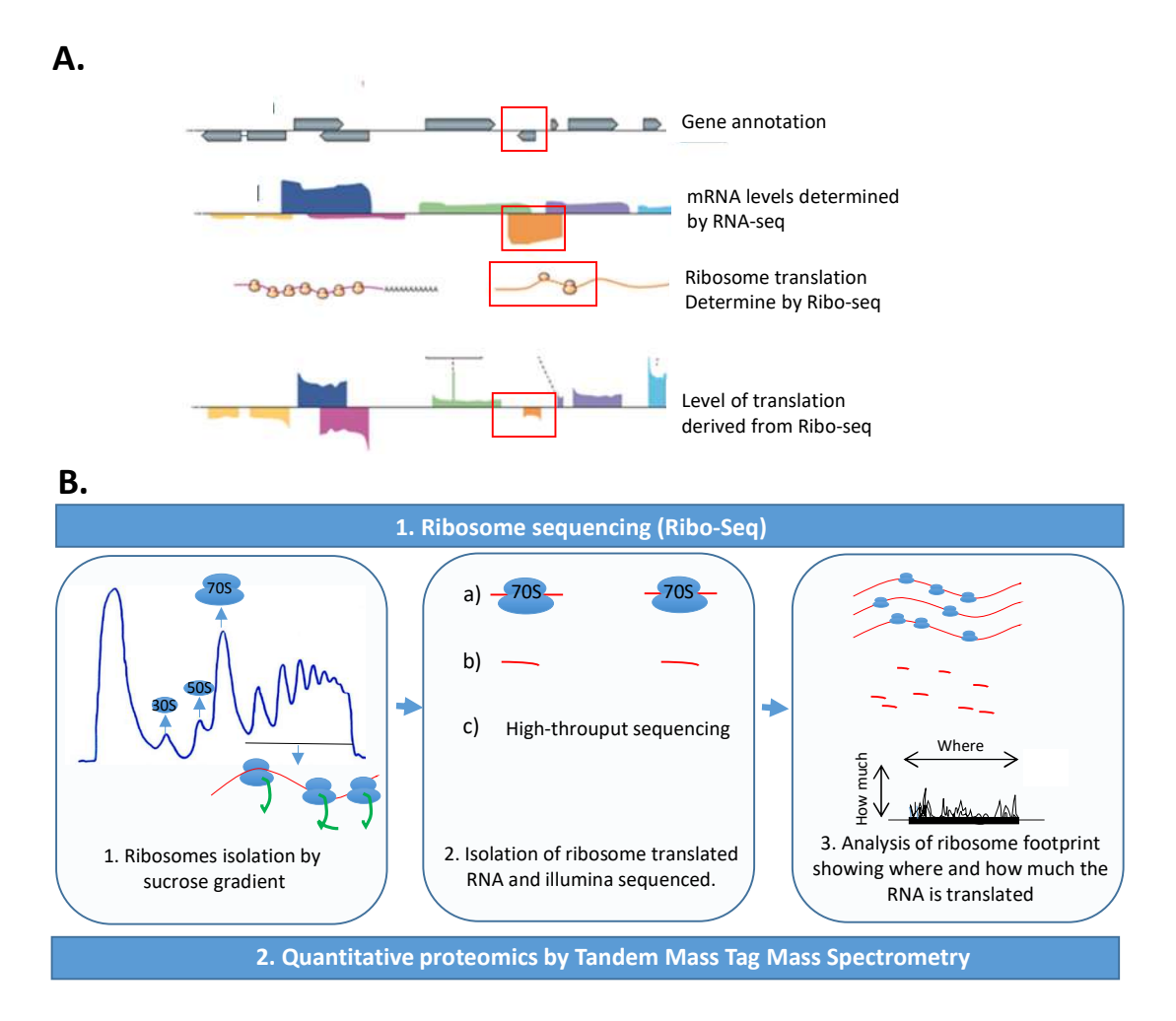


Figure 12. Diagram showing available techniques to analyse gene expression. **A)** Showing how RNA-seq is not always directly correlated with protein levels (Red insert). **B)** Diagram showing the 2 techniques used in this study.

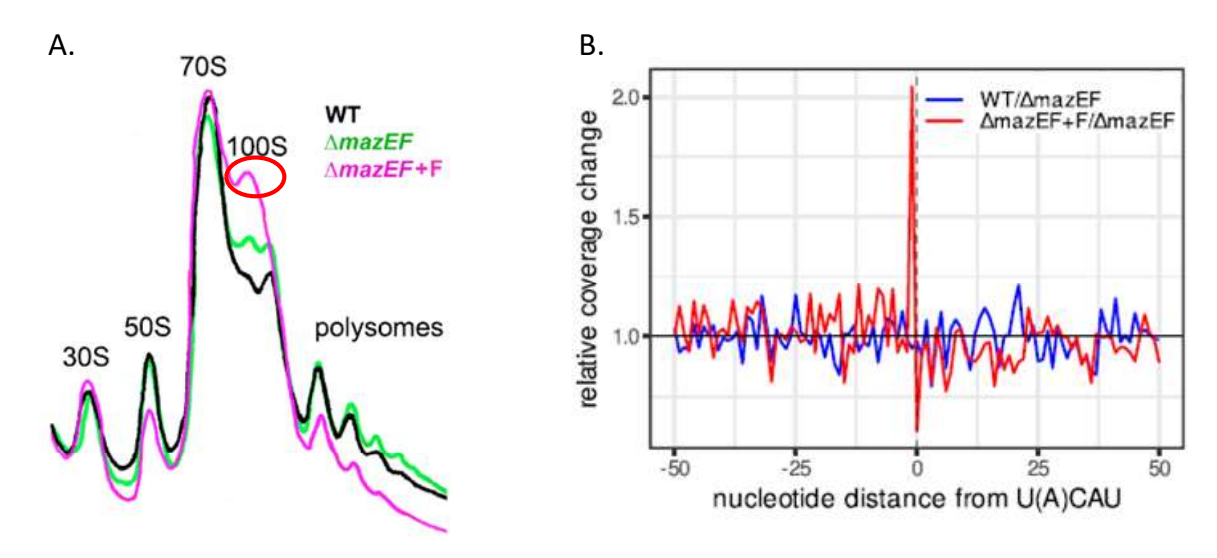


Figure 13. A) Sucrose density gradient analysis of polysomes from WT and *mazEF*-deleted strain carrying either an empty or MazF gene plasmid (+F). Positions of 30S, 70S, 100S and polysomes are indicated. 100S ribosome dimers are indicated by a red circle. **B)** Ribosomes stalling at the end of the transcript cleaved by MazF. Mean change in RPFs between *mazEF*-deleted strain carrying or not MazF gene plasmid (red line) at position -1 relative to U(A)CAU sequences. For comparison mean change in RPFs between WT and *mazEF*-deleted strains.

In conclusion, the impact of MazF encompasses a broad spectrum of mRNA targets, indicated its involvement in a diverse array of cellular processes. MazF inhibits growth but the bacterial cell is still active, as evidenced by the absence of a complete reduction of polysomes. MazF activity reprograms the translation machinery, leading the bacterial cell towards a survival mode via multiple cellular pathways. Our findings point towards mechanisms such as 1-translation rescue and co-translational quality control, 2- Ribosome hibernation and 3- Increased cell-wall thickness and reduced division (Figure 7 of the manuscript) (Bezrukov et al. 2021).

MazF toxin causes alterations in *Staphylococcus* aureus transcriptome, translatome and proteome that underlie bacterial dormancy

Fedor Bezrukov ^{61,*}, Julien Prados ⁶², Adriana Renzoni ^{62,3,*} and Olesya O. Panasenko ^{62,*}

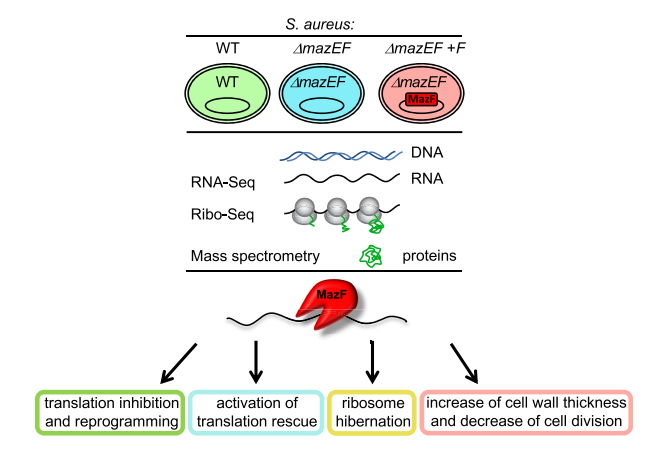
¹Department of Physics and Astronomy, The University of Manchester, Manchester M13 9PL, UK, ²Department of Microbiology and Molecular Medicine, Faculty of Medicine, University of Geneva, Geneva 1211, Switzerland and ³Division of Infectious Diseases, Department of Medicine, Geneva University Hospitals and Medical School, Geneva 1211, Switzerland

Received August 26, 2020; Revised December 07, 2020; Editorial Decision December 24, 2020; Accepted December 28, 2020

ABSTRACT

Antibiotic resistance is a serious problem which may be caused by bacterial dormancy. It has been suggested that bacterial toxin-antitoxin systems induce dormancy. We analyzed the genome-wide role of Staphylococcus aureus endoribonuclease toxin MazF using RNA-Seq, Ribo-Seq and quantitative proteomics. We characterized changes in transcriptome. translatome and proteome caused by MazF, and proposed that MazF decreases translation directly by cleaving mRNAs, and indirectly, by decreasing translation factors and by promoting ribosome hibernation. Important pathways affected during the early stage of MazF induction were identified: MazF increases cell wall thickness and decreases cell division; MazF activates SsrA-system which rescues stalled ribosomes, appearing as a result of MazF mRNA cleavage. These pathways may be promising targets for new antibacterial drugs that prevent bacteria dormancy. Finally, we described the overall impact of MazF on S. aureus cell physiology, and propose one of the mechanisms by which MazF might regulate cellular changes leading to dormancy.

GRAPHICAL ABSTRACT



INTRODUCTION

Staphylococcus aureus is a Gram-positive human pathogen, colonizing about one third of the world's population and causing a variety of diseases, from minor skin infections to life-threatening diseases (1). Antibiotic treatment is one of the main approaches of modern medicine used to combat bacterial infections; however, the effective use of antibiotics is constantly undermined due to the emergence of resistant pathogens, posing a serious public health problem (2).

Antibiotic resistance typically evolves via natural selection through random mutation or horizontal gene transfer, generating resistant cells that survive in the presence of antibiotics. It is now widely appreciated that bacterial cells may escape the bactericidal activity of antibiotics without undergoing genetic change (3). These cells are genetically identical to susceptible bacteria but have entered a non-growing quiescent or dormant state in which cells are metabolically inactive, and, thus, recalcitrant to antibiotics.

^{*}To whom correspondence should be addressed. Tel: +41 22 379 56 51; Email: olesya.panasenko@unige.ch Correspondence may also be addressed to Fedor Bezrukov. Tel: +44 161 306 64 76; Email: Fedor.Bezrukov@manchester.ac.uk Correspondence may also be addressed to Adriana Renzoni. Tel: +41 22 372 40 79; Email: Adriana.Renzoni@hcuge.ch

Dormancy, latency, stasis, quiescence and persistence are conceptually related terms used to describe the propensity of bacteria to arrest their growth in response to environmental or host-imposed stress (3–6). The molecular mechanisms underlying bacterial dormancy are not well understood.

Bacterial toxin–antitoxin systems (TASs) have been proposed as factors primarily responsible for the formation of cell dormancy; however, their role in this process is still unclear. TAS is a two-component ubiquitous module found in almost all bacteria, which is composed of a toxin and an antitoxin counteracting the toxin activity (7–9). By decreasing cell growth, toxins may help to maintain a population of dormant cells, which are not killed by antibiotics in an otherwise sensitive culture. In S. aureus MazEF is a type II TAS that consists of two proteins: a stable toxin MazF, and unstable antitoxin MazE (10,11). MazF is an endoribonuclease that preferentially cleaves mRNAs at UACAU sites (12– 14). In our recent work, MazF cleavage preference has been studied, extending the previously reported cleavage motif (15). The endonucleolytic activity of MazF is neutralized when it binds stoichiometrically to antitoxin MazE (16). Preferential digestion of MazE by stress-inducible ATPdependent ClpCP proteolytic unit frees MazF to exert its toxicity (17,18).

MazF was extensively investigated in E. coli, where it was shown to block protein synthesis (19,20) and is involved in reversible growth inhibition, drug tolerance and persistence generation (21). Later works demonstrated that the role of E. coli MazF in cell dormancy, however, is not yet fully clear (reviewed in (22)). Much less is known about S. aureus MazF, where its properties and function could differ from its E. coli homolog. Not only the MazF cleavage motifs do not entirely coincide, but also the total number of TASs is vastly different: unlike *E. coli* with numerous TASs, S. aureus has only three type II TASs. In S. aureus, MazF may be activated by stress (23), the activation of MazF leads to bacteriostasis (15,24) and alters susceptibility to antibiotics (14). Recently, it has been demonstrated that MazF promotes S. aureus biofilm antibiotic tolerance leading to transition from an acute to chronic infection that cannot be eradicated with antibiotics and is less virulent (25). It has been suggested that MazF not only made the bacteria more tolerant to antibiotics but also made the bacteria more tolerant to the host (25). Thus, the MazEF system may conceivably be one of the important players in S. aureus dormancy and antibiotic tolerance.

Endoribonuclease toxins, when activated, would predictably substantially change gene expression, which can be measured genome-wide by high throughput RNA sequencing (RNA-Seq). However, diverse studies have shown that mRNA levels only partially explain protein levels in the cell because of the complexity of protein translation, which is the most common toxin target. The development of ribosome sequencing (Ribo-Seq) has allowed the global analysis of translation *in vivo* (26–28). Ribo-Seq is based on sequencing of ribosome-protected mRNA fragments (RPFs). In contrast to RNA-Seq, Ribo-Seq only captures those mR-NAs that are being actively translated. However, although Ribo-Seq provides information on which proteins are being translated in the cell and at first approximation on their translation levels, it remains an indirect method to estimate

protein abundance. Only a combination of all three techniques, RNA-Seq, Ribo-Seq and quantitative proteomics can provide definite information about gene expression.

In S. aureus, the genome-wide role of MazEF TAS has not been investigated, although RNA- and Ribo-Seq have been applied to explore MazF toxin in *Eschrichia coli* (29). Herein, we used RNA-Seq, Ribo-Seq and quantitative proteomics to analyze the effect of MazF toxin on the transcriptome, translatome and proteome of S. aureus. We characterized the correlation between transcription, translation, and protein levels and demonstrated that MazF decreases translation directly by cleaving mRNA, and indirectly, by decreasing levels of translation factors, like rrf/frr, levels of genes responsible for amino acid biosynthesis, tRNA aminoacylation and modifications and by promoting ribosome hibernation. Our results suggest a plausible model where MazF not only suppresses transcription and translation but rather changes the translational program in a way that the cell is prepared for dormancy, for instance, promoting ribosome hibernation, increasing cell wall thickness, and decreasing cell division.

MATERIALS AND METHODS

Bacteria strains and plasmids

In this study we use HG003 strain, either wild-type (30), or deleted for mazEF (14). The mazEF deleted strain was constructed as described in (14), without affecting the sigB locus located downstream of the mazEF genes. Briefly, the mazEF knockout mutant was generated by replacing the mazE and mazF open reading frames with a lox flanked erythromycin resistance cassette, without affecting the upstream transcriptional promoter and the downstream rho independent transcriptional terminator. The resistant cassette was further removed, generating a markerless HG003 mazEF deleted mutant (14). Strains were transformed either with an empty pRAB11 vector (31), or a vector carrying HG003 mazF gene under control of inducible anhydrotetracycline (ATc) promoter (pRAB11-mazF) (15,23). Cultures were grown on Mueller Hinton Broth media in the presence of 15 µg/ml of chloramphenicol (Cm) until OD₆₀₀ of 0.5–0.7 at 37°C with shaking. To induce mazF expression, anhydrotetracycline (ATc) was added up to a final concentration 0.2 µM and cultures were incubated 10–180 min at 37°C with shaking.

RNA-Seq

Cultures with either the empty vector or the vector containing mazF were grown untill OD_{600} of 0.5 at 37°C with shaking. ATc induction was done for 10 min. For total RNA isolation 8 ml of culture were immediately mixed with 40 ml of -80° C cold ethanol–acetone mixture (1:1). Cells were collected by centrifugation for 10 min at 4000 g, 4°C. Pellets were washed with 1 ml of cold TE buffer (10 mM Tris–HCl, 1 mM EDTA, pH 8.0), resuspended in 100 μ l of TE with 1 mg/ml of lysostaphin (AMBI) and 2 μ l of RNasinePlus (Promega), and incubated for 5 min at 37°C. Total RNAs were purified with the ReliaPrep RNA kit (Promega) in biological duplicates. Ribosomal RNAs

were depleted with RiboZero rRNA Removal Kit for Bacteria (Illumina). Libraries were created using the Illumina TruSeq stranded mRNA kit. First strand cDNAs were synthesized with random hexamer primer. Libraries were sequenced at Fasteris SA (Geneva, Switzerland) on an Illumina HiSeq 3000/4000, single-reads, 1 × 50 bp.

Analysis of RNA-Seq

Results of RNA-Seq were aligned to RefSeq assembly GCF_000013425.1 (NCTC 8325) combined with pRAB11 sequence (accession JN635500.1) using STAR aligner. The aligned reads were associated with the RefSeq gene annotations (the tmRNA region was added to the annotations manually using the location from AureoWiki). A typical library contained 24–34 million of reads per sample aligned to genome, with a high correlation between biological replicates (Supplementary Figure S1B, Table S1). Only genes with more than 40 reads per sample (average over samples) were retained for further analysis. Read counts were normalized by the total number of reads excluding reads aligned to ribosomal RNA, and differential gene fold changes and *P*-values were obtained by limma/voom (32).

RNA-Seq results were validated using TaqMan reverse transcription real-time quantitative polymerase chain reaction (RTqPCR) with MGB Double-Dye probes (Supplementary Table S4) as described in supplementary methods.

Detection of MazF cleavage sites

The potentially cleaved genes were identified in the genome by the dips in RNA-Seq coverage similar to published methods (29). First, RNA-Seq coverage was constructed from single end sequencing assuming length of fragments to be equal to 200 nt. Gene coverage was analyzed including 50 nt upstream. Second, cleavage ratio was constructed as ratio of the normalized RNA-Seq coverage of $\Delta mazEF+F$ to $\triangle mazEF$ samples. The genes were defined as potential MazF cleavage targets if the difference between minimum and maximum of cleavage ratio along the gene was >8-fold, creating the 'dip' (Supplementary Figure S2B). The genes with RNA-Seq coverage in $\triangle mazEF$ sample below 10 near the cleavage minimum were ignored to evade false positives in low expressed genes. The method described here differs from that of (29), where only the cleavage ratio in the minimum along the gene was used. This difference makes our approach less biased toward detecting down regulated, but not cleaved, genes.

To verify that this method detects mRNA cleavage, we checked that the detected cleavage minima predominantly had a UACAU cleavage motif in the 150 nt vicinity (Supplementary Figure S2C). With the uncertainty on the length of the mRNA fragments in the library, we cannot expect a more precise association of the cleavage minima with cleavage site in each particular gene.

Ribo-Seq

To obtain *S. aureus* polysomes 1 ml of an overnight culture was diluted in 250 ml of media and grown until an OD_{600} of 0.5 at 37°C. ATc induction was done for 10 min. To block

translation Cm was added up to a final concentration of 0.3 mM, and culture was incubated for 2 min at 37°C and then quickly chilled. After centrifugation pellets were washed in 2 ml of cold Resuspension Buffer (RB) (20 mM Tris (pH 8.0), 10 mM MgCl₂, 5 mM CaCl₂, 100 mM NH₄Cl, 1 mM Cm), and resuspended in 0.8 ml of cold Lysis Buffer [RB plus 0.1% IGEPAL, 0.4% Triton X-100, 100 U/ml RNasefree DNase I (Roche), 0.5 U/µl SUPERaseIn (Ambion), Protease Inhibitors (Roche)]. Suspension was incubated on ice for 5 min and frozen in drops in liquid nitrogen. Drops were milled five times with 1-min cycles at 30 Hz in CryoMill MM400 (Retsch) in a 10 ml grinding jar with 15 mm grinding ball.

For cell extract preparation, cell powder was thawed in 50 ml tube and centrifuged at 4000 g, 4°C for 1 min. Supernatant (SN) was clarified at 16 000 g, 4°C for 1 min and centrifuged in a new tube at 16 000 g, 4°C for 10 min.

To obtain ribosome footprints 1000 U of S7 Micrococcal Nuclease S7 (Roche) was added per 1 mg of nucleic acids. Samples were incubated for 1 h at 25°C with rotation at 190 rpm. Reactions were guenched by the addition of EGTA up to a final concentration 6 mM. Nucleic acids (0.5 mg) were loaded onto a linear 10-50% sucrose gradients prepared on Gradient Buffer [20 mM Tris (pH 8.0), 10 mM MgCl₂, 100 mM NH₄Cl]. Tubes were centrifuged at 217 000 g (35 000 rpm, SW41 Ti rotor, Beckman Coulter) for 3 h at 4°C. Fractions were collected using a UA/6 detector (ISCO). After centrifugation fractions (750 μl) were incubated with 10 μl of proteinase K (NEB, 800 U/ml) and 10 μl of SDS 10% overnight at 4°C. RNAs were isolated with phenol-chloroform extraction. Libraries were prepared as described (26,33) and sequenced on an Illumina HiSeq 3000/4000, single-reads, 1×50 bp.

Analysis of Ribo-Seq

Reads were aligned by STAR, with the adap-'-clip 3p Adapter Seqsequence removed using CTGTAGGCACCATCAATAGATCGGAAGAGC ACACGTCTGAACTCCAGTCAC' option. The position of the P-site was determined by the study of the distribution of the positions of the fragments around the beginning of the ORFs, as described (26) using only ORFs without other annotated features 50 nt upstream in the genome (to exclude possible complications of translation of genes within operons). Alignment of the first significant peak of the distribution with the AUG codon corresponded to 3'-end of the fragment being in the nucleotide position 16 of the open reading frame, so the P-site was further defined as the 3'-position of the read minus 15, and only RPF with the length 25–31 were used. The translational signal was defined by the number of RPF with the P-site within gene CDS, excluding first 30 and last 6 nucleotides, to remove the effects of translational initiation and termination. Only genes with >40 reads on average were retained for analysis. The signal was normalized by the total number of reads aligned to the genome (excluding plasmid and rRNA reads). Fold changes were computed by limma/voom (32). Typical number of Ribo-Seq reads corresponding to coding genes was about 4 million per sample with very good reproducibility between biological replicates (Supplementary

Figure S7B, Table S1). Translational efficiency (TE) was defined as the ratio of Ribo-Seq and RNA-Seq signals in RPKM. TE and its fold change was calculated using Xtail (34) allowing to identify the statistical significance of the result.

TMT-MS2 quantitative proteomics

ATc induction was done for 10 min. For total protein extraction 25 ml of cultures with OD_{600} of 0.7 were collected and washed three times with 1 ml of phosphate-buffered saline (PBS) buffer. Cells were lysed in the presence of 400 µl of lysis buffer (LB) [PBS, 200 µg/ml lysostaphin (AMBI), 200 μg/ml DNAse I, protease inhibitors (Roche)] for 20 min at 37°C, chilled on ice, and sonicated 10 times with 30-s cycles using Cell Disrupter B-30 (Branson). Extracts were clarified by centrifugation for 10 min at 14 000 g, 4°C. Total protein concentration was measured in supernatants by the Bradford protein assay. This method permitted to obtain of about 1 mg of total protein with a concentration of about 2.5-3.0 mg/ml. Samples were mixed with Laemmli Sample Buffer (SB) and analyzed by SDS polyacrylamide gel electrophoresis (SDS-PAGE) followed by Coomassie Blue staining or western blot.

Tandem Mass Tags Mass Spectrometry (TMT-MS2) was done at the Proteome Sciences R&D GmbH&Co KG. Samples were digested with trypsin, TMT-labeled, and subjected to Strong Cation Exchange (SCX) chromatography. Each fraction was analyzed by nano LC-MS/MS and MS2 (Thermo LTQ-Orbitrap Velos mass spectrometer). Data were analyzed with the MASCOT and SEQUEST databases. Filtering, normalization and quantification was achieved using Proteome Discoverer (Thermo Scientific). *P*-values and the log-fold change was further obtained using limma package.

Transmission electron microscopy (TEM)

 $\Delta mazEF$ cells carrying either empty vector or vector containing mazF were grown at 37°C until an OD₆₀₀ of 0.5– 0.6. After ATc induction cultures were incubated for 0, 10, 60 and 180 min at 37°C with shaking. 2 ml of cell cultures were collected by centrifugation for 1 min, 10 000 g, 4°C. Pellets were washed with 1 ml of PBS and then resuspended in 1 ml of fresh 4% (v/v) glutaraldehyde in PBS. After 15 min incubation samples were spun for 1 min, 10 000 g, 4°C and washed with 1 ml of PBS. Samples obtained in two independent experiments were analyzed on Morgagni TEM (FEI) at the Microscopy PFMU core platform, CMU, University of Geneva. Cell wall thickness measurements were done using TEM image software: six measurements per cell in 10 different cells of each strain with nearly equatorial cut surfaces were averaged. The P-values were computed using two-sided Wilcoxon signed-rank test. Cell size was analyzed using ImageJ software. For analysis of cell division the Fisher's exact test was used to compare the number of cells with and without division septum.

Antibodies

Polyclonal rabbit anti-MazF antibodies were described in (15) and used in dilution 1:500. Polyclonal rabbit anti-

Hpf antibodies were described in (35) and used in dilution 1:4000. Polyclonal rabbit anti-Pbp4 antibodies were used in dilution 1:5000. Goat anti-rabbit IgG–HRP conjugate (Bio-Rad) were used in dilution 1:5000.

RESULTS

Transcriptome analysis after MazF induction

We expected that MazF modifies *S. aureus* physiology directly by cleavage of mRNA at a specific motif, and/or globally by indirect regulation. This global effect is expected to modify the activation of pathways relevant to dormancy. Using conditional expression of *mazF* (Supplementary Figure S1A) we explored in detail how MazF toxin affects cellular physiology (Figure 1A).

First, we analyzed the effect of mazF induction on the S. aureus transcriptome by RNA-Seq. The RNA-Seq libraries showed high correlation between both biological replicates (Supplementary Figure S1B, Table S1). In the S. aureus genome (NCTC 8325) there are 2843 genes annotated as open reading frames (ORFs). 1684 (60%) of them contain in total 3406 UACAU sequences that are potentially cleaved by MazF. The distribution of this motif over coding gene sequences (CDS) does not have any preferential position bias (Supplementary Figure S2A). In WT both MazE and MazF proteins are present, and even though MazF is neutralized by MazE we cannot exclude some level of endogenous MazF activity, as reported (14). We analyzed the RNA-Seq read coverage 500 nucleotides (nt) before and after each of UACAU sequences (Figure 1B), and observed a decrease of reads around the potential MazF cleavage sites when MazF expression was induced, while no global changes were found between WT and $\triangle mazEF$ strain. This result provides evidence that in WT MazF activity is generally neutralized by MazE, while, in the absence of MazE, MazF leads to mRNA cleavage on UACAU on a genomewide level.

Recently, we identified MazF cleavage motifs *in vivo* using the nEMOTE (non-phosphorylated exact mapping of transcriptome ends) technique (15). This method allows detection of the exact cleavage sites with nucleotide precision. However, it has limitations, and it was possible to identify cleavages only in highly expressed genes. In our analysis herein, we applied a different approach similar to (29,36). We identified MazF cleavages by the pronounced dips in the ratio between $\Delta mazEF+F$ and $\Delta mazEF$ RNA-Seq coverage (Supplementary Figure S2B and C). By this method 339 genes that may be directly cut by MazF were detected (Supplementary Table S2). These cleavages mostly corresponded to the significantly down-regulated genes and have only 10% overlap with the genes identified by nEMOTE in (15) (Supplementary Figure S2D).

In previous studies, it was proposed that *E. coli* MazF cleaves closely upstream of the AUG start codon and generates leaderless mRNAs, which are translated by 'stressribosomes' lacking anti-Shine-Dalgarno sequence also created by MazF (36,37). Later, this finding was argued (29). We analyzed whether *S. aureus* MazF created such transcripts, and found only one gene (SAOUHSC_01137), which was cleaved by MazF in the proximity of the start codon and which was translated slightly better after MazF

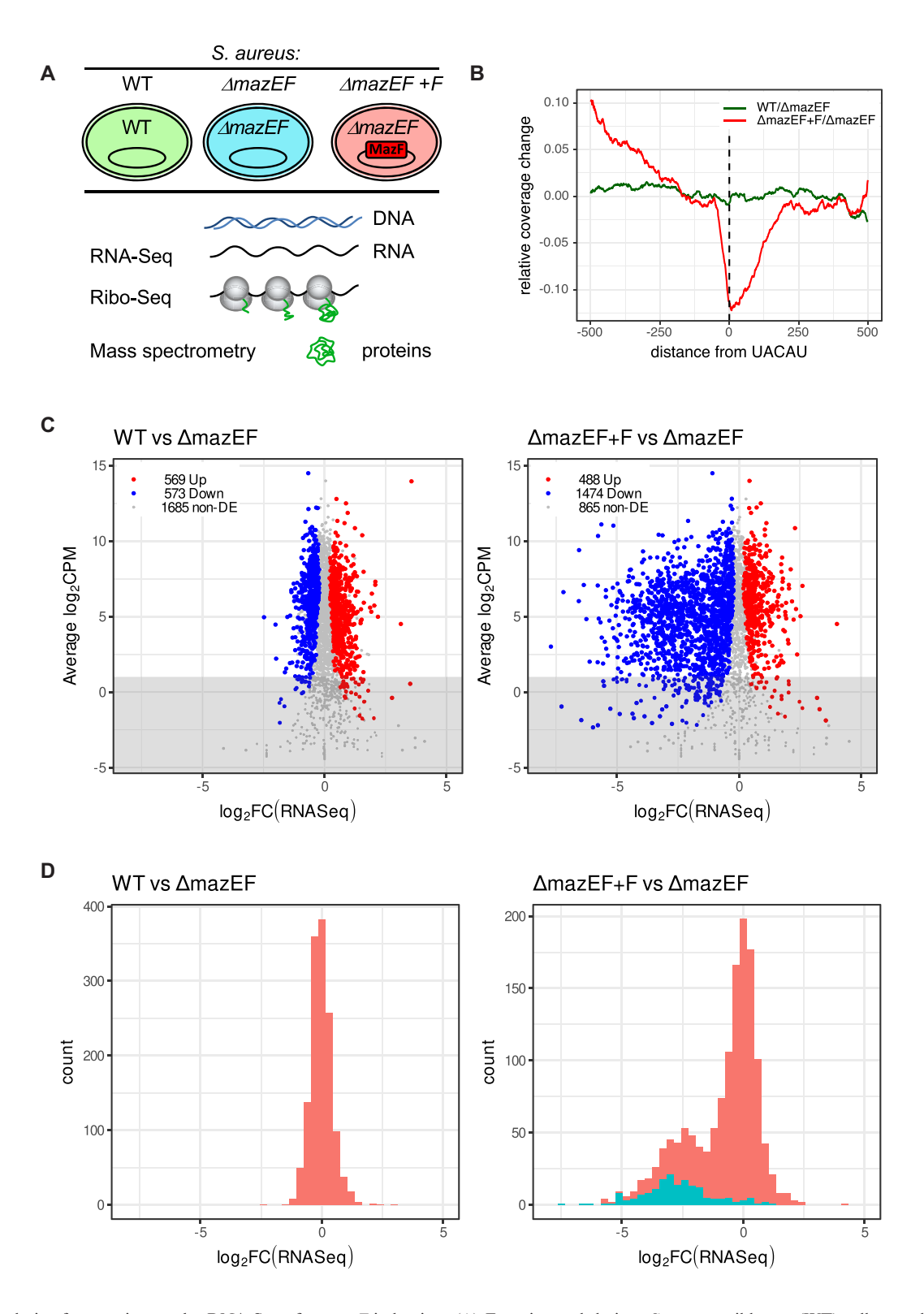


Figure 1. Analysis of transcriptome by RNA-Seq after mazF induction. (A) Experimental design. S. aureus wild type (WT) cells or cells deleted for mazEF ($\Delta mazEF$), were transformed with an empty vector or a vector carrying inducible mazF ($\Delta mazEF+F$). Cells were collected after 10 min of mazF induction when MazF protein had been produced, but cell growth was not yet inhibited (15,23), and analyzed by RNA-Seq, Ribo-Seq and quantitative mass spectrometry. (B) MazF expression leads to mRNA cleavage on UACAU on genome-wide level. Comparison of RNA-Seq coverage 500 nt before and after UACAU sequences: WT to $\Delta mazEF$ (green) and $\Delta mazEF+F$ to $\Delta mazEF$ (red). (C) \log_2 -fold change (\log -FC) in RNA levels of WT compared to $\Delta mazEF$ (left) and of $\Delta mazEF+F$ compared to $\Delta mazEF$ (right). RNA-Seq is expressed in counts per million reads (CPM). Upregulated genes (P < 0.05), downregulated genes (P < 0.05) and non-differentially expressed genes (non-DE) (P > 0.05) are marked in red, blue and grey, respectively. Only genes with more than 40 reads per gene averaged per sample (above the grey highlighted region) were retained for the further analysis. (D) Distribution of the log-FC of RNA-Seq between WT and $\Delta mazEF$ (left) and $\Delta mazEF$ (right). The genes with identified MazF cleavage site are indicated in cyan.

induction. We concluded that MazF does not create translated leaderless transcripts in *S. aureus*.

Principal Component Analysis (PCA) allows to summarize the systematic patterns of variations in the data. PCA demonstrated close similarity of biological duplicates (Supplementary Figure S3A). $\Delta mazEF$ cluster is closer to WT cluster, while $\Delta mazEF+F$ is notably different from the WT and $\Delta mazEF$ groups, indicating that mazF induction leads to larger gene expression changes than deletion of mazEF. Clustering was similar for PCA limited to only high (RPKM $> 2^5$) or low (RPKM $< 2^5$) expressed genes, and even limited to only transcripts with or without UACAU motifs, suggesting that MazF changed expression not only of cleaved genes, but rather impacted the entire transcriptome.

We compared changes in transcriptomes when mazEF was deleted (WT versus $\Delta mazEF$) and when mazF was induced in a $\Delta mazEF$ background ($\Delta mazEF+F$ versus $\triangle mazEF$) (Figure 1C, Supplementary Table S1). Similar number of genes were up- and down-regulated (569) and 573 genes, respectively) in WT compared to $\Delta mazEF$, while transcription of 1685 genes was unchanged. In contrast, we observed that MazF caused considerable perturbation in the transcriptome. Upon mazF induction only 867 genes were not changed, while 488 and 1474 genes were upand down-regulated, respectively, corresponding to about 17% and 52% of analyzed genes. Importantly, upon mazF induction, many genes were significantly down-regulated (with log₂-fold change (log-FC)<-2). 17% of up-regulated genes indicates that, even if MazF decreased transcription and inhibited cell growth, the cell remained biologically active. RNA-Seq data were validated by RTqPCR in independent experiments for 18 transcripts (vraS, lytR, rsbW, htrA1, frr/rrf, murA1, tagA, purR, pbp2, pbp4, stp1, yjbH, fusA, hup, trfA, spx, trxA, hpf) differently affected by MazF (Supplementary Figure S4, Table S4).

The distribution of the RNA-Seq log-FC for the WT to $\Delta mazEF$ comparison showed one peak with the average of zero (Figure 1D, left). In the comparison of $\Delta mazEF+F$ to $\Delta mazEF$, however, the histogram of the RNA-Seg log-FC was bimodal with two pronounced peaks, indicating that there are two families of genes (Figure 1D, right). One group - with the average log-FC of zero, and a second group of significantly down regulated genes with average log-FC –2.5. This distribution suggests that there are two mechanisms of gene regulation by MazF. The genes in the first group did not display an overall decrease of expression, but had a variance in expression change, indicating an indirect effect of MazF on them. For comparison, the distribution of the RNA-Seq log-FC between replicates showed a very narrow peak around zero (Supplementary Figure S3B). The transcripts in the second group probably correspond to those directly cleaved by MazF, leading to strongly reduced expression. Indeed, distribution of the genes that we identified as cut by MazF (Supplementary Table S2), explicitly correlate with the second peak supporting the idea of two mechanisms of gene regulation by MazF (Figure 1D, right). Not all genes from the second group were identified as cleaved, due to the strict criteria of our analysis, chosen to avoid false positive artifacts. It is certainly possible that more genes, if not all, from the second group are MazF targets.

To examine if MazF may generally affect the stability of mRNAs besides it direct cleavage targets we analyzed if the change in mRNA levels upon mazF induction can be attributable to the change of mRNA stability. We performed an RNA stability assay by adding rifampicin to halt de novo mRNA synthesis in $\triangle mazEF$ cells expressing either empty vector or inducible MazF after 10 min of ATc induction. The decay of the mRNAs was monitored by RTqPCR at different time points of rifampicin treatment (Supplementary Figure S5). For transcripts that were not affected by MazF (gyrB), and for transcripts that were decreased upon mazF induction (frr/rrf, hup, fusA), we observed slightly increased mRNA degradation. For the transcripts that were increased upon mazF induction (spx, hpf) we observed slight mRNA stabilization. Although individual decay rates varied for each gene tested, we found evidence of both increased and decreased decay. Thus, there appears to be no global non-specific effect on RNA decay, but rather a gene specific effect.

Analysis of S. aureus translatome

Global impact of MazF on translation was studied by Ribo-Seq (Figure 2A). Ribosome profiles from $\Delta mazEF$ cells slightly differed from the WT. Ribosome profiles after MazF expression in $\Delta mazEF$ background showed decreased polysomes and the appearance of a pronounced 100S peak, representing ribosome dimers (38). The 100S ribosomes are translationally inactive and correspond to the resting form in the ribosome cycle, hence, the process of 100S formation has been named 'ribosomal hibernation'. 100S peak was not affected by RNase treatment and was not observed in Δhpf strain (Supplementary Figure S6). Thus we concluded that MazF expression led to appearance of hibernating ribosomes that are sequestrated from active translation and are preserved in a form of dimers.

The quality of Ribo-Seq analysis depends on the size and homogeneity of ribosome protected fragments (RPFs) obtained after nuclease digestion. Optimal digestion was obtained with 1000 U of \$7 nuclease per 1 mg of total RNA (Supplementary Figure S7A). Libraries were prepared from digested RPFs and, after quality control, subtraction of rRNA and plasmid reads, showed good reproducibility between biological replicates (Supplementary Figure S7B, Table S1). The length distribution of RPFs ranged from 22 to 40 nt and showed a single peak with a maximum at 27 nt and well-defined three-nucleotide periodicity which is a characteristic property of protein coding ORFs (Figure 2B and Supplementary Figure S7C). This was larger than E. coli (24 nt) and smaller than eukaryotic (28–32 nt) RPFs. RPFs of length 25–31 nt, demonstrating good correlation with the 1st nt of codons, were selected for subsequent analysis (Figure 2C).

When MazF cleaves mRNA it creates stop-less transcripts, where ribosomes reaching the end of prematurely truncated mRNA stall because of the absence of a complete codon in the A-site, as was reported for *E. coli* (29). We analyzed changes in RPFs near the MazF cleavage site, and indeed observed accumulation of ribosomes at the position preceding UACAU sequences (Figure 2D).

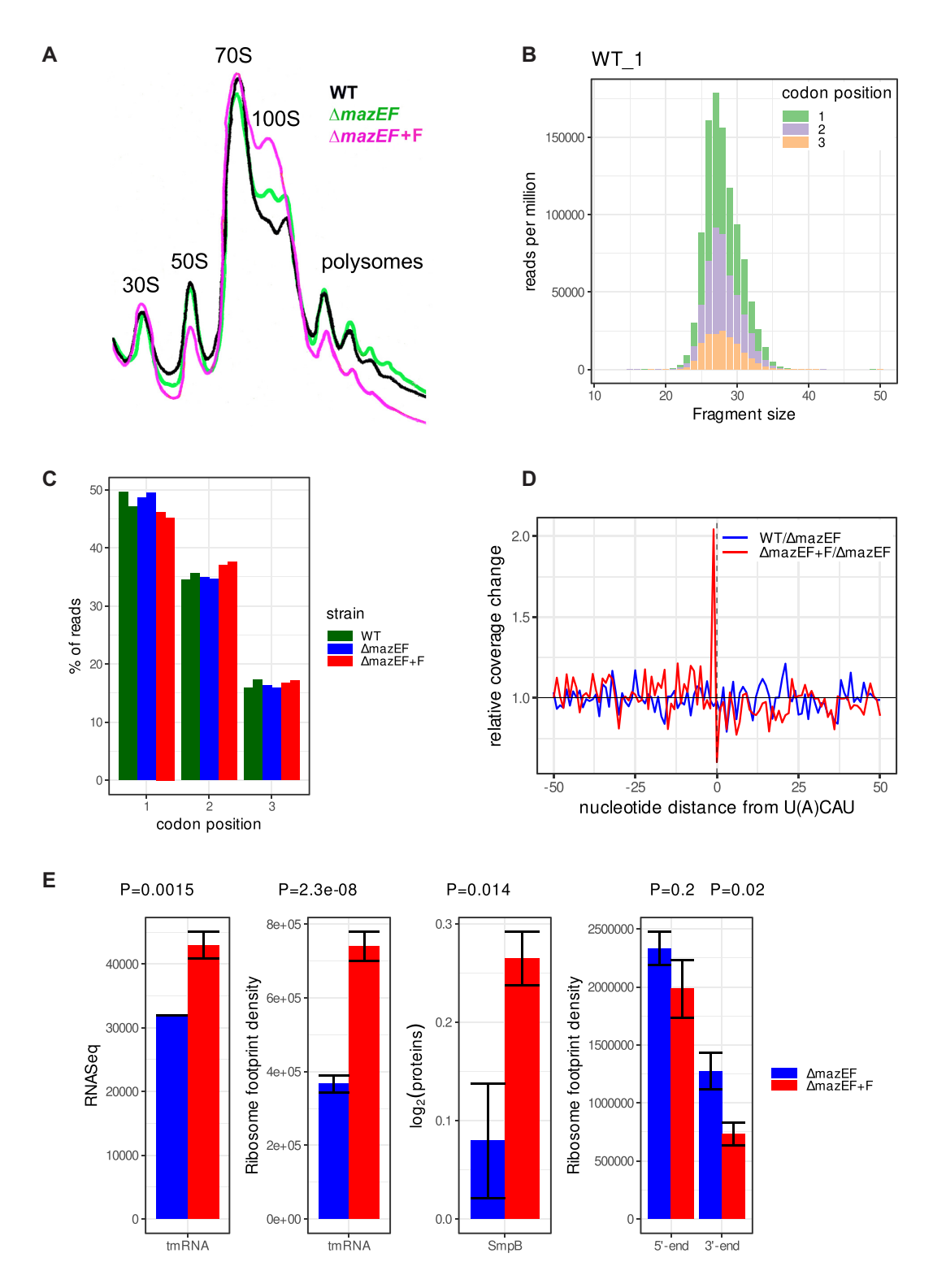


Figure 2. Analysis of translatome after mazF induction by Ribo-Seq. (A) 10-15% sucrose density gradient analysis of polysomes from the WT and $\Delta mazEF$ cells, harboring either empty plasmid or plasmid with mazF gene (F). Positions of 30S, 50S, monosomes (70S), ribosome dimers (100S), and polysomes are indicated. (B) The frequency distribution of RPFs between 21 and 38 nt obtained from nuclease digestion in the WT replicate 1. Codon periodicity for each length fragment is indicated in green, violet, and orange for the 1^{st} , 2^{nd} and 3^{rd} nt position in codon, respectively. (C) Reads attributed to the 1^{st} , 2^{nd} and 3^{rd} nt of a codon in WT (green), $\Delta mazEF$ (blue) and $\Delta mazEF+F$ (red) samples in duplicates. (D) Ribosomes stall at the end of the transcripts cleaved by MazF. Mean change in RPFs between $\Delta mazEF+F$ and $\Delta mazEF$ (ed) at the position -1 relative to U(A)CAU sequences. For comparison, mean change in RPFs between WT and $\Delta mazEF$ (blue) is shown in the same region. (E) MazF induction leads to the activation of SsrA-tagging system, which consists of tmRNA and protein SmpB, and to the decrease of RPFs at the 3' end of transcripts. $\Delta mazEF$ (blue) and $\Delta mazEF+F$ (red) strains were compared for tmRNA levels, ribosome density on MLD part of tmRNA, protein levels of SmpB, and ribosome density at the 5' and 3' ends of transcripts. SmpB protein levels were evaluated by quantitative mass spectrometry (Supplementary Table S1) and have arbitrary normalization. P-values are indicated above.

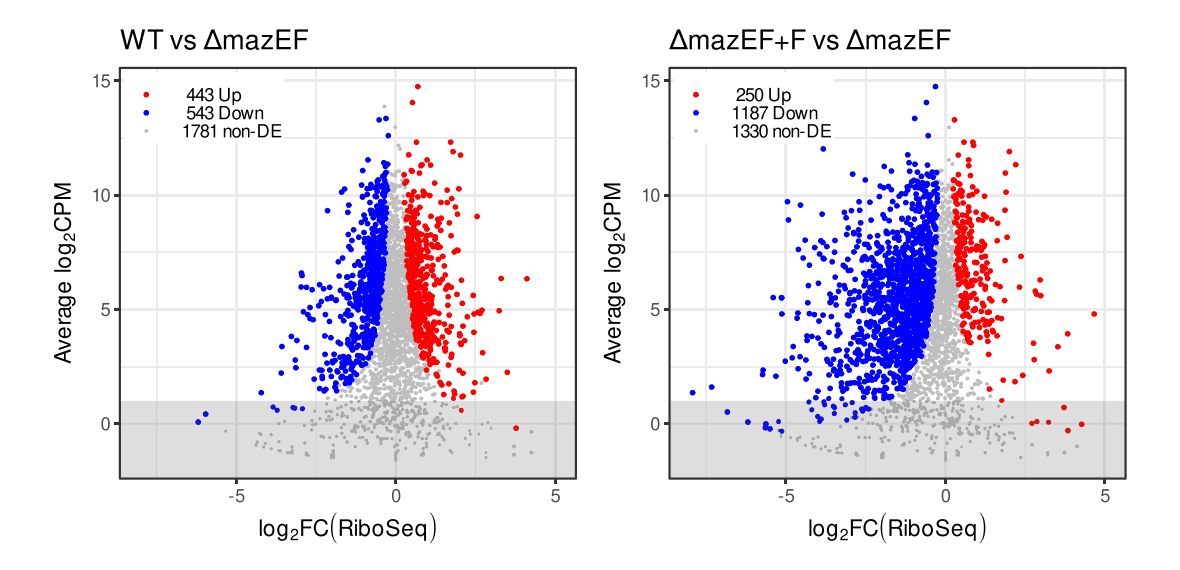


Figure 3. Changes in translatome after mazF induction, log-FC in RPFs in WT compared to $\Delta mazEF$ (left) and in $\Delta mazEF+F$ compared to $\Delta mazEF$ (right). Genes with increased RPFs (P < 0.05), decreased RPFs (P < 0.05) and genes without significant change in RPFs (P > 0.05) are marked in red, blue and grey. Only genes with more than 40 reads per gene averaged per sample (above the grey highlighted region) were retained for the further analysis.

In bacteria the stop-less transcripts are rescued by the SsrA-tagging system, consisting of transfer-messenger RNA (tmRNA) and protein SmpB, in the process called trans-translation. tmRNA is a bifunctional molecule that has tRNA-like domain (TLD) acting as a tRNA, and messenger-like domain (MLD) acting as a mRNA. Elongation factor Tu with the help of SmpB delivers tmRNA to the A-site of the stalled ribosome, where mRNA template is changed with MLD, and translation continues. Most of the knowledge about the bacterial translation rescue systems derives from E. coli (39,40). In S. aureus, there is only one translation rescue system, which is essential. It terminates translation by a normal stop codon and contributes to degradation of partially synthesized proteins by proteases (17,41). We observed increase of tmRNA transcription, increase of RPFs on MLD of tmRNA and increase of SmpB protein production after MazF induction (Figure 2E). We concluded that the SsrA-tagging system, playing an important role in the rescue of stalled ribosomes and in the resumption of protein synthesis, was activated by MazF in S. aureus. MazF induction resulted in about 50% decrease of ribosome footprints at the 3' end of transcripts, due to the ribosomes running off from the 3' end of cleaved transcripts, but did not significantly change the ribosome occupancy at the 5' end of transcripts and within the transcripts (Figure 2E, right). The PCA for Ribo-Seq (Supplementary Figure S8) was similar to those of RNA-Seq, confirming the conclusion that MazF causes indirect regulation of translation of many genes.

Comparison of the Ribo-Seq of WT versus $\Delta mazEF$ and $\Delta mazEF+F$ versus $\Delta mazEF$ (Figure 3, Supplementary Table S1) led to the results similar to RNA-Seq. We found similar numbers of up- and down-regulated genes, 443 and 543, respectively in WT compared to $\Delta mazEF$, while translation of 1781 genes was not changed. MazF led to substantial decrease of RPFs. Only 250 genes had more RPFs, while 1187 genes had less RPFs when MazF was induced, corresponding to 9.0% and 43% of analyzed genes. 1330 genes were unchanged. Many genes were significantly down-regulated with log-FC<-2, indicating the substantial reduction of translation.

Correlation between transcriptome, translatome and proteome

At the first approximation, the change in number of RPFs in Ribo-Seq corresponds to the change in translation and is more directly related to the change in protein levels, than RNA-Seq. However, translation does not always occur with the same speed and outcome. Translation is further modified by additional factors, which may influence protein production, as, e.g. the presence of co-translational factors or chaperones assisting folding of nascent chains. Thus, changes in translation alone also do not necessarily imply changes in the abundance of the translated proteins. By this reasoning, the relation between RNA-Seq, Ribo-Seq and quantitative proteomics data should be analyzed.

Protein abundance was estimated by Tandem Mass Tags Mass Spectrometry (TMT-MS2) under the same conditions of *mazF* induction as before (Supplementary Figure S9A). PCA showed that WT, $\triangle mazEF$ and $\triangle mazEF+F$ duplicates form separated clusters (Supplementary Figure S9B).

To study the relation between RNA-Seq, Ribo-Seq, and proteomics we compared the changes of these parameters between either WT and $\triangle mazEF$ (Figure 4, left), or between $\Delta mazEF+F$ and $\Delta mazEF$ (Figure 4, right). Use of the differential expression allowed to avoid the possible biases associated with overall gene expression or CDS length, and is the only possible approach for proteomics data, which does not provide reliable absolute measurements.

First, we studied the relation between transcriptome and translatome (Figure 4, top). For the case of WT vs $\triangle mazEF$ the Pearson correlation was rather small (0.29) and overall shape of the distribution was round. This indicates, that the

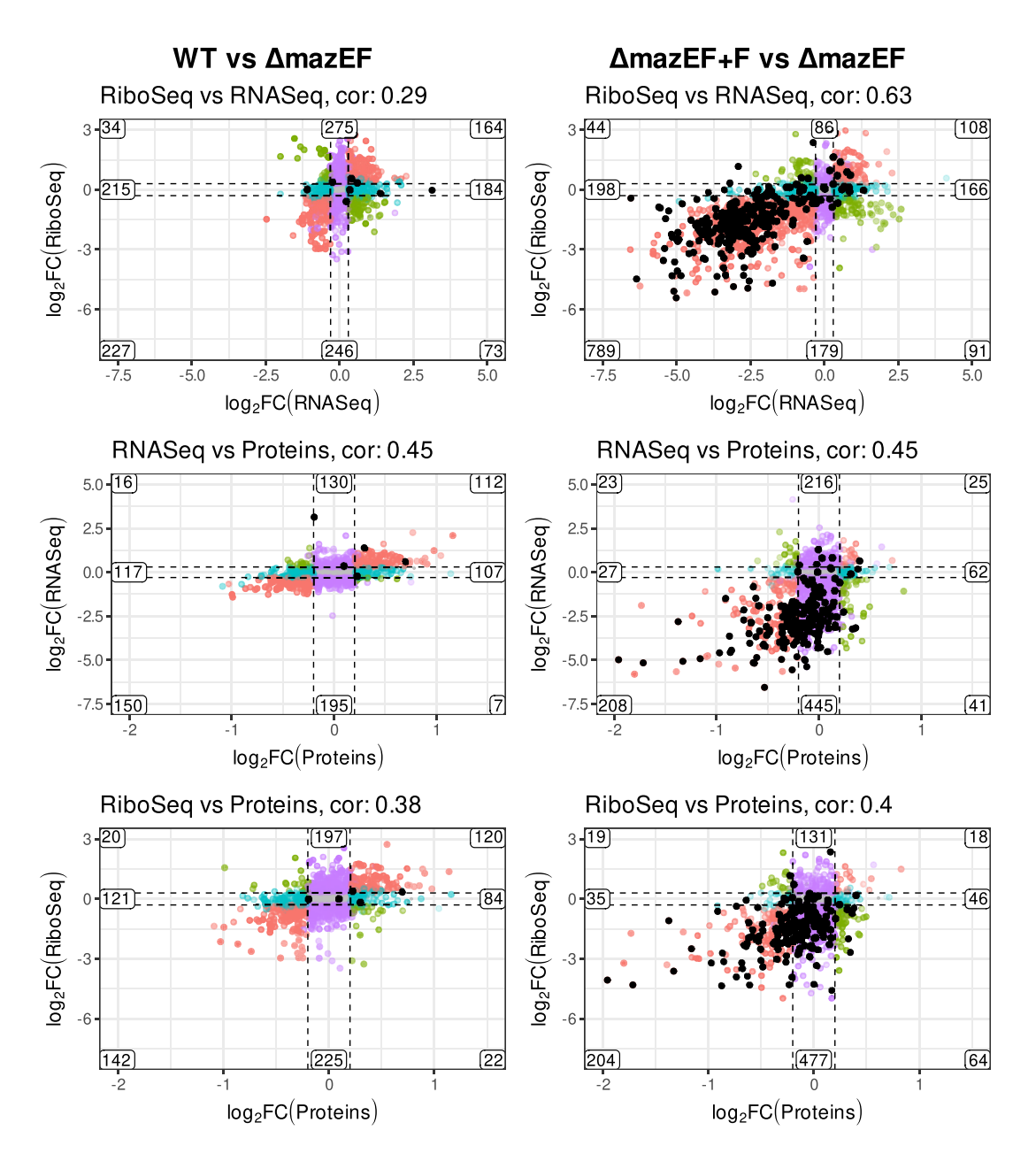


Figure 4. Correlation between changes in RNA-Seq, Ribo-Seq and proteomics. log-FC in RNA-Seq, Ribo-Seq, and proteomics in WT compared to $\Delta mazEF$ (left) and $\Delta mazEF+F$ compared to $\Delta mazEF$ (right). Comparison of Ribo-Seq versus RNA-Seq, RNA-Seq versus proteomics, and Ribo-Seq versus proteomics, are indicated. The scales are the same for the graphs on the right and left side of the picture for the clear comparison. Pearson correlation is indicated above each panel. The numbers of the genes in each group are shown. The genes are defined as differentially expressed for log-FC larger than 0.3 for RNA- and Ribo-Seq, and larger than 0.2 for proteins and P < 0.05. Colors indicate the homodirectional change (red), opposite change (green), change only in x-axis (blue), change only in y-axis (violet), no change (gray). Genes which were identified as a directly cleaved by MazF are indicated by black dots.

difference caused by removal of *mazEF* is not pronounced, and the correlation is mostly dominated by random noise. We can still see, that the number of genes that changed homodirectionally in a statistically significant way (up or down regulated in both RNA- and Ribo-Seq, in red) was larger, than of those that changed in opposite directions (up in RNA- and down in Ribo-Seq, or vice versa, in green), indicating that the changes were indeed related.

The effect of *mazF* induction, on the contrary, caused significant modification of both translatome and transcrip-

tome, with a large number of downregulated genes. With the large changes, the Pearson correlation was higher (0.63), confirming the strong relation between RNA- and Ribo-Seq. The subset of genes showing opposite changes such as increased mRNA but decreased Ribo-Seq, may be explained by mRNA preservation in a translationally inactive, but stable form. Genes showing decreased mRNA levels but increased Ribo-Seq, may be translated more efficiently. More complex scenarios could involve combination of transcriptional and translational regulatory events.

Middle and bottom panels of Figure 4 demonstrated the relation between RNA- and Ribo-Seq and protein levels. Both RNA- and Ribo-Seq clearly correlate with the protein levels (Pearson correlation 0.45 and 0.4) in $\Delta mazEF+F$ vs $\Delta mazEF$ comparison, even if this correlation was, as expected, weaker than between RNA- and Ribo-Seq (0.63). Quite a lot of genes were significantly changed only in RNA- and Ribo-Seq but not in proteome (genes marked in violet). A possible explanation for these genes is the experimental timing. Probably 10 min of mazF induction caused changes in RNA levels, but was not enough for the proteome to fully respond. Also, we did not examine protein stability, only steady-state protein levels.

An important observation is that the transcripts identified as cleaved by MazF (marked by black dots) mainly correspond to the genes downregulated at all stages of gene expression: transcription, translation and protein production. However, we noticed that not all transcripts which were decreased upon *mazF* induction were cleaved by MazF. To demonstrate the spectrum of possible relations between RNA-Seq, Ribo-Seq and MazF cleavage activity we compiled the plots of RNA-Seq and Ribo-Seq density maps and MazF cleavage map in $\triangle mazEF$ and $\triangle mazEF+F$ samples for several representative situations: transcripts which we identified as cleaved by MazF (lytR, pyrR); transcripts which have both RNA- and Ribo-Seq signals decreased but no cleavage detected (vraS, frr/rrf); transcripts which have RNA-Seq signal increased and Ribo-Seq signal increased or not changed (epiE, hpf); transcripts which have RNA-Seq increased and Ribo-Seq decreased (ilvC), and, finally transcripts which have RNA-Seq decreased and Ribo-Seq increased (SAOUHSC_02842) (Supplementary Figure S10).

Quantitative data for both transcript abundances (RNA-Seq) and protein synthesis rates (Ribo-Seq) enabled us to infer the relative translation efficiency (TE). To explain better the crosstalk of transcription and translation, it was proposed to calculate TE as the ratio of Ribo- and RNA-Seq signals (26), which corresponds to the number of ribosomes per length of mRNA, or ribosome density. In our data set changes in TE had very low or even anti-correlation with proteins (0.091 for WT versus $\triangle mazEF$ and -0.22 for $\Delta mazEF+F$ versus $\Delta mazEF$) (Supplementary Figure S11). Thus, TE, calculated in this way, cannot fully explain protein abundance. Indeed, TE depends on many factors such as codon usage, availability of the tRNAs, sequencedependent determinants (like Shine-Dalgarno sequences) and mRNA secondary structures (42). TE can also change over time and conditions for a given mRNA, reflecting dynamic regulation at the level of translation. However, in some particular cases in our data set (see below) TE correlated with protein levels and may explain increased protein even when transcription was decreased.

MazF affects expression of many specific groups of genes, in particular, genes involved in cell wall biosynthesis and cell division

We identified several functional groups of genes where transcription, translation or protein level were changed

upon MazF expression (Figure 5, Supplementary Table S3). MazF cleaves mRNA and reduces polysomes, indicating that translation and protein synthesis are reduced. The decreased translation can be seen, in particular, for the groups connected to protein synthesis, tRNA aminoacylation, signal transduction, transport and binding proteins, energy metabolism, cell envelope and cell division (Figure 5A, Supplementary Table S3). Translation of many others groups of genes, such as amino acid biosynthesis, translation and ribosome recycling factors, tRNA and rRNA modification was reduced (Supplementary Table S3), that is also in agreement with the general translation inhibition. We observed, however, that the translation of some groups of genes was increased upon mazF induction: e.g. groups of genes of the arginine deiminase (ADI) pathway (Figure 5A), ATP dependent chaperones, TCA cycle, glycolysis, gluconeogenesis and the pentose phosphate pathway (Supplementary Table S3), indicating that particular pathways were activated upon MazF induction. Interestingly, upregulation of the ADI pathway was associated with cell wall biosynthesis and increased cell wall thickness (43,44), observed in vancomycin-intermediate S. aureus strains (45).

While overall transcription and translation correlated well with protein levels we observed several examples of the opposite behavior. For example, genes of ribosomal proteins, pyrimidine and purine ribonucleotide biosynthesis, and genes of ATP synthase (Figure 5B, Supplementary Table S3) had decreased translation but increased protein level. In some cases, this may be explained by increased TE, as observed, e.g. for ATP synthase and pyrimidine and purine biosynthesis genes. However, for genes encoding ribosomal proteins the protein levels were increased even without increase in TE.

We found that many genes involved in cell wall biosynthesis, cell division, and fatty acid metabolism were affected upon MazF expression. Some of these genes were cleaved by MazF (Supplementary Table S2) and (15). To address the role of MazF in cell wall structure we examined genes in the *S. aureus* cell wall biosynthetic pathway (Supplementary Figure S12) (44,46–49). Translation and/or protein levels of many key enzymes involved in cell wall biosynthesis and several side pathways connected with cell wall biosynthesis, such as ADI pathway, pyrimidine biosynthesis, TCA cycle, glycolysis were increased by MazF (Supplementary Figure S12, Table S3). Simultaneously MazF suppressed expression of many genes involved in cell division (Supplementary Table S3).

To further verify the effect of MazF on cell wall and cell division we examined cell morphology changes after different times of *mazF* induction by transmission electron microscopy (TEM) (Figure 6 and Supplementary Figure S13). Without induction no visible difference was detected in *AmazEF* cells carrying either the empty vector or the plasmid expressing MazF. After 180 min of MazF induction, we observed an increase of cell wall thickness and a decrease in the number of dividing cells, as determined by the number of cells with a division septum. These effects were also visible after 60 min of induction (Figure 6B, C and Supplementary Figure S13). We concluded that MazF increased cell wall thickness and decreased the number of

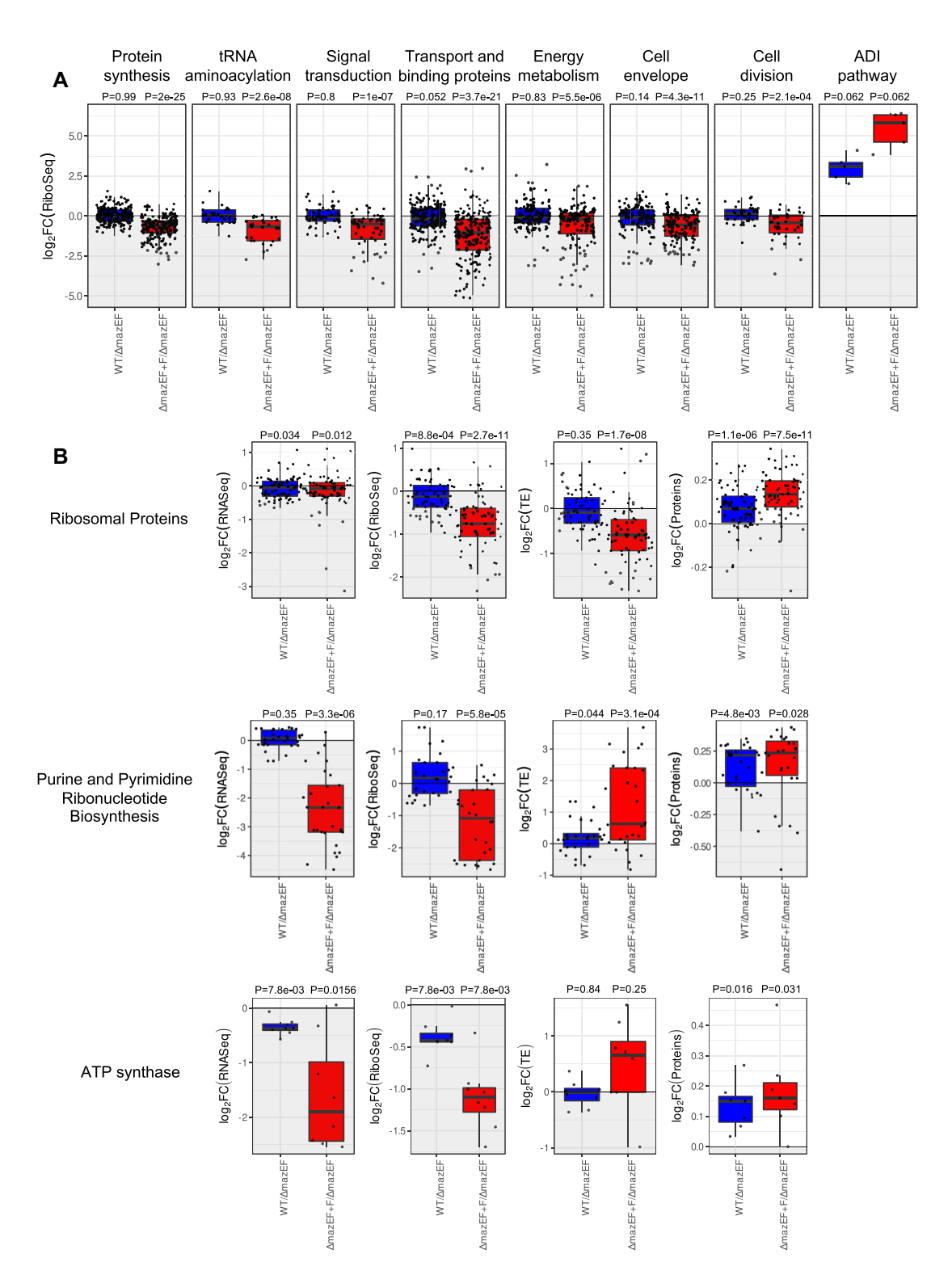


Figure 5. MazF affects specific pathways. (A) Example of groups of genes with decreased and increased translation (log2-FC) represented as a box plot. Comparison of WT to $\Delta mazEF$ (blue) and $\Delta mazEF+F$ to $\Delta mazEF$ (red). The other groups of genes are present in Supplementary Table S3. (B) Examples of groups of genes with decreased translation, but increased protein levels. Changes in transcription (RNA-Seq), translation (Ribo-Seq), translational efficiency (TE), and protein levels for WT compared to $\Delta mazEF$ (blue) and for $\Delta mazEF+F$ compared to $\Delta mazEF$ (red). Genes of ribosomal proteins, purine and pyrimidine biosynthesis and ATP synthase are presented. The P-values for the group of genes being overall differentially expressed are indicated above each group, and were computed using two-sided Wilcoxon test.

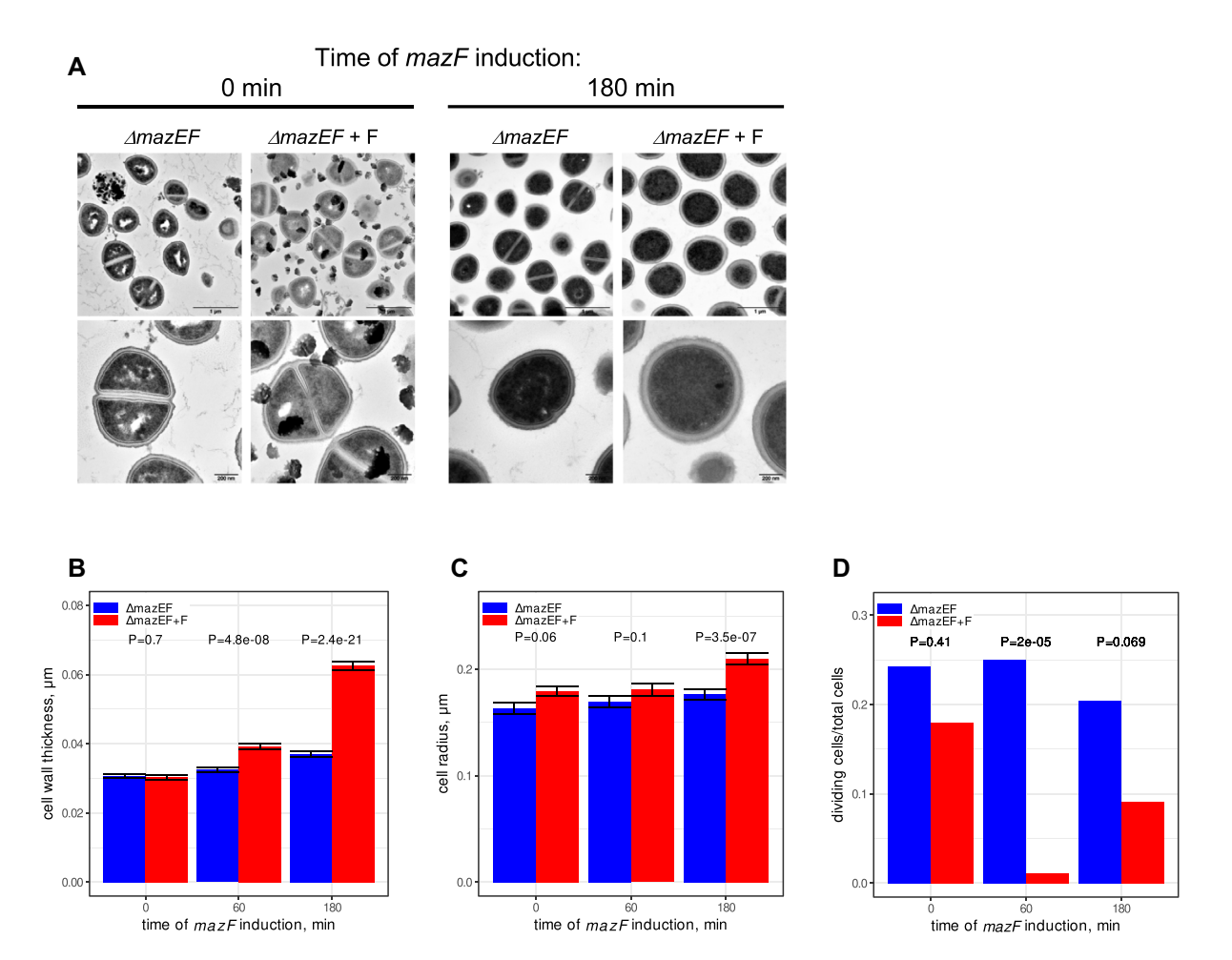


Figure 6. MazF increases thickness of cell wall and decreases cell division. (A) $\Delta mazEF$ cell carrying either empty vector or plasmid expressing MazF ($\Delta mazEF+F$) were treated with ATc for 0, 10, 60 and 180 min to induce mazF expression and analyzed by transmission electron microscopy (TEM). Electron microscopy images are presented at 2 different magnifications (upper and lower panels), and the scale bars indicate 1 μ m or 200 nm, respectively. Images at 0 and 180 min of induction are shown. More images are shown on the Supplementary Figure S13. (B and C) Analysis of cell wall thickness (B) and cell size (C) after 0, 60 and 180 min of mazF induction. $\Delta mazEF+F$ samples are indicated in blue and red, respectively. The error bars indicate standard deviations (SDs). The P-values were computed using two-sided Wilcoxon signed-rank test. (D) Analysis of cell division after 0, 60 and 180 min of mazF induction. The Fisher's exact test was used to compare the number of cells with and without division septum. P-values are indicated.

dividing cells, in agreement with the inhibition of the cell growth and bacteriostasis (15).

DISCUSSION

In this work, we have used multiple techniques to probe the effects of MazF toxin on *S. aureus* physiology in an effort to understand how this toxin might regulate cellular changes leading to dormancy. Understanding the causes of dormancy is critical for the management of antibiotic resistance. Presently, it is not known how many distinct mechanisms culminate in *S. aureus* dormancy, and it is certainly possible that there exists more than one pathway, or that there are redundancies among multiple pathways. Our study now contributes a more comprehensive understanding of the link between MazF toxin and its relation to dormancy. We have summarized our collective observations in a working model (Figure 7) demonstrating examples of the pathways that may be regulated by MazF and lead to bacterial dormancy.

Role of MazF in translation inhibition

Whereas we identified only 339 cleaved genes, MazF expression caused a decrease of about 50% of transcripts according to both RNA- and Ribo-Seq. The cleaved transcripts belonged to many different gene families without any statistically significant enrichment. We concluded that MazF cleaves a wide range of mRNAs as it was described for *E. coli* (29), affecting the entire transcriptome and translatome and causing global changes in cell metabolism.

Even if MazF inhibits cell growth, we did not observe complete drop of polysomes (Figure 2A), showing that the cell remained active, similar to what was reported in *E. coli* (50). We found that about 17% of transcripts were increased upon MazF induction, indicating that some pathways were upregulated. Notably, in *E. coli* MazF selectively enabled the synthesis of about 10% of proteins that either promoted cell death or ensured the survival of small subpopulation under stress conditions (20). We conclude that in *S. aureus* MazF activity does not lead to a complete inhibition but rather to an alteration of the translation program, thereby

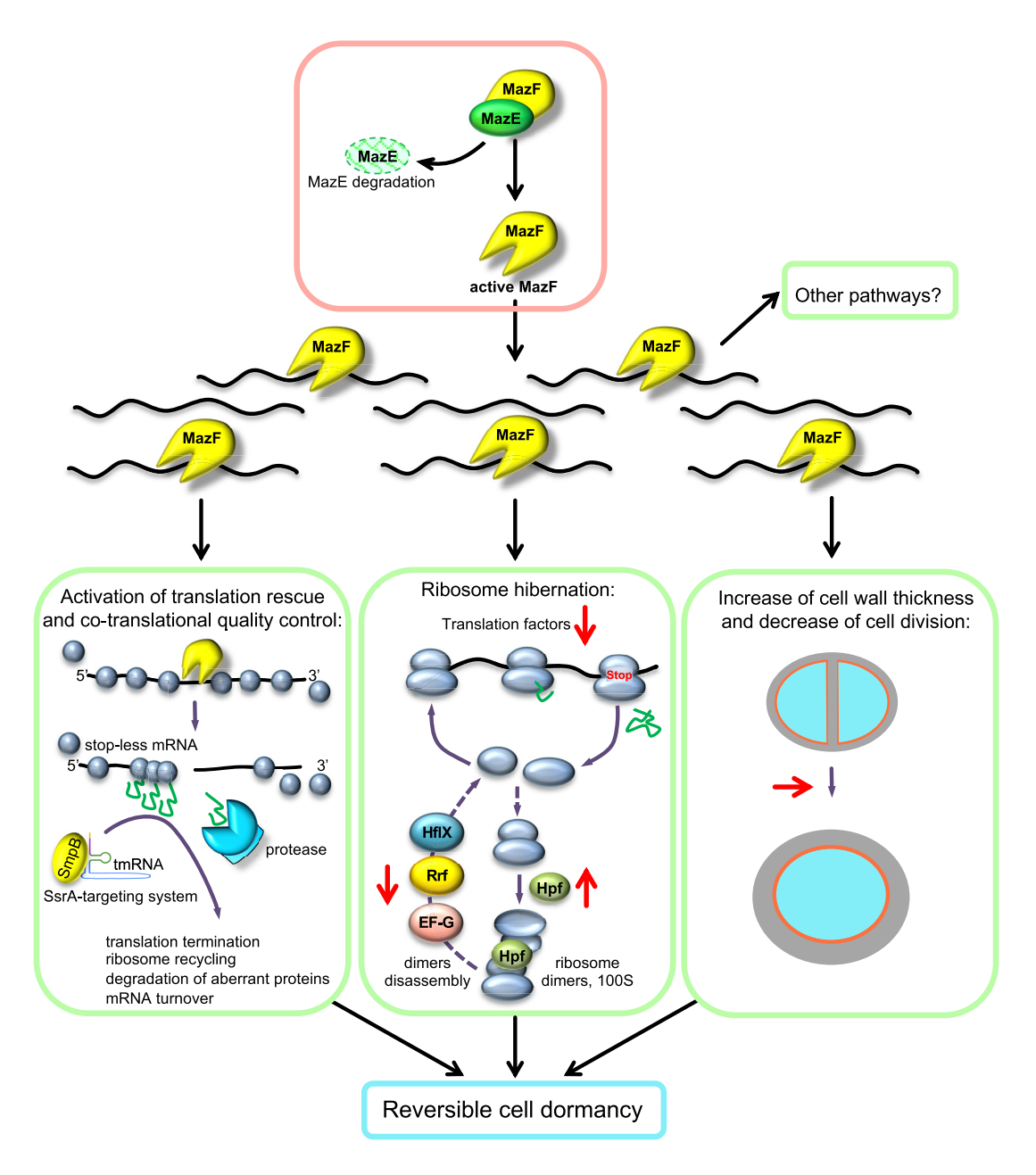


Figure 7. Model of MazF impact on cell physiology and its implication on cell survival and dormancy. MazE degradation unleashes MazF endoribonuclease activity. MazF cleaves many RNAs and suppresses transcription and translation of many genes rather than a particular set of genes. MazF changes the translational program and specifically affects several pathways: co-translational quality control, ribosome hibernation and recycling, cell division and cell wall thickness. Activation of these pathways may contribute to reversible bacteria dormancy, which allow cells to survive unfavorable growth conditions. Impact of MazF is indicated in red arrows. Activation of the other pathways by MazF is also possible.

potentially preparing the cell for long-term survival. In this work, we demonstrated three examples of such pathways that may be activated by MazF, namely translation rescue and co-translational quality control, ribosome hibernation and recycling, and finally, cell division and cell wall thickness (Figure 7).

Role of MazF in translation rescue and co-translational quality control $% \left(\mathbf{r}\right) =\mathbf{r}^{\prime }$

Cleavage by MazF results in the formation of stop-less transcripts, where stalled ribosomes are accumulated. We

observed that MazF activated the SsrA system that rescues stalled ribosomes and resolves non-stop translation. MazF also increased the levels of the ATP-dependent chaperones, which deal with partially synthesized peptides appearing during translation rescue. Both the SsrA system and ATP-dependent chaperones are important players in co-translational quality control mechanisms. Thus, we concluded that in *S. aureus* MazF induction leads to activation of co-translational quality control mechanisms that resume protein synthesis to maintain cell survival upon dormancy and possibly to facilitate the exit from dormancy state later (Figure 7).

Role of MazF in ribosome hibernation and recycling

A role for MazF in translation inhibition was discussed in several studies mostly performed on E. coli, and several targets of MazF were proposed. It was suggested that E. coli MazF reduces translation through cleavage of both mRNAs and rRNAs (19,29,36,37). In particular, it cleaves rRNA and mRNAs encoding ribosomal proteins, leading to disruption of rRNA maturation and ribosome biogenesis, and, thus, decreases cell growth (29). Earlier we also found that MazF cleaves mRNAs encoding ribosomal proteins in S. aureus (15). In this study, we observed reduced translation of these mRNAs, but, surprisingly, without reduction of the protein levels. We observed, however, a significant decrease of factors responsible for translation, tRNA aminoacylation, ribosome disassembly, and increase of hibernation-promoting factor, Hpf (Supplementary Figure S14).

In bacteria the majority of non-translating ribosomes hibernate in the form of 100S dimers, which sequester ribosomes away from active translation, and prevent ribosome degradation by an unknown pathway. In S. aureus Hpf mediates ribosome dimerization and is required for a long-term survival (51). On the one hand, Hpf suppresses translation through titrating active ribosomes. On the other hand, Hpf_{Sa} decreases ribosome turnover and preserves them, thereby the dimers can be dissociated and reassembled into active ribosomes upon the exit of quiescence (38). To resume translation ribosome hibernation is reversed by 100S dissociation. Recently, it was shown that in S. aureus ribosome recycling factor (Rrf, also known as Frr) and elongation factor G (EF-G, also known as FusA) synergistically split 100S dimers and, in certain conditions, this process may include activity of HflX GTPase (52). Notably, we observed that MazF decreased levels of rrf (Supplementary Figure S14A). Levels of EF-G and hflX were also decreased but to a lesser extent (Supplementary Table S3), and both these mRNAs were cleaved by MazF (15). Increased levels of hibernation factor and decreased levels of dimer disassembly factors favors ribosome hibernation. These observations are consistent with a model that in S. aureus MazF suppresses translation mainly acting at the level of translation and ribosome hibernation factors, rather than ribosomal proteins (Figure 7). Such a mechanism allows the cell to rapidly decrease translation but also rapidly restart it if needed, e.g. to exit from the dormant state.

Role of MazF in cell wall thickness

MazF affected translation and protein levels of many genes involved in cell wall biosynthesis as illustrated schematically (Supplementary Figure S12). MazF also altered several side metabolic pathways involved in the synthesis of the cell wall. Namely, translation of ADI pathway genes, arcRCDBA, where ArcR is the transcription activator of arc operon, were significantly increased. Upregulated ADI pathway is associated with elevation of ammonia and activation of Glm pathway, which produces UDP-N-acetyl-glucosamine (GlcNAc), the cardinal precursor metabolite for cell wall peptidoglycan (43), and with elevation of ATP, a substrate necessary for Mur ligases in cell wall synthesis

(44). Both pathways culminate in increased cell wall thickness. Accordingly, increased cell wall thickness, observed in vancomycin-intermediate *S. aureus* strains (VISA), was linked to *arcB* upregulation and elevation of ammonia and ATP (45).

Another example of pathways altered upon MazF expression are purine and pyrimidine biosynthesis and pathways connected to it. Upon MazF expression glycolysis, TCA cycle and pentose phosphate pathway were mostly upregulated in both RNA- and Ribo-Seq, providing substrates for de novo synthesis of nucleotides. We observed that many genes involved in purine and pyrimidine biosynthesis were cleaved by MazF and decreased in both RNA- and Ribo-Seg when *mazF* was expressed. However, TE of those genes was increased, and accordingly, protein abundance also. Increased purine biosynthesis might be needed to maintain at certain level ATP production for the needs of cell wall synthesis, as it was observed for VISA strains where genes involved in purine biosynthesis were upregulated (53), or for S. aureus persistence to rifampicin (54). Increased pyrimidine biosynthesis provides UMP, which is an important substrate for UDP-GlcNAc, required for the cell wall synthesis. Consistent with our observation, metabolomic analysis revealed that MazF in E. coli increases NMP and NDP levels (50).

Several other observations also connect MazF activity to the cell wall thickness. First, increase of cell wall thickness was observed in a $\Delta yjbH$ mutant (55), where MazF was activated (23). Second, deletion of trfA, which stabilized MazE (17), restored sensitivity of cells resistant to cell wall antibiotics (56). Moreover, in other bacteria a possible role of MazF in cell wall biogenesis was also noticed. For example, in $E.\ coli\ mRNAs$ isolated from polysomal fractions and responsible for 'cell structure' were upregulated upon MazF induction (36).

Possible role of MazF in bacterial dormancy/persistence

The terms of dormancy and persistence are often confusing in the literature. Persister cells are non-growing subpopulations tolerant to antibiotics, and often significantly present in biofilms (5). Persisters arise due to dormancy, defined as a state in which cells decrease metabolism and arrest growth (3,5). Dormant bacteria are also often tolerant to antibiotics.

It has been suggested that MazF in *E. coli* is involved in drug tolerance and persistence generation (21). In *S. aureus* activation of MazF leads to quiescence (24) and dormancy (15) and alters susceptibility to antibiotics (14). In this study we induced MazF only for 10 min, thus the changes we observed possibly correspond to a very early stage leading to the entrance to dormancy. In this regard, our observations concerning ribosome hibernation and co-translational quality control systems are very interesting. Both mechanisms promote cell survival and, possibly, reversible cell dormancy instead of cell death (Figure 7).

Ribosome hibernation has emerged as one of the pivotal cellular processes for entry into dormancy and subsequent resuscitation. MazF could favor ribosome hibernation by increasing levels of Hpf, and decreasing ribosome recycling factors. Mechanisms that cause dissociation of the ribo-

some dimers might decrease cell viability and prevent bacterial dormancy. Accordingly, antibiotic tolerance has been mediated by ribosome dimerization in the absence of *Mycobacterial* HflX (57). Disruption of 100S dimers, either by decreasing activity of Hpf, or by increasing activity of EF-G/Rrf/HflX, makes these factors possible and promising targets for future antibacterial drug discovery.

Another important connection to dormancy uncovered in our study is the increased transcription and translation of ADI and TCA cycle genes. Upregulation of ADI pathway had been connected to vancomycin resistance (45), while the increased activity of TCA cycle had been connected to persistence in *S. aureus* (58). Genes encoding enzymes of TCA cycle, ribosomal proteins and ADI pathway were also upregulated in *S. aureus* biofilms (59) that may be linked to persistence.

Increased cell wall thickness and changes in expression of cell wall related genes caused by MazF, described in this study, may be connected to bacterial dormancy (15) and persistence. Accordingly, activation of the cell wall stress stimulon and peptidoglycan biosynthesis was observed in intracellular *S. aureus* persisters upon antibiotic exposure (60). Taken together, our observations are important in the regard that approaches leading to MazF inactivation may synergize bactericidal effects of cell wall antibiotics.

MazEF regulation by stress

MazF endoribonuclease activity is neutralized by antitoxin MazE. MazE protein level is controlled by the ATPdependent ClpCP protease and requires an adaptor protein TrfA (17,18). Transcription of TrfA is regulated in part by activator Spx (61). Spx protein level is, in turn, controlled by ClpXP protease and requires an adaptor protein YibH (62,63). One can imagine, that stress such as antibiotics, that causes inhibition of transcription and/or translation may inhibit mazEF expression, and prevent de novo synthesis of MazE and MazF. The unstable MazE is degraded and nuclease activity of MazF is unleashed. It has been suggested that in E. coli stress induces transcription of TASs without activating toxins and that transcriptional induction results from antitoxin degradation and relief of transcriptional autoregulation (64). However, the S. aureus MazEF system is unique because it does not repress its own promoter (65). Accordingly, recently we demonstrated that YjbH aggregates in response to stress, thereby initiating YjbH-Spx-TrfA cascade, which results in MazE degradation and, consequently, MazF toxin activation (23). These observations were confirmed by the fact that inhibition of cell growth caused by MazF induction was reverted by trfA deletion (15). Therefore, it is very possible that in S. aureus environmental stress, such as antibiotics, may modulate MazEF function and unleash MazF endoribonuclease activity.

CONCLUSION

We characterized changes and correlations in transcriptome, translatome, and proteome caused by MazF. Important pathways affected during the early stage following MazF induction were identified. These pathways may be promising targets for new antibacterial drugs that prevent

bacteria dormancy and synergize the efficacy of conventional antibiotics.

DATA AVAILABILITY

All RNA- and Ribo-Seq data from this study are available at NCBI Gene Expression Omnibus (GSE155036). Mass spectrometry raw data are available at ProteomeXchange (PXD021129).

SUPPLEMENTARY DATA

Supplementary Data are available at NAR Online.

ACKNOWLEDGEMENTS

We kindly thank Friedrich Götz (The University Tübingen, Germany) for supplying the HG003 and the HG003 *mazEF* deleted strains, Mee-Ngan Yap (Saint Louis University, USA) for anti-Hpf antibody, and William L. Kelley (University of Geneva, Switzerland) for invaluable help and critical reading of the manuscript.

FUNDING

Helmut Horten Stiftung (to O.O.P.); Ernst and Lucie Schmidheiny Foundation (to O.O.P.); Swiss National Science Foundation [310030-169404 to A.R.]. Funding for open access charge: Swiss National Science Foundation. *Conflict of interest statement*. None declared.

REFERENCES

- Lowy, F.D. (1998) Staphylococcus aureus infections. N. Engl. J. Med., 339, 520–532.
- Aslam,B., Wang,W., Arshad,M.I., Khurshid,M., Muzammil,S., Rasool,M.H., Nisar,M.A., Alvi,R.F., Aslam,M.A., Qamar,M.U. et al. (2018) Antibiotic resistance: a rundown of a global crisis. *Infect. Drug Resist.*, 11, 1645–1658.
- 3. Balaban, N.Q., Helaine, S., Lewis, K., Ackermann, M., Aldridge, B., Andersson, D.I., Brynildsen, M.P., Bumann, D., Camilli, A., Collins, J.J. *et al.* (2019) Definitions and guidelines for research on antibiotic persistence. *Nat. Rev. Microbiol.*, 17, 441–448.
- 4. Lewis, K. (2010) Persister cells. Annu. Rev. Microbiol., 64, 357-372.
- Wood, T.K., Knabel, S.J. and Kwan, B.W. (2013) Bacterial persister cell formation and dormancy. Appl. Environ. Microbiol., 79, 7116–7121.
- Rittershaus, E.S., Baek, S.H. and Sassetti, C.M. (2013) The normalcy of dormancy: common themes in microbial quiescence. *Cell Host Microbe*, 13, 643–651.
- Masuda, H. and Inouye, M. (2017) Toxins of prokaryotic toxin-antitoxin systems with sequence-specific endoribonuclease activity. *Toxins (Basel)*, 9, 140.
- Otsuka, Y. (2016) Prokaryotic toxin-antitoxin systems: novel regulations of the toxins. *Curr. Genet.*, 62, 379–382.
- Yamaguchi, Y., Park, J.H. and Inouye, M. (2011) Toxin-antitoxin systems in bacteria and archaea. *Annu. Rev. Genet.*, 45, 61–79.
- Schuster, C.F. and Bertram, R. (2016) Toxin-antitoxin systems of Staphylococcus aureus. Toxins (Basel), 8, 140.
- 11. Sierra, R., Viollier, P. and Renzoni, A. (2019) Linking toxin-antitoxin systems with phenotypes: a *Staphylococcus aureus* viewpoint. *Biochim. Biophys. Acta Gene Regul. Mech.*, **1862**, 742–751.
- van Rensburg, J.J. and Hergenrother, P.J. (2013) Detection of endogenous MazF enzymatic activity in *Staphylococcus aureus*. *Anal. Biochem.*, 443, 81–87.
- Zhu, L., Inoue, K., Yoshizumi, S., Kobayashi, H., Zhang, Y., Ouyang, M., Kato, F., Sugai, M. and Inouye, M. (2009) Staphylococcus aureus MazF specifically cleaves a pentad sequence, UACAU, which is unusually abundant in the mRNA for pathogenic adhesive factor SraP. J. Bacteriol., 191, 3248–3255.

- Schuster, C.F., Mechler, L., Nolle, N., Krismer, B., Zelder, M.E., Gotz, F. and Bertram, R. (2015) The MazEF toxin-antitoxin system alters the beta-lactam susceptibility of *Staphylococcus aureus*. *PLoS One*. 10. e0126118.
- Sierra, R., Prados, J., Panasenko, O.O., Andrey, D.O., Fleuchot, B., Redder, P., Kelley, W.L., Viollier, P.H. and Renzoni, A. (2020) Insights into the global effect on *Staphylococcus aureus* growth arrest by induction of the endoribonuclease MazF toxin. *Nucleic Acids Res.*, 48, 8545–8561.
- Fu,Z., Donegan,N.P., Memmi,G. and Cheung,A.L. (2007) Characterization of MazFSa, an endoribonuclease from Staphylococcus aureus. *J. Bacteriol.*, 189, 8871–8879.
- Donegan, N.P., Marvin, J.S. and Cheung, A.L. (2014) Role of adaptor TrfA and ClpPC in controlling levels of SsrA-tagged proteins and antitoxins in Staphylococcus aureus. *J. Bacteriol.*, 196, 4140–4151.
- Donegan, N.P., Thompson, E.T., Fu, Z. and Cheung, A.L. (2010) Proteolytic regulation of toxin-antitoxin systems by ClpPC in Staphylococcus aureus. *J. Bacteriol.*, 192, 1416–1422.
- Zhang, Y., Zhang, J., Hoeflich, K.P., Ikura, M., Qing, G. and Inouye, M. (2003) MazF cleaves cellular mRNAs specifically at ACA to block protein synthesis in Escherichia coli. *Mol. Cell*, 12, 913–923.
- Amitai, S., Kolodkin-Gal, I., Hananya-Meltabashi, M., Sacher, A. and Engelberg-Kulka, H. (2009) Escherichia coli MazF leads to the simultaneous selective synthesis of both "death proteins" and "survival proteins". *PLoS Genet.*, 5, e1000390.
- Tripathi, A., Dewan, P.C., Siddique, S.A. and Varadarajan, R. (2014)
 MazF-induced growth inhibition and persister generation in Escherichia coli. *J. Biol. Chem.*, 289, 4191–4205.
- Fraikin, N., Goormaghtigh, F. and Van Melderen, L. (2020) Type II toxin-antitoxin systems: evolution and revolutions. *J. Bacteriol.*, 202, e00763-19.
- Panasenko, O.O., Bezrukov, F., Komarynets, O. and Renzoni, A. (2020)
 YjbH solubility controls Spx in *Staphylococcus aureus*: implication for MazEF toxin-antitoxin system regulation. *Front. Microbiol.*, 11, 113.
- 24. Fu,Z., Tamber,S., Memmi,G., Donegan,N.P. and Cheung,A.L. (2009) Overexpression of MazFsa in *Staphylococcus aureus* induces bacteriostasis by selectively targeting mRNAs for cleavage. *J. Bacteriol.*, 191, 2051–2059.
- 25. Ma,D., Mandell,J.B., Donegan,N.P., Cheung,A.L., Ma,W., Rothenberger,S., Shanks,R.M.Q., Richardson,A.R. and Urish,K.L. (2019) The toxin-antitoxin MazEF drives staphylococcus aureus biofilm formation, antibiotic tolerance, and chronic infection. *mBio*, **10**, e01658-19.
- Ingolia, N.T., Ghaemmaghami, S., Newman, J.R. and Weissman, J.S. (2009) Genome-wide analysis in vivo of translation with nucleotide resolution using ribosome profiling. *Science*, 324, 218–223.
- Ingolia, N.T. (2014) Ribosome profiling: new views of translation, from single codons to genome scale. *Nat. Rev. Genet.*, 15, 205–213.
- 28. Brar, G.A. and Weissman, J.S. (2015) Ribosome profiling reveals the what, when, where and how of protein synthesis. *Nat. Rev. Mol. Cell Biol.*, **16**, 651–664.
- Culviner,P.H. and Laub,M.T. (2018) Global analysis of the E. coli toxin mazf reveals widespread cleavage of mRNA and the inhibition of rRNA maturation and ribosome biogenesis. *Mol. Cell*, 70, 868–880.
- 30. Herbert, S., Ziebandt, A.K., Ohlsen, K., Schafer, T., Hecker, M., Albrecht, D., Novick, R. and Gotz, F. (2010) Repair of global regulators in Staphylococcus aureus 8325 and comparative analysis with other clinical isolates. *Infect. Immun.*, 78, 2877–2889.
- Helle, L., Kull, M., Mayer, S., Marincola, G., Zelder, M.E., Goerke, C., Wolz, C. and Bertram, R. (2011) Vectors for improved Tet repressor-dependent gradual gene induction or silencing in Staphylococcus aureus. *Microbiology*, 157, 3314–3323.
- Law, C.W., Chen, Y., Shi, W. and Smyth, G.K. (2014) voom: Precision weights unlock linear model analysis tools for RNA-seq read counts. *Genome Biol.*, 15, R29.
- McGlincy, N.J. and Ingolia, N.T. (2017) Transcriptome-wide measurement of translation by ribosome profiling. *Methods*, 126, 112–129.
- Xiao, Z., Zou, Q., Liu, Y. and Yang, X. (2016) Genome-wide assessment of differential translations with ribosome profiling data. *Nat. Commun.*, 7, 11194.

- 35. Basu, A. and Yap, M.N. (2017) Disassembly of the *Staphylococcus aureus* hibernating 100S ribosome by an evolutionarily conserved GTPase. *Proc. Natl. Acad. Sci. U.S.A.*, **114**, E8165–E8173.
- Sauert, M., Wolfinger, M.T., Vesper, O., Muller, C., Byrgazov, K. and Moll, I. (2016) The MazF-regulon: a toolbox for the post-transcriptional stress response in *Escherichia coli*. Nucleic. Acids. Res., 44, 6660–6675.
- 37. Vesper,O., Amitai,S., Belitsky,M., Byrgazov,K., Kaberdina,A.C., Engelberg-Kulka,H. and Moll,I. (2011) Selective translation of leaderless mRNAs by specialized ribosomes generated by MazF in Escherichia coli. *Cell*, **147**, 147–157.
- Basu, A. and Yap, M. N. (2016) Ribosome hibernation factor promotes Staphylococcal survival and differentially represses translation. *Nucleic. Acids. Res.*, 44, 4881–4893.
- 39. Neubauer, C., Gillet, R., Kelley, A.C. and Ramakrishnan, V. (2012) Decoding in the absence of a codon by tmRNA and SmpB in the ribosome. *Science*, 335, 1366–1369.
- Huter, P., Muller, C., Arenz, S., Beckert, B. and Wilson, D.N. (2017) Structural basis for ribosome rescue in bacteria. *Trends Biochem. Sci.*, 42, 669–680
- Flynn, J.M., Levchenko, I., Seidel, M., Wickner, S.H., Sauer, R.T. and Baker, T.A. (2001) Overlapping recognition determinants within the ssrA degradation tag allow modulation of proteolysis. *Proc. Natl.* Acad. Sci. U.S.A., 98, 10584–10589.
- 42. Gingold, H. and Pilpel, Y. (2011) Determinants of translation efficiency and accuracy. *Mol. Syst. Biol.*, 7, 481.
- 43. Cui, L., Murakami, H., Kuwahara-Arai, K., Hanaki, H. and Hiramatsu, K. (2000) Contribution of a thickened cell wall and its glutamine nonamidated component to the vancomycin resistance expressed by Staphylococcus aureus Mu50. *Antimicrob. Agents Chemother.*, 44, 2276–2285.
- Lovering, A.L., Safadi, S.S. and Strynadka, N.C. (2012) Structural perspective of peptidoglycan biosynthesis and assembly. *Annu. Rev. Biochem.*, 81, 451–478.
- 45. Tan, X.E., Neoh, H.M., Looi, M.L., Chin, S.F., Cui, L., Hiramatsu, K., Hussin, S. and Jamal, R. (2017) Activated ADI pathway: the initiator of intermediate vancomycin resistance in Staphylococcus aureus. *Can. J. Microbiol.*, **63**, 260–264.
- Barreteau, H., Kovac, A., Boniface, A., Sova, M., Gobec, S. and Blanot, D. (2008) Cytoplasmic steps of peptidoglycan biosynthesis. FEMS Microbiol. Rev., 32, 168–207.
- 47. Swoboda, J.G., Campbell, J., Meredith, T.C. and Walker, S. (2010) Wall teichoic acid function, biosynthesis, and inhibition. *ChemBioChem*, 11, 35–45.
- 48. Brown, S., Santa Maria, J.P. Jr. and Walker, S. (2013) Wall teichoic acids of gram-positive bacteria. *Annu. Rev. Microbiol.*, 67, 313–336.
- Sobral, R. and Tomasz, A. (2019) The staphylococcal cell wall. *Microbiol Spectr*, 7, doi:10.1128/microbiolspec.GPP3-0068-2019.
- Mok, W.W., Park, J.O., Rabinowitz, J.D. and Brynildsen, M.P. (2015)
 RNA futile cycling in model persisters derived from MazF accumulation. *MBio*, 6, e01588-15.
- Ueta, M., Wada, C. and Wada, A. (2010) Formation of 100S ribosomes in *Staphylococcus aureus* by the hibernation promoting factor homolog SaHPF. *Genes Cells*, 15, 43–58.
- Basu, A., Shields, K.E. and Yap, M.F. (2020) The hibernating 100S complex is a target of ribosome-recycling factor and elongation factor G in Staphylococcus aureus. *J. Biol. Chem.*, 295, 6053–6063.
- Mongodin, E., Finan, J., Climo, M.W., Rosato, A., Gill, S. and Archer, G.L. (2003) Microarray transcription analysis of clinical Staphylococcus aureus isolates resistant to vancomycin. J. Bacteriol., 185, 4638–4643.
- 54. Yee, R., Cui, P., Shi, W., Feng, J. and Zhang, Y. (2015) Genetic screen reveals the role of purine metabolism in *Staphylococcus aureus* persistence to rifampicin. *Antibiotics (Basel)*, **4**, 627–642.
- 55. Renzoni, A., Andrey, D.O., Jousselin, A., Barras, C., Monod, A., Vaudaux, P., Lew, D. and Kelley, W.L. (2011) Whole genome sequencing and complete genetic analysis reveals novel pathways to glycopeptide resistance in *Staphylococcus aureus*. *PLoS One*, 6, e21577.
- 56. Renzoni, A., Kelley, W.L., Barras, C., Monod, A., Huggler, E., Francois, P., Schrenzel, J., Studer, R., Vaudaux, P. and Lew, D.P. (2009) Identification by genomic and genetic analysis of two new genes playing a key role in intermediate glycopeptide resistance in Staphylococcus aureus. Antimicrob. Agents Chemother., 53, 903–911.

- Rudra, P., Hurst-Hess, K.R., Cotten, K.L., Partida-Miranda, A. and Ghosh, P. (2020) Mycobacterial HflX is a ribosome splitting factor that mediates antibiotic resistance. *Proc. Natl. Acad. Sci. U.S.A.*, 117, 629–634.
- 58. Wang, W., Chen, J., Chen, G., Du, X., Cui, P., Wu, J., Zhao, J., Wu, N., Zhang, W., Li, M. et al. (2015) Transposon mutagenesis identifies novel genes associated with staphylococcus aureus persister formation. Front. Microbiol, 6, 1437.
- Resch, A., Rosenstein, R., Nerz, C. and Gotz, F. (2005) Differential gene expression profiling of Staphylococcus aureus cultivated under biofilm and planktonic conditions. *Appl. Environ. Microbiol.*, 71, 2663–2676.
- Peyrusson, F., Varet, H., Nguyen, T.K., Legendre, R., Sismeiro, O., Coppee, J.Y., Wolz, C., Tenson, T. and Van Bambeke, F. (2020) Intracellular *Staphylococcus aureus* persisters upon antibiotic exposure. *Nat. Commun.*, 11, 2200.
- 61. Jousselin, A., Kelley, W.L., Barras, C., Lew, D.P. and Renzoni, A. (2013) The *Staphylococcus aureus* thiol/oxidative stress global regulator Spx

- controls trfA, a gene implicated in cell wall antibiotic resistance. *Antimicrob. Agents Chemother.*, **57**, 3283–3292.
- Engman, J. and von Wachenfeldt, C. (2015) Regulated protein aggregation: a mechanism to control the activity of the ClpXP adaptor protein YjbH. Mol. Microbiol., 95, 51–63.
- 63. Engman, J., Rogstam, A., Frees, D., Ingmer, H. and von Wachenfeldt, C. (2012) The YjbH adaptor protein enhances proteolysis of the transcriptional regulator Spx in Staphylococcus aureus. *J. Bacteriol.*, **194**, 1186–1194.
- LeRoux, M., Culviner, P.H., Liu, Y.J., Littlehale, M.L. and Laub, M.T. (2020) Stress can induce transcription of toxin-antitoxin systems without activating toxin. *Mol. Cell.* 79, 280–292.
- Donegan, N.P. and Cheung, A.L. (2009) Regulation of the mazEF toxin-antitoxin module in Staphylococcus aureus and its impact on sigB expression. *J. Bacteriol.*, 191, 2795–2805.

3. Conclusion and Perspectives

In the following paragraphs, I will described the research contributions highlighted by this privat-docent thesis (points 1-3), and at the end, I will add clinical contributions based on my basic research work. These clinical contributions were not develop in this thesis but merit presentation (4).

Our basic research contributions involve the discovery of novel *S. aureus* antibiotic defence pathways, as depicted below. These antibiotic defense pathways converge towards the modification of the cell-wall and dormancy induction (Figure 14).

- 1. By a complete genetic reconstitution, we showed for the first time that *S. aureus* uses simultaneously multiple sensor and stress pathways to resist to cell-wall active antibiotics increasing cell-wall thickness. While our investigation shed light on this phenomenon, the complete spectrum of factors contributing to the modulation of cell-wall thickness remain to be identified.
- 2. The presence of antibiotics triggers a response through phospho-signaling systems, potentially activating an arsenal of proteins involved in cell-wall modification to avoid killing. Transcription and translation of these arsenal of cell-wall proteins are two evident mechanisms that could be modified for this metabolic adaptation. However, our investigation has shed light into an additional mechanisms involving extracellular protein folding and lipoprotein modification. Indeed, we identified a two-component system (VraRS) regulating transcription of a lipid-anchored membrane protein (PrsA), which, in turn assist folding of the most important penicillin binding protein (PBP2A) conferring resistance to B-lactam antibiotics. Interestingly, our results also suggest that lipoprotein modification may play a role to modulate antibiotic resistance. Studying the phenomenon of see-saw between Daptomycin and B-lactam antibiotics, we observed that sensitization to B-lactams was not due to a decreased transcription or translation of PBP2A but an increase of protein secretion into the extracellular media. We proposed a model where the abnormal secretion can be due to changes in lipoprotein modifications affecting in turn location and function of PrsA, required for the correct PBP2A membrane folding and activity

(Figure 14A and B). Future studies may be conducted to show and identify more exactly the mechanisms of lipoprotein modifications in *S. aureus* affecting antibiotic resistance.

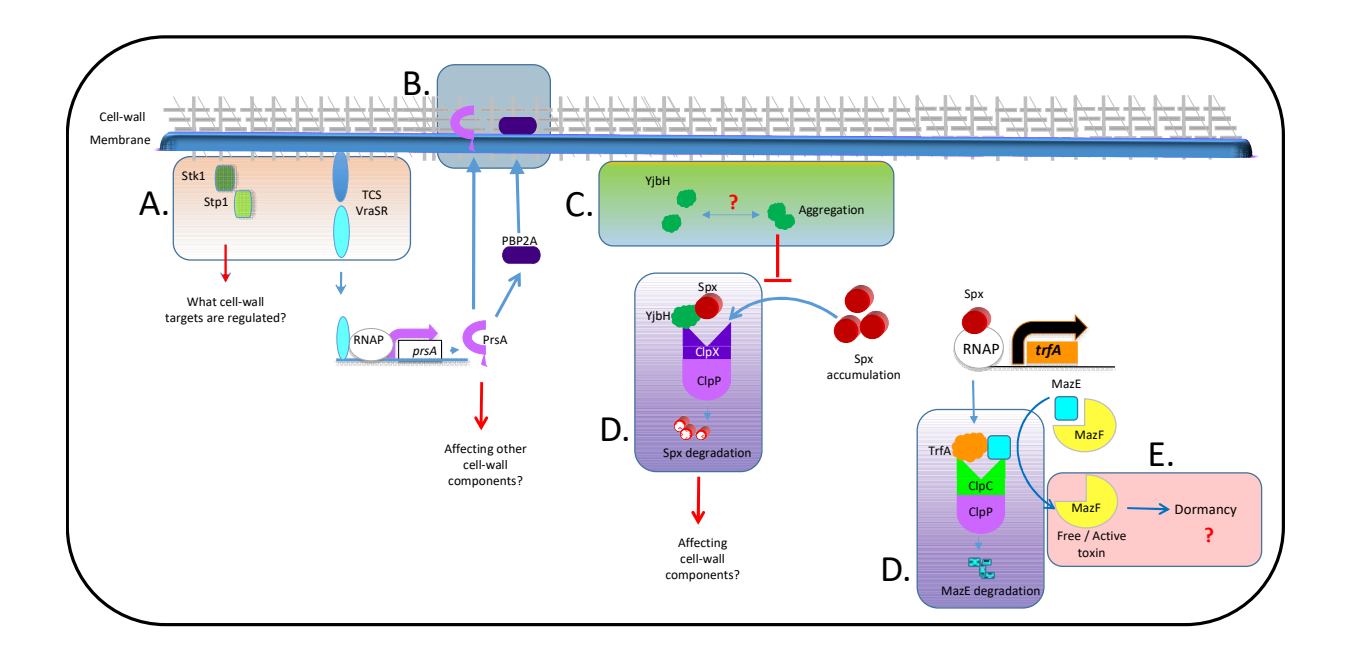


Figure 14. Schematic representation of *S. aureus* strategic defences against antibiotic treatment, identified by my research program. Two resistant defences are depicted: modulation of cell-wall metabolism to respond to cell-wall active antibiotics and dormancy induction. Specifically, our work identified the following new strategic defences. To overcome antibiotic attack, *S. aureus* uses simultaneously phosphor-signalling systems (A) and oxidative stressed pathways (Spx) to modulate of cell-wall metabolism. Protein secretion, folding and lipoprotein modification are involved in this process (B). Protein aggregation (C), protein degradation systems (D) and toxin-antitoxin systems are involved in bacterial dormancy induction. The exact mechanisms and potential interplay of all identified key points are still to be defined. Red arrows and question marks depicted important points for future investigation.

- 3. We profoundly contributed to study *S. aureus* bacterial dormancy. Before starting our research project, it was known that *S. aureus* MazEF TAS system was involved in growth arrest and only few RNA targets were identified.
- a) We applied several new technologies and confirmed that indeed MazF toxin overexpression induces growth stasis. We identified MazF in vivo genome-wide RNA targets allowing not only the identification of several potential metabolic genes involved in *S. aureus* entry into dormancy but also the identification of an extended alternative RNA motif recognized and cleaved by MazF.

- b) MazF activity does not lead to a complete inhibition but rather an alteration of translation. This observation correlates with MazF cleavage of mRNA encoding ribosomal proteins, however we further observed by Ribo-seq a reduced translation of these mRNAs without, surprisingly, reduction of protein levels. This observation is probably due to a very short time of proteome analysis after *mazF* reduction in RNA levels. Perhaps 10 min was not enough for the proteome to fully respond. We observed however, a significant decrease of factors responsible for translation or formation of ribosome dimers upon MazF overexpression. Ribosome dimer formation is a bacterial mechanism to protect ribosomes under stress conditions. We can speculate that MazF induces entry into dormancy by activating ribosome dimer formation which will not only decrease protein translation but will also protect ribosomes to reactivate translation when needed, rescuing cells from dormancy state.
- c) It is clear that bacteria can enter and exit from dormancy state, implying that reversible molecular pathways may be involved. In *S. aureus* the dormancy-related MazEF TAS is controlled by two proteolytic systems involving TrfA and YjbH adapto protiens. Interestingly, we decipher upstream pathways that can inhibit or reactivate MazEF TAS activity. YjbH adaptor protein of the ClpXP proteolytic system is prone to aggregation, upon environmental stresses or antibiotics (C) affecting activity of the downstream protein degradation systems (D) and culminating in regulation of MazE degradation and MazF activation. Our studies contributed to understand le molecular pathways controlling MazF expression in vitro. The clinical importance of regulation of MazF activity, highlighted by studies showing the role of MazF expression in chronic *S. aureus* infections, indicates the importance to decipher in future studies the in vivo conditions leading to modulation of MazF expression and activity.

We must improve our understanding of the molecular mechanisms regulating bacterial dormancy. These results will be key for the discovery of novel targets for antibiotic development. Understanding, for example, of bacterial translation during dormancy, will help to identify new translational inhibitors to destroy dormant bacteria

4. We have established the fundamental research program, presented above, focused on *S. aureus* antibiotic resistance, with the aim of developing molecular markers capable of identifying the emergence of low-level glycopeptide resistant strains prior to the selection of high-level resistant strains or the onset of cross-resistance. In parallel, we dedicated efforts to enhancing clinical diagnostic laboratory techniques aimed at detecting these challenging bacteria.

Glycopeptides (vancomycin and teicoplanin) are employed as valuable therapies for severe MRSA infections and used under some special circumstances to treat MSSA infections. However, their usage selects for low-level glycopeptide resistant strains, including vancomycin-intermediate (VISA) or heterogeneous vancomycin-intermediate (hVISA) in MSSA or MRSA strains. Their resistant classification is based on determination of the minimal concentration of antibiotic capable to inhibit bacterial growth (MIC breakpoints). For glycopeptides, the MIC breakpoint is is $\leq 2 \mu g/ml$ for "susceptible", 4-8 $\mu g/ml$ for "intermediate", and $\geq 16 \mu g/ml$ for "resistant" strains, following clinical and laboratory standards institute (CLSI) recommendations (Clinical and Laboratory Standards Institute. 2009. M100-S19.Wayne, PA). The European Committee on Antimicrobial Susceptibility Testing (EUCAST) removed the intermediate category and recommended clinical breakpoints of $\leq 2 \mu g/ml$ for "susceptible" and $\geq 2 \mu g/ml$ for resistant strains.

VISA isolates are strains having vancomycin intermediate resistance, and frequently display heterogeneous resistance to glycopeptides (hVISA/hGISA) (Hiramatsu et al. 1997; Hubert et al. 1999) means that a vast majority (sometimes >99.99%) is still killed by the vancomycin or teicoplanin concentrations (≤2 μg/ml) that are effective against glycopeptide-susceptible isolates, whereas a small minority (sometimes <0.01%) can resist these antibiotic concentrations. They are typically found at a frequency of ≤10⁻⁵ to 10⁻⁶ colony forming units. The appearance of VISA and hVISA strains represents a significant risks because their phenotypic detection is often difficult. Phenotypic detection of VISA is generally achieved by determination of their MIC by broth microdilution, the gold standard recommended by the European Committee on Antimicrobial susceptibility testing (EUCAST). An intrinsic difficulty of the VISA detection method is its lack of sensitivity, which can only detect two-fold increases or decreases in MICs. Therefore, any minor increase (< 2-fold) in MIC may escape detection by the standard methodology. The phenotypic detection of hVISA

is even more challenging as they are classified as susceptible strains by current clinical detection methods, they display an unstable phenotype complicating their detection because only a subset of the microbial population (perhaps as few as 10^{-6} cells) express glycopeptide resistance and can escape detection (van Hal et al. 2011). Moreover, there is a wide consensus that the phenotypic expression of low-level glycopeptide resistance is variable, being significantly influenced by several technical parameters, including the composition of liquid or solid test media, and varying time frames and inoculum sizes (van Hal et al. 2011; Vaudaux et al. 2010).

Alternative to the broth microdilution method, VISA/hVISA detection methods, such as the modified population analysis profile, Etest macromethod, and Etest GRD, were developed (Howden et al. 2010; van Hal et al. 2011) Despite the use of more appropriate bacterial inocula and incubation periods, these alternative VISA/hVISA detection methods are not reliable or labor-intensive, such as the (PAP)-area under the curve (AUC) method, thus being inappropriate for clinical laboratory use.

Our research program contributed to the improvement of clinical detection of low-level glycopeptide resistance, by developing more sensitive phenotypic methods to detect glycopeptide resistance in clinical isolates (Vaudaux et al. 2010; Vaudaux et al. 2012; Uckay et al. 2012). We showed that the macrodilution and agar testing methods significantly improved the detection rates of GISA isolates. Interestingly, the detection of elevated teicoplanin MICs was a reliable marker of the GISA phenotype and predicted to facilitate the detection of isolates expressing vancomycin-intermediate resistance. We further validated our method for detecting GISA strains analyzing the impact of low-level glycopeptide resistance on therapeutic outcomes of MRSA bacteremic patients (Uckay et al. 2012) and in orthopedic devices related to MRSA infections (Vaudaux et al. 2012). Both studies support the concept that evaluation of low-level teicoplanin resistance may improve the detection of GISA isolates.

Accurate strain detection enables clinicians to optimize treatment strategies, to reduce mortality rates and length of hospital stays. New detection methods should be capable of identifying the onset of resistance before high resisitance levels are attained. To have the ability to direct identify resistant strains from human samples eliminating the need for subcultures and aiding the detection of hVISA and sVISA phenotypes.

4. REFERENCES

- Arede, P., J. Ministro, and D. C. Oliveira. 2013. 'Redefining the role of the beta-lactamase locus in methicillin-resistant Staphylococcus aureus: beta-lactamase regulators disrupt the MecI-mediated strong repression on mecA and optimize the phenotypic expression of resistance in strains with constitutive mecA expression', *Antimicrob Agents Chemother*, 57: 3037-45.
- Balaban, N. Q., S. Helaine, K. Lewis, M. Ackermann, B. Aldridge, D. I. Andersson, M. P.
 Brynildsen, D. Bumann, A. Camilli, J. J. Collins, C. Dehio, S. Fortune, J. M. Ghigo, W.
 D. Hardt, A. Harms, M. Heinemann, D. T. Hung, U. Jenal, B. R. Levin, J. Michiels, G.
 Storz, M. W. Tan, T. Tenson, L. Van Melderen, and A. Zinkernagel. 2019. 'Definitions and guidelines for research on antibiotic persistence', *Nat Rev Microbiol*, 17: 441-48.
- Bayer, A. S., T. Schneider, and H. G. Sahl. 2013. 'Mechanisms of daptomycin resistance in Staphylococcus aureus: role of the cell membrane and cell wall', *Ann N Y Acad Sci*, 1277: 139-58.
- Berger-Bachi, B., A. Strassle, J. E. Gustafson, and F. H. Kayser. 1992. 'Mapping and characterization of multiple chromosomal factors involved in methicillin resistance in Staphylococcus aureus', *Antimicrob Agents Chemother*, 36: 1367-73.
- Bezrukov, F., J. Prados, A. Renzoni, and O. O. Panasenko. 2021. 'MazF toxin causes alterations in Staphylococcus aureus transcriptome, translatome and proteome that underlie bacterial dormancy', *Nucleic Acids Res*, 49: 2085-101.
- Bigger, J. W. 1944. 'Treatment of staphylococcal infections with penicillin by intermittent sterilisation', *Lancet*, 244: 497-500.
- Camargo, I. L., H. M. Neoh, L. Cui, and K. Hiramatsu. 2008. 'Serial daptomycin selection generates daptomycin-nonsusceptible Staphylococcus aureus strains with a heterogeneous vancomycin-intermediate phenotype', *Antimicrob Agents Chemother*, 52: 4289-99.
- Castro-Roa, D., A. Garcia-Pino, S. De Gieter, N. A. J. van Nuland, R. Loris, and N. Zenkin. 2013. 'The Fic protein Doc uses an inverted substrate to phosphorylate and inactivate EFTu', *Nat Chem Biol*, 9: 811-7.
- Chen, C. J., Y. C. Huang, and C. H. Chiu. 2015. 'Multiple pathways of cross-resistance to glycopeptides and daptomycin in persistent MRSA bacteraemia', *J Antimicrob Chemother*, 70: 2965-72.
- Cong, Y., S. Yang, and X. Rao. 2020. 'Vancomycin resistant Staphylococcus aureus infections: A review of case updating and clinical features', *J Adv Res*, 21: 169-76.
- Conlon, B. P. 2014. 'Staphylococcus aureus chronic and relapsing infections: Evidence of a role for persister cells: An investigation of persister cells, their formation and their role in S. aureus disease', *Bioessays*, 36: 991-6.
- Conlon, B. P., E. S. Nakayasu, L. E. Fleck, M. D. LaFleur, V. M. Isabella, K. Coleman, S. N. Leonard, R. D. Smith, J. N. Adkins, and K. Lewis. 2013. 'Activated ClpP kills persisters and eradicates a chronic biofilm infection', *Nature*, 503: 365-70.
- Coussens, N. P., and D. A. Daines. 2016. 'Wake me when it's over Bacterial toxin-antitoxin proteins and induced dormancy', *Exp Biol Med (Maywood)*, 241: 1332-42.

- Cui, L., T. Isii, M. Fukuda, T. Ochiai, H. M. Neoh, I. L. Camargo, Y. Watanabe, M. Shoji, T. Hishinuma, and K. Hiramatsu. 2010. 'An RpoB mutation confers dual heteroresistance to daptomycin and vancomycin in Staphylococcus aureus', *Antimicrob Agents Chemother*, 54: 5222-33.
- Cui, L., E. Tominaga, H. M. Neoh, and K. Hiramatsu. 2006. 'Correlation between Reduced Daptomycin Susceptibility and Vancomycin Resistance in Vancomycin-Intermediate Staphylococcus aureus', *Antimicrob Agents Chemother*, 50: 1079-82.
- Darby, E. M., E. Trampari, P. Siasat, M. S. Gaya, I. Alav, M. A. Webber, and J. M. A. Blair. 2023. 'Molecular mechanisms of antibiotic resistance revisited', *Nat Rev Microbiol*, 21: 280-95.
- De Lencastre, H., S. W. Wu, M. G. Pinho, A. M. Ludovice, S. Filipe, S. Gardete, R. Sobral, S. Gill, M. Chung, and A. Tomasz. 1999. 'Antibiotic resistance as a stress response: complete sequencing of a large number of chromosomal loci in Staphylococcus aureus strain COL that impact on the expression of resistance to methicillin', *Microb Drug Resist*, 5: 163-75.
- Donegan, N. P., J. S. Marvin, and A. L. Cheung. 2014. 'Role of adaptor TrfA and ClpPC in controlling levels of SsrA-tagged proteins and antitoxins in Staphylococcus aureus', *J Bacteriol*, 196: 4140-51.
- Donegan, N. P., E. T. Thompson, Z. Fu, and A. L. Cheung. 2010. 'Proteolytic regulation of toxinantitoxin systems by ClpPC in Staphylococcus aureus', *J Bacteriol*, 192: 1416-22.
- Dorr, T., M. Vulic, and K. Lewis. 2010. 'Ciprofloxacin causes persister formation by inducing the TisB toxin in Escherichia coli', *PLoS Biol*, 8: e1000317.
- Fowler, V. G., Jr., H. W. Boucher, G. R. Corey, E. Abrutyn, A. W. Karchmer, M. E. Rupp, D. P. Levine, H. F. Chambers, F. P. Tally, G. A. Vigliani, C. H. Cabell, A. S. Link, I. DeMeyer, S. G. Filler, M. Zervos, P. Cook, J. Parsonnet, J. M. Bernstein, C. S. Price, G. N. Forrest, G. Fatkenheuer, M. Gareca, S. J. Rehm, H. R. Brodt, A. Tice, S. E. Cosgrove, S. aureus Endocarditis, and Group Bacteremia Study. 2006. 'Daptomycin versus standard therapy for bacteremia and endocarditis caused by Staphylococcus aureus', N Engl J Med, 355: 653-65.
- Fu, Z., N. P. Donegan, G. Memmi, and A. L. Cheung. 2007. 'Characterization of MazFSa, an endoribonuclease from Staphylococcus aureus', *J Bacteriol*, 189: 8871-9.
- Fu, Z., S. Tamber, G. Memmi, N. P. Donegan, and A. L. Cheung. 2009. 'Overexpression of MazFsa in Staphylococcus aureus induces bacteriostasis by selectively targeting mRNAs for cleavage', *J Bacteriol*, 191: 2051-9.
- Harms, A., D. E. Brodersen, N. Mitarai, and K. Gerdes. 2018. 'Toxins, Targets, and Triggers: An Overview of Toxin-Antitoxin Biology', *Mol Cell*, 70: 768-84.
- Harms, A., E. Maisonneuve, and K. Gerdes. 2016. 'Mechanisms of bacterial persistence during stress and antibiotic exposure', *Science*, 354.
- Hiramatsu, K. 2001. 'Vancomycin-resistant Staphylococcus aureus: a new model of antibiotic resistance', *Lancet Infect Dis*, 1: 147-55.
- Hiramatsu, K., N. Aritaka, H. Hanaki, S. Kawasaki, Y. Hosoda, S. Hori, Y. Fukuchi, and I. Kobayashi. 1997. 'Dissemination in Japanese hospitals of strains of Staphylococcus aureus heterogeneously resistant to vancomycin', *Lancet*, 350: 1670-3.
- Hiramatsu, K., Y. Katayama, M. Matsuo, T. Sasaki, Y. Morimoto, A. Sekiguchi, and T. Baba. 2014. 'Multi-drug-resistant Staphylococcus aureus and future chemotherapy', *J Infect Chemother*, 20: 593-601.

- Hososaka, Y., H. Hanaki, C. Yanagisawa, Y. Yamaguchi, H. Matsui, T. Nakae, S. Iwata, I. Hayashi, and K. Sunakawa. 2006. 'Nosocomial infection of beta-lactam antibiotic-induced vancomycin-resistant Staphylococcus aureus (BIVR)', *J Infect Chemother*, 12: 181-4.
- Howden, B. P., J. K. Davies, P. D. Johnson, T. P. Stinear, and M. L. Grayson. 2010. 'Reduced vancomycin susceptibility in Staphylococcus aureus, including vancomycin-intermediate and heterogeneous vancomycin-intermediate strains: resistance mechanisms, laboratory detection, and clinical implications', *Clin Microbiol Rev*, 23: 99-139.
- Howden, B. P., A. Y. Peleg, and T. P. Stinear. 2014. 'The evolution of vancomycin intermediate Staphylococcus aureus (VISA) and heterogenous-VISA', *Infect Genet Evol*, 21: 575-82.
- Hubert, S. K., J. M. Mohammed, S. K. Fridkin, R. P. Gaynes, J. E. McGowan, Jr., and F. C. Tenover. 1999. 'Glycopeptide-intermediate Staphylococcus aureus: evaluation of a novel screening method and results of a survey of selected U.S. hospitals', *J Clin Microbiol*, 37: 3590-3.
- Hyyrylainen, H. L., B. C. Marciniak, K. Dahncke, M. Pietiainen, P. Courtin, M. Vitikainen, R. Seppala, A. Otto, D. Becher, M. P. Chapot-Chartier, O. P. Kuipers, and V. P. Kontinen. 2010. 'Penicillin-binding protein folding is dependent on the PrsA peptidyl-prolyl cistrans isomerase in Bacillus subtilis', *Mol Microbiol*, 77: 108-27.
- Jousselin, A., W. L. Kelley, C. Barras, D. P. Lew, and A. Renzoni. 2013. 'The Staphylococcus aureus thiol/oxidative stress global regulator Spx controls trfA, a gene implicated in cell wall antibiotic resistance', *Antimicrob Agents Chemother*, 57: 3283-92.
- Jousselin, A., C. Manzano, A. Biette, P. Reed, M. G. Pinho, A. E. Rosato, W. L. Kelley, and A. Renzoni. 2015. 'The Staphylococcus aureus Chaperone PrsA Is a New Auxiliary Factor of Oxacillin Resistance Affecting Penicillin-Binding Protein 2A', *Antimicrob Agents Chemother*, 60: 1656-66.
- Jousselin, A., A. Renzoni, D. O. Andrey, A. Monod, D. P. Lew, and W. L. Kelley. 2012. 'The posttranslocational chaperone lipoprotein PrsA is involved in both glycopeptide and oxacillin resistance in Staphylococcus aureus', *Antimicrob Agents Chemother*, 56: 3629-40.
- Katayama, Y., H. Murakami-Kuroda, L. Cui, and K. Hiramatsu. 2009. 'Selection of heterogeneous vancomycin-intermediate Staphylococcus aureus by imipenem', *Antimicrob Agents Chemother*, 53: 3190-6.
- Keren, I., D. Shah, A. Spoering, N. Kaldalu, and K. Lewis. 2004. 'Specialized persister cells and the mechanism of multidrug tolerance in Escherichia coli', *J Bacteriol*, 186: 8172-80.
- Lowy, F. D. 2003. 'Antimicrobial resistance: the example of Staphylococcus aureus', *J Clin Invest*, 111: 1265-73.
- Masuda, H., Q. Tan, N. Awano, K. P. Wu, and M. Inouye. 2012. 'YeeU enhances the bundling of cytoskeletal polymers of MreB and FtsZ, antagonizing the CbtA (YeeV) toxicity in Escherichia coli', *Mol Microbiol*, 84: 979-89.
- Mehta, S., A. X. Cuirolo, K. B. Plata, S. Riosa, J. A. Silverman, A. Rubio, R. R. Rosato, and A. E. Rosato. 2012. 'VraSR two-component regulatory system contributes to mprF-mediated decreased susceptibility to daptomycin in in vivo-selected clinical strains of methicillin-resistant Staphylococcus aureus', *Antimicrob Agents Chemother*, 56: 92-102.
- Mishra, N. N., A. S. Bayer, P. A. Moise, M. R. Yeaman, and G. Sakoulas. 2012. 'Reduced susceptibility to host-defense cationic peptides and daptomycin coemerge in methicillin-resistant Staphylococcus aureus from daptomycin-naive bacteremic patients', *J Infect Dis*, 206: 1160-7.

- Mishra, N. N., J. McKinnell, M. R. Yeaman, A. Rubio, C. C. Nast, L. Chen, B. N. Kreiswirth, and A. S. Bayer. 2011. 'In vitro cross-resistance to daptomycin and host defense cationic antimicrobial peptides in clinical methicillin-resistant Staphylococcus aureus isolates', *Antimicrob Agents Chemother*, 55: 4012-8.
- Mok, W. W., M. A. Orman, and M. P. Brynildsen. 2015. 'Impacts of global transcriptional regulators on persister metabolism', *Antimicrob Agents Chemother*, 59: 2713-9.
- Mok, W. W., J. O. Park, J. D. Rabinowitz, and M. P. Brynildsen. 2015. 'RNA Futile Cycling in Model Persisters Derived from MazF Accumulation', *MBio*, 6: e01588-15.
- Mutschler, H., M. Gebhardt, R. L. Shoeman, and A. Meinhart. 2011. 'A novel mechanism of programmed cell death in bacteria by toxin-antitoxin systems corrupts peptidoglycan synthesis', *PLoS Biol*, 9: e1001033.
- Page, R., and W. Peti. 2016. 'Toxin-antitoxin systems in bacterial growth arrest and persistence', *Nat Chem Biol*, 12: 208-14.
- Panasenko, O. O., F. Bezrukov, O. Komarynets, and A. Renzoni. 2020. 'YjbH Solubility Controls Spx in Staphylococcus aureus: Implication for MazEF Toxin-Antitoxin System Regulation', *Front Microbiol*, 11: 113.
- Park, J. H., Y. Yamaguchi, and M. Inouye. 2011. 'Bacillus subtilis MazF-bs (EndoA) is a UACAU-specific mRNA interferase', *FEBS Lett*, 585: 2526-32.
- Proctor, R. A., A. Kriegeskorte, B. C. Kahl, K. Becker, B. Loffler, and G. Peters. 2014. 'Staphylococcus aureus Small Colony Variants (SCVs): a road map for the metabolic pathways involved in persistent infections', *Front Cell Infect Microbiol*, 4: 99.
- Renzoni, A., D. O. Andrey, A. Jousselin, C. Barras, A. Monod, P. Vaudaux, D. Lew, and W. L. Kelley. 2011. 'Whole genome sequencing and complete genetic analysis reveals novel pathways to glycopeptide resistance in Staphylococcus aureus', *PLoS One*, 6: e21577.
- Renzoni, A., W. L. Kelley, C. Barras, A. Monod, E. Huggler, P. Francois, J. Schrenzel, R. Studer, P. Vaudaux, and D. P. Lew. 2009. 'Identification by genomic and genetic analysis of two new genes playing a key role in intermediate glycopeptide resistance in Staphylococcus aureus', *Antimicrob Agents Chemother*, 53: 903-11.
- Renzoni, A., W. L. Kelley, R. R. Rosato, M. P. Martinez, M. Roch, M. Fatouraei, D. P. Haeusser, W. Margolin, S. Fenn, R. D. Turner, S. J. Foster, and A. E. Rosato. 2017. 'Molecular Bases Determining Daptomycin Resistance-Mediated Resensitization to beta-Lactams (Seesaw Effect) in Methicillin-Resistant Staphylococcus aureus', *Antimicrob Agents Chemother*, 61.
- Reygaert, W. C. 2018. 'An overview of the antimicrobial resistance mechanisms of bacteria', *AIMS Microbiol*, 4: 482-501.
- Roch, M., P. Clair, A. Renzoni, M. E. Reverdy, O. Dauwalder, M. Bes, A. Martra, A. M. Freydiere, F. Laurent, P. Reix, O. Dumitrescu, and F. Vandenesch. 2014. 'Exposure of Staphylococcus aureus to subinhibitory concentrations of beta-lactam antibiotics induces heterogeneous vancomycin-intermediate Staphylococcus aureus', *Antimicrob Agents Chemother*, 58: 5306-14.
- Sader, H. S., D. J. Farrell, R. K. Flamm, and R. N. Jones. 2015. 'Analysis of 5-year trends in daptomycin activity tested against Staphylococcus aureus and enterococci from European and US hospitals (2009-2013)', *J Glob Antimicrob Resist*, 3: 161-65.
- Sader, H. S., and R. N. Jones. 2006. 'The activity of daptomycin against wild-type Staphylococcus aureus and strains with reduced susceptibility to vancomycin', *Clin Infect Dis*, 43: 798-9; author reply 99-800.

- Shaw, G. J., J. M. Meunier, J. Korfhagen, B. Wayne, K. Hart, C. J. Lindsell, and G. Fermann. 2015. 'Randomized Controlled Noninferiority Trial Comparing Daptomycin to Vancomycin for the Treatment of Complicated Skin and Skin Structure Infections in an Observation Unit', *J Emerg Med*, 49: 928-36.
- Sierra, R., J. Prados, O. O. Panasenko, D. O. Andrey, B. Fleuchot, P. Redder, W. L. Kelley, P. H. Viollier, and A. Renzoni. 2020. 'Insights into the global effect on Staphylococcus aureus growth arrest by induction of the endoribonuclease MazF toxin', *Nucleic Acids Res*, 48: 8545-61.
- Sierra, R., P. Viollier, and A. Renzoni. 2018. 'Linking toxin-antitoxin systems with phenotypes: A Staphylococcus aureus viewpoint', *Biochim Biophys Acta Gene Regul Mech*.
- Skiest, D. J. 2006. 'Treatment failure resulting from resistance of Staphylococcus aureus to daptomycin', *J Clin Microbiol*, 44: 655-6.
- Stefani, S., F. Campanile, M. Santagati, M. L. Mezzatesta, V. Cafiso, and G. Pacini. 2015. 'Insights and clinical perspectives of daptomycin resistance in Staphylococcus aureus: A review of the available evidence', *Int J Antimicrob Agents*, 46: 278-89.
- Tong, S. Y., J. S. Davis, E. Eichenberger, T. L. Holland, and V. G. Fowler, Jr. 2015. 'Staphylococcus aureus infections: epidemiology, pathophysiology, clinical manifestations, and management', *Clin Microbiol Rev*, 28: 603-61.
- Uckay, I., L. Bernard, M. Buzzi, S. Harbarth, P. Francois, E. Huggler, T. Ferry, J. Schrenzel, A. Renzoni, P. Vaudaux, and D. P. Lew. 2012. 'High prevalence of isolates with reduced glycopeptide susceptibility in persistent or recurrent bloodstream infections due to methicillin-resistant Staphylococcus aureus', *Antimicrob Agents Chemother*, 56: 1258-64.
- van Hal, S. J., M. Jones, I. B. Gosbell, and D. L. Paterson. 2011. 'Vancomycin heteroresistance is associated with reduced mortality in ST239 methicillin-resistant Staphylococcus aureus blood stream infections', *PLoS One*, 6: e21217.
- Vaudaux, P., T. Ferry, I. Uckay, P. Francois, J. Schrenzel, S. Harbarth, and A. Renzoni. 2012. 'Prevalence of isolates with reduced glycopeptide susceptibility in orthopedic device-related infections due to methicillin-resistant Staphylococcus aureus', Eur J Clin Microbiol Infect Dis, 31: 3367-74.
- Vaudaux, P., P. Francois, B. Berger-Bachi, and D. P. Lew. 2001. 'In vivo emergence of subpopulations expressing teicoplanin or vancomycin resistance phenotypes in a glycopeptide-susceptible, methicillin-resistant strain of Staphylococcus aureus', *J Antimicrob Chemother*, 47: 163-70.
- Vaudaux, P., E. Huggler, L. Bernard, T. Ferry, A. Renzoni, and D. P. Lew. 2010. 'Underestimation of vancomycin and teicoplanin MICs by broth microdilution leads to underdetection of glycopeptide-intermediate isolates of Staphylococcus aureus', Antimicrob Agents Chemother, 54: 3861-70.
- Vulin, C., N. Leimer, M. Huemer, M. Ackermann, and A. S. Zinkernagel. 2018. 'Prolonged bacterial lag time results in small colony variants that represent a sub-population of persisters', *Nat Commun*, 9: 4074.
- Windels, E. M., B. Van den Bergh, and J. Michiels. 2020. 'Bacteria under antibiotic attack: Different strategies for evolutionary adaptation', *PLoS Pathog*, 16: e1008431.
- Yamaguchi, Y., H. Hanaki, C. Yanagisawa, Y. Ikeda-Dantsuji, T. Hashimoto, H. Yazaki, K. Sugahara, T. Yanagisawa, H. Kawajiri, S. Sato, A. Ishizaki, R. Tachihara-Sato, Y. Takahashi, T. Ono, Y. Kageyama, T. Kawaguchi, A. Tamura, K. Hagane, and K. Sunakawa. 2009. 'Characterization of beta-lactam antibiotic-induced vancomycin-

- resistant MRSA (BIVR) in a patient with septicemia during long-term vancomycin administration', *J Infect Chemother*, 15: 274-8.
- Yang, S. J., Y. Q. Xiong, P. M. Dunman, J. Schrenzel, P. Francois, A. Peschel, and A. S. Bayer. 2009. 'Regulation of mprF in daptomycin-nonsusceptible Staphylococcus aureus strains', *Antimicrob Agents Chemother*, 53: 2636-7.
- Zhu, L., K. Inoue, S. Yoshizumi, H. Kobayashi, Y. Zhang, M. Ouyang, F. Kato, M. Sugai, and M. Inouye. 2009. 'Staphylococcus aureus MazF specifically cleaves a pentad sequence, UACAU, which is unusually abundant in the mRNA for pathogenic adhesive factor SraP', *J Bacteriol*, 191: 3248-55.